Impact of climate change on severe storms in Europe : attribution and projection

Mireia Ginesta Fernandez

université PARIS-SACLAY

Impact of climate change on severe storms in Europe: attribution and projection

Impact du changement climatique sur les tempêtes sévères en Europe: attribution et projection

Thèse de doctorat de l'université Paris-Saclay

École doctorale n°129, Sciences de l'Environnement d'Île de France (SEIF)
Spécialité de doctorat: Géosciences
Graduate School : Géosciences, Climat, Environnement, Planètes
Référent : Université de Versailles-Saint-Quentin-en-Yvelines

Thèse préparée dans l'unité de recherche **Laboratoire des sciences du climat et de l'environnement (Université Paris-Saclay, CNRS, CEA, UVSQ)**, sous la direction de **Davide Faranda**, directeur de recherche CNRS, et la co-direction de **Pascal Yiou**, directeur de recherche CEA.

Thèse soutenue à Paris-Saclay, le 14 juin 2024, par

Mireia GINESTA FERNANDEZ

Composition du jury

Membres du jury avec voix délibérative

Fabio D'ANDREA Directeur de Recherche CNRS, Laboratoire de Météorologie Dynamique Ecole Normale Supérieure	Président
Florian PANTILLON Chargé de recherche CNRS, Laboratoire d'Aérologie, Université de Toulouse	Rapporteur et Examinateur
Rachel WHITE Assistant Professor, University of British Columbia	Rapporteure et Examinatrice
Suzana CAMARGO Professeure à Lamont-Doherty Earth Observatory, Columbia University	Examinatrice
Joaquim PINTO Professeur à Karlsruher Institut für Technologie	Examinateur

THESE DE DOCTORAT
NNT : 2024UPASJ009

université PARIS-SACLAY
ÉCOLE DOCTORALE
Sciences de l'Environnement d'Île-de-France (SEIF)

Title: Impact of climate change on severe storms in Europe: attribution and projection

Keywords: extratropical cyclones; extreme events; extreme event attribution; climate change

Abstract: Global warming is altering the frequency and severity of extreme weather events, such as heatwaves, floods, and cyclones. These events have immediate, observable impacts, such as economic losses or loss of life. Extreme event attribution, initially conceived as a tool for assessing liability for damages, has rapidly evolved into various approaches aimed at quantifying the influence of climate change on the dynamics, hazards, and impacts of such extreme events. For some extremes, particularly those predominantly influenced by dynamics such as extratropical storms, confidence in attribution and future projections remains low.

In this thesis, we assess changes in observed severe extratropical storms and their meteorological hazards across Western Europe in a warmer climate. Some of the storms analyzed are Alex, in October 2020, Xynthia, in February 2010, and Eunice, in February 2022. Each of them exhibits unique characteristics, yet we can identify similar patterns for comparative analysis. Hence, we explore the concept of weather analogues, which represent recurrent patterns of atmospheric circulation. We identify analogues of severe extratropical storms in two different climates, characterized by weak and strong human influence on climate, in both reanalysis and climate models. We found an increase in precipitation and wind speed associated with these storms in a warmer world, with the drivers of such changes varying from case to case.

While analyzing average large-scale patterns in storms across the North Atlantic is fundamental for understanding general trends in dynamics and hazards in various locations, focusing on specific storms, as conducted in this thesis, can offer additional perspectives. Specific storms result from a combination of complex processes that might not be fully captured in large-scale trends; thus, they can serve as case studies for investigating the influence of climate change on their behavior. By examining specific patterns and their analogues, we acknowledge the chaotic nature of the atmosphere, and by providing localized assessments, we consider the specificities of the area.

The tools presented here can be applied to other extratropical storms worldwide to enhance our comprehension and provide local assessments. Our research combines meteorological knowledge with climate science, aiming to understand the evolving nature of severe storms and the hazards of climate change.

université PARIS-SACLAY

ÉCOLE DOCTORALE
Sciences de l'Environnement d'Île-de-France (SEIF)

Titre: Impact du changement climatique sur les tempêtes sévères en Europe: attribution et projection

Mots clés: tempêtes extratropicales; événements extrêmes; attribution des événements extrêmes; changement climatique

Résumé: Le réchauffement climatique altère la fréquence et la sévérité des événements météorologiques extrêmes, tels que les vagues de chaleur, les inondations et les tempêtes. Ces événements ont des impacts immédiats et observables, tels que des pertes économiques ou des pertes de vie. L'attribution des événements extrêmes, initialement conçue comme un outil d'évaluation de la responsabilité des dommages, a rapidement évolué vers différentes approches visant à quantifier l'influence du changement climatique sur la dynamique, les risques et les impacts de tels événements extrêmes. Pour certains extrêmes, en particulier ceux principalement influencés par la dynamique tels que les tempêtes extratropicales, la confiance dans l'attribution et les projections futures reste faible.

Dans cette thèse, nous évaluons les changements observés dans les tempêtes extratropicales sévères et leurs risques météorologiques en Europe occidentale dans un climat plus chaud. Certaines des tempêtes analysées sont Alex, en octobre 2020, Xynthia, en février 2010, et Eunice, en février 2022. Chacune présente des caractéristiques uniques, mais nous pouvons identifier des motifs similaires pour une analyse comparative. Ainsi, nous explorons le concept d'analogues météorologiques, qui représentent des motifs récurrents de circulation atmosphérique. Nous identifions des analogues de tempêtes extratropicales sévères dans deux climats différents, caractérisés par une faible et une forte influence humaine sur le climat, dans les réanalyses et les modèles climatiques. Nous avons constaté des augmentations cohérentes des précipitations et de la vitesse du vent associées à ces tempêtes dans un monde plus chaud, les facteurs de ces changements variant d'un cas à l'autre.

Alors que l'analyse des modèles à grande échelle des tempêtes à travers l'Atlantique Nord est fondamentale pour comprendre les tendances générales dans la dynamique et les risques dans divers endroits, se concentrer sur des tempêtes spécifiques, comme réalisé dans cette thèse, peut offrir des perspectives supplémentaires. Des tempêtes spécifiques résultent d'une combinaison de processus complexes, ce qui en fait des études de cas précieuses pour étudier l'influence du changement climatique sur leur comportement. En examinant des motifs spécifiques et leurs analogues, nous reconnaissons la nature chaotique de l'atmosphère, et en fournissant des évaluations localisées, nous tenons compte des spécificités de la région.

Les outils présentés ici peuvent être appliqués à d'autres tempêtes extratropicales dans le monde entier pour améliorer notre compréhension et fournir des évaluations locales. Notre recherche combine les connaissances météorologiques avec les sciences climatiques, dans le but de comprendre la nature évolutive des tempêtes violentes et les risques du changement climatique.

This thesis has been funded by the European Union's Horizon 2020 research and innovation programme under the Marie Sklodowska-Curie grant agreement No. 956396, EDIPI (European weather extremes: drivers, predictability and impacts).

Remerciements

I am deeply grateful to my supervisor, Davide Faranda, for guiding me throughout these three years. Davide; you have valued me and, more importantly, believed in me, which made me believe in myself too. You have understood me during my frustrating moments, consistently supported me, made me laugh (a lot), taken me to conferences, and introduced me to this world. You are a true role model, and I owe my amazing PhD experience to you. I also want to extend my heartfelt thanks to my co-supervisor, Pascal Yiou. Your door has always been open, providing a place of peace for me and for everyone. Talking to you is always a pleasure; you listen, understand, and share your vast knowledge with us. I have learned so much from you, and this field, especially our team, is immensely fortunate to have you.

I am thankful to the jury members: Florian Pantillon, Rachel White, Suzana Camargo, Joaquim Pinto, and Fabio d'Andrea. I admire each of you, and it has been a pleasure to receive your support and feedback.

I am grateful to the members of my committee, Carmen Alvarez and Gwendal Riviere, for guiding, supporting, and motivating me to keep pushing forward in my research. I also want to thank Pascal Maugis for showing genuine interest in both my research and my overall well-being.

I am grateful to my colleagues, with whom I have had the pleasure of sharing this journey. A special thanks to the small family of ESTIMR. Particularly to Flavio Pons, for being an extraordinary scientific and moral support, and for becoming a friend. To Paula, for being the best office mate. To Camille, for always being ready to help and laugh, organize get-togethers, and for becoming an adventure companion in remote countries. To Robin, my thesis brother, whom I admire greatly, both scientifically and personally. To Nemo, the other thesis brother, for his immense kindness. To Meriem, for her support and friendship. To Soulivanh Thao, for helping me whenever I needed it. To Yoann Robin, for always being willing to share code and help his colleagues. To Clara and Greta, my "gluten-free gang"; I wish I had met you sooner, but I'm happy to finally have met you and look forward to sharing more experiences in the future. To Gisela and Yann, it was wonderful getting to know you outside the lab; I hope to keep in touch. To Stella, Lucas, Laura, Germain, George, Pradeebane, Bastien, Burak, and many more with whom I have had the pleasure of exchanging experiences.

I am incredibly fortunate to have had my EDIPI colleagues by my side. We are a big family, and I am very grateful for all the nice memories with each one of you. Vinnie, thank you for being my Parisian sister, for your sweetness, and for becoming a true friend. Ferran, a compatriot; I feel very lucky to have met you and to have a kind, lifelong friend. To Emma, for your endless support; simply thank you for being there, specially when I needed it the most. To Anastasyia, for your friendship and for making my (and everyone's) experience in Sweden and elsewhere unforgettable. To Aleksa; I admire you greatly, you always have a smile for everyone, you are empathetic, and always willing to help, thank you for being you. To Anupama; you have been a great discovery for me, I admire you a lot, and I had the great pleasure of sharing my experience in Brussels (and more!) with you. To Valeria, for being so sweet and an inspiration to me and many other women; I know you will have a brilliant future, and I hope to be part of it. To Bianca, for being an adventure companion with whom I look forward to sharing even more trips. To Jamie, for sharing your energy and light with me and with the whole group. To Federico, for always bringing us good vibes and

lots of music. To Innovasita, for your daily smile and the little stories you share with us. To Sohan, for your bravery and for never losing your smile for us. And to Thessa, for your strong courage and resilience. Thank you all.

From EDIPI, I would also like to thank Gabriele Messori, the project coordinator. I believe we are the luckiest to have you as the captain of our ship; I'm not sure if there is a more supportive and organized coordinator out there. To Andra, for her endless energy and support; to Elisa, for being trustworthy, sweet, and for becoming one of us; to Murat, for bravely taking on the role of Andra and Elisa, and doing so at the same incredible level. To Stephane, for welcoming me to RMI and sharing your vast knowledge. And to all the supervisors, especially those who made the amazing training events possible and those who were there to meet and support us.

A mis amigos y familia de París. Muchas gracias, Lia, por ser mi compañera y hermana de aventuras, por quererme y estar siempre a mi lado. A Pablo, por su infinito apoyo. A Irmi, por ser una hermana mayor y pequeña a la vez. A Mateo, por nuestra complicidad. A Joaquín, por ser el pilar de esta pequeña familia. A Marina, por ser nuestra estrella. A Anna, mi hermana perdida que tengo por ahí a la que admiro mucho. Y a Stefan, por quererme y aceptarme tal como soy, y por estar siempre a mi lado.

Agradezco a todas las personas que han sido parte de mi hogar. A todxs lxs trabajadorxs de la Residencia Colegio de España, por cuidarnos tanto, y a los compañeros de residencia del Colegio y de la casa de Suecia. A Eric; aunque la vida nos lleve por caminos diferentes, siempre te agradeceré que nuestros caminos se hayan cruzado y haber tenido el placer de compartir un pedacito de ella contigo.

Als meus amics de sempre. Especialment a la Laia, la Núria i la Glòria, per ser-hi des dels tres anys. A la Cris i al Miquel, per haver estat també des de ben petits. Als amics de la uni (Carme, Paula, Guillem, Pablo, Gorge, Marina, Joan, Jordi, Carles, Willy, Marc i Òscar). Als del màster, especialment a en Pep i en Carlos. Al Mario, per ser una inspiració i el meu gran suport abans d'aquesta aventura. Als meus professors del màster, especialment al Javi, per obrir-me les portes d'aquest món.

A la meva familia, especialment a la tieta Mai i tiet Pedro, per cuidar-me com si fos una filla.

Als meus pares, Toni i Rosa; no tinc paraules suficients d'agraïment per tot el que heu fet per mi, per creure en mi, per valorar-me i estimar-me. Al Kiwi, per ser el millor gos del món. I a la meva germana Sandra: ets el meu pilar fonamental i un exemple a seguir. Tot el que he aconseguit és gràcies a vosaltres; ho devem a l'esforç compartit. Us estimo infinitament.

Contents

Remerciements **v**

1 Introduction **1**

1.1 Extreme Event Attribution 2

1.2 Extratropical Cyclones 13

1.3 Research Questions 22

2 An Introduction to a Conditional Extreme Event Attribution Approach **27**

2.1 Introduction 28

2.2 Article published in Climate Dynamics 28

2.3 Additional analyses 29

2.4 Summary and conclusions 36

3 A Multivariate Extreme Event Attribution Approach **39**

3.1 Introduction 40

3.2 Methodology and example of application: Acqua Alta events 40

3.3 Refined Multivariate Approach and application to the Emilia-Romagna floods of May 2023 43

3.4 Summary and conclusions 58

4 Future projections of Explosive Cyclones in a Changing Climate **61**

4.1 Introduction 62

4.2 Article under review in Journal of Climate 62

4.3 Additional analyses 64

4.4 Summary and conclusions 76

5 Conclusions **79**

5.1 Overview of the thesis 79

5.2 Limitations and Implications 80

5.3 Future research directions 82

References **85**

A Article "A methodology for attributing severe extratropical cyclones to climate change based on reanalysis data: the case study of storm Alex 2020" **101**

B Article "Anthropogenic climate change will intensify European explosive storms similar to Alex, Eunice, and Xynthia in the future" **127**

C Manuscript in preparation "Future projections of the concurrences of atmospheric rivers and explosive cyclones in the North Atlantic" **173**

C.1 Scientific background 173

C.2 Data and methods 174

D Coauthored articles **177**

Chapter 1

Introduction

Contents

2.1 Introduction 28
2.2 Article published in Climate Dynamics 28
2.3 Additional analyses 29
2.3.1 Parameter sensitivity tests 30
a) Number of analogues 30
b) Spatial domain to identify analogues 32
2.3.2 Assessment of the role of internal variability 32
2.3.3 Comparison with general trends of North Atlantic Winter Cyclones 33
2.4 Summary and conclusions 36

Objectives

This chapter aims to introduce background knowledge about Extreme Event Attribution and extratropical cyclones, as well as the research question and motivation of this thesis.

1.1 Extreme Event Attribution

In 1856, Eunice Newton Foote conducted pioneering experiments in her home laboratory, discovering the greenhouse effect through observations of carbon dioxide and water vapor. Despite her groundbreaking work, her recognition in the scientific community remains limited. It was not until 1896 that Svante Arrhenius's paper, 'On the Influence of Carbonic Acid in the Air upon the Temperature of the Ground,' gained widespread acknowledgment for proposing the link between burning fossil fuels, increased carbon dioxide, and rising temperatures.

In the 1960s, concerns about climate change emerged. In 1967, Syukuro Manabe and Richard T. Wetherald estimated that doubling the CO_2 concentration would lead to a 2 K increase in atmospheric temperature (Manabe and Wetherald, 1967). Manabe's remarkable contributions earned him the 2021 Nobel Prize in Physics, shared with Klaus Hasselmann and Giorgio Parisi, for creating a model that links weather and climate and developing methods for identifying human influence on climate (Nobel Prize Outreach AB, 2024).

The scientific community progressed in detecting and attributing climate change. Detection involves observing statistically significant changes in the climate system, such as mean temperature or extreme events. Attribution is the process of linking these observed changes to specific causes, particularly discerning the extent of human activities' contribution.

Following these advances, the Intergovernmental Panel on Climate Change (IPCC) was established by the United Nations in 1988. The IPCC aims to provide comprehensive reviews and regular assessments based on scientific evidence. The reports include a chapter on detection and attribution. The IPCC's Third Assessment Report in 2001 presented 'new and stronger evidence that most of the warming observed over the last 50 years is attributable to human activities' (Watson and Core Writing Team (Eds.), 2001).

Discerning long-term, large-scale changes in the climate proves challenging. In contrast, our daily lives are impacted by weather variations. In 2003, Myles Allen underscored the significant damage caused by extreme weather (Allen, 2003). To illustrate, he referenced an ongoing event in his region—a flooding of the River Thames. Allen noted that people are generally more responsive to immediate concerns like rising insurance premiums and falling property values than to broader global sustainability issues. Stressing the need for a scientific foundation for fair compensation, he proposed quantifying the change in the likelihood of an event relative to its preindustrial value, marking the beginning of the Extreme Event Attribution (EEA) field.

Since then, more than 500 attribution studies disentangle the role of climate change on extreme events (Carbon Brief, 2022), with an annual special issue in The Bulletin of the American Meteorological Society (BAMS) since 2011 (Herring et al., 2022; Peterson et al., 2012). The most studied events include heatwaves, rain and flooding events, droughts, storms, and wildfires. However, there are still limited capabilities for attributing some, especially smaller-scale events requiring high-resolution data, such as

localized floods, particularly in the Global South.

The motivation behind EEA research is diverse. Jézéquel et al. (2020) explored EEA scientists' motivations, identifying two main categories: (i) contributing to collective knowledge and (ii) potential instrumental applications, such as climate litigation or infrastructure design. This thesis aligns more with the first group. The research presented aims to enhance our understanding of impactful **extratropical cyclones**, those that lead to **wet and windy extremes**, in the context of climate change.

In the following sections, I summarize the diverse approaches that have evolved over the last few decades in EEA. I present various definitions of extreme events, tailored to the objectives of studies. I also highlight some commonly used datasets in EEA, and explore potential applications of this field.

1.1.1 Evolution of different approaches of EEA

The approaches I will describe subsequently can be grouped into two main categories: the *unconditional* approach and the *conditional* approach. When comparing a climate with natural forcings only to another with historical forcings, even with a certain level of conditioning on atmospheric composition, the oceanic and atmospheric states are left unconstrained. This is the unconditional approach, exemplified by the risk-based approach. On the opposite end of the spectrum, the approaches that constrain the dynamics leading to the event, such as the analogues approach in which the synoptic atmospheric circulation is somehow fixed, are the conditional approaches. Both approaches may assess changes in the likelihood of the event, its magnitude, or a combination of both.

a) Unconditional Approaches

Risk-Based Approach To the best of our knowledge, the first EEA study was done by Stott et al. (2004). They applied the approach proposed by Allen (2003) on the European heatwave of 2003, which has been estimated to cause 70,000 deaths (Robine et al., 2008). Stott et al. (2004) introduced the Fraction of Attributable Risk (FAR) as an index designed to quantify the change in the probability of occurrence in a climate influenced by anthropogenic radiative forcing in comparison to a climate without climate change. They found that the heatwave was at least two times more probable than it would have been without climate change. The approach of comparing the change in probabilities between two different worlds, generally with and without climate change, has been called the *risk-based approach*.

As the first approach of EEA, many studies have been based on it (Philip et al., 2020; Van Oldenborgh, 2007). In fact, most of the BAMS studies are based on this probabilistic approach (Jézéquel et al., 2018b). These studies define a *factual* period, which is generally a period characterized by a strong climate change signal (such as the historical or more recent period), and a *counterfactual* period, representing the

world that would have been without climate change (such as the pre-industrial climate). There are variations, such as using atmosphere-only simulations and using sea surface temperatures (SSTs) and sea ice as boundary conditions (Pall et al., 2011). Others also use climate projections to evaluate the role of a stronger global warming signal in the event's future occurrence (e.g. Fischer and Knutti, 2015). Evaluating future projections, as well as the possibility of unprecedented events (Harrington et al., 2022), provides valuable information for the processes involved in adaptation decision-making (Hazeleger et al., 2015).

It is important to note that this approach attributes a *class of events*, that is, events of a similar or higher magnitude that the one observed. Taking the study by Emanuel (2017) on hurricane Harvey as an example, the question to answer would be "how likely is it that hurricane-induced flooding of Harvey's magnitude will occur again?".

Impacts Attribution More recently, studies have applied the probabilistic approach to directly attribute real impacts, such as mortality rates or economic losses, to anthropogenic climate change. A pioneering study by Mitchell et al. (2016), quantified the influence of anthropogenic climate change on heat-related mortality in Europe during the 2003 heatwave. This study established a connection between temperature and mortality through the use of an impact assessment model, and applied the FAR statistics. Another example was presented by Litzow et al. (2021), who assessed the impact on the sustainability of fisheries using Bayesian regression models. Perkins-Kirkpatrick et al. (2022) attributed the maximum daily mortality in the UK during the summer of 2006 and the financial damages from a high rainfall event in New Zealand on April 4, 2017. They employed "transfer functions" to link weather variables with impacts. Additionally, they emphasized that the relationship between meteorological hazards and real impacts is usually nonlinear, advocating for the inclusion of an assessment of both in all attribution studies to better quantify the real impacts.

These impact attribution studies typically assume anthropogenic forcing as the primary driver without accounting for changes in other factors, such as exposure or the "transfer function." In some cases, it is crucial to consider these factors. For instance, increasing trends in damages due to natural disasters are often associated with an increase in vulnerability and exposure (Visser et al., 2014). Therefore, while recent advancements in this field have been noteworthy, there is room for improvement, such as accounting for changes in additional factors to enhance the accuracy of the real impacts.

b) Conditional Approaches

Storyline approach Trenberth et al. (2015) highlighted the challenges associated with the risk-based approach when analyzing events strongly influenced by atmospheric circulation patterns. They emphasized that forced circulation changes induced by external factors like human activities are often smaller than the internal variability dominating short-lived events. In addition, as pointed out by Shepherd (2014), uncertainty in the future projections of dynamic changes is much higher than for the thermodynamics response. Consequently, Trenberth et al. (2015) introduced an alternative approach.

Instead of comparing probabilities of an event, their aim was to address a different question: given the weather pattern of an extreme event, how did the contributing factors unfold, and how the known thermodynamics signal played a role in each of them? They illustrated this reasoning with examples, such as the 'snowmaggedon' in Washington DC in February 2010, where unusually high SSTs contributed to the intensification of the event by enhancing moisture content in the storm. The general approach of disentangling the physical processes leading to the event assessing the role of climate change on them, was later termed the *storyline approach* by Shepherd (2016). In such approach, what is evaluated is the event itself, rather than a class of events. Some examples or interpretations of the storyline approach are listed below.

Boulder Approach In a review paper on EEA, Otto (2017) mentioned the "Boulder Approach", although other studies consider it part of the storyline approach (Jézéquel et al., 2018b). This approach aims to analyze causal factors of extreme events without quantifying their influence on the occurrence and without explicitly constraining the circulation. One of the first examples was proposed by Hoerling et al. (2013), who analyzed the 2011 Texas drought/heat wave and estimated the anthropogenic contribution of the drivers to the event.

Analogues Approach This method consists in dynamically constraining the circulation pattern leading to extreme events (Yiou, 2014). An early example was presented by Yiou et al. (2007), who identified analogues of the exceptionally warm fall/winter of 2006/2007 and observed that flow analogues were associated with colder temperatures. Similarly, in a study by Cattiaux et al. (2010), daily-flow analogues of the cold winter of 2010 were identified, and they showed that analogues in a past climate were linked to even lower temperatures. The analogues approach has also been used to separate the dynamics and thermodynamics signals (Vautard et al., 2016; Vautard et al., 2023; Yiou et al., 2017).

Recently, Faranda et al. (2022) that I co-authored (included in Appendix D), introduced a novel methodology within the analogues approach. We identified a specified number of circulation patterns resembling those leading to extreme events in two climates—with weak and strong climate change signals—referring to them as analogues of the event. Subsequently, we conducted a comparison of the meteorological hazards, such as temperature or precipitation, of these analogues in both climates. Another example of this approach was shown by Ginesta et al. (2023) (included in Appendix A). In this study, we identified changes in meteorological hazards between the present and a recent past climate of extratropical cyclone Alex, constraining the atmospheric sea level pressure pattern to reassemble to the cyclonic low that caused the event. Chapter 2 is based on these two studies.

Spectrally nudged storyline Dynamic conditions are constrained through the application of global spectral nudging (van Garderen et al., 2020). This technique consists in constraining the large-scale circulation patterns of a high resolution model, such as divergence and vorticity at upper levels in van Garderen et al. (2020), towards reanalysis data. By employing this technique, it becomes possible to simulate extreme weather events with high detail, and an assessment of the role of thermodynamics in driving such extremes.

Forecast-based approach To our knowledge, the first study using a weather forecast model for attribution was Lackmann et al 2015, who analyzed Hurricane Sandy in pre-industrual and future climates using the Weather Research and Forecasting regional model (WRF) driven by reanalysed SSTs. Meredith et al. (2015) performed an ensemble sensitivity simulations using the WRF model and evaluated the role of the SST in the Black sea in amplifying the 2012 Krymsk precipitation extreme. Another methodology using weather forecasting models was proposed by Leach et al. (2021), in which they used the ECMWF medium-range forecast model to attribute partially an increased CO2 concentrations to the European winter heatwave in February 2009. Notably, the degree of conditioning to atmospheric circulation can be adjusted by modifying the lead time of the simulations. Shorter lead times tightly constrain the circulation to the event, while larger lead times incorporate dynamic responses.

c) On the gradual differences of the EEA framing

In unconditional approaches, the signal-to-noise ratio is low when the event is largely driven by dynamics, resulting in inconclusive results on the role of climate change. In addition, while using the null hypothesis of no climate change, they are prone to Type II errors or false negatives. In such cases, Trenberth et al. (2015) proposed that assessing how contributing factors might have been affected by known thermodynamics could be more effective. This is because conditioning on dynamics filters out variability significantly, leaving a more noticeable thermodynamic signal. However, they are prone to false positives or Type I error. In addition, as noted by Otto et al. (2016), dynamics can sometimes counteract or reinforce the thermodynamics signal, adding complexity to the analysis (Faranda et al., 2020).

One of the earliest EEA studies where distinct approaches yielded apparently opposite climate change signals was observed in two studies that attributed the Russian Heatwave of 2010. In one study, the authors stated that the event was largely driven by natural variability (Dole et al., 2011). The other study, by Rahmstorf and Coumou (2011), indicated that climate change increased the likelihood of occurrence. Otto et al. (2012) conducted a study with the aim of reconciling these approaches, stating that one study evaluated the magnitude of the event while the other assessed its frequency, leading to potentially divergent climate change signals. However, they emphasized that these studies are complementary, serving different purposes.

As stated by Lloyd and Oreskes (2018), some defenders of the conventional risk-based approach argued that it would be more useful for stakeholders to know changes in the overall risk or probability of an extreme rather than disentangling the different factors that lead to it (or the deterministic storyline approach). However, Lloyd and Oreskes (2018) suggested that there is "no single most relevant approach to all situations and all questions". The EEA studies combine different approaches and serve different purposes. As stated by Otto (2023), differences in the EEA methods are gradual rather than fundamental, and ideally a combination of different methods would provide a complete and comprehensive attribution assessment (e.g. Tanaka et al., 2023). I interpret then that EEA studies can be placed along a spectrum based on their framing, with different approaches and purposes. I depict such gradual differences in figure 1.3, with a few

studies mentioned earlier to illustrate these distinctions.

Figure 1.1: **Unconditional**: Stott et al. (2004) compared two climates, one with natural forcing (NAT) and a historical climate (HIST) considering anthropogenic forcing. Pall et al. (2011) used an atmospheric circulation model with prescribed sea surface temperature (SST) and sea ice depicting two different climates. **Conditional**: Faranda et al. (2022) used the analogues approach to identify changes in the magnitude of the events. Jézéquel et al. (2018a) compute the trends in the likelihood of the atmospheric circulation pattern that lead to a particular extreme event. Leach et al. (2021) is a forecast-based approach in which, by changing the lead time of the simulations, they are able to change the level of conditioning (the lead time closest to the time of the event is the most conditioned on the circulation).

1.1.2 Definition of an extreme event: dynamics, hazards, or impacts

While all Extreme Event Attribution (EEA) studies share a common overarching purpose – evaluating the role of climate change in observed extreme events – they diverge in the definition of the extreme event. The definition of an extreme event is a subjective key choice that might impact quantitatively the results of the attribution (Cattiaux and Ribes, 2018). The choice of definition takes into account the variables considered, and has an influence on the choice of the approach and datasets used. I categorize EEA studies into three groups based on their definition, and show one example of each in figure 1.2:

- **Attribution by Dynamics:** This category encompasses studies focused on understanding the dynamic processes leading to extreme events, often associated with the storyline approach. For instance, consider a heatwave that produced extreme temperatures. Attribution by dynamics would involve examining the synoptic circulation that lead to the extreme temperatures.
- **Attribution by Hazards:** This category focuses on defining an event by its meteorological hazards, such as high precipitation rates or extreme temperatures. In the same heatwave example, attribution by hazards would consist in attributing the extreme temperatures themselves, often using risk-based approaches.
- **Attribution by Impacts:** This category includes studies directly attributing impacts, such as mortality rates or economic losses, to climate change. Continuing

with the heatwave example, attribution by impacts would directly evaluate the impact of climate change on the heat-related deaths.

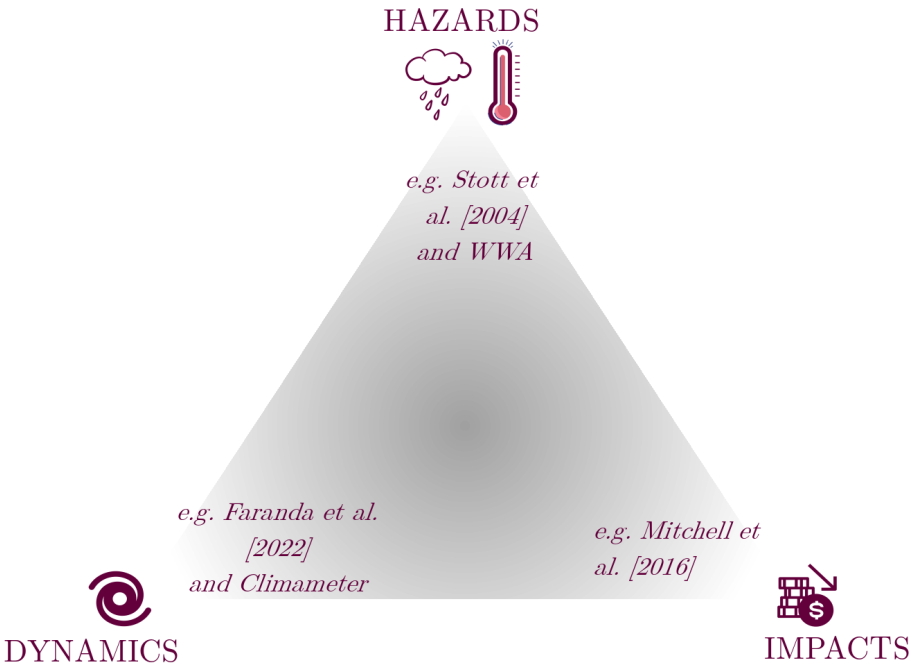

Figure 1.2: Stott et al. (2004) defines an extreme event as a threshold in temperature. World Weather Attribution is an academic collaboration of rapid attribution studies using the unconditional approach, by defining events as exceedances of a threshold of, for example, temperature, precipitation, or wind speed. Faranda et al. (2022) defines an extreme event based on its atmospheric circulation pattern. Climameter is an academic collaboration of rapid attribution studies using the conditional approach, by defining events based on their synoptic pressure pattern. Climameter and WWA are further discussed in section 1.1.4. Mitchell et al. (2016) defines the event as the heat related mortality.

1.1.3 Datasets

Observations or Reanalyses EEA studies incorporate observations and/or reanalyses–which are climate models that assimilate historical observational data–to quantitatively define the events. This step is crucial, as every EEA study requires sufficient meteorological data to link it with observed impacts (Otto, 2023). For example, Tradowsky et al. (2023) defined a flooding event based on the precursor rainfall due to the lack of hydrological data. Many studies use observational data to complement their attribution studies evaluating ongoing trends (King et al., 2015; Terray, 2023).

In some cases, studies base their results solely on observations or reanalysis datasets. This proves particularly useful in cases where climate models struggle to reproduce the event, and to avoid model uncertainty or hypothesize less about the data. Additionally,

the near real-time availability of these datasets enables rapid attribution studies. However, the challenge lies in the potential influence of the dataset's length, as long-term observations are essential for discerning trends associated with anthropogenic climate change, as well as on the data quality. Yet, the presence of internal variability in such datasets can mask these trends. Some examples that base their results in observations are Cattiaux et al. (2010) and Van Oldenborgh et al. (2012). These observational studies assess the overall effect of climate change trends, and to attribute these trends specifically to anthropogenic radiative forcing requires either the use of climate models or a thorough evaluation of the role of internal variability on the observed trends.

Weather Models Medium-range and seasonal weather forecasts have also been incorporated due to their capability to simulate specific extreme events (Hoerling et al., 2013; Leach et al., 2021). Such forecast-based methodology requires the event to have been well forecasted and represented as it happened. If this condition is accomplished, this methodology has the advantage of not needing verification against observations, as well as a higher-resolution and better representation of atmospheric and oceanic processes.

Climate Models The use of general circulation models (GCM) is important in attribution studies because they enable the creation of two scenarios, factual and counterfactual, with two different configurations to evaluate the role of specific factors. Generally, a large ensemble is used to simulate both worlds, either by employing a single model and slightly changing the initial conditions or physics, or using several models to account for model uncertainty (e.g., from the Coupled Model Intercomparison Project, CMIP), or a combination of these (e.g. Lewis et al., 2019; Lewis and Karoly, 2013).

A prerequisite for a model to fit for purpose is its ability to simulate the extreme event studied. Therefore, the choice of model configuration firstly depends on the type of extreme event under consideration. For example, some studies use regional high resolution models capable of simulating events like tropical cyclones (Lackmann, 2015), while others can rely on relatively lower resolution models for events that are better represented such as heatwaves that are highly affected by thermodynamics (Philip et al., 2022). General circulation models are also employed to assess the role of specific factors by constraining the simulations to them such as sea surface temperatures, atmospheric CO2, or aerosols. For example, comparing two atmosphere-only simulations with different prescribed SSTs and sea ice (Christidis et al., 2013; Massey et al., 2015).

1.1.4 Applications of EEA

Despite the rapid growth of the EEA field, the majority of results have primarily aimed at advancing knowledge and raising awareness. Limited attention has been given to potential applications, such as supporting litigation or informing loss and damage negotiations. In the following section, I provide a few notions of some applications of the EEA.

Liability The question Allen posed in the paper that gave birth to the EEA field was as follows: "Will it ever be possible to sue anyone for damaging the climate?" This question was the initial motivation of EEA — specifically, providing robust scientific evidence to inform potential legal actions. Some studies have already been employed in legal cases (Burger et al. (2020) and Marjanac and Patton (2018), for reviews on climate litigation and EEA).

Legal Case Example: 'Juliana v. United States' (Burger et al., 2020; Lloyd and Shepherd, 2021). In 2015, 21 plaintiffs sued the United States. They claimed the government, despite knowing about climate change for 50 years, failed to take sufficient steps to cut fossil fuel emissions. The plaintiffs argued the government violated their rights to a safe climate, causing harm to their life, well-being, and property, among others. They sought a stronger plan for fossil fuel reduction, not monetary compensation for the damages. The climate scientist Dr. Trenberth backed the plaintiffs with several EEA studies, using the storyline approach (Juliana v. United States, 2016; Lloyd and Shepherd, 2021; Trenberth et al., 2015). Trenberth analyzed factors behind each event for each plaintiff, assessing the role of climate change. Defense counsel John Weyant argued the claims were not precise, and the method ignored confounding factors, like poor forest management leading to severe fires (Juliana v. United States, 2018; Lloyd and Shepherd, 2021). However, Lloyd and Shepherd (2021) argued that making statements about individual events based on general knowledge (the storyline approach) is legitimate and valid when supported by evidence and an understanding of the factors involved. The 'Juliana v. United States' case is still ongoing (APNews, 2023; Kluger, 2024).

Loss and damage In the 'loss and damage' (L&D) framework, the idea is that parties more responsible for climate change compensate those less responsible for its impacts, but its definition remains unclear. At COP27 in Egypt in 2022, a significant outcome was the announcement of a planned L&D fund to assist low-emitting nations facing climate change impacts, including extreme events.

Some suggest that EEA science could inform responsibilities for climate change (Burger et al., 2020; Otto et al., 2017). However, its feasibility is still under discussion. Jézéquel et al. (2019) explored the diversity of views regarding the use of EEA for L&D through a series of interviews to both EEA scientists and L&D delegates. They highlighted several hurdles that complicate the use of EEA for L&D, including technical challenges, such as a lack of confidence in EEA results and difficulties in attributing events in the most vulnerable countries, and political challenges, like the allocation of responsibilities among emitters.

A recent debate has emerged on using EEA in L&D (King et al., 2023a; Noy et al., 2023). King et al. (2023a) argues that EEA field is not ready yet to support the L&D decision-making. They argue that there are few impact attribution studies, which in turn pose several challenges (Perkins-Kirkpatrick et al., 2022). Additionally, King et al. (2023a) point out limitations in attributing localized extreme events, such as hail or tornadoes, and a lack of analyses in the Global South, among other issues. On the other hand, a few months later, Noy et al. (2023) offered a contrasting perspective in

direct response. They argue that EEA can play a constructive role in L&D, even if it cannot capture local and small-scale events, suggesting that a regional assessment would be sufficient. The article emphasizes that the most damaging events, such as extreme temperatures or droughts, are well-modeled and captured by EEA. They further state that existing literature on EEA, even in regions with less research, provides valuable information on future events. They also stress the importance of considering literature from related fields like economics or sociology, which have long studied changes in exposure and vulnerability, especially in low-income regions. The conclusion drawn is that EEA, while not perfect, is currently the best tool to inform L&D allocation, and collaboration with vulnerable developing countries is essential.

Operationalization and Rapid Attribution There is an increasing interest in operationalizing EEA as it plays a crucial role in raising awareness, as well as possibly providing information for decision-making regarding adaptation or addressing loss and damage (Stott and Christidis, 2023). The rapid evolution of this field has led to the development of various projects by different groups aimed at providing rapid attribution assessments or helping to build them:

- World Weather Attribution (WWA): Established in 2015, WWA employs peer-reviewed methods (Philip et al., 2020) to offer a rapid and unconditional attribution of recent extreme events. WWA evaluates changes in the intensity and likelihood of extreme events globally, including cold spells, heatwaves, droughts, storms, wildfires, and extreme rainfall. The events are defined in terms of meteorological hazards, such as accumulated rainfall or temperature. They determine if there is any detectable trend in intensity or probability using observational data, as well as the return period of the event. Using climate models, they further assess the change in the likelihood and magnitude in two 'worlds': the current world with 1.2 K of global warming and a hypothetical world without anthropogenic climate change. The methods are also being explored for potential application in National Weather Services (Otto et al., 2022).

- Climameter: Founded in 2023, Climameter is a rapid and conditional attribution framework primarily conceived by my supervisor, Davide Faranda, and further supported by our team ESTIMR and international collaborators. Using peer-reviewed methods (Faranda et al., 2022), Climameter uses reanalysis data to assess changes in meteorological hazards conditional on the synoptic pattern of the latest extreme weather events worlwide. Consequently, the event is defined based on its dynamics, specifically its atmospheric synoptic pressure pattern.

- *C20C + D&A project* This is a subproject of the World Climate Research Programme's (WCRP) Climate Variability Programme's (CLIVAR) Climate of the 20th Century Plus Project (C20C+). It aims at providing public large samples of climate model data at relatively high resolution for rapid detection and attribution purposes.

- *Met Office Hadley Centre* In this center, part of the United Kingdom's national weather service, they adapted a methodology for the attribution of extremes in

near-real time and include the analysis in their assessements (Christidis, 2021). They use an unconditional attribution approach, following the traditional risk-based approach, and use coupled model data from large multi-model ensembles of the CMIP6 project.

The rapid attributions by WWA and Climameter have gained substantial media attention worldwide. While the primary goal of increasing awareness has shown promising results, further investigation is required to determine the potential to fulfill additional objectives.

1.1.5 Types of Extreme Events

The approaches described earlier can generally be applied to any type of extreme event. The figure illustrates the number of attribution studies conducted between 2011 and 2022 in online searches through journals, including BAMS (statistics taken from Carbon Brief (2022)), of the most extensively studied extremes. While the field of EEA is expanding rapidly, with numerous additional studies in just two years, this overview offers an approximation of the current state of the art.

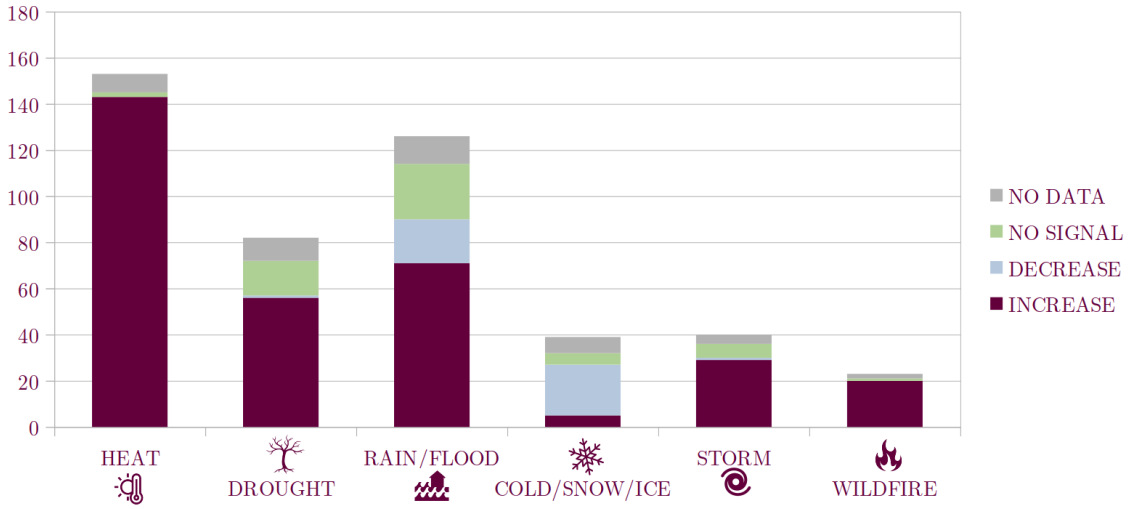

Figure 1.3: Source: statistics taken from Carbon Brief (2022).

In this thesis, our focus is on attributing extratropical cyclones (ETCs)—synoptic-scale low-pressure systems in the mid-latitudes. The location and temporal variability of ETCs determines the midlatitude climate. ETCs contribute substantially to total precipitation, accounting for approximately 70% in extensive areas of Europe and North America and up to 90% locally (Hawcroft et al., 2012). Moreover, the largest wind speeds on record are associated with ETCs (Ulbrich et al., 2001). The upcoming section provides insights into the nature of ETCs, with a special focus on the North Atlantic and Mediterranean.

1.2 Extratropical Cyclones

Extratropical cyclones, also referred to as mid-latitude storms, have the potential to intensify and cause significant damages when making landfall. They pose the greatest meteorological hazard in Europe, associated with both economic and non-economic damages (Cusack, 2023). For instance, in the U.S., one of the most damaging ETCs in recent years was Uri, causing economic losses of around $30 billion and insured losses of approximately $15 billion (MunichRe, 2023). One of the most recent impactful European ETCs, Eunice (or Zeynep), hit western central Europe resulting in an economic loss of nearly $6 billion and insured losses of almost $5 billion (MunichRe, 2023). Future projections indicate an increased risk of windstorms in Europe (Pinto et al., 2012; Priestley et al., 2023).

Conceptual models In contrast to the relatively recent field of EEA, the study of ETCs has a rich history spanning over a century (Hinman, 1888; Schultz et al., 2019). In the 1920s, the renowned Bergen school of meteorology, founded by Vilhelm Bjerknes, focused on understanding ETCs using weather station data. Their key contribution was the Norwegian cyclone model, a simple conceptual model of understanding ETC structure and development (Bjerknes, 1919; Bjerknes and Solberg, 1922). In such a model, a low pressure system is formed from a perturbation in the polar front, with cold and warm fronts emerging from the center. As the system evolves, the cold front "catches up" the warm front (or more correctly the fronts "wrap up", a clarification by Schultz and Vaughan (2011)), causing the warm sector to narrow, and subsequently forming the occluded front.

Advancements in technology, such as weather satellites and numerical weather prediction models, have significantly enhanced our comprehension of these phenomena. Several modelling studies that were able to simulate more realistic cyclones did not reproduce the Norwegian-type of cyclone. Furthermore, these models frequently struggled to forecast the development of explosive ETCs, commonly defined as those deepening by at least 24 hPa in 24 hours and latitudinally adjusted (Sanders and Gyakum, 1980). An example was the Presidents' Day Snowstorm 1979 (Bosart, 1981), an explosive ETC causing heavy snowfall in the northeastern USA. The difficulty in forecasting such impactful ETCs triggered extensive research in the field.

Shapiro and Keyser (1990) observed that, for many cyclones, specially the most intense, the structure did not correspond to the Norwegian model, and proposed another conceptual model (depicted in figure 1.4, from Martínez-Alvarado et al. (2014)). In the development stage, they observed a cold fracture, that is, a separation of the cold front aligning near perpendicular to the warm front–a shape that has been called T-bone structure. In later stages, the warm front wraps up in the center of the cyclone forming a warm-core seclusion. This study demonstrates that a universal model capable of perfectly describing the lifecycles of all ETCs does not exist, given the broad spectrum of characteristics and evolution inherent in these cyclones. Each ETC is unique due to the complex interplay between baroclinic and diabatic processes that contribute to their formation, development, and dissipation.

Advancements in numerical modeling have yielded new conceptual models and identified mesoscale features that play a role in ETC development (Dacre, 2020). THe main airflows include:

- Warm Conveyor Belt (WCB): Warm, moist airstream that flows northeastward into the cyclone, originating in the warm sector of the cyclone (or ahead of the cold front). It plays a crucial role in transporting warm and moist air into the cyclone's core.

- Cold Conveyor Belt (CCB): A cold airstream that flows southward and eastward, wrapping around the western side of the cyclone. It originates from the northwest quadrant of the cyclone and brings cold air equatorward.

- Dry Intrusion (DI): A drier airstream that descends from the upper troposphere into the cyclone's circulation. Dry intrusions often occur on the western side of the cyclone and can disrupt cloud patterns and affect the structure of the ETC.

- Sting Jets (SJ): Mesoscale wind maxima at the south of the low center associated with descent air from the mid-troposphere formed along the bent-back front (BBF). They are typically found in cyclones over the ocean that exhibit the evolution of Shapiro–Keyser cyclone. This phenomenon is rarer than the previous ones.

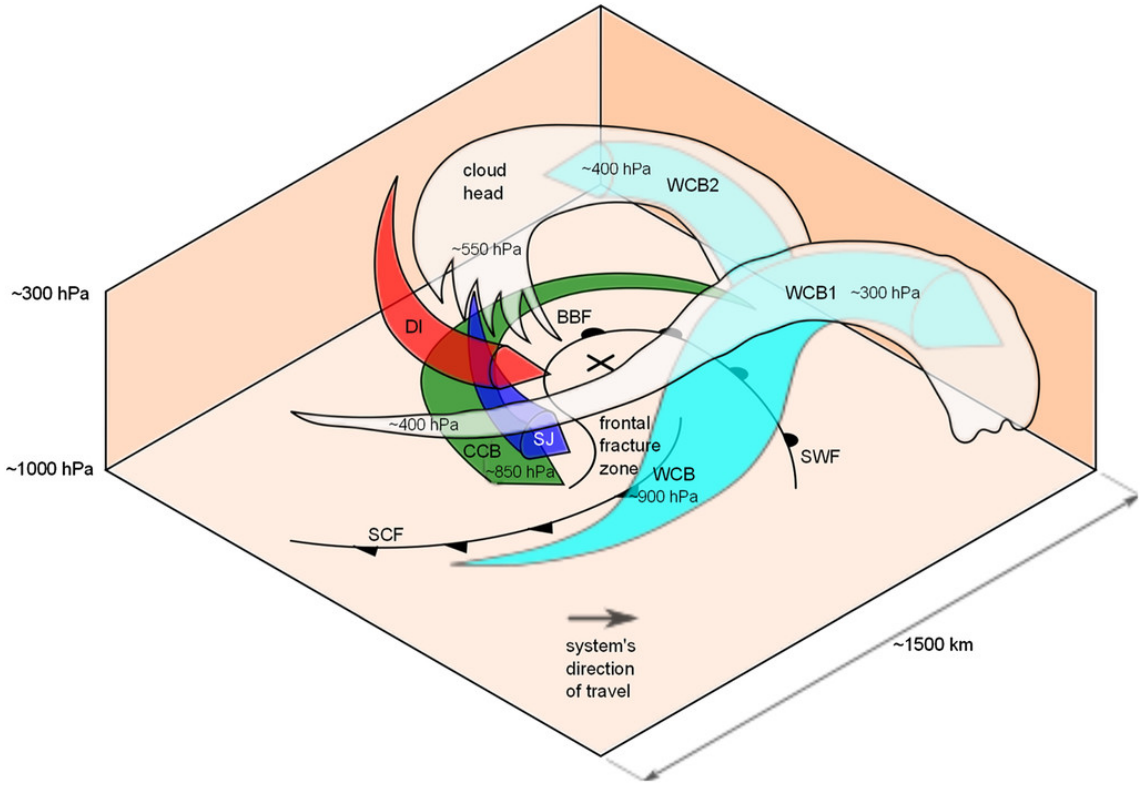

Figure 1.4: Figure from Martínez-Alvarado et al. (2014). Structure of a Shapiro-Keyser type cyclone in the Northern Hemisphere (NH).

1.2.1 Climatology and variability of storm tracks

Storm tracks, the preferred regions where ETCs travel, have been under study since the mid-nineteenth century (Hinman, 1888). Petterssen (1956) identified, based on weather charts, three regions with the maximum number of ETCs in the Northern Hemisphere: from east China extending across the Pacific, from the eastern Rockies extending across the Atlantic, and over the Mediterranean. Notably, cyclogenesis predominantly occurs on the westward side of these basins, and this spatial distribution remains consistent today. The methods employed to study storm tracks can be broadly categorized into two approaches:

Eulerian approach The Eulerian approach focuses on the spatial distribution and frequency of ETCs in a particular region, analyzing them at fixed points in space. This method is especially useful for understanding the climatology and long-term patterns of storm tracks. One technique involves applying time filtering to gridded analysis maps, for example identifying disturbances with 2-6 day (synoptic) periods. This approach can be applied to various variables at different levels, such as sea level pressure, 300 hPa height, 500hPa wind statistics, 850 hPa temperature, or eddy poleward heat flux (Blackmon et al., 1977; Hoskins and Hodges, 2002).

Lagrangian approach The Lagrangian approach consists of following the paths of individual ETCs or weather systems. It is useful for studying specific individual ETCs. The variables used to identify and track such systems include, for example, minima in mean sea level pressure or maxima in low-level relative vorticity (Hoskins and Hodges, 2002). The ETCs counts and tracks may vary substantially depending on the tracking algorithm used, specially for weak ETCs (Neu et al., 2013).

The seasonal climatology has been extensively studied using both Eulerian and Lagrangian approaches. Figure 1.5, from Shaw et al. (2016), shows the winter storm tracks in the Northern Hemisphere (NH) (December–February, DJF) and Southern Hemisphere (SH) (June-August, JJA).

In this thesis, we focus on the ETCs in the North Atlantic and Mediterranean. In the North Atlantic, the position of the storm track is strongly linked to the North Atlantic Oscillation (NAO), which is the principal mode of atmospheric variability in the basin. In NAO positive phases, the storm track and jet are shifted northeastward, and extreme and explosive ETCs occur more frequently (Gómara et al., 2014; Pinto et al., 2009). In NAO negative phases, the storm track shifts southward, and ETCs tracks are more zonally oriented. The North Atlantic storm track density has a maximum in winter, when the meridional temperature gradient is strongest (Hoskins and Hodges, 2019a). In winters of strong jet, a midwinter minimum in the Atlantic storm activity has been recently identified (Afargan and Kaspi, 2017). The ETC intensity is minimum in summer, when the meridional temperature gradient is weakest, and the tracks are generally displaced polewards until autumn. Notably, in the eastern North Atlantic and parts of western Europe, this poleward shift is less pronounced, and there is almost no

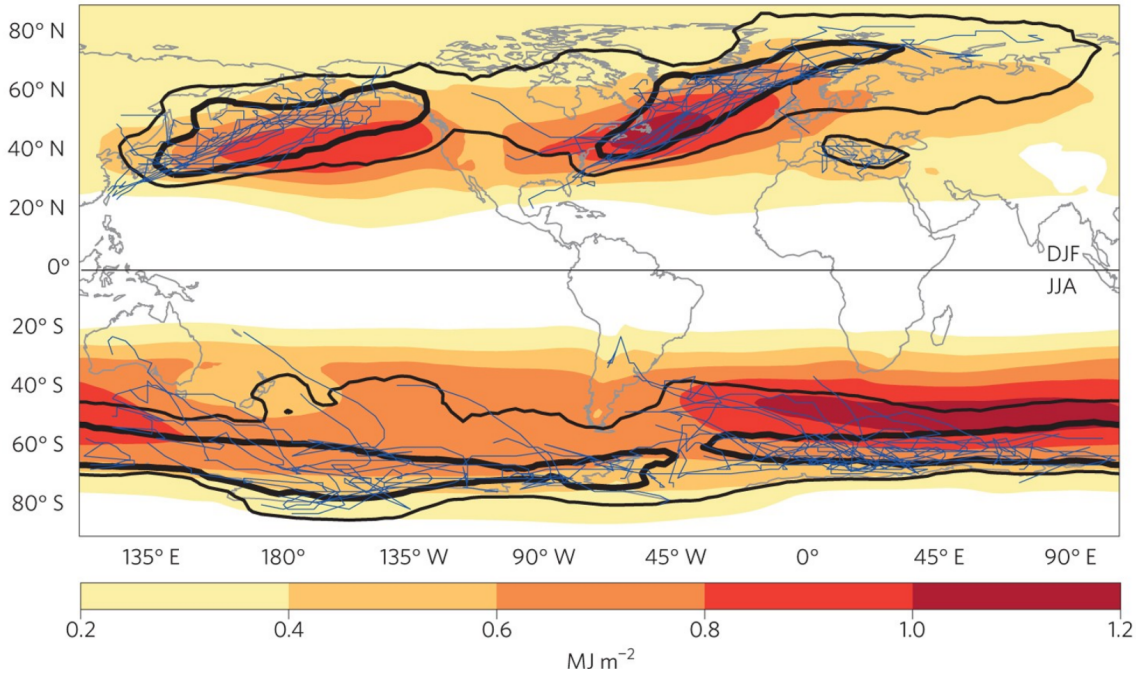

Figure 1.5: Winter storm tracks in the Northern Hemisphere (NH) (December–February, DJF) and Southern Hemisphere (SH) (June-August, JJA) using ERA-Interim reanalysis. Black contours show ETC track density. Blue lines show individual ETCs tracks for the top 0.5% most intense cyclones. Shading corresponds to the eddy kinetic energy. Figure from Shaw et al. (2016).

shift from September to March (Hoskins and Hodges, 2019b).

In the Mediterranean, ETCs are generally shorter-lived, slower, and smaller in size compared to the Atlantic ETCs (Flaounas et al., 2022). Mediterranean ETCs are more frequent in winter, while in summer ETCs occurrences are frequent over North Africa. Intense ETCs predominantly occur in winter in the northwestern part of the basin, covering the Tyrrhenian and Adriatic seas (figure 1.6), with frequent cyclogenesis leeward of the Alps. Explosive Mediterranean ETCs mainly occur over the Ligurian sea (Kouroutzoglou et al., 2011).

1.2.2 Processes and dynamics of cyclogenesis

a) Baroclinic Instability

The fundamental mechanism in the formation of ETCs is baroclinic instability (Charney, 1947; Eady, 1949). Baroclinic instability is closely related to an horizontal temperature gradient in the atmosphere. In the approximation of the wind being geostrophic and in hydrostatic equilibrium, this gradient is proportional to the vertical wind shear, a relationship known as the thermal wind balance. The magnitude of low-level baroclinicity is often assessed through the maximum Eady Growth Rate, which is directly

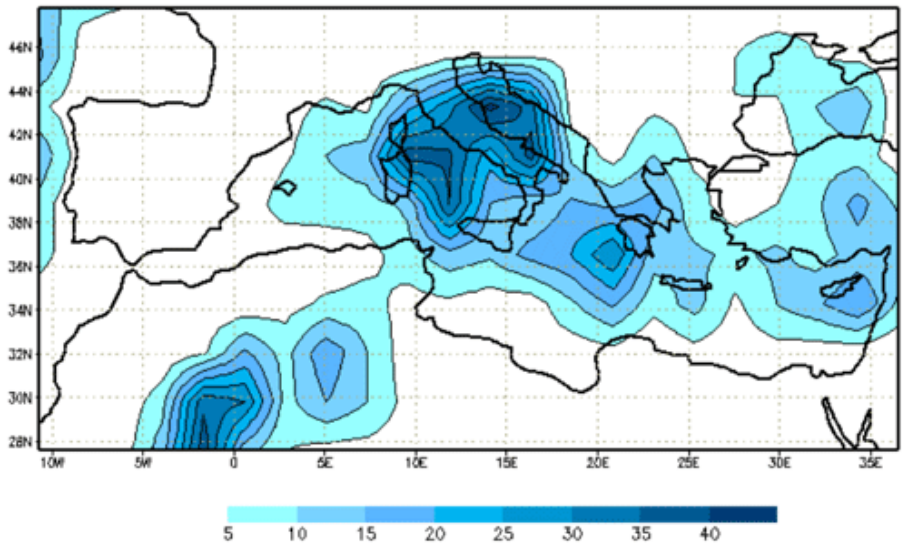

Figure 1.6: Number of intense cyclones over the 45 years of the ERA-40 period at mature stage. Figure from Homar et al. (2006), modified by Flaounas et al. (2022).

proportional to the meridional temperature gradient and inversely proportional to static stability, and serves as an indicator of the possibility of development of ETCs. High baroclinicity is observed on the eastern coast of the US, driven by a strong meridional temperature gradient resulting mainly from land-sea temperature contrast and the Gulf Stream, along with the influence of orography (Brayshaw et al., 2009, 2011). The interaction with Rossby waves, characterized by large-scale meanders or undulations on the upper-level flow, amplifies or triggers the growth of unstable waves in these regions, which manifest as a series of ETCs separated by regions of high pressure. These cyclones grow by converting available potential energy into kinetic energy.

A useful way to describe baroclinic instability is through the potential vorticity (PV) framework (Hoskins et al., 1985). PV, proportional to the product of absolute vorticity and stability, is conserved under adiabatic conditions. Changes in PV are determined by advection, with further changes attributed to non-conservative processes or diabatic effects. Understanding the ETC development from the PV perspective involves a combination of different PV anomalies: an upper-level trough (or positive PV anomaly) moving over a region of baroclinicity or a meridional temperature gradient, along with diabatically produced low-level PV anomalies that can intensify the ETC (Davis and Emanuel, 1991). Diabatic heating and low-level PV production mainly occur from latent heat release of cloud formation in the WCB (Wernli and Davies, 1997).

Diabatic PV production can intensify ETCs, playing a significant role in the rapid intensification of ETCs (Binder et al., 2016; Schemm, 2023). Case studies on explosive ETCs highlight the crucial role of latent heating in explosively intensifying ETCs (Fink et al., 2012; Ludwig et al., 2014). However, the relative contribution of diabatic effects on the cyclone intensification can vary significantly from case to case.

b) Influential factors of cyclogenesis

The synoptic conditions that lead to the development of ETCs might be diverse. There have been attempts to classify them according to, for example, their upper level versus lower level forcings (Catto (2016) for a review on ETCs classification). Petterssen and Smebye (1971) categorized two types of ETC; the first being predominantly low-level forced and with a constant tilt between the surface low and upper trough, while the second is strongly upper-level forced with a decreasing westward tilt along development. Dacre and Gray (2009) noted a prevalence of this second type in the western Atlantic. Deveson et al. (2002) introduced a third type as those characterized by strong upper-level forcing, weak low-level baroclinicity, and a significant role of diabatic heating in their intensification. Dacre and Gray (2009) found that they are more prevalent in the eastern North Atlantic than in the western region. This type exhibits shorter lifetimes, faster intensification, and develops in regions with weaker low-level baroclinicity and lower stability. Priestley et al. (2020a) noted that in the central and eastern Atlantic, ETCs often form on the trailing fronts of preexisting ETCs, a type known as *secondary* ETCs. Many secondary ETCs develop explosively, posing significant hazards in Europe.

Flaounas et al. (2021) analyzed Mediterranean ETCs from a PV perspective and showed that stronger baroclinic forcing is associated with a decreased influence of diabatic processes on cyclone development, and vice versa; their relative contribution might vary from case to case. In addition, the complex topography in the Mediterranean, specially high mountain ranges such as the Alps, plays a key role in cyclogenesis (Buzzi et al., 2020; Speranza et al., 1985). Deep lee ETCs often occur when upper-level PV anomalies approach the Alps from the northwest, and the block of the mountains leads to a drop in pressure on the south side of the mountains. This creates a reinforcement between the upper and lower level PV anomalies. Additional mechanisms may arise from the extratropical transition of hurricanes in the tropical Atlantic, such as directly moving to the Mediterranean basin, inducing strong humidity advection, or perturbing the mid-latitude flow downstream. When hurricanes interact with the mid-latitude flow, they can perturb cyclogenesis in remote regions from the hurricane, potentially leading to intense precipitation events in the Mediterranean (Grams et al., 2011; Pantillon et al., 2013; Pantillon et al., 2015).

1.2.3 ETCs representation

a) Reanalyses

Typically, the performance of models used in simulating ETCs is compared with reanalysis products. Hodges et al. (2011) compared four reanalyses and observed an overall improvement in agreement with the higher-resolution versions, consistent with advancements in models, data assimilation, and increased observational input. In general, higher-resolution reanalyses identify more ETCs, although there is more agreement among reanalyses of different resolutions regarding deep cyclones (Tilinina et al., 2013; Wang et al., 2016).

In this thesis we use the recent presatellite backward extension of ERA5 reanalysis to 1950 Hersbach et al. (2020). ERA5 reanalysis is the fifth version of the ECMWF reanalysis, within the Copernicus Climate Change Service (C3S). It is based on the Integrated Forecasting System (IFS) Cy41r2, and has a resolution of 31 km and hourly output data. Bell et al. (2021) showed satisfactory performance of the backward extension, particularly in terms of inter-monthly variability in precipitation and temperature trends. They further found high confidence in the representation of synoptic details of the 1953 North Sea storm, along with an improvement over lower temporal and spatial resolution reanalysis. Recent findings by Karwat et al. (2022) highlight agreement with the standard ERA5 reanalysis spanning from 1979, and found to perform well in depicting Northern Hemisphere storm-related characteristics, including frequency, size, and intensity.

b) General Circulation Models

The General Circulation Models (GCMs) contributing to the CMIP project have been shown to capture the general characteristics such as frequency and intensity of the ETCs. However, the models generally depict a too zonal storm track and too zonal jet stream in the North Atlantic winter, and an underestimation of the ETCs density in summer (Priestley et al., 2020b). Priestley et al. (2020b) further found that CMIP6 models tend to underestimate the frequency and intensity of explosive cyclones, especially in lower-resolution models. Such biases show a progressive reduction in later versions, with CMIP6 performing better than CMIP5 and CMIP3 (Harvey et al., 2020). These later versions have made improvements mainly in model physics and increased resolution.

In chapter 4 we mainly use a large ensemble from the GCM Community Earth System Model (CESM–LE) (Kay et al., 2015). Dolores-Tesillos et al. (2022) assessed the model's performance in reproducing ETCs comparing with ERA-Interim. They found that the model tends to underestimate the number of ETCs over the North Atlantic ocean and particularly over the western Mediterranean, and to overestimate it between Iceland and Norway. In contrast to many CMIP models, the model does not exhibit a too zonal storm track. Raible et al. (2018) noted that the CESM slightly overestimates ETC depth and underestimates ETC-associated precipitation and radius. However, despite these biases, both studies demonstrate that the model effectively reproduces ETCs, with biases becoming more apparent when analyzing weak cyclones.

Joos et al. (2023) evaluated the CESM performance in capturing the WCBs, which, as discussed, are the ascending airstreams responsible for most of the precipitation of the ETCs. They found that, overall, the model effectively represents WCBs characteristics, including frequency and pressure evolution. Differences identified were suggested to be at least partially attributed to internal variability. In addition, Binder et al. (2023) found that in the winter Northern Hemisphere, the model captures well the deepening rates of the ETCs, although it underestimates those of the most explosive ones. For the ETCs with the strongest deepening and most intense WCBs, the diabatically produced low-level PV anomaly is underestimated.

c) Regional Climate Models

In this thesis we also use Regional Circulation Models (RCMs). RCMs are capable of enhancing regional details, including topography, and depict smaller-scale processes more effectively than GCMs. Reale et al. (2022) and Flaounas et al. (2022) have shown the accurate representation of the climatology of Mediterranean cyclones by RCMs. However, it is essential to acknowledge certain limitations of RCMs, such as the influence of boundary conditions provided by driving GCMs. In chapter 3, we use the existing EURO-CORDEX simulations—a coordinated downscaling experiment, part of the CORDEX initiative by the World Climate Research Programme (WCRP), to produce improved regional climate change projections.

1.2.4 Observed changes and future projections

Several studies have examined the impacts of climate change on ETCs. The pattern of such changes in the North Atlantic is complex, shaped by a tug of war between different opposing processes (Shaw et al., 2016). These include a decrease in the lower-troposphere baroclinicity due to the Arctic Amplification and an increase in the upper-level baroclinicity due to the upper tropospheric warming (Shaw et al., 2016; Stendel et al., 2021). Further factors involve changes in atmospheric latent heat release (Binder et al., 2023; Willison et al., 2013), vertical stratification (Pfahl et al., 2015), or land-sea temperature contrast (Portal et al., 2022). The effects of these complex changes on ETCs can manifest diversely, ranging from shifts in their frequency of occurrence to changes in their intensity.

Observed Changes Tilinina et al. (2013) identified substantial decadal variability in the number of very deep cyclones (<960 hPa) in the North Atlantic, with an increase from 1979 to 1990 followed by a subsequent decline. They further found an increase in the number of winter ETCs, and a decrease in summer. As stated in Chapter 11 of the last IPCC Sixth Assessment Report Working Group 1, there is "*low confidence* in past-century trends in the number and intensity of the strongest ETCs". More recently, Karwat et al. (2022) found a non-significant positive trend in the number of North Atlantic ETCs and a significant northward shift, using the ERA5 reanalysis from 1950. They also observed an increase in intensity and persistence, and higher wind speeds in the most intense ETCs since 1979.

Future Projections In a warmer climate, an increase in precipitation associated with ETCs is one of the most robust projections under climate change, linked to an increase in low-level moisture content (Seneviratne et al., 2021). However, changes in ETC dynamics can counteract the thermodynamic effect on overall precipitation regionally; for example, a projected decline in Mediterranean ETC activity leads to a localized decrease in total precipitation (Zappa et al., 2015). Changes in dynamics, including ETC-associated wind speed or the storm track position, are more uncertain. Zappa et al. (2013) used CMIP5 models, and identified a tripolar pattern in the frequency

of winter ETCs in the North Atlantic: an increase in central Europe and a decrease in the Norwegian and Mediterranean Seas. Seiler and Zwiers (2016) found a localized increase in the number of explosive ETCs in the British Isles and North Sea, as well as a general decrease in the North Atlantic, albeit with a slight intensification. Catto et al. (2019), Feser et al. (2015), Seneviratne et al. (2021), and Ulbrich et al. (2009) provide complete reviews on the future trends. Figure 1.7 summarizes the processes involved in the future changes to ETCs features, taken from the review by Catto et al. (2019). Below, I update these reviews with more recent studies.

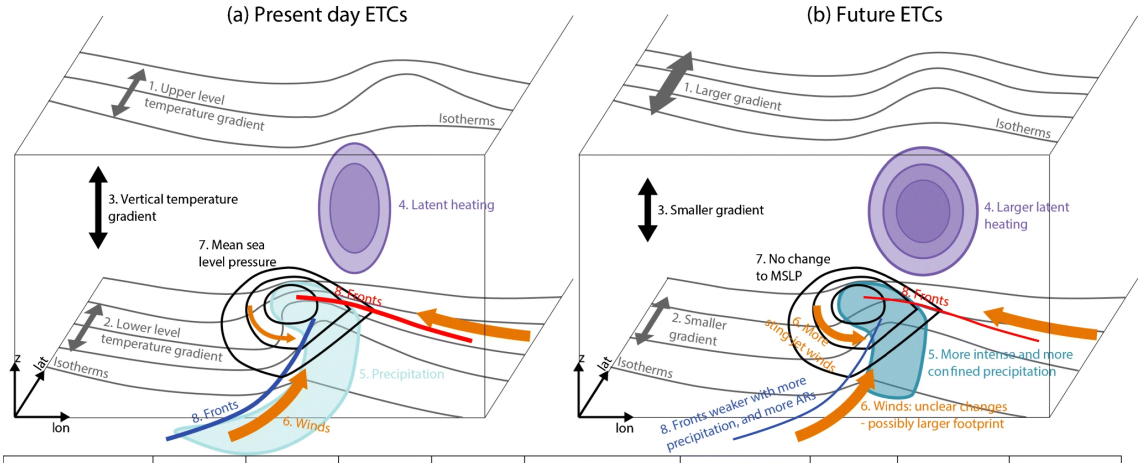

Feature	1	2	3	4	5 (intensity)	5 (extent)	6	7	8
Confidence	High	High	High	High	High	Low	Low	Medium	Low

Figure 1.7: Schematic diagram summarizing future changes to ETCs in the NH. Figure from Catto et al. (2019).

Priestley and Catto (2022) used historical simulations and various future scenarios of several models of the CMIP6. They identified a winter extension of the storm activity into Europe, and decrease in the Mediterranean, aligning with the findings by Zappa et al. (2013) using an older generation of CMIP. Additionally, they identified an increase in Northern Hemisphere ETC intensity, particularly in the most extreme cyclones (higher vorticity and lower mean sea level pressure), and an increase in the ETC-associated wind speed on the southern flank. Little et al. (2023) found a similar pattern. Dolores-Tesillos et al. (2022) used the large ensemble CESM-LE with the worst-case scenario from the CMIP5 project. They identified an increase frequency of ETCs north of the UK, especially for the most intense ETCs, and a decrease in the Mediterranean. They also found a reduced ETC intensity in the Mediterranean but an increase in western Scandinavia and central Europe, measured by 850hPa relative vorticity.

Focusing on the Mediterranean region, Reale et al. (2022) used multiple regional climate models from the Med-CORDEX initiative (Ruti et al., 2016). They found a winter decrease in ETC activity, consistent with Zappa et al. (2015), along with a decrease in ETC intensity (measured using mean sea level pressure) and increased ETC-associated wind speed in the Central Mediterranean.

1.3 Research Questions

Numerous EEA studies have investigated extreme wet or windy events using the probabilistic unconditional approach (Eden et al., 2018; Philip et al., 2018; Tradowsky et al., 2023). Vautard et al. (2019) analyzed the influence of climate change on two explosive ETCs that occurred in January 2018, Friederike and Eleanor. They defined the events as an exceedance of a threshold of winter maximum daily wind speed over a limited region.

In the context of storyline attribution studies of storms, much of the focus has been on tropical cyclones (e.g. Patricola and Wehner, 2018). The prevalent approach involves using high-resolution weather forecast simulations, incorporating the climate change effect into the initial and/or boundary conditions. However, there has been relatively less exploration in attributing ETCs through a conditional approach. Hawkins et al. (2023) employed a reanalysis-based approach, by re-runs with perturbed sea surface temperatures. Ermis et al. (2023) (conference abstract) applied a forecast-based approach similar to that in Leach et al. (2021) to analyze storm Eunice, which notably impacted the United Kingdom in February 2022, and which will later appear again in this thesis.

The last IPCC report stated that "Specific studies attributing changes in the most extreme ETCs are not available. The human influence on individual extreme ETC events has been considered only a few times and there is overall low confidence in the attribution of these changes" (Seneviratne et al. (2021), section 11.7.2.3).

The primary objective of this thesis is to address this gap by adapting the conditional analogues approach to the analysis of severe ETCs, and illustrating the methods on high impact case studies. Hence, we aim at answering the following questions:

- **Q1: How can we define an analogue of an ETC that leads to a wet and windy extreme event?**

  We explore different definitions of an analogue based on the dynamics (Chapters 2 and 4) and a combination of both, dynamics and hazards (Chapter 3).

- **Q2: Can we identify ongoing changes in the meteorological hazards, such as precipitation and wind speed, in a severe ETC?**

  We address this question in Chapter 2. This chapter presents a methodology to identify analogues based on the dynamics that lead to the wet and windy extreme event. In particular, we identify analogues of the sea level pressure pattern of an ETC that affected France and Italy in October 2020, named storm Alex. We compare the meteorological hazards of the analogues, namely precipitation and wind speed, between factual and counterfactual periods.

- **Q3: How can we apply the analogues approach in ETCs that occur in regions of complex topography and are associated with heavy rainfall or strong winds regionally?**

In Chapter 3, we introduce a multivariate approach for identifying analogues based on the sea level pressure pattern, as well as meteorological hazards. This methodology is particularly suitable for small-scale, shallow ETCs with the potential to induce substantial local impacts, influenced by factors such as topography or the advection of warm, humid air. To illustrate this approach, we examine two extreme events in Italy driven by Mediterranean ETCs: flooding (Acqua Alta) events in Venice, characterized by exceptionally high water levels in the Venetian Lagoon, and flooding events in Emilia Romagna.

- **Q4: How will some North Atlantic explosive ETCs that had strong impacts in Europe change in a future climate in terms of frequency and magnitude?**

  Chapter 4 identifies analogues of the track of an ETC until its mature stage to consider its explosive deepening. We further assess changes in the frequency and magnitude of explosive ETCs, as well as the dynamics behind such changes. We illustrate this with three explosive ETCs that affected the western coast of Europe: Xynthia in February 2010, Alex in October 2020, and Eunice in February 2022.

Résumé en Français

Attribution des Événements Extrêmes

Le domaine de l'attribution des événements extrêmes (EEA) a émergé au début des années 2000. Son objectif est d'évaluer comment le changement climatique en cours a influencé les événements extrêmes observés, tels que les cyclones extratropicaux intenses. Depuis lors, plus de 500 études d'attribution ont analysé le rôle du changement climatique sur les événements extrêmes.

Les approches de l'EEA peuvent être regroupées en deux grandes catégories: l'approche inconditionnelle et l'approche conditionnelle. L'approche inconditionnelle, qui repose sur une méthode probabiliste (appelée "risk based"), est la plus traditionnelle. Dans cette approche, l'événement est défini par un indice, tel que les précipitations sur une période donnée ou les températures extrêmes dans une région spécifique. La probabilité de cet événement est évaluée dans deux climats différents: l'un avec le réchauffement climatique et l'autre sans. Les circulations atmosphériques et océaniques ne sont pas restreintes à l'événement observable. D'un autre côté, les approches qui contraignent les dynamiques conduisant à l'événement, comme l'approche par analogues où la circulation atmosphérique synoptique est en quelque sorte fixée, relèvent de l'approche conditionnelle. Ces deux approches peuvent évaluer les changements dans la probabilité de l'événement, son intensité, ou une combinaison des deux. De plus, les événements extrêmes peuvent être définis par leur dynamique, comme la circulation atmosphérique qui mène à l'événement; par leurs aléas, incluant des facteurs comme les précipitations ou la vitesse du vent; ou par leurs impacts, tels que la mortalité due à la chaleur ou les pertes économiques d'une tempête. Les applications de l'EEA sont diverses, incluant la communication auprès des média et du public, l'adaptation au changement climatique, et l'évaluation de la responsabilité ou les pertes et préjudices.

Dans cette thèse, je vais appliquer les méthodes de l'EEA pour améliorer notre compréhension de l'impact du changement climatique sur certains cyclones extratropicaux observés dans l'Atlantique Nord et en Méditerranée, particulièrement ceux qui entraînent des extrêmes pluvieux et venteux.

Cyclones Extratropicaux

Les cyclones extratropicaux (CET), ou tempêtes de latitudes moyennes, sont des systèmes synoptiques de basse pression dans les latitudes moyennes. L'emplacement et la variabilité temporelle des CET déterminent le climat des latitudes moyennes. Les CET intenses représentent le plus grand danger météorologique en Europe, associés à des dommages économiques et non économiques.

Le mécanisme fondamental derrière la cyclogenèse, ou formation d'un CET,

est l'instabilité barocline. L'instabilité barocline est étroitement liée à un gradient de température horizontal dans l'atmosphère, et elle est maximale en hiver (Décembre à Février dans l'hémisphère nord). L'activité des CET est la plus intense dans le bassin nord-est de l'Atlantique, près de Terre-Neuve, en hiver, lorsque le gradient de température méridienne est le plus prononcé. La trajectoire des tempêtes, c'est-à-dire les régions préférées où les CET se déplacent, est inclinée du sud-est au nord-ouest. En Méditerranée, les CET sont généralement de plus courte durée, plus lents et plus petits par rapport aux CET de l'Atlantique. Les CET méditerranéens intenses se produisent principalement en hiver dans la partie nord-ouest du bassin.

Plusieurs études ont examiné les impacts du changement climatique sur les CET. La manière dont ces changements se produisent dans l'Atlantique Nord est complexe, influencée par un équilibre délicat entre différents processus contradictoires. Ceux-ci incluent une diminution de la baroclinicité de la troposphère inférieure due à l'amplification arctique et une augmentation de la baroclinicité de la troposphère supérieure due au réchauffement troposphérique supérieur. D'autres facteurs impliquent des changements dans la libération de chaleur latente atmosphérique, la stratification verticale ou le contraste de température entre la terre et la mer. Comme indiqué dans le chapitre 11 du dernier rapport d'évaluation du GIEC du groupe de travail 1, il y a une faible confiance dans les tendances du siècle passé concernant le nombre et l'intensité des CET les plus forts.

Dans un climat plus chaud, une augmentation des précipitations associées aux CET est l'une des projections les plus robustes sous le changement climatique, liée à une augmentation de la teneur en humidité des basses couches. Les changements dans la dynamique, y compris leur vitesse de vent associée ou la position de la trajectoire des tempêtes, sont plus incertains. Plusieurs études ont identifié un modèle tripolaire dans la fréquence et l'intensité des CET hivernaux dans l'Atlantique Nord: une augmentation en Europe centrale et une diminution dans les mers norvégienne et méditerranéenne.

Problématiques de Recherche

Alors que l'analyse des tendances générales du comportement des tempêtes offre une compréhension fondamentale des dangers potentiels du changement climatique, il est crucial de reconnaître que des tempêtes spécifiques peuvent présenter des caractéristiques uniques. Cela découle du fait que ces tempêtes sont influencées par une combinaison de facteurs qui peuvent ne pas être précisément capturés dans les tendances globales, en raison de la nature chaotique de l'atmosphère et des interactions non linéaires. De plus, différentes régions peuvent présenter des conditions environnementales uniques, telles que la topographie locale ou les courants océaniques, ce qui influe sur le comportement des tempêtes de manière variée selon les zones. Le dernier rapport du GIEC indique que "les études spécifiques attribuant des changements aux cyclones extratropicaux les plus extrêmes

ne sont pas disponibles. L'influence humaine sur les événements individuels de cyclones extratropicaux extrêmes n'a été considérée que quelques fois et il y a une confiance globalement faible dans l'attribution de ces changements". L'objectif principal de cette thèse est de combler cette lacune en adaptant l'approche des analogues conditionnels à l'analyse des cyclones extratropicaux sévères et en illustrant ces méthodes à travers des études de cas à fort impact. Ainsi, nous cherchons à répondre aux questions suivantes:

- Q1: Comment pouvons-nous définir un analogue d'un CET qui mène à un événement extrême pluvieux et venteux?
- Q2: Pouvons-nous identifier des changements en cours dans les dangers météorologiques, tels que les précipitations et la vitesse du vent, dans un CET sévère?
- Q3: Comment pouvons-nous appliquer l'approche des analogues aux CET qui se produisent dans des régions de topographie complexe et sont associés à de fortes précipitations ou des vents forts régionalement?
- Q4: Comment certains CET explosifs de l'Atlantique Nord, qui ont eu de forts impacts en Europe, changeront-ils dans un climat futur en termes de fréquence et de magnitude?

Chapter 2

An Introduction to a Conditional Extreme Event Attribution Approach

Objectives

In this chapter, I present a conditional approach for attributing extratropical cyclones to climate change, using the method of analogues of sea level pressure pattern. This approach is illustrated through an analysis of Storm Alex, which impacted France and Italy in early October 2020.

Contents

3.1 Introduction . . . 40
3.2 Methodology and example of application: Acqua Alta events . . . 40
3.3 Refined Multivariate Approach and application to the Emilia-Romagna floods of May 2023 . . . 43
3.3.1 Introduction and context of the study . . . 43
3.3.2 Datasets and Methods . . . 44
a) Methods . . . 45
b) Performance of EURO-CORDEX models . . . 49
3.3.3 Results . . . 49
a) Detected changes – ERA5 . . . 49
b) Projections with EURO-CORDEX models . . . 52
3.3.4 Discussion . . . 54
3.3.5 Supplementary material . . . 55
3.4 Summary and conclusions . . . 58

2.1 Introduction

When I joined the laboratory as a PhD student, my supervisors and other colleagues were actively engaged in various projects related to the detection and attribution of extreme events (e.g., XAIDA and EDIPI, two European Union's Horizon 2020 research and innovation programmes under grant agreements No 101003469 and No 956396, respectively). A key objective of our group was to formulate a methodology for attributing extreme events to climate change conditioned on the atmospheric circulation. My task was to adapt this methodology to extratropical cyclones leading to wet and windy extremes.

This exploration resulted in my first two publications. The first, a collaborative effort with colleagues and led by Davide Faranda, introduces a methodology within the analogues approach to attribute extreme events conditioned on the atmospheric circulation (Faranda et al., 2022). This study, included in Appendix D, illustrates the methodology on several extreme events that happened in 2021. I was responsible to analyze storm Filomena, which affected Spain in January 2021 with high amounts of snow. The second publication, led by myself, sets the basis of the methodology for extratropical cyclones (Ginesta et al., 2023).

To illustrate the methodology, we chose to examine storm Alex that impacted France and Italy in 2020. Our choice reflects the tendency among climate scientists to investigate extreme phenomena that directly affect their own regions, as highlighted by Jézéquel et al. (2018b). In addition, there was raising concern in French media on understanding this event and my supervisors were interviewed. Consequently, the choice of this storm emerged from its proximity and its significance in both scientific and media contexts.

2.2 Article published in Climate Dynamics

The article is included in the Appendix A. I provide below an extended summary.

Ginesta, M., Yiou, P., Messori, G., Faranda, D. A methodology for attributing severe extratropical cyclones to climate change based on reanalysis data: the case study of storm Alex 2020. Clim Dyn 61, 229–253 (2023). https://doi.org/10.1007/s00382-022-06565-x

Extended Summary

Storm Alex impacted southwestern Europe at the beginning of October 2020, resulting in over 20 fatalities and an estimated economic loss exceeding 2.5 billion euros. Regions in southern France and northern Italy recorded unprecedented levels of precipitation, such as 630 mm in just 24 hours in Sambughetto.

We use ERA5 reanalysis data (Hersbach et al., 2020) —which combines observational data with model outputs — as a proxy for the true state of the atmosphere to assess ongoing changes. We define two different climate periods: a past period from 1950 to 1984 (counterfactual), and a more recent period, from 1986 to 2021 (factual). The latter represents a climate largely influenced by anthropogenic emissions, whereas in the former, the human influence on climate is comparatively weaker. This assumption is supported by a substantial change in the effective-radiative forcing from the 1980s onwards, as shown in Figure 2.10 of Chapter 2 in the last IPCC Sixth Assessment Report (Gulev et al., 2021). However, due to the relatively short time periods used, our findings may also be influenced by internal variability of the climate system.

We identify 30 analogues of Alex when the cyclone reached its minimum sea-level pressure on October 2, 2020, at 06:00 UTC in each of the periods. To do this, we calculate the Euclidean distance between Alex's sea-level pressure map and all other timesteps and select the 30 with the minimum spatially-averaged distance.

We observed that the pressure field of the factual analogues shows a more meridionally elongated wave pattern compared to the counterfactual analogues, characterized by positive anomalies at both the surface and mid-troposphere in the North Atlantic and negative surface anomalies on the southern flank of the low-pressure system (Fig. 2.1). We then compared the meteorological hazards in both periods and found an increase in precipitation and wind gusts in Southern France and Northern Italy, the regions most affected by the cyclone, in the factual period compared to the counterfactual (Fig. 2.2). We further found that Alex-like storms are more persistent in the factual and that they become more frequent in autumn. Therefore, these changes collectively indicate that Alex-like storms are more impactful and common in a warmer climate.

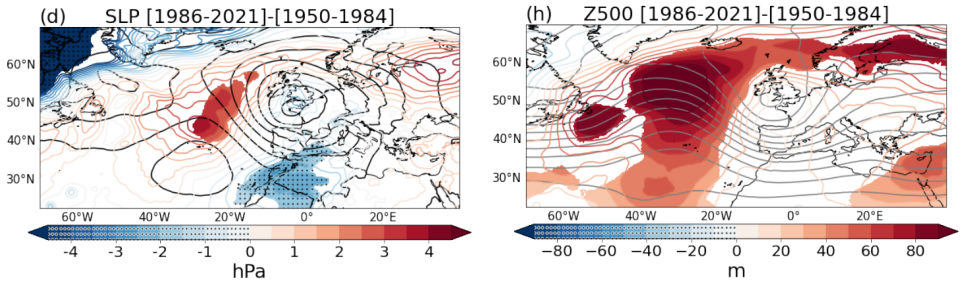

Figure 2.1: Factual minus counterfactual differences of sea level pressure (SLP, d) and geopotential height at 500hPa (Z500, h). Coloured contours show the differences while grey contours show the counterfactual absolute values. Shading shows statistically significant differences. In all panels, negative values are stippled. This figure corresponds to Figures 2(d) and 2(h) of Ginesta et al. (2023).

2.3 Additional analyses

In the following sections, I perform additional analyses to Ginesta et al. (2023) to: validate the findings by testing them under different parameters (section 2.3.1), quantify

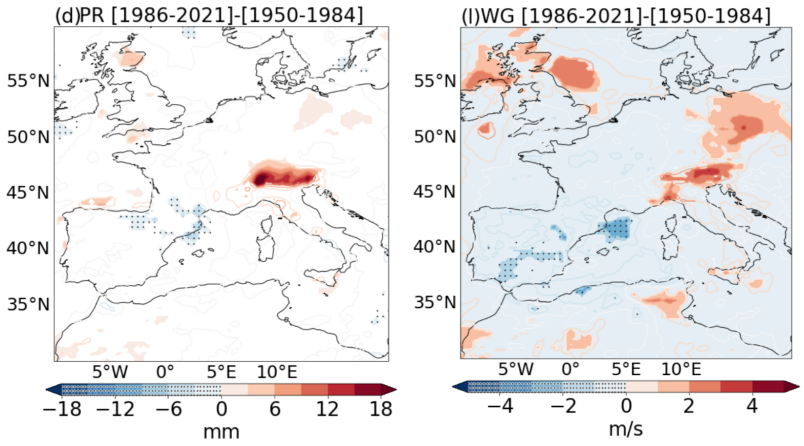

Figure 2.2: Difference between the composite of factual and counterfactual analogues for (d) 24-hour accumulated precipitation (PR) and (l) maximum 10m wind gust within 24 hours (WG). This figure corresponds to to Figures 7(d) and 7(l) of Ginesta et al. (2023).

the contribution of internal variability (section 2.3.2), and compare with other studies that asses general trends averaging over multiple cyclones in the North Atlantic basin (section 2.3.3). These additional analyses serve to strengthen the robustness of our results.

2.3.1 Parameter sensitivity tests

The presented methodology depends on different parameters, such as the number of analogues and the spatial domain used to identify the analogues.

a) Number of analogues

We explored the sensitivity to a selection of $K = 30$ analogues by calculating the Euclidean distance between Alex and its analogues across a range of analogue numbers, spanning from $K = 5$ to $K = 150$ with 5-unit intervals (Fig. 2.3a). The Euclidean distance exhibits a pronounced increase from 5 to approximately 50 analogues, after which it levels off (Fig. 2.3a). We also determined the slope at each point, representing the change in distance for a specific number of analogues (Fig. 2.3b). Notably, the point at 30 aligns approximately with the elbow of the slope curve. This particular point reflects a compromise, balancing the need for statistical robustness with the need for relatively high-quality analogues. Moreover, beyond this point, the rate of change in Euclidean distances starts to slow down significantly, indicating that adding more analogues after this point does not substantially enhance the overall accuracy of the analysis.

We repeated the study using 25 and 50 analogues without finding substantial changes

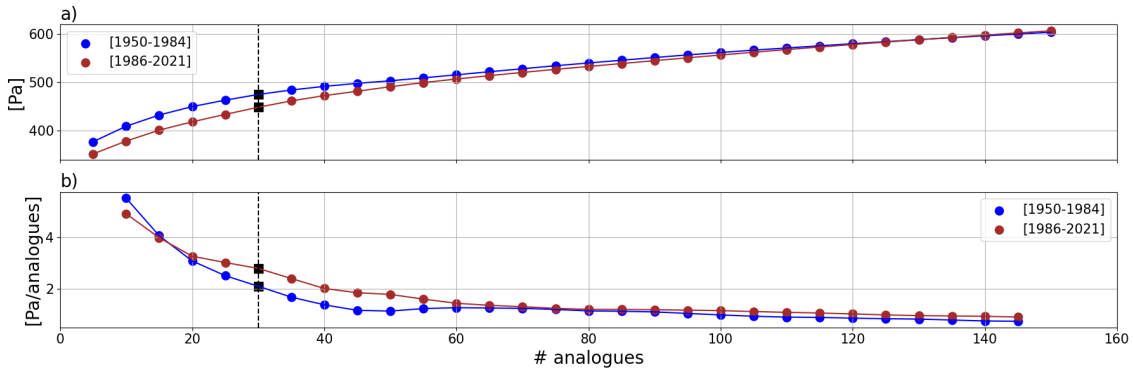

Figure 2.3: a) Mean Euclidean distance between the sea level pressure map of Alex and its analogues as a function of the number of analogues. b) Slope of the mean Euclidean distance curve as a function of the number of analogues.

(Fig. 2.4). However, for more than 50 analogues the factual minus counterfactual differences become weaker. Hence, for a number of analogues larger than 50, the differences might be largely marked by the diversity in the cyclone patterns and are therefore not statistically significant.

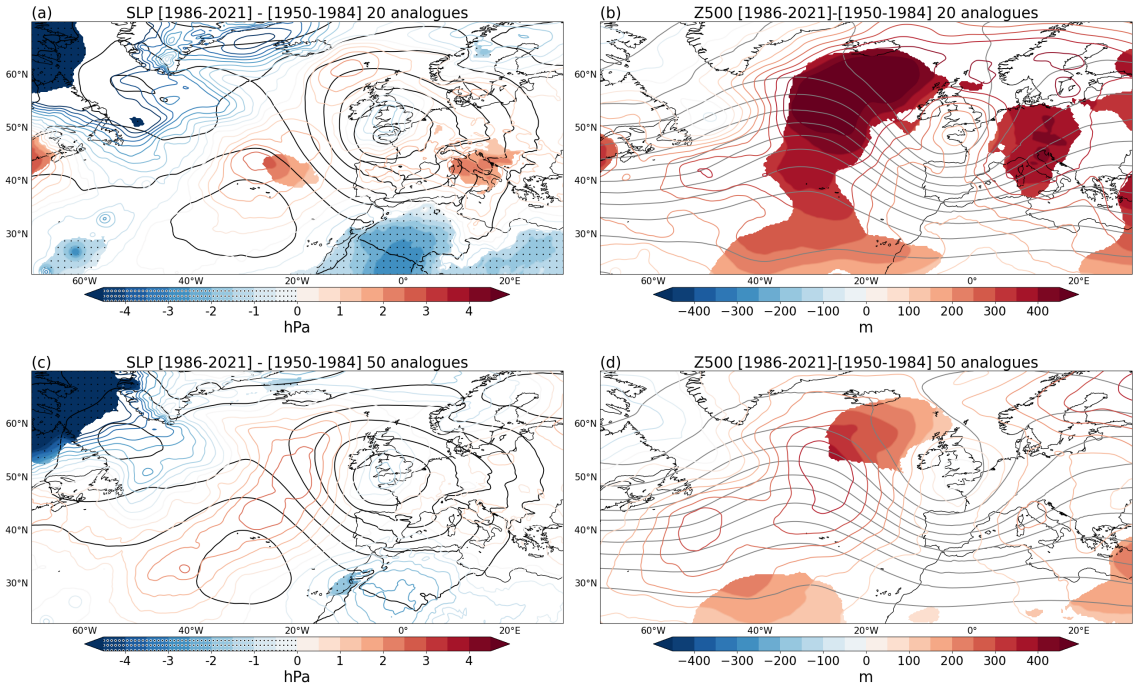

Figure 2.4: Factual minus counterfactual differences of sea level pressure (a, c) and Z500 (b, c) of the composites with 20 analogues (a, b) and 50 analogues (c, d). Colored contours indicate differences, while grey contours represent counterfactual absolute values. Shading shows statistically significant differences. Negative values in (a,c) are stippled.

Hence, the sensitivity analysis on the number of analogues showed that selecting

30 analogues is a trade-off between statistical robustness and analogues quality, as it aligns with an elbow in the Euclidean distance curve. Repeating the study with 25 and 40 analogues showed no substantial changes, while beyond 50 analogues, differences in outcomes became weaker, potentially influenced by cyclone pattern diversity.

b) Spatial domain to identify analogues

We conducted sensitivity tests by changing the spatial domain for identifying analogues, extending the search by up to 10 degrees in both longitude and latitude (dashed black boxes in Fig. 2.5). When opting for a larger domain, the positive sea level pressure anomalies within the cyclone core are more pronounced compared to a smaller domain (Fig. 2.6). In the North Atlantic, negative anomalies are weaker for the larger domain, but the large-scale spatial patterns are similar. The differences, i.e., factual minus counterfactual, in sea level pressure and geopotential height are also larger in magnitude for the smaller domain than the larger one (Fig. 2.5). By construction, for the smaller domain the analogues do not give any weight to the large-scale circulation over the eastern North Atlantic, within which cyclone Alex matured. Thus the quality of the analogues is closely steered by the core of the depression itself, while larger variations can occur elsewhere in the domain. On the contrary, for a larger domain, remote circulation features that do not have a direct impact on Alex, and the subsequent extreme weather in Europe play a role in determining analogue quality.

2.3.2 Assessment of the role of internal variability

Changes in weather patterns across distant locations on Earth can be attributed to common climate variability phenomena, including El Niño, i.e. warm SST anomalies in the eastern tropical Pacific, and other large-scale atmospheric oscillations. This simultaneous alteration of weather conditions in two remote locations influenced by the same climate variability phenomena is referred to as teleconnection, representing a manifestation of atmospheric internal variability (Bjerknes, 1969; Liu and Alexander, 2007). This teleconnection is facilitated by atmospheric circulation patterns that transfer information, such as the propagation of Rossby waves. Numerous studies have investigated the impact of specific climate variability phenomena and their associated teleconnections on European weather. For instance, the El Niño-Southern Oscillation (ENSO) has traditionally been associated with the North Atlantic Oscillation (NAO) pattern, wherein a positive (negative) ENSO aligns with a negative (positive) NAO, and some studies have further evaluated the nonlinearities of such teleconnection (King et al., 2023b). However, recent work by Mezzina et al. (2020) has raised questions about the robustness of this ENSO-NAO relationship. The mechanisms and dynamics governing teleconnection patterns and their impacts remain subjects of uncertainty and ongoing investigation.

We evaluate the possible link of the main sources of internal variability, namely ENSO, Atlantic Multidecadal Oscillation (AMO), and the Pacific Decadal Oscillation (PDO), with the observed changes. We determine the ENSO, AMO, and PDO in-

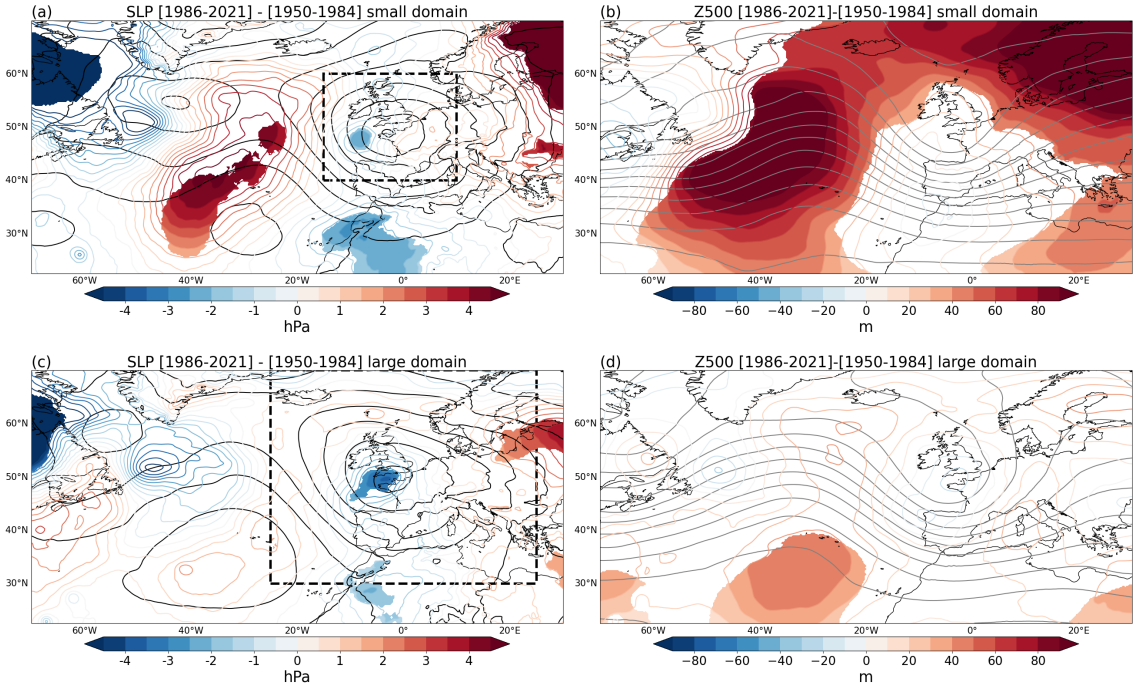

Figure 2.5: Factual minus counterfactual differences of sea level pressure (a, c) and Z500 (b, d) of the analogues found with a smaller domain (a, b) and a larger domain (c, d). The domain used for analogue identification is depicted by the dashed black box. Colored contours indicate differences, while grey contours represent counterfactual absolute values. Shading shows statistically significant differences.

dices for the analogues of each corresponding period. Figure 2.7 shows the distribution of these indices. This analysis reveals no substantial change in the internal variability indices of AMO and PDO. However, ENSO may have contributed to the observed changes, as evidenced by a shift towards positive values in the factual climate. Consequently, we conclude that the previously observed results might be partially attributed to alterations in the ENSO pattern.

2.3.3 Comparison with general trends of North Atlantic Winter Cyclones

During the time I conducted the revisions of this paper, Karwat et al. (2022) were also undergoing peer review for their study on the Long-Term Trends of Northern Hemispheric Winter Cyclones, using the recently updated Extended ERA5 Reanalysis. They showed that the pre-satellite ERA5 data in the Backward Extension (1950–1978) is suitable for long-term studies, and is consistent with the previous ERA5 dataset (1979–2021). This offers further validation of the dataset in our analysis. Their results also show a non-significant increase in the number of extratropical cyclones in the North Atlantic, as well as an increase in storminess or cyclone intensity. They observed a decrease in cyclone speed, indicative of increased persistence, and a poleward displacement

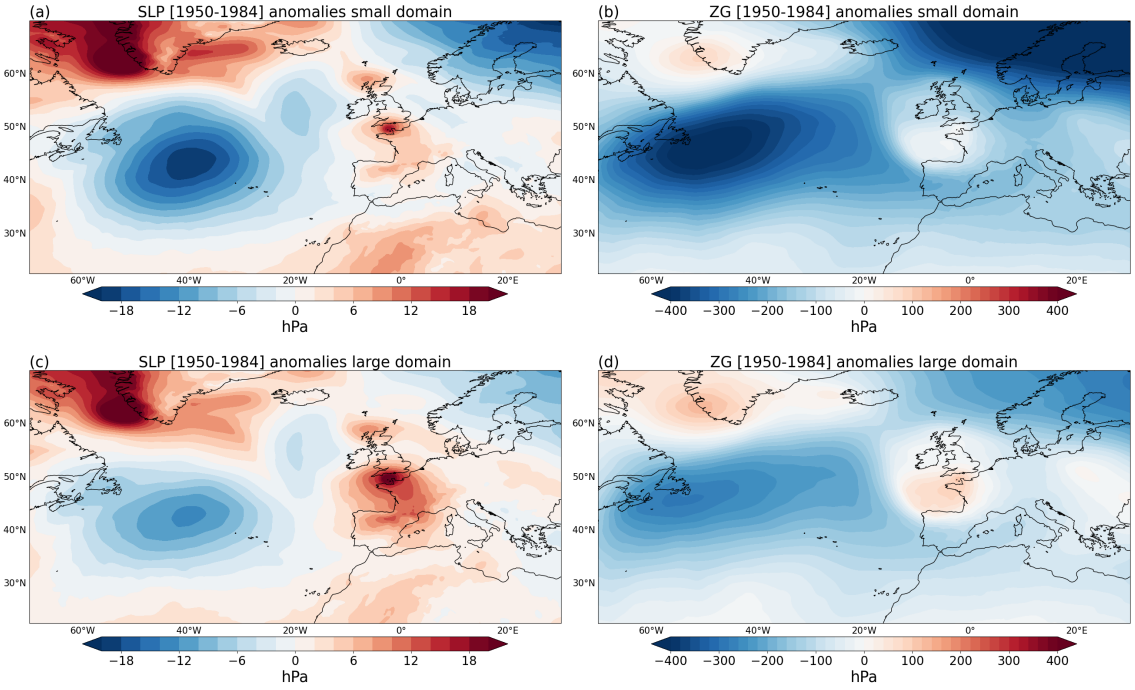

Figure 2.6: Counterfactual anomalies of sea level pressure (a, c) and Z500 (b, d) of the analogues found with the smaller domain (a, b) and the larger domain (c, d).

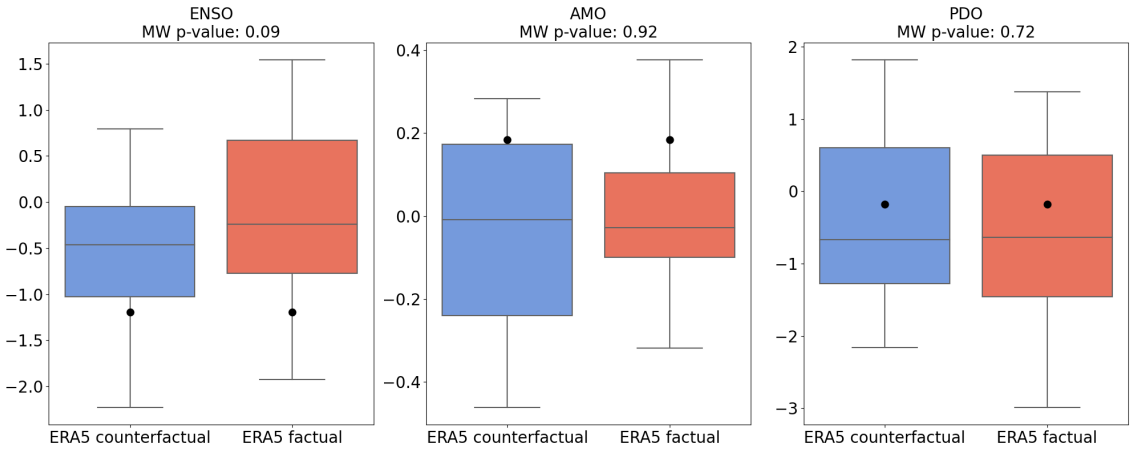

Figure 2.7: Boxplots for all analogues in both counterfactual and factual periods of the different internal variability indices: ENSO, AMO, and PDO. A Mann-Whitney test is used to identify statistical differences in both distributions, with the null hypothesis of no significant difference between the periods. The p-value is shown in the title. We use monthly indices produced by NOAA/ERSSTv5; for ENSO the index is Nino3.4. Dots show the values for Alex.

of the cyclones. Thus, the increase in persistence and the latitudinal displacement of Alex agree with the trends in the basin. Conversely, Karwat et al. (2022) found a significant decrease in the mean precipitation associated with the cyclones, but an increase

in the years with extremes. They also found an increase in the maximum wind gust of the most intense cyclones in the most recent period, from 1979 to present, but no trends considering the whole period.

Considering both the similarities and differences of trends of Alex compared to general patterns, I argue that while general trends often reflect dominant patterns observed across larger scales, individual storms can deviate from these trends due to their sensitivity to localized conditions and the dynamic nature of atmospheric and oceanic processes.

2.4 Summary and conclusions

In this chapter, we introduced a methodology that enables the comparison of precipitation and wind speed in two climates, counterfactual and factual, conditioned on the observed pressure pattern. We illustrated it on storm Alex, and found that similar cyclones exhibit increased persistence and precipitation in the factual climate compared to the counterfactual.

Building on the work of Faranda et al. (2022), our studies contribute to a novel methodology for attributing extreme events. These studies served as methodological validation for the development of Climameter led by Davide Faranda (https://www.climameter.org/). This accessible tool facilitates rapid attribution studies of extreme events, supporting media efforts to raise awareness of the effects of climate change.

While Climameter adopts a conditional approach, the "World Weather Attribution" (WWA) is another collaborative initiative of rapid extreme event attribution that uses an unconditional framework. WWA defines events based on meteorological hazards, including precipitation, wind speed, and temperature (https://www.worldweatherattribution.org/). The next chapter presents a methodology that aims to combine these two approaches by defining an event and its analogues based on both dynamics and hazards.

Résumé en Français

Dans ce chapitre, je présente une méthodologie pour attribuer les cyclones extratropicaux observés au changement climatique, en l'illustrant avec la tempête Alex. Cette méthodologie est décrite dans l'article publié dans Climate Dynamics intitulé "A methodology to attribute extratropical cyclones to climate change: the case study of Storm Alex 2020".

La tempête Alex a touché le sud-ouest de l'Europe au début d'octobre 2020, causant plus de 20 morts et des pertes économiques estimées à plus de 2,5 milliards d'euros. Des régions du sud de la France et du nord de l'Italie ont enregistré des niveaux de précipitations sans précédent.

Nous utilisons les données de réanalyse ERA5 et définissons deux périodes climatiques différentes: une période passée de 1950 à 1984 (contre-factuelle), et une période plus récente, de 1986 à 2021 (factuelle). Cette dernière représente un climat largement influencé par les émissions anthropiques, et dans la première l'influence humaine sur le climat est comparativement plus faible. Nous identifions 30 analogues d'Alex lorsque le cyclone a atteint sa pression au niveau de la mer minimale le 2 octobre 2020, à 06:00 UTC pour chaque période (factuelle et contre-factuelle). Pour ce faire, nous calculons la distance euclidienne entre la carte de pression au niveau de la mer d'Alex et toutes les autres étapes de temps, puis sélectionnons les 30 étapes – analogues – avec la distance spatiale moyenne minimale.

Nous avons observé que le champ de pression des analogues factuels montre une configuration d'onde plus allongée méridionalement par rapport aux analogues contre-factuels, caractérisé par des anomalies de pression positives à la surface et en moyenne troposphère dans l'Atlantique Nord et des anomalies négatives à la surface sur le flanc sud du système de basse pression. Nous avons ensuite comparé les aléas météorologiques dans les deux périodes et constaté une augmentation des précipitations et des rafales de vent dans le sud de la France et le nord de l'Italie, les régions les plus touchées par le cyclone, dans la période factuelle par rapport à la période contre-factuelle. Nous avons également constaté que les tempêtes de type Alex sont plus persistantes dans la période factuelle et deviennent plus fréquentes en automne. Ces changements indiquent collectivement que les tempêtes de type Alex sont plus impactantes et communes dans un climat plus chaud. Nous avons également trouvé que la variabilité interne, en particulier le mode ENSO (Oscillation australe El Niño), pourrait expliquer en partie ces différences.

Chapter 3

A Multivariate Extreme Event Attribution Approach

Objectives

In this chapter, I expand on the conditional approach introduced in Chapter 2, presenting a multivariate approach to identify analogues of extratropical cyclones. Analogues are defined based on sea level pressure patterns and other relevant meteorological variables, such as precipitation and wind speed. The first part illustrates the approach on flooding events in Venice (Acqua Alta), while the second part refines the methodology and applies it to attribute and project the Emilia Romagna floods in 2023.

Contents

4.1 Introduction . . . 62
4.2 Article under review in Journal of Climate . . . 62
4.3 Additional analyses . . . 64
4.3.1 Tracking comparison . . . 64
a) TempestExtremes detection and tracking (TE) . . . 66
b) M02 detection and tracking . . . 68
c) Analogues quality comparisons between M20, TE, and M02 . . . 69
d) Conclusion . . . 70
4.3.2 CMIP6 comparison . . . 71
4.3.3 Concurrences with atmospheric rivers . . . 73
4.4 Summary and conclusions . . . 76

3.1 Introduction

In this chapter, I revisit the methodology introduced in Chapter 2, where we initially defined an analogue as a function of the atmospheric pressure pattern. Here, I extend the definition of an event to encompass meteorological hazards, including precipitation and wind speed. The integration of meteorological hazards on the event definition aligns with the risk-based approach, while maintaining the definition based on the pressure pattern corresponds to the analogues approach. Therefore, the goal of this chapter is to bring these two approaches together, combining the quantification of meteorological hazards with the synoptic-scale configuration of the atmosphere — an approach we term *multivariate approach*.

I first applied this multivariate approach to abnormal high-water events in Venice, known as Acqua Alta. In a paper led by Davide Faranda (Faranda et al., 2023), included in Appendix D, we attributed the Acqua Alta events to ongoing climate change. My contribution involved formulating and applying the methodology; I defined an analogue considering the atmospheric pressure pattern as well as regional precipitation and the Sirocco wind — a warm, humid southeasterly wind from the Adriatic Sea—relevant to the local Acqua Alta phenomena. The approach and application are shown in section 3.2.

Furthermore, in section 3.3 I illustrate the methodology to flooding events in Emilia Romagna in May 2023, marked by three storms on the 2nd, 10th, and 16th. I assess how the magnitude of the event has changed compared to the past and examine future projections. To achieve this, I use ERA5 reanalysis and the high-resolution regional multi-model ensemble EURO-CORDEX (Jacob et al., 2014).

3.2 Methodology and example of application: Acqua Alta events

The analogue method starts by identifying the variables that best represent the event. Subsequently, events with similar characteristics in terms of these variables are identified. In this multivariate approach, two categories of variables are distinguished: those associated with the atmospheric circulation pattern and dynamics, which could be represented, for example, by sea level pressure, and others that incorporate meteorological hazards variables providing insights into the physical state of the atmosphere, such as precipitation or wind speed. Consequently, the goal is to identify analogues based on atmospheric pressure patterns, with a further focus on narrowing down this search to regional meteorological hazards.

I applied this approach to four Acqua Alta events in Venice (Faranda et al., 2023). The atmospheric configuration in all the events was a low-pressure system over the northwestern Mediterranean, and can be characterized by the sea level pressure pattern. The meteorological variables that are linked to Acqua Alta events are precipitation and Scirocco winds. The Scirocco wind is a local wind over the Adriatic Sea from the

southeast (135°) that advects warm, humid air into the Gulf of Venice. Scirocco wind is calculated using the 10m zonal (u) and meridional (v) wind components (eq. (3.1)):

$$ws = u_{10m}\cos(135°) + v_{10m}\sin(135°). \tag{3.1}$$

Thus, the three variables — sea level pressure (slp), total precipitation (pr), and Scirocco wind speed (ws) — are used to identify analogues of Acqua Alta events. Figure 3.1a–c shows the slp, pr, and ws components of the Acqua Alta event on the 4th of November 1966.

We then normalize each field $\phi = \{\text{slp, pr, ws}\}$ at each grid point. We use min-max normalization, based on the minimum and maximum values observed throughout the 1950-2022 period (eq. (3.2)). This process ensures that each variable is transformed into a comparable scale from 0 to 1 across the specified time period. The normalized fields are depicted in Figure 3.1d–f.

$$\phi_{scaled,i,j} = \frac{\phi(t)_{i,j} - \phi_{\min,i,j}}{\phi_{\max,i,j} - \phi_{\min,i,j}}. \tag{3.2}$$

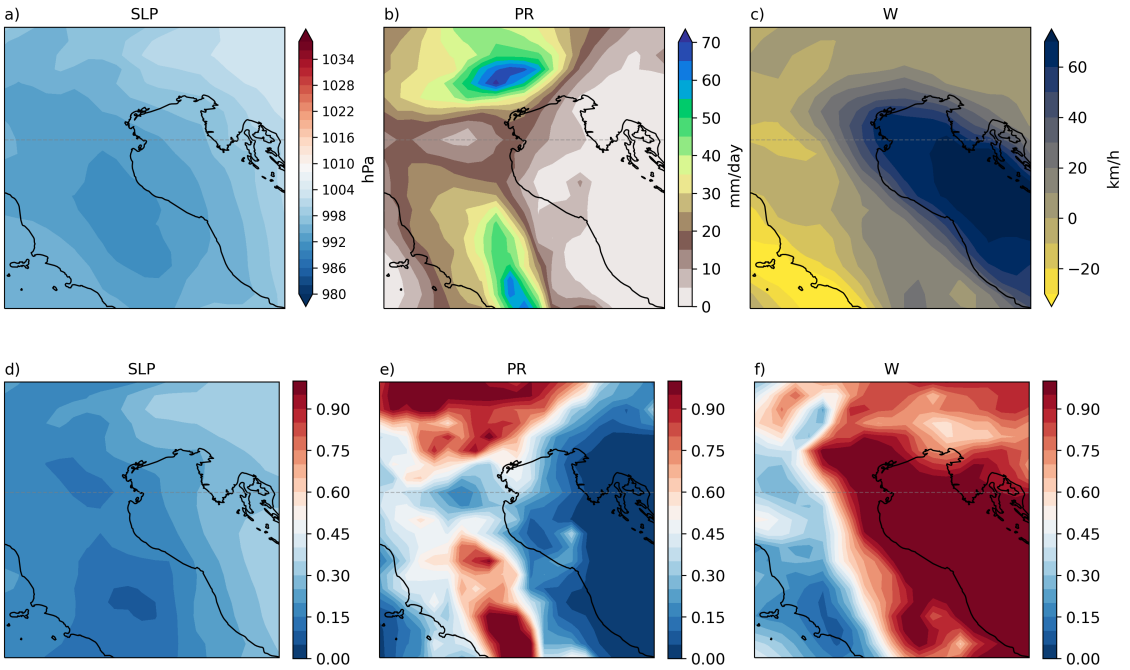

Figure 3.1: (a–c) ERA5 6–hourly sea level pressure (slp), total precipitation (pr), and Scirocco wind speed (ws) on the 4th November 1966 at 12 UTC. (d–f) Normalized fields of figure 3.1, using 1950-2022 as reference period.

Subsequently, spatially averaged Euclidean distances are computed for the normalized fields, resulting in three time series representing the Euclidean distances between

the event and all other time steps. These individual Euclidean distances are then combined to form the *pseudo-distance* (eq. (3.3)):

$$d(t) = \sqrt{d_{slp}(t)^2} + \sqrt{d_{pr}(t)^2 + d_{ws}(t)^2}. \tag{3.3}$$

We term it a pseudo-distance rather than a distance because it does not satisfy the properties of a Euclidean distance within the given phase space of slp, pr, and ws. The combination used to calculate pseudo-distances inherently assigns more weight to the slp distances compared to pr or ws. The slp field tends to be smoother than pr or ws. pr and ws are significantly influenced by topography and have a higher frequency of variations both temporally and locally. Consequently, the Euclidean distances between normalized slp fields are considerably smaller than those of pr and ws. This reasoning justifies the prioritization of the slp or the consideration of a separate dynamical part.

In the final step, identifying the best analogues involves selecting those with the lowest pseudo-distances. Following Ginesta et al. (2023), the search for analogues is prohibited within a seven-day window centered on the event date and the event itself is excluded within its respective period.

This methodology was specifically tailored for these events. In the following section, I introduce a broader multivariate approach where I define a total distance that treats all variables equally. This approach can be used for a wider range of events and combinations of different variables.

3.3 Refined Multivariate Approach and application to the Emilia-Romagna floods of May 2023

3.3.1 Introduction and context of the study

The March–May period of 2023 was the third-warmest on record globally and the 19th warmest in Italy on record (NOAA, 2023). Southwestern Europe, including northern Italy, was experiencing drought conditions. However, the drought in Italy was partially recovered at the beginning of May due to regional intense rainfall. In May, the region of Emilia Romagna in the northeastern part of Italy, with its capital in Bologna, experienced a sequence of flooding events over the first two weeks. The first flood occurred on the 2nd of May, resulting in the loss of two lives. The second event, on the 10th of May, was comparatively less severe. The third event, on the 16th of May, was the most impactful one resulting in 16 fatalities.

These three events were caused by a serial clustering of three extratropical cyclones, that is, the passage of three low pressure systems over the same region in a short period of time (Dacre and Pinto, 2020; Pinto et al., 2014). The three cyclones were located over the Thyrrenian sea when they caused high amounts of rainfall. Notably, the first rainfall event, on the 2nd of May, occurred after a prior period of drought, causing high amounts of rainfall over the dry and impermeable ground. The subsequent heavy rainfall events were followed by intensified flooding, as the soil was already saturated. The combination of these factors triggered rapid saturation and runoff.

A study by the World Weather Attribution (WWA), published soon after the event, found a limited role of climate change in the heavy rainfall that led to the floods in Emilia Romagna (Barnes et al., 2023). The report gained coverage in international and Italian media soon shortly after publication (Fraser-Baxter, 2023; Lombroso, 2023; Rinnovabili.it, 2023; Sabelli, 2023). The WWA study was a rapid unconditional attribution study that defined the extreme event as the maximum accumulated precipitation over 21 days between April and June over Emilia Romagna. The study used observational data from weather stations, reanalyses, and multi-model ensembles, to evaluate trends from observations, model performance, and multi-method multi-model attribution. They found that in the present the event has a return period of 1 in a 200 years event, with no change in a past climate. In addition, they found that none of the models show statistically significant changes in the likelihood or intensity of such event.

We acknowledge certain limitations in the study. The severity of the event was not solely determined by continuous rainfall over 21 days but was also influenced by the intensity of each of the three storms. Additionally, the combination of dry soil conditions before the event and saturated runoff conditions after the initial flooding played a significant role. To address these limitations, collaboration was initiated with researchers from Italy, including Erika Coppola, Chen Lu, Valerio Lembo, Tommaso Alberti, and Federico Grazzini.

In collaboration with these researchers, our aim is to provide a complementary analysis from different perspectives. Chen Lu and Erika Coppola applied a risk-based

approach, defining the event as the wettest 3 days in May. Preliminary results indicate a significant increase in both intensity and likelihood of the event with global warming, although these results are provisional and not presented here.

My role is to specifically focus on the impact of climate change on the intensity of each of the three storms separately, using the analogue multivariate approach. In the following sections, I present the analogue multivariate approach, redefined with respect to the previous section. We assess detected changes in pressure, precipitation, and wind speed of the events by comparing a past counterfactual with a factual climate using ERA5. Following that, we evaluate future projections using a high resolution multi-model ensemble within the World Climate Research Program Coordinated Regional Downscaling Experiment EURO-CORDEX initiative (https://cordex.org/; Giorgi et al. (2009)). We compare the present-like or factual climate with a future counterfactual represented by the climate at the end of the 21st century. It is important to note that we only use a subset of the EURO-CORDEX simulations, specifically those publicly accessible and hosted on our server. We are currently working on applying the following methodology to all EURO-CORDEX simulations.

3.3.2 Datasets and Methods

We use the ERA5 reanalysis dataset (Hersbach et al., 2020) for the characterisation of the events and the identification of the analogues in two climates. The atmospheric horizontal resolution is 31 km. We evaluate ongoing changes in the magnitude of the events from 1950 to 2022. We split the period in two 35–year periods, similar to Ginesta et al. (2023); a factual period, from 1987 to 2022, and a counterfactual period, from 1950 to 1985. We refer to them as **past** and **present**, respectively. We use daily data for the months of March, April, May, and June (MAMJ), of sea level pressure (slp), daily averaged precipitation rate (referred to as precipitation from hereafter, pr), and daily averaged wind speed (ws).

We use high-resolution regional climate models (RCMs) due to their added value in simulating phenomena over complex topography and smaller-scale atmospheric processes compared to general circulation models (GCMs) (Feser et al., 2011). Our study involves 19 simulations within the World Climate Research Program Coordinated Regional Downscaling Experiment EURO-CORDEX initiative at 0.11° (around 12 km) horizontal atmospheric resolution. The regional simulations were obtained by downscaling several GCMs from the Coupled Model Intercomparison Project 5 (CMIP5) global climate projections. The driving GCMs and the driven RCMs used are listed in Table 3.1. We compare two climates: a factual one from 1970 to 2000 representing a present-like climate and a future counterfactual from 2070 to 2100, using the Representative Concentration Pathway RCP8.5, representing the worst-case scenario. We refer to them as **historical** and **future**, respectively.

To allow a comparison between models and ERA5 we interpolate the horizontal grid of the higher resolution (model) to match that of the lower resolution (ERA5). To do that, we use the CDO — Climate Data Operators software (Schulzweida et al., 2019). We employ nearest neighbor remapping for pr, "cdo remapnn," and distance-weighted

average remapping for slp and ws, "cdo remapdis". The nearest neighbors remapping is suitable for pr due to its discontinuous nature, ensuring an accurate representation of localized effects. In contrast, distance-weighted average remapping is applied to slp and ws to ensure a seamless transition between grid points, particularly for variables with smooth and gradual changes.

RCM	**GCM**	**Institute ID**	Label
GERICS-REMO2015	CCCma-CanESM2	GERICS	A
GERICS-REMO2015	CNRM-CERFACS-CNRM-CM5	GERICS	B
GERICS-REMO2015	IPSL-IPSL-CM5A-MR	GERICS	C
GERICS-REMO2015	MIROC-MIROC5	GERICS	D
GERICS-REMO2015	NCC-NorESM1-M	GERICS	E
CLMcom-CCLM4-8-17	CNRM-CERFACS-CNRM-CM5	CLMcom	F
CLMcom-CCLM4-8-17	MPI-M-MPI-ESM-LR	CLMcom	G
CLMcom-ETH-COSMO-crCLIM-v1-1	ICHEC-EC-EARTH	CLMcom-ETH	H
CLMcom-ETH-COSMO-crCLIM-v1-2	MPI-M-MPI-ESM-LR	CLMcom-ETH	I
DMI-HIRHAM5	ICHEC-EC-EARTH	DMI	J
DMI-HIRHAM6	MPI-M-MPI-ESM-LR	DMI	K
KNMI-RACMO22E	ICHEC-EC-EARTH	KNMI	L
KNMI-RACMO22E	MPI-M-MPI-ESM-LR	KNMI	M
IPSL-WRF381P	IPSL-IPSL-CM5A-MR	IPSL	N
IPSL-WRF381P	MOHC-HadGEM2-ES	IPSL	O
IPSL-WRF381P	NCC-NorESM1-M	IPSL	P
CNRM-ALADIN63	MPI-M-MPI-ESM-LR	CNRM	Q
CNRM-ALADIN63	NCC-NorESM1-M	CNRM	R
MPI-CSC-REMO2009	MPI-M-MPI-ESM-LR	MPI-CSC	S

Table 3.1: List of RCM-GCM combinations with corresponding institutions. Last column shows the label for figures 3.6, 3.10,3.11,3.12.

a) Methods

Similar to Faranda et al. (2022) and Ginesta et al. (2023), we identify a fixed number of analogues in two distinct periods characterized by different radiative forcing. Analogues are determined based on slp, pr and ws. Unlike the previous section, we do not constrain the wind speed to have a specific direction due to limitations in data availability from high-resolution models. Nevertheless, our analysis using ERA5 data reveals no significant differences when considering the northeastern component of the wind speed, which is the one mostly linked to rain in the region (not shown).

For searching analogues, we constrain variables within two different domains: a large-scale domain [4E–21E, 36N–49N] for slp and a regional domain [10E–15E, 43N–46N] for pr and ws (see figure 3.3). This two-domain approach enables us to account for the entire low-pressure system configuration leading to the event while emphasizing the region with the highest meteorological hazards.

We proceed with normalizing the fields using quantile normalization. First, we compute the empirical cumulative distribution function (ECDF), a statistical tool that represents cumulative probability against data values. Mathematically, the ECDF $p(x)$ is expressed as:

$$p(x) \approx \Pr\{X \leq x\}$$

For illustration purposes, figure 3.2 displays the ECDF for slp, pr, and ws using ERA5 data, for a random grid point, at 43.5° of latitude and 12° of longitude. Given its highly skewed distribution, values equal to 0 were excluded from the computation of the ECDF for pr. This exclusion simply ensures a better representation of the normalized fields up to saturation in figure 3.2b. Consequently, the ECDF for pr saturates at approximately 0.8, indicating that around 20% of values are missing—specifically, the values equal to 0 that were removed. The horizontal dashed red line in the figure represents the normalized value for the event on the 2nd of May at this grid point. The reference periods for ECDF computation are 1950 to 2022 for ERA5 data and the historical period for the EURO-CORDEX models.

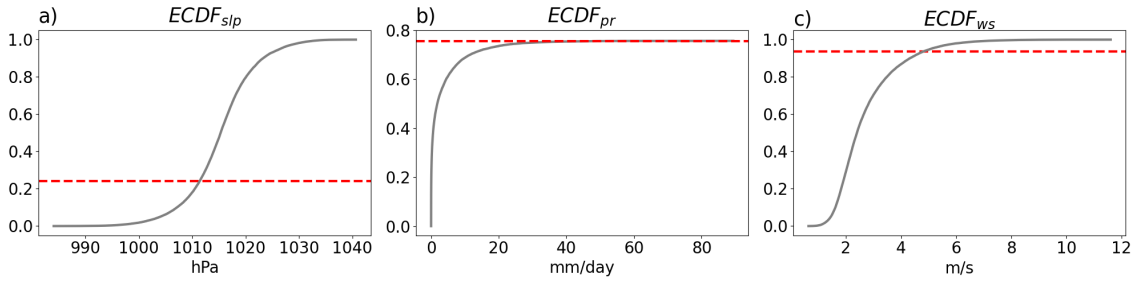

Figure 3.2: Empirical Cumulative Distribution Function (ECDF) for a specific grid point [43.5°N 12°E] using ERA5 data from 1950 to 2022. The red dashed lines indicate the point or quantile to which the ECDF for the event on the 2nd of May 2023 at this specific grid point belongs. a) shows the ECDF for sea level pressure, b) for precipitaiton, and c) for wind speed.

To identify analogues, we create a matrix containing the ECDF for every grid point for ERA5 and each model simulation. Subsequently, we determine the quantile of the ECDF to which each grid point in each timestep belongs for both the event and all available data, with respect to their ECDF reference matrix. Euclidean distances are then computed between the quantiles of the event and those of all other available data, with spatial averaging applied to these distances. This process generates a time series of the distances between the quantiles.

Figures 3.3a–c show the three fields during the time of the event, in this case the first storm on the 2nd of May of 2023. Figures 3.3d–f depict the normalized fields, representing the quantiles at each grid point with respect to the ECDF of ERA5.

Next, we combine the Euclidean distances of the normalized fields to obtain the total distance $d(t)$:

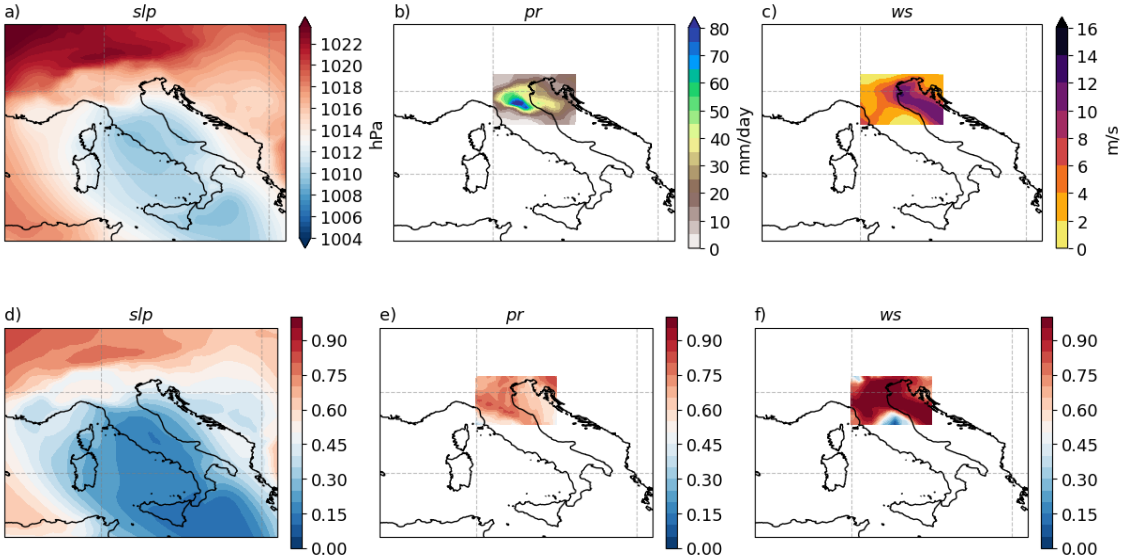

Figure 3.3: (a–c) Sea level pressure (slp), precipitation (pr), and wind speed (ws) on the 2nd of May of 2023 using ERA5 daily data. (d–f) Normalized fields, representing the quantiles with respect to the ERA5 ECDF.

$$d(t) = \sqrt{d_{slp}(t)^2 + d_{pr}(t)^2 + d_{ws}(t)^2}. \tag{3.4}$$

Contrary to the pseudo-distance defined in the previous section 3.2, the mathematical properties of a distance are satisfied with eq. (3.4).

Figure 3.4 shows the histogram of the distances of the normalized fields, or quantiles, for the present period of ERA5. As expected, distributions across variables are comparable. We achieved this by transforming the original values of each variable onto a common scale based on their cumulative distribution functions.

Figure 3.5a shows $d(t)$ for the event of the 2nd of May in the ERA5 present data. Figures 3.5b,c,d show the contribution of the individual distances $d_{slp}(t)$, $d_{pr}(t)$, and $d_{ws}(t)$, respectively. The colored crosses indicate the 20 chosen analogues. For example, the analogue on the 20th of May 1995 is the closest one to the event in terms of pr but not in terms of slp. Conversely, the analogue of the 24th of March 1991 resembles the event in terms of slp but is the least similar in terms of pr. In employing this multivariate approach, it is important to note that the selected analogues reflect a balance across all three variables of interest, recognizing that they may not perfectly align in each individual variable but collectively represent a meaningful trade-off between them.

Finally, we analyze future changes in meteorological hazards by calculating the difference in spatially averaged pr values between factual and counterfactual climates over the regional domain (see Fig. 3.3b or the dashed black box in Fig. S1h). While ws was also considered in finding analogues to better condition the event, we focus only on pr for assessing future changes due to its direct potential to cause flooding in the area. Notably, changes in pr can still be detected even if we constrain our analogues to pr.

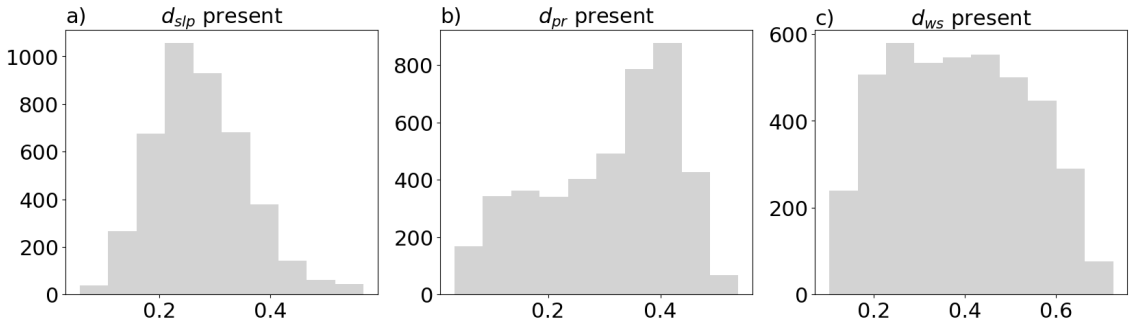

Figure 3.4: Histogram of the Euclidean distances between the event of the 2nd of May and all other timesteps in the ERA5 past period for slp (a), pr (b), and ws (c).

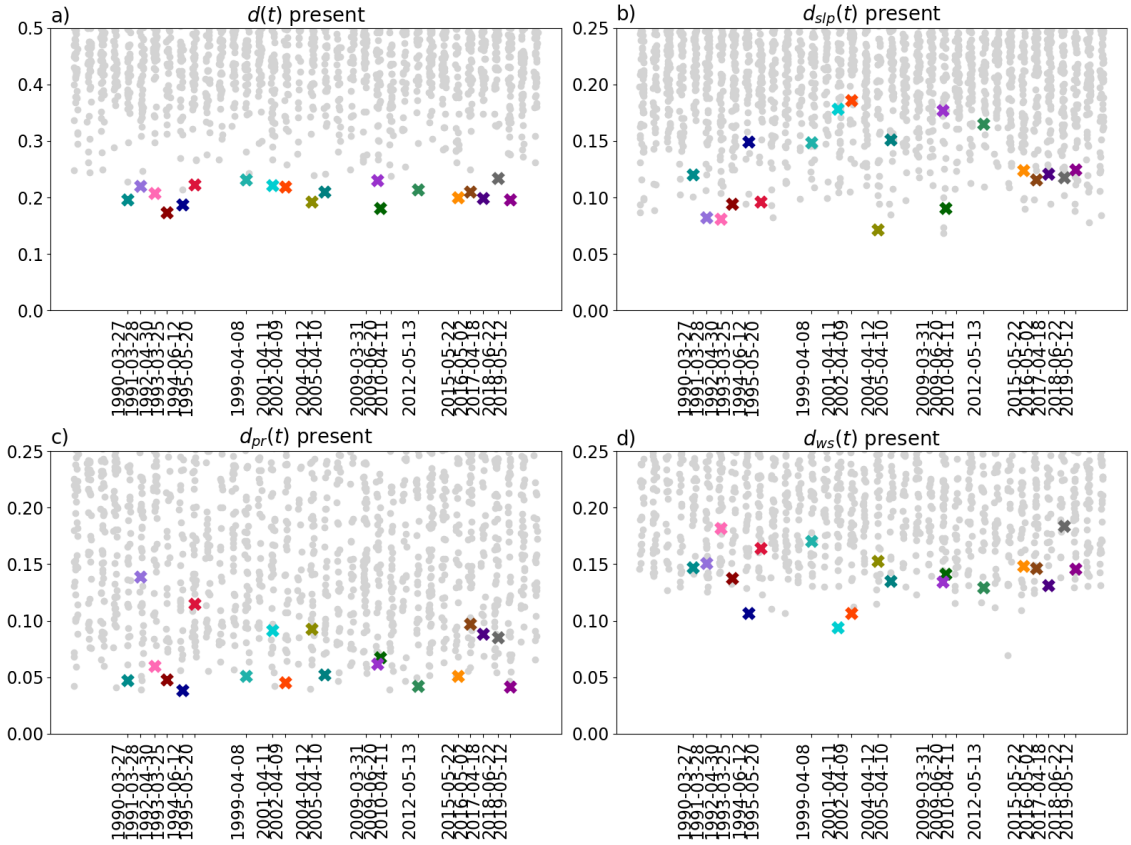

Figure 3.5: a) Timeseries of the spatially averaged total Euclidean Distance according to equation (3.5) for the present period to the event of the 2nd of May 2023. b,c,d) show the distances of the normalized fields of sea level pressure (slp), precipitation (pr), and wind speed (ws), each contributing equally to the total distance $d(t)$. Coloured crosses show the distances of the 20 analogues of the present period.

This is because we are using a multi-variable approach, which effectively sets pr more free, and even if we used only pr, the observed signal in pr would serve as an indicator of how closely the analogues match the event.

b) Performance of EURO-CORDEX models

To assess how well EURO-CORDEX simulations reproduce similar events, we evaluate the representation of the meteorological hazards of the analogues, specifically focusing on pr over the regional domain as shown in figure 3.3b. The evaluation includes calculating the spatially averaged Euclidean distance between the precipitation patterns over the regional domain for each present analogue, both from ERA5 and models, and the precipitation pattern of the event characterized using ERA5 data. This evaluation, termed *analogues quality*, serves as an indicator of how closely the analogues align with the hazards observed in the event.

Figure 3.6 shows the *analogues quality* for the three events. Across all events, distances to the event are consistently lower for ERA5 analogues compared to EURO-CORDEX models. This suggests that ERA5 analogues resemble more the events, indicating higher quality compared to the models. This higher quality in ERA5 is particularly evident for the first event, on the 2nd of May. The lower representation of the models may be linked to the systematic bias of most of the EURO-CORDEX models, which tend to simulate drier conditions in the Po Valley, specially in summer (Kotlarski et al., 2014). Consequently, the analogues identified in the models are associated with lower precipitation values, resulting in higher Euclidean Distances to the event.

The range between the lowest and highest quartiles of ERA5 encompasses the median quartile of the models. This suggests that, while ERA5 outperforms the models, the models demonstrate a consistent capability to reproduce the event to a certain extent. This finding provides confirmation that these models can be used to assess changes in the future period.

3.3.3 Results

a) Detected changes – ERA5

Figure 3.7 shows the ERA5 analogues composite analysis for the event of the 2nd of May. The first column shows the values of slp, pr and ws on the date of the event. The second column shows the analogues composites of the past period, the third column the analogues composites of the present period, and the fourth column the statistical significant present-minus-past differences. The analogues in both periods are able to reproduce the pressure pattern that leads to northeasterly wind advection in the Emilia Romagna region (Fig. 3.7b,c). However, we note that the analogues exhibit a different synoptic pressure pattern than the event itself, with the two lows that characterized the event being more spatially separated than in the actual event (Fig. 3.7a). In addition, the analogues underestimate the precipitation over the impacted region in both past and present periods, highlighting the extreme nature of the event and the challenge of reproducing identical precipitation patterns (3.7f,g).

The slp present-minus-past differences indicate positive anomalies in the northern and southern flanks of the cyclone (3.7d). These anomalies contribute to an increased

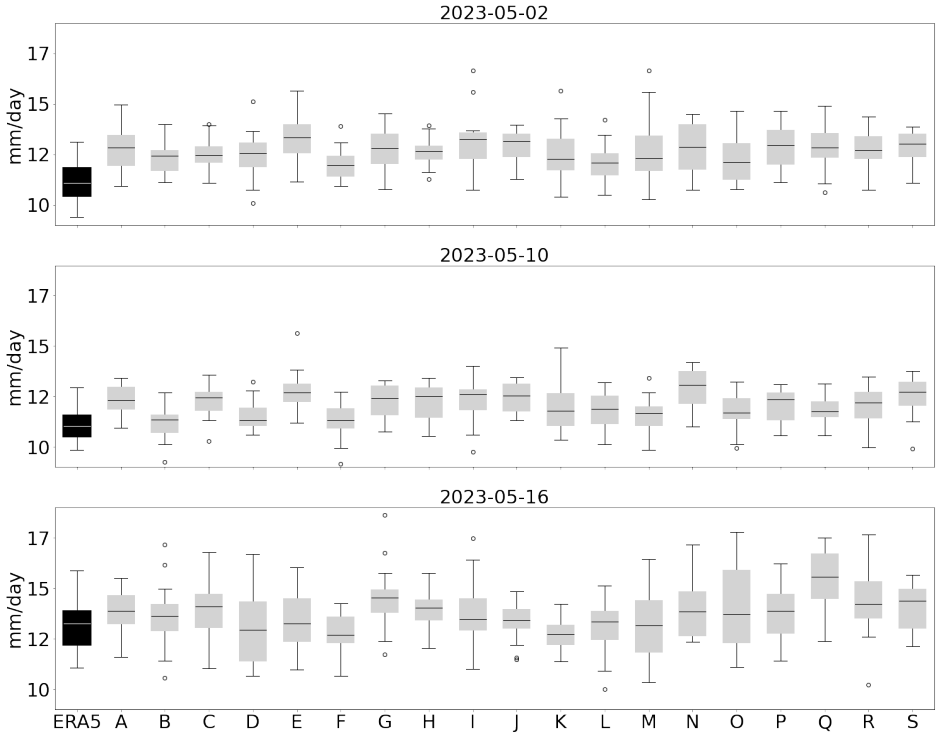

Figure 3.6: Analogues quality computed as the spatially averaged Euclidean distance between the pr of the events in ERA5 and the pr of the 20 analogues for each simulation over the regional domain. Each letter is a simulation, corresponding to table 3.1.

slp gradient in the cyclone, resulting in an increase in wind speed in the northern flank (3.7l). Figure 3.7h shows an increase in pr in the Emilia Romagna region, particularly in the northern flank and over the Gulf of Genoa. Hence, events similar to the 2nd of May may be more intense in the present period compared to the past. Caution is needed in interpreting these results, as they are found locally in a small region of the domain, as the correction for the false discovery rate has not yet been applied (Wilks, 2016).

The analogues composite analysis for event of the 10th of May is shown in figure 3.8. The analogues in both past and present periods simulate the synoptic pressure pattern fairly well, with a main cyclone centered over the gulf of Genova (Fig. 3.8b,c), However, the precipitation is underestimated (Fig. 3.8f,g), similar to the previous event. No significant changes are found in the precipitation pattern over the Emilia Romagna region (Fig. 3.8h).

Figure 3.9 shows the analogues composite analysis for ERA5 data for the third event, on the 16th of May. Figure 3.9h shows an increase in pr southwest of the Emilia Romagna region, specially over Toscana and Lazio. Furthermore, negative anomalies in

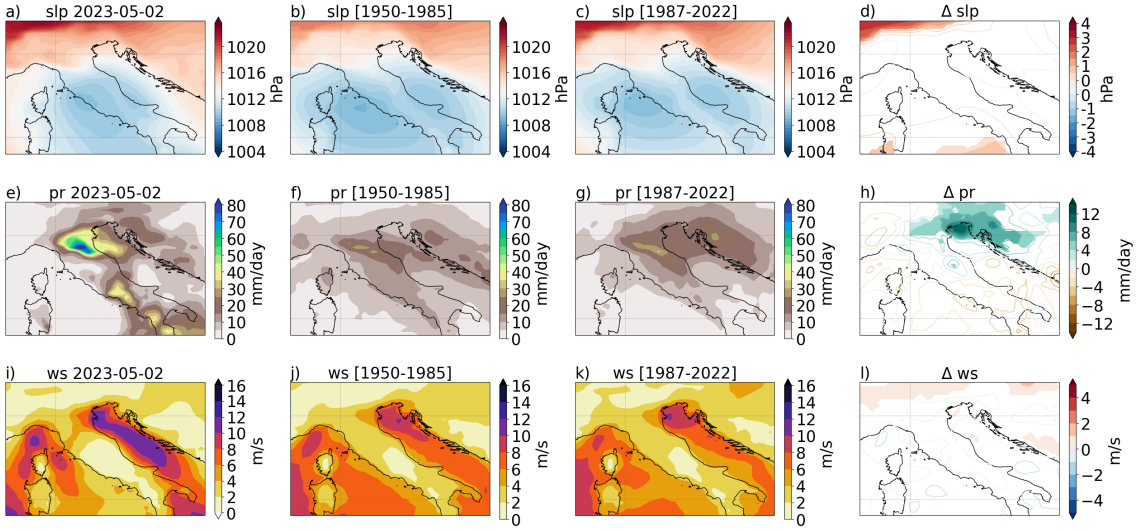

Figure 3.7: Sea level pressure (a), precipitation (e), and wind speed (i) on the 2nd of May 2023 using ERA5 data. slp composites of the 20 analogue storms for the past (b) and present (c) periods, and the corresponding pr (f,g) and ws (j,k) composites. Present minus past differences of slp, pr and ws are shown in (d,h,l). Shading in shows statistically significant differences. A bootstrap test was conducted with a confidence level of 95%.

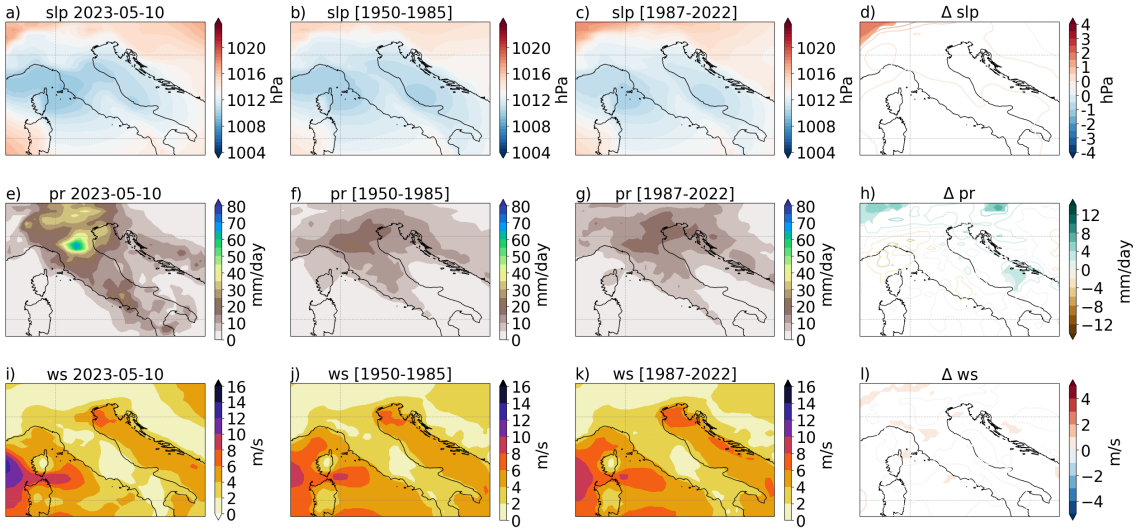

Figure 3.8: Same as figure 3.7 but for the 10th of May 2023

sea level pressure on the northwestern flank of the cyclone suggest a deeper and more spatially extended cyclone in the present period. As a result, wind speed increases in the Lazio region.

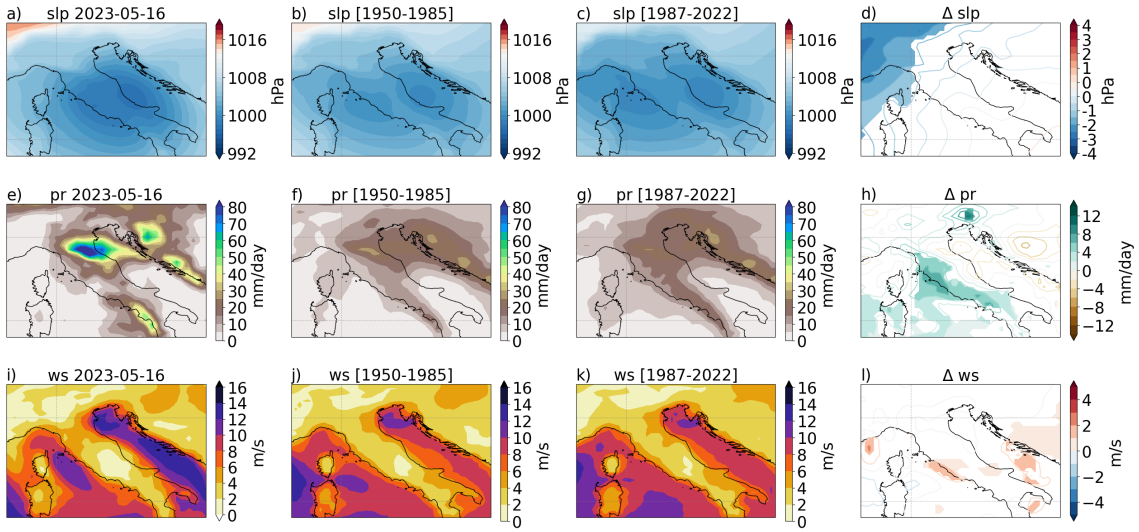

Figure 3.9: Same as figure 3.7 but for the 16th of May 2023

b) Projections with EURO-CORDEX models

The analogues composite analysis for EURO-CORDEX simulations for the event of the 2nd of May is shown in figure S1 in the supplementary material section (section 3.3.5). The analogues composites of slp for both historical and future projections depict a low pressure centered between Corsica and the Italian peninsula (Fig. S1b-c). Both show a similar pattern to the event (Fig. S1a), which means that models are able to capture the atmospheric circulation characteristics that lead the event. However, both historical and future composites show underestimated precipitation of the event, consistent with the previously discussed bias in EURO-CORDEX models. Notably, this bias is also evident in the analogues derived from ERA5 past and present (Fig. 3.7), emphasizing the challenge of finding suitable analogues for such extreme events.

There are no discernible future minus historical significant changes in slp, pr, nor ws (Fig. S1d, h, f). The lack of significance could be attributed to averaging simulations with diverse changes and spatial patterns, resulting in the attenuation of changes. To better discern changes in pr over the regional domain, indicated with a black dashed box in figure S1h, we compute spatially averaged future minus historical pr of the analogues. These changes are presented in Figure 3.10 and, as defined in the previous section, constitute the changes in the meteorological hazards. 14 out of 19 simulations show an increase in precipitation in this region, although only three of them are statistically significant. No simulation exhibits a statistically significant decrease in precipitation. Despite the lack of robust agreement among the models, we argue that positive changes were identified in some simulations, suggesting a potential influence of a warmer climate in increasing the precipitation of this type of event.

For the second event, which occurred on the 10th of May, the models successfully capture the atmospheric low over the Gulf of Genoa that led to the event (Fig. S2b, c). However, there are no satisfactory analogues identified in terms of pr during either of

the two periods. Nevertheless, among the 19 models examined, 7 indicate an increase in precipitation in a future climate compared to historical conditions, while 2 suggest a negative, albeit weaker, signal, over the regional domain (Fig. 3.11). The regional model GERICS-REMO2015 shows 3 simulations with positive signal and 1 negative, while DMI-HIRHAM5 shows 1 positive and 1 negative. Despite considerable variability and lack of consensus among simulations, the majority of models indicate a positive precipitation change. Therefore, we cannot dismiss the role of climate change in influencing this event. However, caution is necessary when interpreting the results due to the poor quality of precipitation analogues and the substantial variability among the models.

For the last and most impactful event on the 16th of May, models successfully capture the distinctive synoptic low-pressure system characterizing the event (Fig. S3b, c). Similar to the previous events, the precipitation of analogues is underestimated compared to that of the event (Fig. S3f, g). Precipitation changes over the regional domain exhibit general agreement among simulations, with 15 indicating positive signal and 9 being significant (Fig. 3.12). Only one simulation shows a significant negative change.

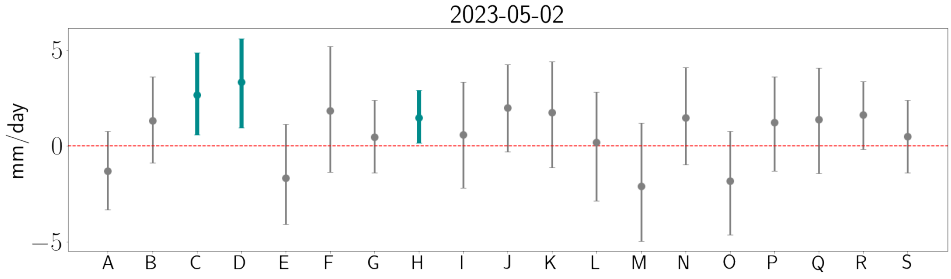

Figure 3.10: Future minus present precipitation (pr) of the analogues over the regional domain (Fig. S1h dashed black box) for the event of the 2nd of May 2023. The mean is represented by a dot, and the confidence interval at a 90% confidence level is depicted by vertical bars, computed using a bootstrap test. Blue denotes positive significant change and brown negative. Each letter is a simulation, corresponding to table 3.1.

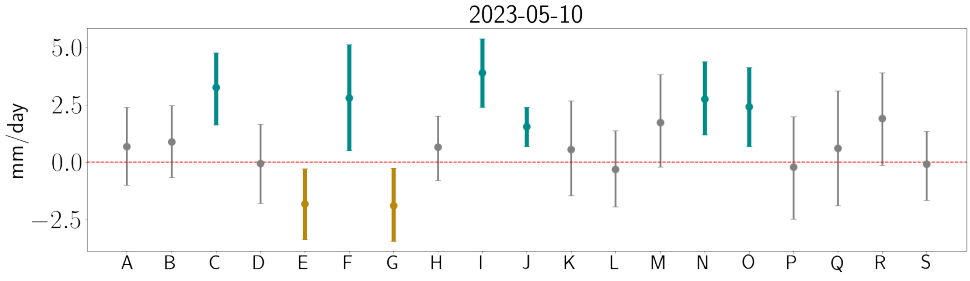

Figure 3.11: Same as figure S1 but for the 10th of May 2023

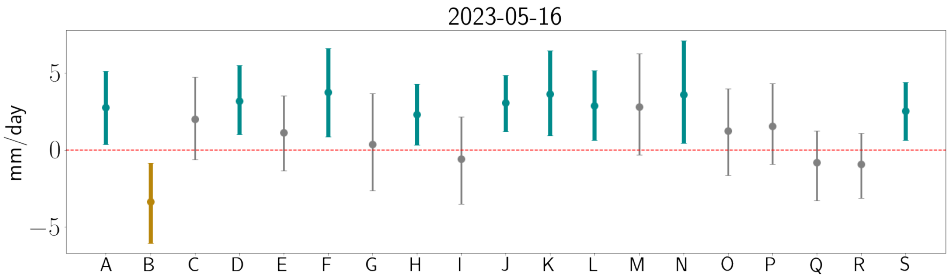

Figure 3.12: Same as figure S1 but for the 16th of May 2023

3.3.4 Discussion

This study conducts an assessment of detected changes and future projections regarding the pressure, precipitation, and wind speed for three storms that caused severe flooding in the Emilia Romagna region on the 2nd, 10th, and 16th of May 2023. We describe and employ a multivariate approach to identify analogues—events similar in terms of sea level pressure, precipitation, and wind speed—in two different climates and we compare these patterns of the analogues. To detect ongoing changes, we use ERA5 reanalysis data, comparing past [1950–1985] and present [1987–2022]. To assess future changes, we perform a multi-model study with high-resolution regional models within the EURO-CORDEX program, comparing historical [1970–2000] and future projections [2070–2100] using the Representative Concentration Pathway RCP8.5 from the CMIP5 project, representing the worst-case scenario.

The analysis of detected changes, using ERA5, shows positive precipitation anomalies in the present period compared to the past over or nearby the Emilia Romagna region for the first and third events—the 2nd and 16th of May. Despite biases and limitations, EURO-CORDEX models demonstrate a certain capability to capture event characteristics. However, ERA5 outperforms models in terms of meteorological hazards of the analogues, emphasizing the need for continued improvements in modeling extreme events. The positive precipitation projections identified in some model simulations in the future conditions with compared to the historical simulations suggest a potential influence of climate change, specially for the 2nd and 16th of May. Notably, the event of the 10th of May, the weakest among the three in terms of meteorological hazards and featuring a shallower sea level pressure structure, does not show significant changes in ERA5 and there is higher variability in the future projections among models. Hence, our findings suggest a possible role of climate change potentially for the most impactful events.

Barnes et al. (2023) found no climate change role in the Emilia Romagna flooding events, while our findings suggest a possible role. This apparent discrepancy could stem from differences in the definition of the extreme event, as they use accumulated precipitation in 21 days, or the unconditional framework they employ, potentially mixing different types of drivers. In contrast, our approach assesses the changes in each specific cyclone, conditional to the atmospheric pressure pattern. Hence, one could argue that

the results are not opposing, but rather stem from addressing distinct aspects of the issue.

We use EURO-CORDEX simulations as they have proved better in simulating heavy precipitation events and have shown higher daily precipitation intensities compared to general circulation models (Jacob et al., 2014). However, the simulations used here were driven by CMIP5 models, representing an earlier version of the CMIP experiments, and were conducted a decade ago. While some enhancements have been implemented in the transition from CMIP5 to CMIP6, such as an increase in the intensity of extratropical cyclones in the Northern Hemisphere (Priestley et al., 2020b), a multi-model ensemble of high-resolution regional simulations employing the latest CMIP6 version is currently unavailable. We acknowledge that these limitations underscore the necessity for an updated analysis employing high-resolution models driven by CMIP6 simulations.

Further investigations should delve into discerning the role of internal variability versus forced signals in this multi-model experiment, providing deeper insights into the role of climate change in modulating such extreme precipitation events. Additionally, it is important to note that this approach does not consider compound effects, such as the combination of extremely dry soils right before the first cyclone with subsequent extreme precipitation leading to flooding. Adapting this multivariate approach to encompass compound effects, incorporating additional variables and diverse time frames, offers an interesting direction for future research, and we leave this exploration for subsequent research efforts.

3.3.5 Supplementary material

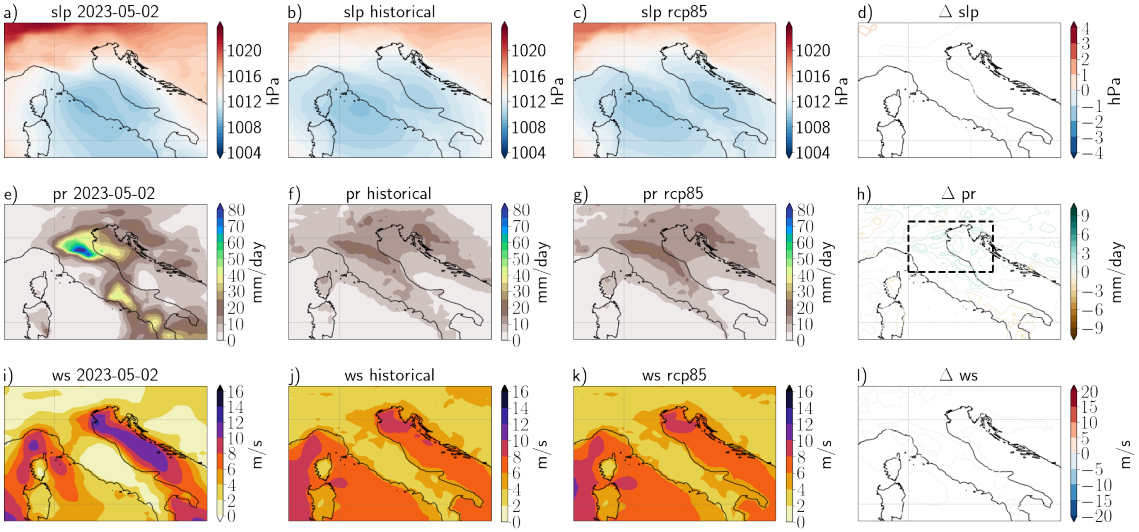

Figure S1: Sea level pressure (a), precipitation (e), and wind speed (i) on the 2nd of May 2023 using ERA5 data. slp composites of the 20 analogue storms for the historical (b) and future (c) simulations using the EURO-CORDEX models, and the corresponding pr (f,g) and ws (j,k) composites. Future minus historical differences of slp, pr and ws are shown in (d,h,l). Shading in shows statistically significant differences. A bootstrap test was conducted with a confidence level of 95%.

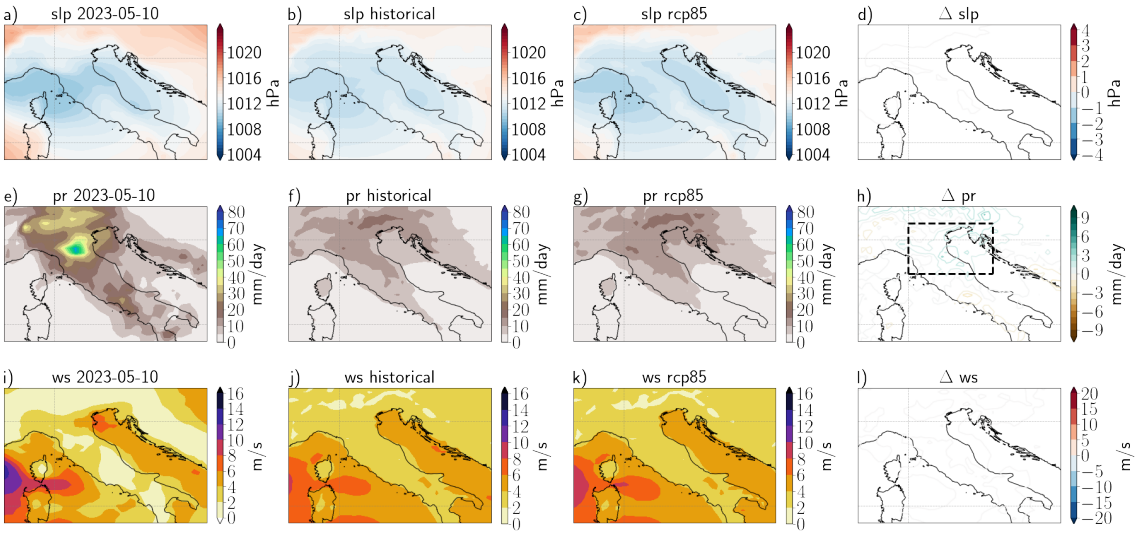

Figure S2: Same as figure S1 but for the 10th of May 2023

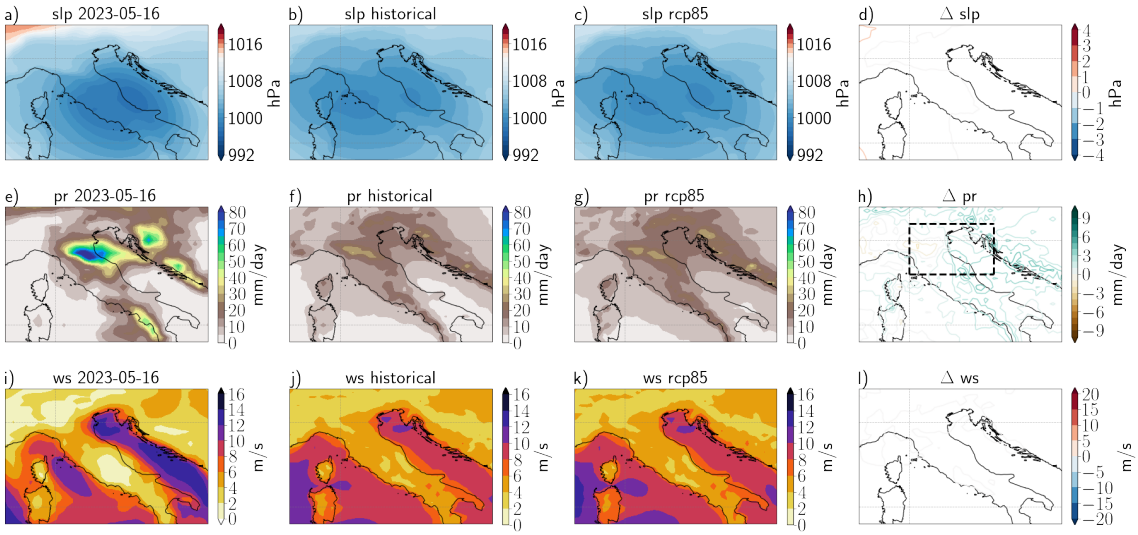

Figure S3: Same as figure S1 but for the 16th of May 2023

3.4 Summary and conclusions

In this chapter, we redefined an analogue of an extreme event by incorporating meteorological hazards alongside the atmospheric circulation pattern. In the first part, we introduced a *pseudo-distance*, defined as a combination of two Euclidean distances: on one side, atmospheric circulation pattern, and on the other side, the combination of meteorological hazards. This methodology was specifically tailored for Acqua Alta events in Venice. It proves particularly useful when considering events primarily defined by mesoscale phenomena, as exemplified in Acqua Alta events where Scirocco winds play a crucial role in elevating water levels.

In the second part, we extended this approach to a more general methodology by introducing a *total Euclidean distance*. This measure assigns equal weight to all variables used in defining an analogue. The broader applicability of this approach is demonstrated through its application to Emilia Romagna high precipitation events. One notable advantage of this methodology lies in its flexibility, allowing for the incorporation of additional variables into consideration. Furthermore, it offers a route to explore defining events arising from compound effects.

This approach proves useful for events like Mediterranean cyclones, which tend to be weaker, smaller in size, and shorter in lifetime compared to North Atlantic extratropical cyclones (Flaounas et al., 2022). Despite their relatively smaller size, these cyclones can have a notable impact at the regional level. Such relatively small cyclones may not be adequately captured, in terms of sea level pressure structure, by the scales resolved in ERA5. Thus, relying solely on sea level pressure for such events might cause us to overlook essential features that made the storms impacts unprecedented.

In the next chapter, we shift our focus to North Atlantic extratropical cyclones. We introduce another framework tailored to identify analogues of explosive cyclones, thereby taking into account not only their high deepening rates but also their distinctive tracks.

Résumé en Français

Dans ce chapitre, nous avons redéfini un analogue d'un cyclone extratropical en intégrant les aléas météorologiques avec la configuration de la circulation atmosphérique. Dans la première partie, nous avons introduit une "pseudo-distance", qui combine deux distances euclidiennes: une pour le champ de pression et une autre pour la combinaison des aléas météorologiques. Cette méthodologie a été spécifiquement développée pour les événements Acqua Alta à Venise et s'avère particulièrement efficace pour les événements influencés par des phénomènes à méso-échelle, tels que les événements Acqua Alta où les vents Sirocco affectent significativement les niveaux marins.

Dans la deuxième partie, nous avons généralisé cette approche en introduisant une "distance euclidienne totale". Cette mesure attribue une importance égale à toutes les variables utilisées pour définir un analogue. Nous appliquons cette approche généralisée aux événements de fortes précipitations en Émilie-Romagne en mai 2023. Un avantage notable de cette méthodologie réside dans sa flexibilité, permettant l'inclusion de variables supplémentaires. De plus, elle offre une voie pour explorer les événements définis par des effets composés.

Cette approche est avantageuse pour des événements tels que les cyclones méditerranéens, qui sont généralement plus faibles, aux dimensions plus modestes et de durée plus courte par rapport aux cyclones extratropicaux de l'Atlantique Nord. Malgré leur taille plus réduite, ces cyclones peuvent avoir des impacts régionaux significatifs. Les échelles résolues dans ERA5 peuvent ne pas capturer de manière adéquate la structure de pression au niveau de la mer de ces cyclones relativement petits. Par conséquent, se fier uniquement à la pression au niveau de la mer pour de tels événements peut conduire à négliger des caractéristiques cruciales qui ont contribué aux impacts sans précédent de ces tempêtes.

Chapter 4

Future projections of Explosive Cyclones in a Changing Climate

Objectives

In this chapter, I use future projections from a single climate model to assess the impact of climate change on specific explosive storms in Europe. The novelty lies in the definition of an analogue, which is based on the development and mature stages of these storms, and in assessing changes in both frequency and magnitude.

Contents

5.1 Overview of the thesis 79
5.2 Limitations and Implications 80
5.2.1 Limitations 80
5.2.2 Implications 81
5.3 Future research directions 82

4.1 Introduction

I had numerous discussions about the methodology employed in Chapter 2 during conferences, workshops, and seminars in my first year of PhD. The two primary concerns were the scarcity of analogues and the potential mismatch in the life stage of the storms when making comparisons. To address these challenges, I refined the analogue methodology by incorporating Lagrangian storm tracks as well as information on the development and mature stages of the storms. In addition, the methodology takes into account the change in frequency of the analogues, rather than specifying a fixed number.

The dataset we used for this study comes from a collaborative work with Dr. Emmanouil Flaounas, a researcher I met in the Future Risks and Impacts of Intense Mediterranean Cyclones Workshop in Baeza, Spain. Flaounas proposed to use a large ensemble of the Community Earth System model, available in the server of his former institution, ETH Zurich. Using a large ensemble of simulations not only alleviated the issue of limited number of analogues but also provided a means to filter out internal variability, allowing a clearer focus on the radiative forcing signal (as suggested by Deser et al. (2012)). The collaboration extended to ETH Zurich, especially with Professor Heini Wernli and his Atmospheric Dynamics group. My visit to ETH Zurich involved discussions with this group and researchers from other groups, as well as access to their server to get the data that I needed.

In the manuscript presented in this chapter (Ginesta et al., 2024), we use the term "storm" as a synonym of "extratropical cyclone." This choice is straightforward: the events under examination are recent extratropical cyclones commonly referred to as storms in the media. As midlatitude storms and extratropical cyclones are considered synonymous in this context (Catto, 2016), I opted to use 'storm' throughout the manuscript to keep things simple and consistent with widely known terminology.

It is important to note that the focus of this study is on the projection of specific events rather than attribution. Unlike attribution studies that examine present and past scenarios or compare worlds with and without climate change, our approach involves projecting the behavior of individual events in a future scenario and compare them with an historical–previously referred to present– climate. Such projections may provide insights for preparing adaptation strategies.

4.2 Article under review in Journal of Climate

The article Ginesta et al. (2024) is currently undergoing its second round of revisions. I included it in the Appendix B.

Ginesta, M., E. Flaounas, P. Yiou, and D. Faranda (2024). "Anthropogenic climate change will intensify European explosive storms similar to Alex, Eunice, and Xynthia in the future". In: Journal of Climate. under review

Extended Summary

The study identifies analogues — storms with similar tracks before reaching their mature stage — of three explosive storms and evaluates changes in frequency and intensity in a future climate. Explosive storms are commonly defined as those deepening by at least 24 hPa in 24 hours at 60°N (Sanders and Gyakum, 1980). The storms, which impacted several western European countries, are Alex (October 2020), Eunice (January 2022), and Xynthia (February 2010). We use a large ensemble of 105 members from the Community Earth System Model version 1 (CESM1). The present climate is represented by historical simulations [1991–2000] and the future climate follows the RCP8.5 scenario from CMIP5 [2091–2101]. Thus, the experiment consist of 1050 years in total for each period.

We first analyzed the ability of the model to reproduce explosive storms. There is an underestimation of storm numbers in the model compared to reanalysis, specially in the ocean. However, this bias is considerably smaller over land. Additionally, the Normalized Deepening Rates (NDR, equation (1) of Ginesta et al. (2024)) of the storms in the model are comparable to those in the ERA5 reanalysis, though the model slightly underestimates the most explosive storms. The comparative analysis, together with assessments by Binder et al. (2023), Dolores-Tesillos et al. (2022), and Joos et al. (2023), gives confidence in the model capability to simulate explosive storms making landfall on the western coast of Europe.

Frequency: We mainly found a decrease in the number of analogues but a relative increase in the number of explosive analogues of storms Alex (Fig. 4.1b,c) and Xynthia, as well as a significant increase in the number of explosive analogues for storm Eunice, in a future climate with respect to the present. In addition, there is an increase of the deepening rates of explosive analogues of Alex (Fig. 4.1b,c) and Xynthia.

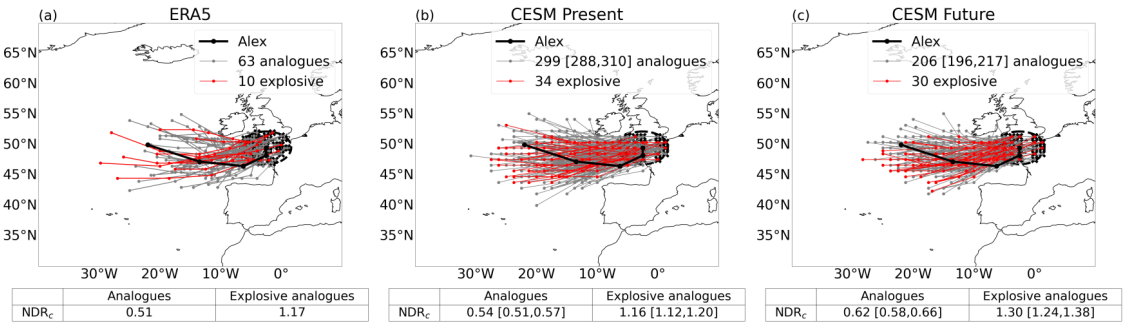

	Analogues	Explosive analogues
NDR_c	0.51	1.17

	Analogues	Explosive analogues
NDR_c	0.54 [0.51,0.57]	1.16 [1.12,1.20]

	Analogues	Explosive analogues
NDR_c	0.62 [0.58,0.66]	1.30 [1.24,1.38]

Figure 4.1: 24-hour track of the development stage of storm **Alex** (thick black line) and its analogues (thin grey lines), for ERA5 (a), CESM present (b), and CESM future (c). Explosive analogues' tracks are highlighted in red. The figure legend shows the number of analogues and explosive analogues. The tables beneath the figures depict the Normalized Deepening Rates. 95 % confidence intervals for CESM present and CESM future, determined using a bootstrap test, are denoted in brackets. This figure corresponds to figure 3 of Ginesta et al. (2024) included in Appendix B.

Meteorological Hazards: Figure 4.2 illustrates the changes observed for storm Alex, including sea level pressure (SLP, a), gradient of equivalent potential temperature ($\Delta\theta_e$, b) to indicate the position of the fronts, precipitation (PR, c), and near-surface wind severity (W, d). We found an increase in total precipitation and wind severity for the explosive analogues of all three storms in a future climate (Fig. 4.2c,d). Specifically, for Alex and Xynthia-like storms, we noted a cyclonic relocation of the weather fronts (e.g. Fig. 4.2b). This suggests a stronger intensification of the storms (consistent with the increase in the deepening rates).

Drivers: For storm Xynthia, we observed no change in low-level baroclinicity during cyclogenesis, but a significant increase in both convective and large-scale precipitation. This suggests that the changes are mainly diabatically driven, resulting from an increase in latent heat that may reinforce the cyclone. On the contrary, Eunice-like storms show a significant increase in low-level baroclinicity during cyclogenesis, suggesting that changes are, at least partially, baroclinically-driven. For storm Alex, there is also an increase, albeit smaller, in baroclinicity.

These findings highlight the potential hazards of explosive storms altered by climate change on western Europe. They offer evidence to support preparation and improve adaptation procedures in the regions.

4.3 Additional analyses

In the following sections, I aim to strengthen the robustness of the findings presented in Ginesta et al. (2024). I provide a comparison with alternative detection and tracking methods (section 4.3.1) and with other CMIP6 models (section 4.3.2). In addition, I present a more general analysis on the concurrences of atmospheric rivers and explosive cyclones over the North Atlantic basin in a future climate, which may offer further understanding of our findings (section 4.3.3).

4.3.1 Tracking comparison

In recent decades, numerous Lagrangian detection and tracking algorithms for extratropical storms have been developed (e.g. Flaounas et al., 2023; Pinto et al., 2005; Sinclair, 1994). Typically, these methods involve the selection of one or more variables for storm identification, with mean sea level pressure or lower tropospheric vorticity being commonly chosen. The selection of the variable depends on the emphasis sought, such as the mass field for mean sea level pressure, which better represents the low-frequency, or the wind field for vorticity, which better represents high-frequency synoptic scale (Hodges et al., 2003; Neu et al., 2013). This variability in selection results in different storm center positions. However, even if the same input variables are used, the storm center positions might differ among methods, due to additional criteria such as thresholds values or gradient fields. To assess the impact of different automated methods on extratropical storm climatologies, Neu et al. (2013) conducted an intercomparison

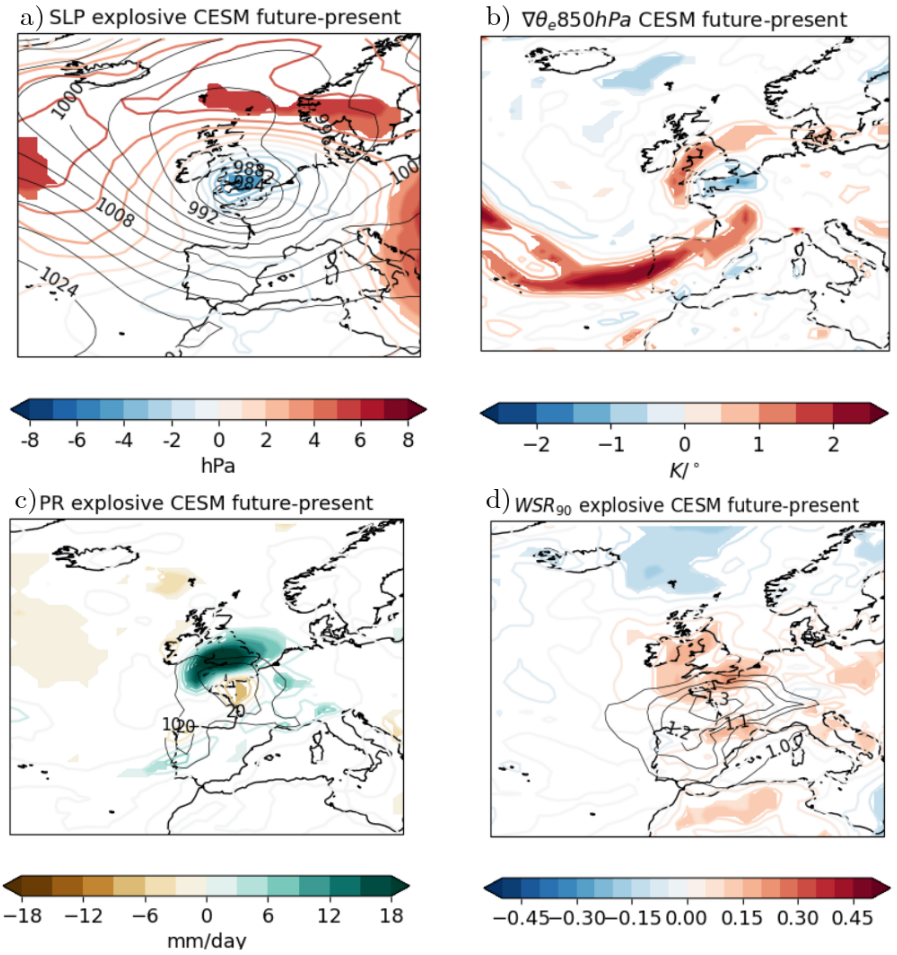

Figure 4.2: Shading: CESM future minus present differences in the composites of **explosive analogues** of storm **Alex** of (g) sea-level pressure, (c) horizontal gradient of equivalent potential temperature at 850 hPa, (h) hourly mean precipitation rate, and (i) hourly mean wind speed. Black contours show the CESM present composites, from 980 hPa and every 4 hPa for SLP, from 10 mm/day and every 5 mm/day for PR, and from 10 m/s and every 2 m/s for W. These figures correspond to figures 9g, 10c, 9h, 9i, of Ginesta et al. (2024) included in Appendix B, respectively.

project involving fifteen international teams. While there is general agreement among methods regarding geographical distribution and interannual variability, significant disparities emerge in total storms numbers and the detection of weaker storms. Better consistency is observed for strong storms.

The methodology employed in Ginesta et al. (2024) is based on Wernli and Schwierz (2006), corresponding to M20 in Neu et al. (2013). Storms are identified as local minima in the SLP field, with a value smaller than that of their eight neighboring grid points. The outermost closed contour is determined by searching for enclosing contours at specific intervals and identified as the one preceding the inclusion of a second local minimum. Then, a straightforward tracking algorithm is used, which predicts the continuation of storms centers based on their positions (Wernli and Schwierz, 2006).

Notably, this method results in a higher number of identified storms than other methods that use more restrictive criteria. Introducing additional criteria, such as a gradient threshold between the SLP minima and its neighbouring points, would reduce the number of identified storms (Haak and Ulbrich, 1996).

Given that our study heavily relies on storm tracks, I opted to compare with two other storm tracking methods: the TempestExtremes software (TE) by Ullrich et al. (2021), and the dataset produced by the "Regional Climate and Weather Hazards" research team led by Prof. Dr. Joaquim Pinto at the Karlsruhe Institute of Technology (KIT), corresponding to the M02 method in Neu et al. (2013). From now on, I refer to M20 to the method used in Ginesta et al. (2024), TE to the TempestExtremes, and M02 to the dataset produced by the group of Prof. Dr. Pinto.

a) TempestExtremes detection and tracking (TE)

I used the TempestExtremes detection and tracking method, an open command-line software developed by Ullrich et al. (2021). This software encompasses two primary functions, **DetectNodes** and **StitchNodes**. The former detects candidates corresponding to local extrema of a given variable; in this case, minimum of SLP. The latter connects candidate points in time to form a track. I adjusted the parameters to detect a minimum of SLP enclosed by a contour of 200 Pa within 6.0° (in degrees great-circle-distance, GCD), candidates within 3.0°GCD of one another are merged, the maximum distance between candidates is 6.0°GCD, cyclone must persist for at least 24 h, cyclones must move at least 6.0°GCD from the start to the end of the track, and the minimum SLP is lower than 1000hPa.

Figure 4.3 shows the 24-hour track of the development stage of the three storms, Alex (a), Eunice (b) and Xynthia (c) (thick black line), and its analogues using the TE method. This would be the equivalent of figures 1, 3, and 5 in the manuscript presented in this chapter. The number of analogues identified for each storm is approximately half of those tracked using the method outlined in the manuscript. As anticipated, the TE method is more restrictive, incorporating additional criteria such as a minimum gradient between the SLP minima and their neighboring points, resulting in fewer storms being detected. However, despite the reduced overall number of storms identified, the ratio of explosive analogues to total analogues remains similar to that observed with the M20 method for storms Alex and Eunice. For Xynthia, the ratio is higher, possibly attributed to a lack of sampling in the alternative method.

Future projections

I further applied the TE algorithm to track storms within the CESM large ensemble. I compare the Figures 3b and 3c from Ginesta et al. (2024), in which we used the M20 method, with figure 4.4, in which we used TE. This supplementary analysis aims to assess potential variations in the frequency changes and meteorological hazards introduced by this new tracking method.

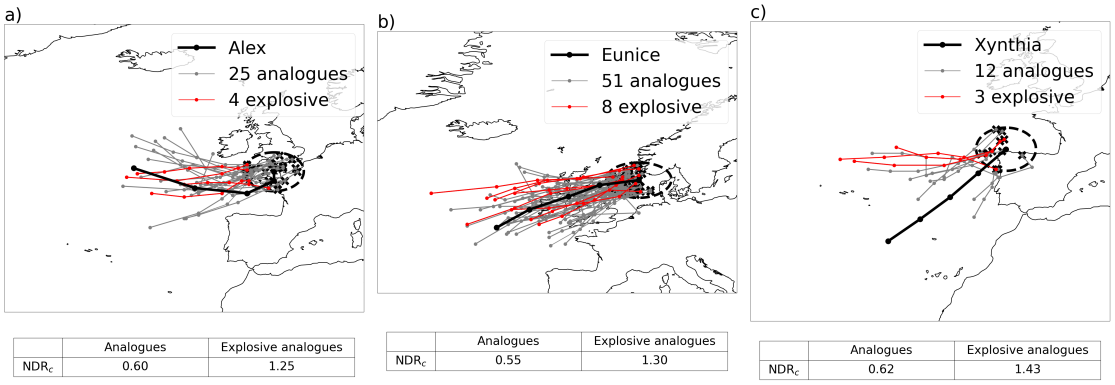

	Analogues	Explosive analogues
NDR_c	0.60	1.25

	Analogues	Explosive analogues
NDR_c	0.55	1.30

	Analogues	Explosive analogues
NDR_c	0.62	1.43

Figure 4.3: 24-hour track of the development stage of storm Alex (thick black line) and its analogues (thin grey lines) for ERA5 for storm Alex (a), Eunice (b), and Xynthia (c), using TE tracking method. Explosive analogues' tracks are highlighted in red. The dashed-line circle indicates the 300-km area used to identify mature stage storms. The figure legend shows the number of analogues and explosive analogues. The tables beneath the figures depict the Normalized Deepening Rate values. These plots would be the equivalent of figures 1a, 3a, and 5a, of the manuscript using M20 tracking method.

Subsequently, figure 4.4 shows the development stages of analogues and explosive analogues during both present (a) and future (b) periods, using the TE method. Consistent with the M20 method, a notable reduction of approximately 30% in the number of analogues is observed in the future period compared to the present. However, there is an increase in the frequency of explosive analogues. Consequently, the ratio of explosive analogues to total analogues rises from around 9% in the present to approximately 16% in the future. This shift in the frequency of explosive storms is slightly higher than that observed with the M20 method, where the ratios were 11% in the present and 15% in the future.

Figure 4.5 shows future minus present differences of the SLP, PR, W of analogues and explosive analogues of storm Alex using the TE tracking method. This figure is similar to Figure 7 (d–i) of the manuscript Ginesta et al. (2024) in which we used the M20 method. The SLP differences of the analogues show lower values in the center of the storms in the future compared to the present, aligning with the findings using the M20 method. No significant differences are observed in the SLP of the explosive analogues, except for a small marginal decrease to the northwest of the storm core. The pattern of PR differences of the analogues closely resembles that of the original analysis, indicating an increase of PR, especially in the northern flank of the storm's core. Similarly, explosive analogues exhibit increased PR in the northern flank and downstream and a decrease in the storm core—a pattern similar to the manuscript's findings, which we suggested to be linked to a weather front relocation. Regarding W, both analogues and explosive analogues exhibit an increase in the western part of the storm's core. However, in the manuscript, the increase in W was located mainly in the northern flank of the storm's core, while in figure 4.5 the increase is upstream, probably in the cold sector of the storms.

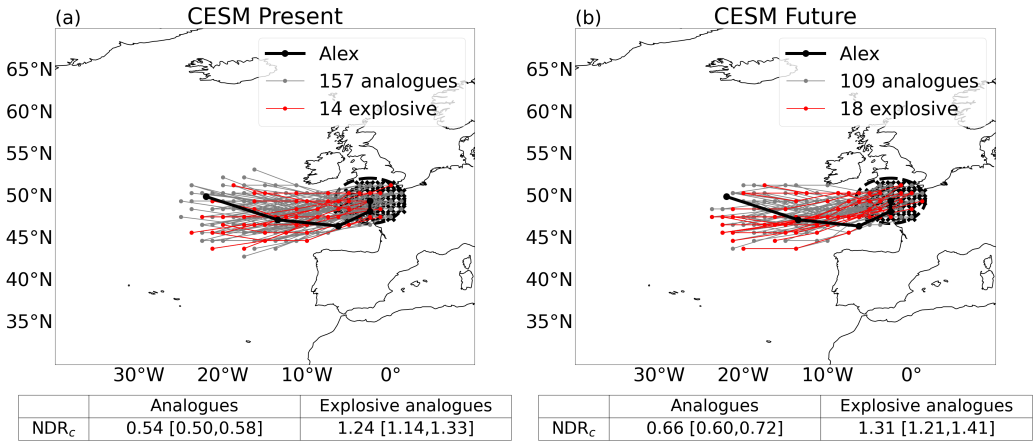

	Analogues	Explosive analogues
NDR_c	0.54 [0.50,0.58]	1.24 [1.14,1.33]

	Analogues	Explosive analogues
NDR_c	0.66 [0.60,0.72]	1.31 [1.21,1.41]

Figure 4.4: 24-hour track of the development stage of storm Alex (thick black line) and its analogues (thin grey lines) for ERA5 for storm Alex for CESM present (a) and CESM future (b) periods using TE tracking method. Explosive analogues' tracks are highlighted in red. The dashed-line circle indicates the 300-km area used to identify mature stage storms. The figure legend shows the number of analogues and explosive analogues. The tables beneath depict the Normalized Deepening Rate values. These plots would be the equivalent of figures 1b,c of the manuscript, in which M20 tracking method was used.

The comparison between the M20 method, as presented in the manuscript, and the TE method reveals consistent outcomes concerning the future-minus-present differences in analogue frequency, along with the spatial pattern and magnitude of pressure and precipitation changes. However, in the context of wind speed, while both methods suggest an increase, there is some variation in the spatial pattern. This highlights the necessity for further analysis, considering other variables such as the position and intensity of weather fronts, to distinguish the differences in wind speed patterns derived from both tracking methods.

b) Mo2 detection and tracking

In addition to the TE method, I conducted a comparative analysis using the storm tracks dataset developed by the "Regional Climate and Weather Hazards" research team led by Prof. Dr. Joaquim Pinto at the Karlsruhe Institute of Technology (KIT), Institute of Meteorology and Climate Research (IMK-TRO). The reanalysis used is ERA5 spanning from 1959 to 2021. The tracking method employed for generating this dataset is detailed in Pinto et al. (2005) and similar to Murray and Simmonds (1991), and corresponds to the M02 method in Neu et al. (2013). The M02 method identifies a maximum in the quasi-geostrophic relative vorticity, computed as the Laplacian of SLP. Candidates are identified as a local minima of SLP within 1200 km of the maximum in vorticity. Candidates over a topography above 1500 m are removed to eliminate potential irregularities introduced by pressure extrapolation. The relative vorticity has to be greater than 0.1 hPa per degree latitude, and they retain only the strongest candidates within a radius

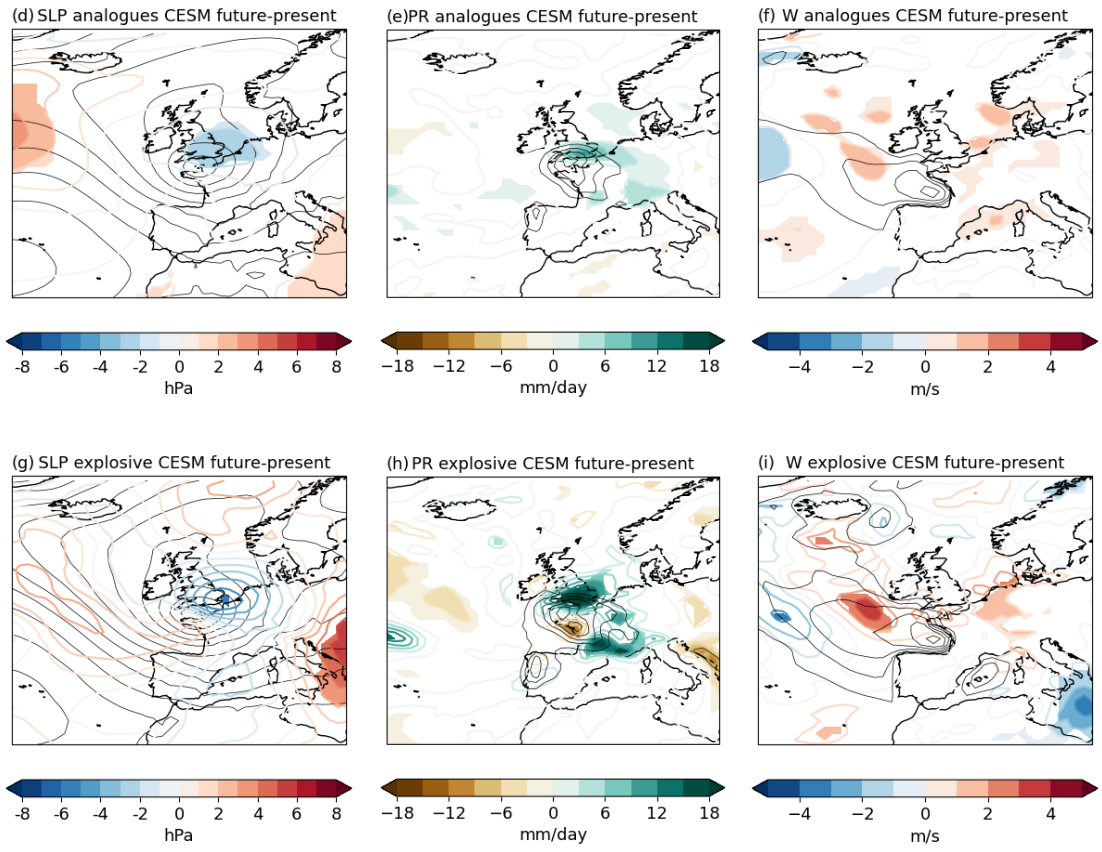

Figure 4.5: Equivalent to figure 7 (d–i) of the manuscript but using TE tracking method to identify analogues.

of 3°. They tracked the candidates using a prediction velocity similar to Murray and Simmonds (1991), with further restrictions such as a minimum lifetime of 24 hours or the system being identified as closed and intense at least once during its lifetime.

Figure 4.6 shows the 24-hour track of the development stage of the three storms, Alex (a), Eunice (b) and Xynthia (c) (thick black line), and its analogues using the storm tracks dataset that follows M02 tracking method. Fewer analogues and explosive analogues are identified with respect to the M20 method. The ratio of explosive analogues to total analogues is slightly lower than the two other methods, M20 and TE, and specially lower than TE for storm Xynthia.

c) Analogues quality comparisons between M20, TE, and M02

Figure 4.7 shows the analogues quality, computed as the euclidean distance between the analyzed storm and its analogues averaged over their 4 grid points, for Alex (a), Eunice (b), ad Xynthia (c). M20 shows larger variability of the analogues quality in all cases, and overall the analogues quality is lower than in the other two methods. This discrepancy may stem from the detection of more mature stage storms in M20

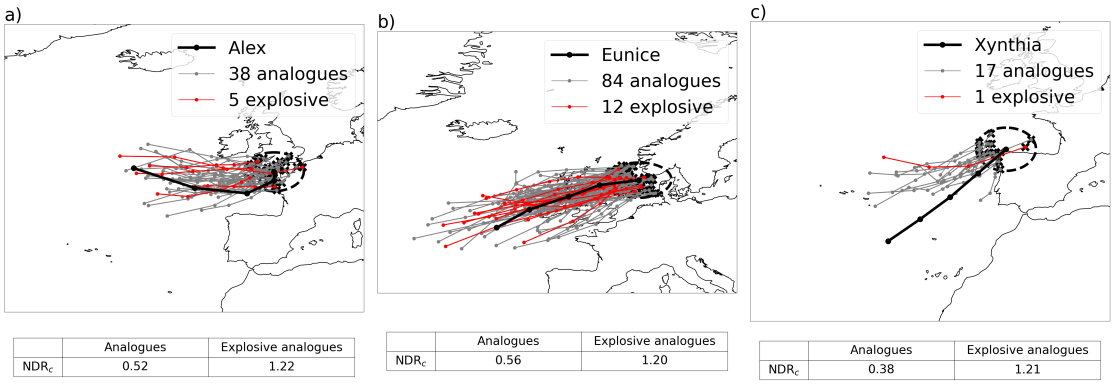

	Analogues	Explosive analogues
NDR_c	0.52	1.22

	Analogues	Explosive analogues
NDR_c	0.56	1.20

	Analogues	Explosive analogues
NDR_c	0.38	1.21

Figure 4.6: 24-hour track of the development stage of storm Alex (thick black line) and its analogues (thin grey lines) for ERA5 for storm Alex (a), Eunice (b), and Xynthia (c), using TE tracking method. Explosive analogues' tracks are highlighted in red. The dashed-line circle indicates the 300-km area used to identify mature stage storms. The figure legend shows the number of analogues and explosive analogues. The tables beneath the figures depict the Normalized Deepening Rate values. These plots would be the equivalent of figures 1a, 3a, and 5a of the manuscript, in which M20 tracking method was used.

that originate from diverse locations. Consequently, when selecting the 20% closest analogues, the resulting tracks are more diverse. M02 emerges as the method yielding better analogues, characterized by lower distances and consequently higher analogues quality.

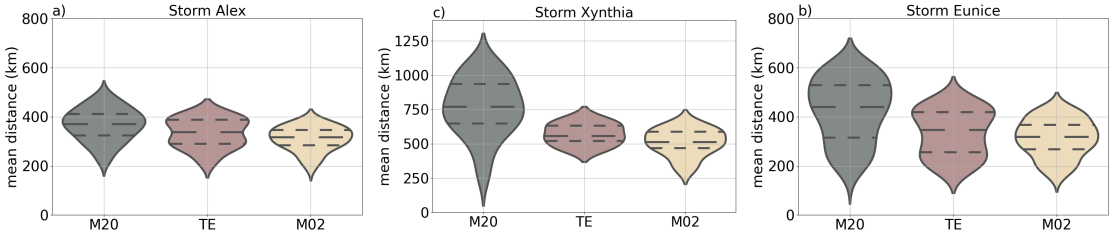

Figure 4.7: Mean Euclidean distances between the 24–hour track of the development stage of storm Alex and its analogues for ERA5 using three tracking methods, M20, TE, and M02, for storm Alex (a), storm Eunice (b), and storm Xynthia (c).

d) Conclusion

To summarize, while the M20 method identifies a greater number of analogues compared to TE and M02, the ratios of explosive analogues to total analogues remain relatively consistent across all methods, indicating robustness in the essential findings. Additionally, the comparison between the M20 method and TE method reveals consistent results in terms of future-minus-present differences in frequency and in the spatial pattern and magnitude of pressure and precipitation changes.

4.3.2 CMIP6 comparison

To assess the sensitivity of trends in number of analogues to the chosen climate model and future scenario, I conducted an analysis based on simulations available in the laboratory's server of different climate models. This encompassed simulations that provided 6-hourly output instantaneous sea level pressure data. In addition, data had to be available for historical period [1982–2013] as well as for the mid and end of the century [2021-2060, 2060–2100] for both SSP2-4.5 and SSP5-8.5 scenarios from CMIP6.

As showed in the previous section, the outcomes are relatively robust to storm tracking methodologies. Consequently, the initial step involves tracking all storms using the TempestExtremes software, as outlined in the preceding section. The list of models and runs used are shown in table 4.1.

GCM	**Runs**	**Nominal atmospheric resolution**
ACCESS-CM2	r1	250 km
BCC-CSM2-MR	r1	100 km
EC-Earth3	r1, r4	100 km
MPI-ESM1-2-HR	r1, r2	100 km
MPI-ESM1-2-LR	r1, r2, r3, r4, r5, r6, r7, r8, r9, r10	250 km

Table 4.1: List of General Circulation Models (GCM) and runs used with their respective nominal atmospheric resolutions.

For the comparative analysis, I initially calculated the number of mature stage storms and then identified the 20% closest tracks to define analogues. The resulting count represents the number of analogues. It is important to note that, in this context, I adjusted the diameter used to define mature stage storms to 500 km. This adjustment was made to slightly relax the criteria for mature stage storms, in order to facilitate the identification of more storms and enhance statistical robustness.

Figure 4.8 depicts the percentage change in the number of analogues across different CMIP6 runs relative to the historical period. The dashed black line represents the corresponding percentage change observed in the CESM large ensemble under the RCP8.5 scenario found in Ginesta et al. (2024). In the SSP2-4.5 scenario, there is greater variability among models for the three storms, specially in the 2020-2061 period, which could be attributed to a smaller signal-to-noise ratio of the forcing signal versus internal variability. Overall, there is agreement among models for storms Alex and Xynthia in the SSP5-8.5 scenario, indicating a decline in the number of analogues in the future scenarios. Results for Eunice also show overall agreement among models, with most of them projecting minor changes or a decrease. However, some models show a more substantial decrease in the number of analogues than the CESM large ensemble, reaching up to a 20% in certain cases.

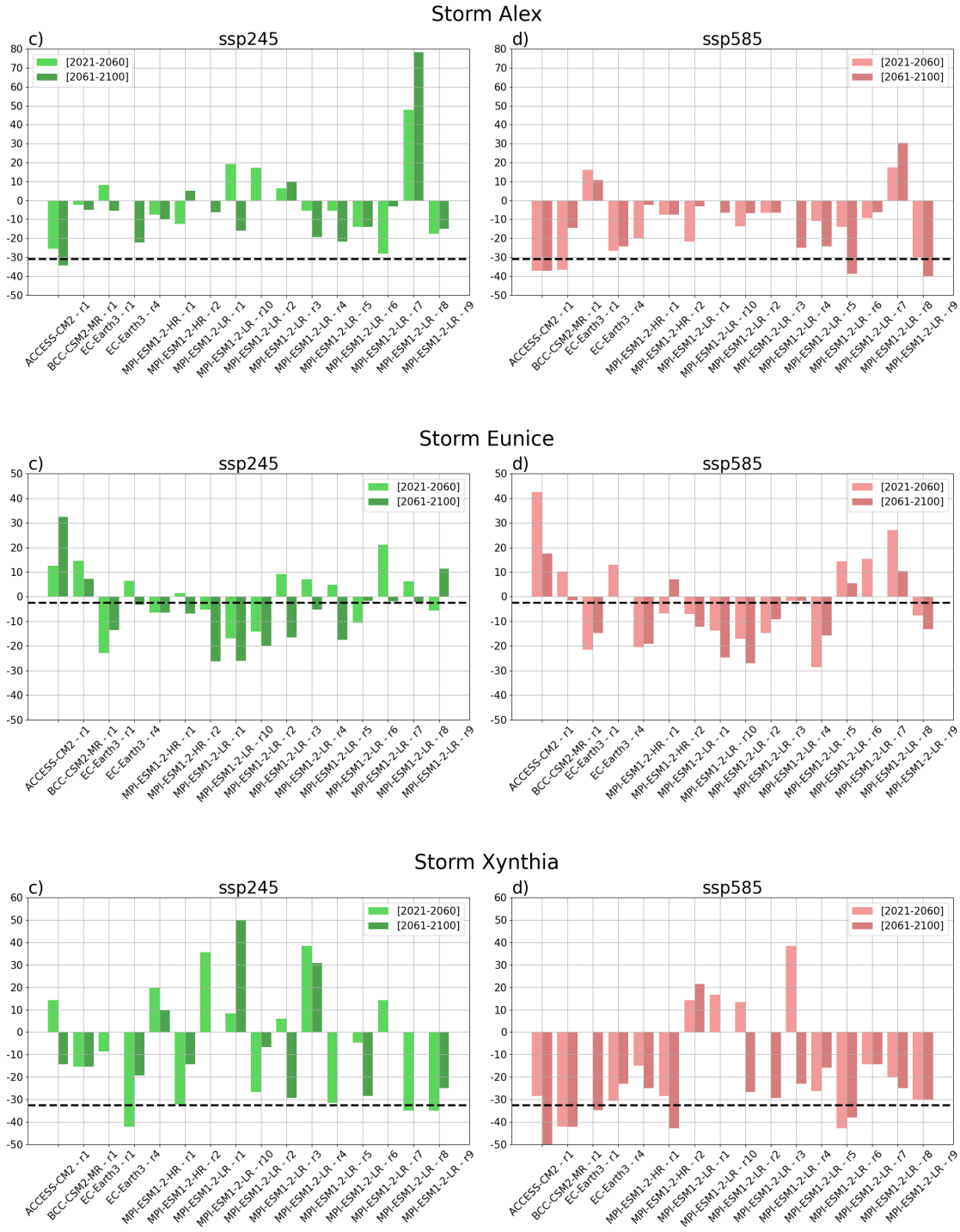

Figure 4.8: Percentage change in the number of analogues for 16 CMIP6 runs under the SSP2-4.5 (a) and SSP5-8.5 (b) scenarios, computed with reference to the historical period [1986-2013]. The analysis covers two future periods: mid-century [2021-2060] and end of the century [2061-2100]. The black dashed line represents the percentage change in the end-of-century period [2091-2100] for the CESM large ensemble under the RCP8.5 scenario, as reported in the manuscript.

4.3.3 Concurrences with atmospheric rivers

Some of the explosive storms analyzed were associated with atmospheric rivers (AR), such as Storm Alex (Davolio et al., 2023) or storm Xynthia (Fig. 4.9). In this section, I explore the relationship between explosive storms and atmospheric rivers in a changing climate in the North Atlantic basin. I present some of the findings of a study that I am co-leading with Ferran Lopez Marti, PhD student from Uppsala University, as part of the European EDIPI project. Data and methods are detailed in the supplementary chapter C.

According to the Glossary of Meteorology of the American Meteorological Society, ARs are "a long, narrow, and transient corridor of strong horizontal water vapour transport that is typically associated with a low-level jet stream ahead of the cold front of an extratropical cyclone" (Ralph et al., 2018). When forced upwards, such as by topography or embedded in the warm conveyor belt of ETCs, they can produce extreme rainfall. Explosive ETCs are often associated with ARs, which may play a key role in the rapid deepening of the cyclone through latent heat release (Eiras-Barca et al., 2018).

We employ the TempestExtremes algorithm to detect and track ARs. We identify ridges on the integrated water vapor transport (IVT), with a minimum IVT value set at 250 kg m^{-1} s^{-1} and a minimum area of 4×10^5 km^{-2}. Additional requirements are outlined in the supplementary chapter C.

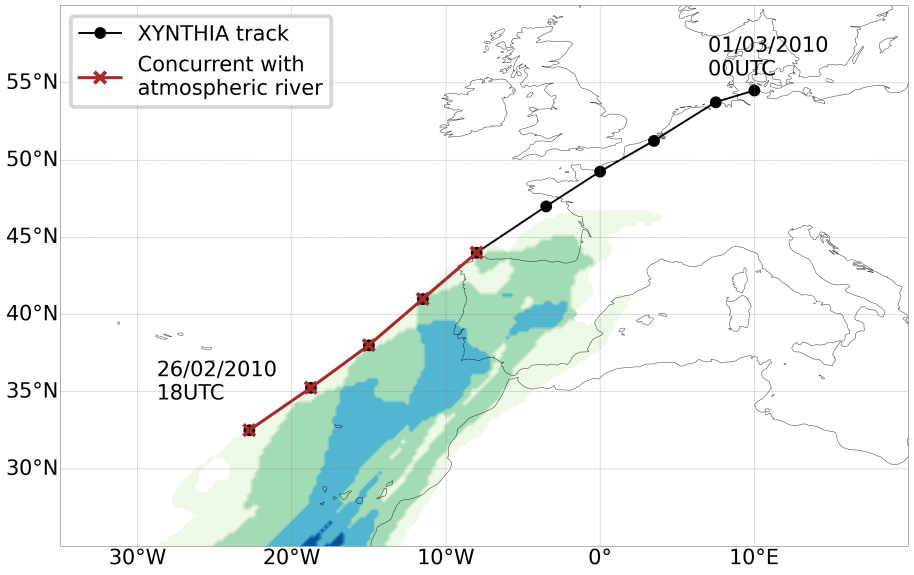

Figure 4.9: Detection and tracking of explosive storm Xynthia and its associated atmospheric river. Red indicates concurrent time steps with the atmospheric river and explosive development of the storm, in black the subsequent time steps. The shading represents the overlaying atmospheric river masks for each timestep, with darker colors indicating overlapping over timesteps.

Figure 4.10a shows the ratio between the number of explosive storms with ARs and

the total number of explosive storms in the North Atlantic basin for ERA5 and CMIP6 models for the historical period [1980–2009]. The highest ratio occurs 6 hours after the maximum deepening point (MDP) of the storm. In ERA5, the ratio at the MDP is approximately 0.6, indicating that 60% of the explosive ETCs are associated with an AR. However, all models tend to overestimate the ratio of explosive ETCs with AR.

The discrepancies between ERA5 and models may arise from biases in model performance or from internal variability. The computation of the IVT for the detection and tracking of ARs may introduce additional biases. We calculated IVT using specific pressure levels, while the IVT from ERA5 was obtained directly from the publicly available data on the Copernicus server. We are currently refining this process to ensure direct comparability among them.

Figure 4.10b shows the ratio for the historical period and future projections [2070-2099] under different scenarios. There is an almost linear increase in future projections with respect to the historical climate, with the lowest increase for the SSP1-2.6 (best-case scenario) and the highest for the SSP5-8.5 (worst-case scenario). In the latter, the multi-model mean reaches maximum values of 0.83, indicating that few hours after the MDP, 83% of the explosive cyclones will be associated with an atmospheric river.

Figure 4.11 shows the spatial distribution of the change in the ratios for western Europe. There is a linear increase in future scenarios, with the highest increase for the SSP5-8.5 scenario. Additionally, there is an increase in the level of agreement among models; under the SSP5-8.5 scenario, all models show an increase over most of Western Europe.

This analysis offers an overview of the changes in the statistical relationship between explosive storms and atmospheric rivers in a future climate. There is an increasing trend towards a higher number of atmospheric rivers associated with explosive storms, especially in the worst-case scenario, on the western European coast. An increase of atmospheric rivers associated implies an increase in the water vapor content of the storm, and thus a possible increase in precipitation. Hence, the findings we found for specific explosive storms may follow the general changes in the North Atlantic basin.

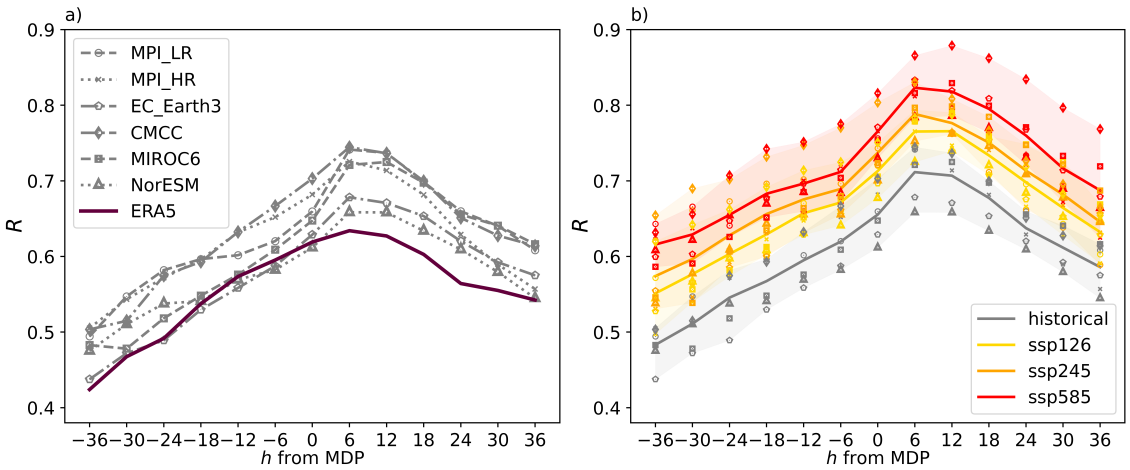

Figure 4.10: a) Ratio (R) between the number of explosive storms with atmospheric river and the total number of explosive storms as a function of the time distance to the Maximum Deepening Point (MDP) for ERA5 and the historical period of CMIP6 models [1980–2009]. b) R for the CMIP6 models for the historical period and the future period [2070–2099] for the scenarios SSP1-2.6, SSP2-4.5, and SSP5-8.5.

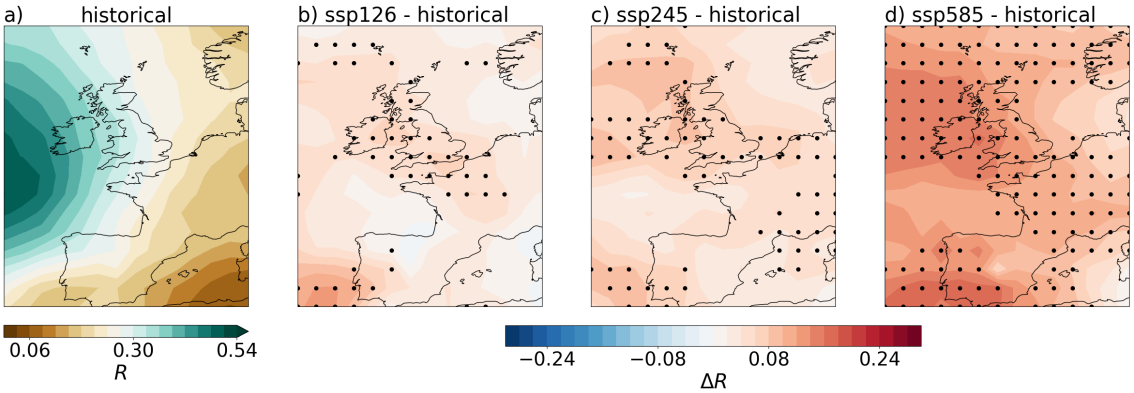

Figure 4.11: a) Ratio (R) between the number of explosive storms with AR and the total number of explosive storms for the multi-model mean of CMIP6 historical period. b–d) Differences in R between the future scenarios and the historical period. Dots indicate the grid points where all six models agree on the sign.

4.4 Summary and conclusions

This chapter has presented a method for isolating the impact of anthropogenic forcing on specific impactful storms, assessing the frequency in two climates, present and future, as well as the meteorological hazards when they make landfall. In addition, two additional tracking methods have been compared, and found similar output. Single runs of other models and scenarios have been used to assess trends in the frequency of the analyzed storms, finding overall agreement among simulations. Finally, an increase in CMIP6 future scenarios of the occurrences of explosive storms with atmospheric rivers in the North Atlantic basin has been found.

Throughout various seminars and conferences where I have presented this work, there has been a recurring expectation for a more generalized analysis that would involve the analysis of numerous storms and the depiction of overarching trends on a geographical map. It is important to clarify that the primary focus of this project lies in the in-depth projection of specific severe storms, rather than a large-scale analysis of a large set of storms. However, automating the methodology to systematically analyze various storms and discern common patterns could provide invaluable insights into the diverse behaviors of storms across different regions. This would be different from the general trends analysis, such as those in Zappa et al. (2013) and Priestley and Catto (2022), in the sense that here we focus on the selection of storms with similar development stages, and we take observed large impactful storms as reference. Therefore, this study could offer more specific insights into storm behavior, such as the relocation of weather fronts observed in Alex and Xynthia, which may be common in certain regions or types of storms — an aspect not assessed in previous studies.

Résumé en Français

L'objectif de cette étude est de projeter des tempêtes spécifiques dans le futur. Contrairement aux études d'attribution qui examinent les scénarios actuels et passés, ou comparent des mondes avec et sans changement climatique, notre approche consiste à projeter le comportement d'événements individuels dans un scénario futur et à les comparer à un climat historique (ou présent). De telles projections peuvent offrir des clés pour préparer des stratégies d'adaptation. Cet article est basé sur un manuscrit en cours de révision dans le Journal of Climate intitulé "Athropogenic climate change will intensify European explosive storms similar to Alex, Eunice, and Xynthia in the future".

L'étude identifie des analogues — des tempêtes avec des trajectoires similaires avant d'atteindre leur stade mature — de trois tempêtes explosives et évalue les changements de fréquence et d'intensité dans un climat futur. Les tempêtes explosives sont couramment définies comme celles qui s'approfondissent d'au moins 24 hPa en 24 heures à 60°N. Les tempêtes qui ont impacté plusieurs pays d'Europe occidentale sont Alex (octobre 2020), Eunice (janvier 2022) et Xynthia (février 2010). Nous utilisons un grand ensemble de 105 membres du Community Earth System Model, version 1 (CESM1). Le climat actuel est représenté par des simulations historiques [1991-2000] et le climat futur suit le scénario RCP8.5 du CMIP5 [2091-2101]. Ainsi, l'expérience comprend un total de 1050 années pour chaque période.

Nous avons d'abord analysé la capacité du modèle à reproduire les tempêtes explosives. Il y a une sous-estimation du nombre de tempêtes dans le modèle par rapport à la réanalyse, notamment au-dessus l'océan. Cependant, ce biais est considérablement plus faible sur les terres. De plus, les taux d'approfondissement normalisés des tempêtes dans le modèle sont comparables à ceux de la réanalyse ERA5, bien que le modèle sous-estime légèrement les tempêtes les plus explosives. L'analyse comparative donne confiance dans la capacité du modèle à simuler les tempêtes explosives touchant la façade ouest de l'Europe.

En termes de fréquence, nous avons principalement observé une diminution du nombre d'analogues, mais une augmentation relative du nombre d'analogues explosifs des tempêtes Alex et Xynthia, ainsi qu'une augmentation significative du nombre d'analogues explosifs pour la tempête Eunice, dans un climat futur par rapport au présent. Nous avons également observé une diminution de la pression au niveau de la mer des analogues explosifs pour les trois cyclones. En ce qui concerne les aléas météorologiques, nous avons observé une augmentation des précipitations et de la sévérité du vent dans les trois tempêtes dans le climat futur par rapport au présent.

Chapter 5

Conclusions

5.1 Overview of the thesis

I began this thesis by outlining the emergence of Extreme Event Attribution, a relatively recent field aimed at understanding the influence of climate change on extreme events, with potential applications such as compensation for damages. Subsequently, I introduced various methodological approaches that have evolved over time, presenting them along a spectrum ranging from unconditional to conditional to the dynamics leading to the observed extremes. I emphasized the limitations of each approach and highlighted their complementary nature when combined. Additionally, I explored diverse event definitions, considering hazards, dynamics, and impacts.

Because of its novelty, the conditional approach is relatively less studied than the unconditional approach. For instance, more attention has been given to evaluating how climate change has influenced the frequency of observed wet and windy extremes, rather than analyzing how the phenomenon that leads to such extremes – such as an explosive cyclone – has changed in a warmer world. Hence, this thesis aims to address this precise question: how climate change influences the dynamics, magnitude, or frequency of certain observed extratropical cyclones that lead to wet and/or windy extremes. To investigate the impact of climate change on extratropical cyclones through a conditional approach, we rely primarily on the analogues approach to identify cyclones resembling those observed in two distinct climates. The first research question introduced in this thesis was: ***Q1*** *How can we define an analogue of an extratropical cyclone?* Each chapter explores a different definition of an analogue.

In Chapter 2, we address ***Q2****: Can we identify ongoing changes in the meteorological hazards, such as precipitation and wind speed, in a severe ETC?* We introduced a methodology wherein we define an analogue of an extratropical cyclone based on its synoptic sea level pressure pattern. Using Storm Alex in early October 2020 as a case study, we observed that Alex-like storms in a more recent climate, characterized by higher anthropogenic emissions, resulted in increased local precipitation in regions most affected by heavy rainfall, compared to a past climate. We found a deepening

of cyclones at low levels in the present climate. Additionally, using dynamical system metrics, we observed an increase in the persistence of storms.

Chapter 3 addresses ***Q3****: How can we apply the analogues approach in ETCs that occur in regions of complex topography and are associated with heavy rainfall or strong winds regionally?* We presented a multivariate approach, where we define an analogue based on both its sea level pressure pattern (dynamics) and precipitation and wind speed (meteorological hazards). For the first Emilia-Romagna flooding event, we observed increased precipitation locally in a more recent climate compared to the past. Future projections using high-resolution regional models showed an overall agreement for the last flooding event, indicating an increase in precipitation over the region in a future climate. However, there was less agreement regarding the first two events.

In Chapter 4, we address ***Q4****: How will some North Atlantic explosive ETCs that had strong impacts in Europe change in a future climate in terms of frequency and magnitude?* We identify analogues of the development stage of cyclones in present and future projections using a general circulation model. Focusing on three explosive cyclones that hit Western Europe in recent decades, we found that in the future world, these cyclones are associated with higher precipitation and wind speed. Moreover, we found an increase in the frequency of the explosive analogues. For two of them, we observed a clear cyclonic relocation of weather fronts, suggesting an increase in the deepening rate of the cyclones over the ocean.

Throughout the thesis, we have thus used three definitions for identifying an analogue of an extratropical cyclone. In dynamical system metrics, analogues are defined as the points in the vicinity of a specific point in phase space, corresponding to an instantaneous atmospheric state. Hence, by changing the definition of an extreme extratropical cyclone, we change the entire phase space. For instance, in the multivariate approach presented in Chapter 3, our phase space is defined by sea level pressure, precipitation, and wind speed, thus defining analogues as those that are similar in terms of these variables. Consequently, the definition of an analogue is inherently tied to the definition of the extreme extratropical cyclone itself. This underscores the subjective nature of defining analogues, as it is intrinsically linked to our interpretation of what makes a cyclone characteristic, as well as the criteria we use to define it effectively.

5.2 Limitations and Implications

5.2.1 Limitations

Several limitations must be considered regarding the results and analyses presented in this study. Firstly, in Chapter 2, we relied on ERA5 data to assess ongoing trends in Storm Alex. Although ERA5 is one of the most advanced reanalyses available, it is not a direct representation of reality. Moreover, limitations exist in the number of analogues available for analysis. Additionally, isolating the climate change signal from internal variability remains challenging, even with 35-year average-periods. While efforts were made to mitigate this limitation by assessing changes in internal variability indices, the

influence of internal variability on the trends observed cannot be entirely ruled out.

In Chapter 3, a multivariate approach was employed, again using ERA5 data to analyze trends in specific Mediterranean cyclones. Similar limitations to those outlined in Chapter 2 apply here, in addition to the relatively short 30-year periods used in Euro-CORDEX simulations. In addition, we did not consider other factors at play in driving extremes, such as extremely dry soil conditions before rainfall for some events, and saturation for some others.

Lastly, Chapter 4 used a large ensemble of the CESM model to better isolate the climate change signal from internal variability. While this approach offers robustness due to the extensive simulations, and even if previous studies have demonstrated the CESM model's reliability in simulating extratropical cyclones in the North Atlantic, it is important to note that results may vary in other models.

5.2.2 Implications

While these findings may not be directly applicable to all cyclones or regions, they align closely with previous research on changes in extratropical cyclones in a warmer world (Dolores-Tesillos et al., 2022; Priestley and Catto, 2022; Seiler and Zwiers, 2016; Zappa et al., 2013). Most notably, these studies indicate an increase in precipitation associated with cyclones in warmer climates, alongside a general decrease in storm numbers but localized increases near the British Isles. Some also suggest heightened cyclone-associated wind speeds.

What sets this study apart is its focus on assessing a single extratropical cyclone. Given the chaotic nature of the atmosphere and climate system, each cyclone is unique, resulting from a combination of various baroclinic and diabatic processes, further influenced by regional characteristics such as topography. While broader studies averaging different factors across various cyclones are crucial for understanding general trends, the specificity of our analysis offers valuable insights. By dissecting the characteristics and behaviour of a single cyclone, we can gain deeper insights into the impacts of climate change on specific meteorological phenomena.

Demonstrating that specific extratropical cyclones leading to extreme wet or windy conditions have been enhanced by climate change, or are more likely to occur, is crucial information specially for local residents and policymakers. It raises awareness of how climate change can impact tangible and direct events, such as extreme weather, beyond global mean temperature increases. Moreover, it offers practical applications, such as information for potential resilience-building measures. For instance, if we anticipate that cyclones like Eunice will become more frequent and severe, communities may choose to reinforce infrastructures accordingly.

5.3 Future research directions

Addressing the limitations identified in this thesis opens the opportunity for future research to further advance our understanding of the influence of climate change on observed extratropical cyclones. One of the main limitations stems from the limited number of analogues, attributed to the constrained temporal coverage. Hence, one could use an ensemble of simulations to address this issue. This approach would automatically imply a better assessment of the role of internal variability in driving the changes observed.

Incorporating additional variables in the multivariate approach presents another promising direction for future research. By expanding the set of variables used to define extreme events, such as incorporating measures of atmospheric moisture content or vertical wind shear, we can better capture the complex dynamics driving cyclone development and intensity. This would enable a more precise identification of analogues that closely match the conditions associated with such extremes. Furthermore, we could explore changes in the frequency of such analogues, rather than restricting our analysis to change in magnitude of hazards.

Furthermore, many of these events involve small-scale processes that are not well-captured in current models or reanalyses. Using convection-permitting simulations, which better resolve convective processes crucial to short-duration extremes, could address this limitation.

For future projections, a promising approach is to combine the meteorological hazards found with changes in adaptation to assess impacts, similar to what was proposed by Visser et al., 2014. For example, incorporating possible scenarios of radiative forcing as well as scenarios of adaptation, and then assessing in detail the differences among the combinations. This approach would involve translating scientific insights into actionable information. I see this interdisciplinary approach not only bridging the gap between scientific research and real-world applications but also providing directly applicable information to policymakers.

Advancements in machine learning techniques hold promise for enhancing our modeling capabilities and optimizing our techniques. For example, in the context of this thesis, machine learning techniques could improve the assessment of the domain used to find analogues, determine which variables to include, or optimize the selection of analogues.

Finally, I believe that we should put more efforts to observe, model, and expand our analysis of extremes to the Global South. It is crucial that we deepen our understanding of the consequences of climate change for the most vulnerable populations. Personally, I see Extreme Event Attribution as a potential tool to support loss and damage processes at a large scale. By focusing on these regions and communities, we can not only enhance our scientific understanding but also contribute to more equitable and effective responses to the challenges posed by climate change.

Résumé en Français

La première question de recherche introduite dans cette thèse était: ***Q1*** *Comment pouvons-nous définir un analogue d'un cyclone extratropical (CET)?* Chaque chapitre explore une définition différente d'un analogue. Dans le chapitre 2, nous abordons ***Q2****: Pouvons-nous identifier des changements en cours dans les dangers météorologiques, tels que les précipitations et la vitesse du vent, lors d'un CET sévère?* Nous avons introduit une méthodologie où nous définissons un analogue d'un cyclone extratropical en fonction de sa configuration synoptique de pression au niveau de la mer. Le chapitre 3 aborde ***Q3****: Comment pouvons-nous appliquer l'approche des analogues dans les CET qui surviennent dans des régions à topographie complexe et sont associés à des précipitations abondantes ou à des vents forts à l'échelle régionale?* Nous avons présenté une approche multivariée, où nous définissons un analogue basé à la fois sur son schéma de pression au niveau de la mer (dynamique) et sur les précipitations et la vitesse du vent (dangers météorologiques). Dans le chapitre 4, nous abordons ***Q4****: Comment certains CET explosifs de l'Atlantique Nord ayant eu un fort impact en Europe changeront-ils dans un climat futur en termes de fréquence et d'intensité?* Nous identifions des analogues du stade de développement des cyclones dans les projections actuelles et futures à l'aide d'un modèle de circulation générale. En nous concentrant sur trois cyclones explosifs ayant frappé l'Europe occidentale au cours des dernières décennies, nous avons constaté que dans le monde futur, ces cyclones sont associés à des précipitations et à des vitesses de vent plus élevées.

Limitations et Implications

Plusieurs limitations doivent être prises en compte concernant les résultats et analyses présentés dans cette étude. La principale concerne le nombre limité d'années et d'analogues pour les chapitres 2 et 3. Isoler le signal du changement climatique par rapport à la variabilité interne reste difficile, même avec des périodes moyennes de 35 ans. Bien que des efforts aient été déployés pour atténuer cette limitation en évaluant les changements dans les indices de variabilité interne, l'influence de la variabilité interne sur les tendances observées ne peut être entièrement écartée. Pour le chapitre 4, nous avons utilisé un seul modèle; il est important de noter que les résultats peuvent varier dans d'autres modèles.

Ce qui distingue cette étude est son focus sur l'évaluation d'un seul cyclone extratropical. Étant donné la nature chaotique de l'atmosphère et du système climatique, chaque cyclone est unique, résultant d'une combinaison de divers processus barocliniques et diabatiques, influencés davantage par des caractéristiques régionales telles que la topographie. Alors que les études plus larges qui moyennent différents facteurs à travers divers cyclones sont cruciales pour comprendre les tendances générales, la spécificité de notre analyse offre des perspectives supplémentaires. En analysant les caractéristiques et le comportement d'un seul cyclone, nous pouvons obtenir des informations plus precises sur les impacts du changement climatique sur des phénomènes météorologiques spécifiques.

Démontrer que des cyclones extratropicaux spécifiques entraînant des conditions extrêmement humides ou venteuses ont été renforcés par le changement

climatique, ou sont plus susceptibles de se produire, est une information crucial notamment pour les résidents locaux et les décideurs. Cela sensibilise à la manière dont le changement climatique peut affecter des événements tangibles et directs, tels que les phénomènes météorologiques extrêmes, au-delà de l'augmentation moyenne mondiale des températures. De plus, cela offre des applications pratiques, telles que des informations pour des mesures potentielles de renforcement de la résilience au changement climatique.

Orientations futures de la recherche

Une des principales limitations découle du nombre limité d'analogues; il serait donc opportun d'utiliser un ensemble de simulations pour aborder cette question. De plus, les simulations qui résolvent les processus convectifs cruciaux pour les événements extrêmes de courte durée pourraient être utilisées, car elles simulent mieux les cyclones de méso-échelle. Pour les projections futures, une approche prometteuse consiste à combiner les risques météorologiques identifiés avec les projections d'adaptation au changement climatique, afin de les évaluer ainsi que d'évaluer l'impact total.

Je pense que nous devrions déployer davantage d'efforts pour observer, modéliser et étendre notre analyse des extrêmes vers le Sud Global. Il est crucial d'approfondir notre compréhension des conséquences du changement climatique pour les populations les plus vulnérables. Personnellement, je considère l'Attribution d'Événements Extrêmes comme un outil potentiel pour soutenir les processus de pertes et dommages à grande échelle. En nous concentrant sur ces régions et ces communautés, nous pouvons non seulement améliorer notre compréhension scientifique, mais aussi contribuer à des réponses plus équitables et efficaces aux défis posés par le changement climatique.

References

Afargan, H. and Y. Kaspi (2017). "A Midwinter Minimum in North Atlantic Storm Track Intensity in Years of a Strong Jet". In: *Geophysical Research Letters* 44.24, pp. 12, 511–12, 518. DOI: https://doi.org/10.1002/2017GL075136 (→ page 15).

Allen, M. (2003). "Liability for climate change". In: *Nature* 421.6926, pp. 891–892 (→ pages 2, 3).

APNews (2023). *Oregon youths' climate lawsuit against US government can proceed to trial, judge rules*. Accessed on: February 25, 2024 (→ page 10).

Barnes, C., D. Faranda, E. Coppola, F. Grazzini, M. Zachariah, et al. (2023). "Limited net role for climate change in heavy spring rainfall in Emilia-Romagna". In: DOI: https://doi.org/10.25561/104550 (→ pages 43, 54).

Bell, B., H. Hersbach, A. Simmons, P. Berrisford, P. Dahlgren, et al. (2021). "The ERA5 global reanalysis: Preliminary extension to 1950". In: *Quarterly Journal of the Royal Meteorological Society* 147.741, pp. 4186–4227. DOI: https://doi.org/10.1002/qj.4174 (→ page 19).

Binder, H., M. Boettcher, H. Joos, and H. Wernli (2016). "The Role of Warm Conveyor Belts for the Intensification of Extratropical Cyclones in Northern Hemisphere Winter". In: *Journal of the Atmospheric Sciences* 73.10, pp. 3997–4020. DOI: 10.1175/JAS-D-15-0302.1 (→ page 17).

Binder, H., H. Joos, M. Sprenger, and H. Wernli (2023). "Warm conveyor belts in present-day and future climate simulations–Part 2: Role of potential vorticity production for cyclone intensification". In: *Weather and Climate Dynamics* 4.1, pp. 19–37 (→ pages 19, 20, 63).

Bjerknes, J. (1919). "On the structure of moving cyclones". In: *Monthly Weather Review* 47.2, pp. 95–99. DOI: 10.1175/1520-0493(1919)47<95:OTSOMC>2.0.CO;2 (→ page 13).

Bjerknes, J. and H. Solberg (1922). "Life cycle of cyclones and the polar front theory of atmospheric circulation". In: *Geophysisks Publikationer* 3.1, pp. 1–18 (→ page 13).

Bjerknes, J. (1969). "Atmospheric teleconnections from the equatorial Pacific". In: *Monthly weather review* 97.3, pp. 163–172 (→ page 32).

Blackmon, M. L., J. M. Wallace, N.-C. Lau, and S. L. Mullen (1977). "An Observational Study of the Northern Hemisphere Wintertime Circulation". In: *Journal of Atmospheric Sciences* 34.7, pp. 1040–1053. DOI: 10.1175/1520-0469(1977)034<1040:AOSOTN>2.0.CO;2 (→ page 15).

Bosart, L. F. (1981). "The Presidents' Day Snowstorm of 18–19 February 1979: A Subsynoptic-Scale Event". In: *Monthly Weather Review* 109.7, pp. 1542–1566. DOI: 10.1175/1520-0493(1981)109<1542:TPDSOF>2.0.CO;2 (→ page 13).

Brayshaw, D. J., B. Hoskins, and M. Blackburn (2009). "The Basic Ingredients of the North Atlantic Storm Track. Part I: Land–Sea Contrast and Orography". In: *Journal of the Atmospheric Sciences* 66.9, pp. 2539–2558. DOI: 10.1175/2009JAS3078.1 (→ page 17).

— (2011). "The Basic Ingredients of the North Atlantic Storm Track. Part II: Sea Surface Temperatures". In: *Journal of the Atmospheric Sciences* 68.8, pp. 1784–1805. DOI: 10.1175/2011JAS3674.1 (→ page 17).

Burger, M., J. Wentz, and R. Horton (2020). "The law and science of climate change attribution". In: *Colum. J. Envtl. L.* 45, p. 57 (→ page 10).

Buzzi, A., S. Davolio, and M. Fantini (2020). "Cyclogenesis in the lee of the Alps: a review of theories". In: *Bulletin of Atmospheric Science and Technology* 1, pp. 433–457 (→ page 18).

Carbon Brief (2022) (→ pages 2, 12, 95).

Cattiaux, J., C. C. R. Vautard, P. Yiou, V. Masson-Delmotte, and F. Codron (2010). "Winter 2010 in Europe: A cold extreme in a warming climate". In: *Geophysical Research Letters* 37. DOI: https://doi.org/10.1029/2010GL044613 (→ pages 5, 9).

Catto, J. L., D. Ackerley, J. F. Booth, A. J. Champion, B. A. Colle, et al. (2019). "The future of midlatitude cyclones". In: *Current Climate Change Reports* 5, pp. 407–420 (→ pages 21, 95).

Catto, J. (2016). "Extratropical cyclone classification and its use in climate studies". In: *Reviews of Geophysics* 54.2, pp. 486–520 (→ pages 18, 62).

Charney, J. G. (1947). "The dynamics of long waves in a baroclinic westerly current". In: *Journal of Atmospheric Sciences* 4.5, pp. 136–162. DOI: 10.1175/1520-0469(1947)004<0136:TDOLWI>2.0.CO;2 (→ page 16).

Christidis, N. (2021). *Using CMIP6 multi-model ensembles for near real-time attribution of extreme events* (→ page 12).

Christidis, N., P. A. Stott, A. A. Scaife, A. Arribas, G. S. Jones, et al. (2013). "A New HadGEM3-A-Based System for Attribution of Weather- and Climate-Related Extreme Events". In: *Journal of Climate* 26.9, pp. 2756–2783. DOI: 10.1175/JCLI-D-12-00169.1 (→ page 9).

Cusack, S. (2023). "A long record of European windstorm losses and its comparison to standard climate indices". In: *Natural Hazards and Earth System Sciences* 23.8, pp. 2841–2856. DOI: 10.5194/nhess-23-2841-2023 (→ page 13).

Dacre, H. (2020). "A review of extratropical cyclones: observations and conceptual models over the past 100 years". In: *Weather* 75.1, pp. 4–7. DOI: https://doi.org/10.1002/wea.3653 (→ page 14).

Dacre, H. F. and J. G. Pinto (2020). "Serial clustering of extratropical cyclones: A review of where, when and why it occurs". In: *NPJ Climate and Atmospheric Science* 3.1, p. 48 (→ page 43).

Dacre, H. F. and S. L. Gray (2009). "The spatial distribution and evolution characteristics of North Atlantic cyclones". In: *Monthly Weather Review* 137.1, pp. 99–115 (→ page 18).

Davis, C. A. and K. A. Emanuel (1991). "Potential vorticity diagnostics of cyclogenesis". In: *Monthly weather review* 119.8, pp. 1929–1953 (→ page 17).

Davolio, S., M. Vercellino, M. M. Miglietta, L. D. Pitura, S. Laviola, et al. (2023). "The influence of an atmospheric river on a heavy precipitation event over the western Alps". In: *Weather and Climate Extremes* 39, p. 100542 (→ page 73).

Deser, C., A. Phillips, V. Bourdette, and H. Teng (2012). "Uncertainty in climate change projections: the role of internal variability". In: *Climate dynamics* 38, pp. 527–546 (→ page 62).

Deveson, A. C. L., K. A. Browning, and T. D. Hewson (2002). "A classification of FASTEX cyclones using a height-attributable quasi-geostrophic vertical-motion diagnostic". In: *Quarterly Journal of the Royal Meteorological Society* 128.579, pp. 93–117. DOI: https://doi.org/10.1256/00359000260498806 (→ page 18).

Dole, R., M. Hoerling, J. Perlwitz, J. Eischeid, P. Pegion, et al. (2011). "Was there a basis for anticipating the 2010 Russian heat wave?" In: *Geophysical research letters* 38.6 (→ page 6).

Dolores-Tesillos, E., F. Teubler, and S. Pfahl (2022). "Future changes in North Atlantic winter cyclones in CESM-LE – Part 1: Cyclone intensity, potential vorticity anomalies, and horizontal wind speed". In: *Weather and Climate Dynamics* 3.2, pp. 429–448. DOI: 10.5194/wcd-3-429-2022 (→ pages 19, 21, 63, 81).

Eady, E. T. (1949). "Long Waves and Cyclone Waves". In: *Tellus* 1.3, pp. 33–52. DOI: https://doi.org/10.1111/j.2153-3490.1949.tb01265.x (→ page 16).

Eden, J. M., S. F. Kew, O. Bellprat, G. Lenderink, I. Manola, et al. (2018). "Extreme precipitation in the Netherlands: An event attribution case study". In: *Weather and Climate Extremes* 21, pp. 90–101. DOI: https://doi.org/10.1016/j.wace.2018.07.003 (→ page 22).

Eiras-Barca, J., A. M. Ramos, J. G. Pinto, R. M. Trigo, M. L. Liberato, et al. (2018). "The concurrence of atmospheric rivers and explosive cyclogenesis in the North Atlantic and North Pacific basins". In: *Earth System Dynamics* 9.1, pp. 91–102 (→ pages 73, 173, 175).

Emanuel, K. (2017). "Assessing the present and future probability of Hurricane Harvey's rainfall". In: *Proceedings of the National Academy of Sciences* 114.48, pp. 12681–12684. DOI: 10.1073/pnas.1716222114 (→ page 4).

Ermis, S., N. Leach, F. Lott, S. Sparrow, and A. Weisheimer (2023). "Extreme event attribution for a mid-latitude windstorm with medium-range forecasts". In: *XXVIII General Assembly of the International Union of Geodesy and Geophysics (IUGG)*. GFZ German Research Centre for Geosciences (→ page 22).

Espinoza, V., D. E. Waliser, B. Guan, D. A. Lavers, and F. M. Ralph (2018). "Global analysis of climate change projection effects on atmospheric rivers". In: *Geophysical Research Letters* 45.9, pp. 4299–4308 (→ page 174).

Eyring, V., S. Bony, G. A. Meehl, C. A. Senior, B. Stevens, et al. (2016). "Overview of the Coupled Model Intercomparison Project Phase 6 (CMIP6) experimental design and organization". In: *Geoscientific Model Development* 9.5, pp. 1937–1958. DOI: 10.5194/gmd-9-1937-2016 (→ page 174).

Faranda, D., S. Bourdin, M. Ginesta, M. Krouma, R. Noyelle, et al. (2022). "A climate-change attribution retrospective of some impactful weather extremes of 2021". In: *Weather and Climate Dynamics* 3.4, pp. 1311–1340. DOI: 10.5194/wcd-3-1311-2022 (→ pages 5, 7, 8, 11, 28, 36, 45, 95).

Faranda, D., M. Ginesta, T. Alberti, E. Coppola, and M. Anzidei (2023). "Attributing Venice Acqua Alta events to a changing climate and evaluating the efficacy of MoSE adaptation strategy". In: *npj climate and atmospheric science* 6.1, p. 181 (→ page 40).

Faranda, D., M. Vrac, P. Yiou, A. Jézéquel, and S. Thao (2020). "Changes in Future Synoptic Circulation Patterns: Consequences for Extreme Event Attribution". In: *Geophysical Research Letters* 47.15. e2020GL088002 10.1029/2020GL088002, e2020GL088002. DOI: https://doi.org/10.1029/2020GL088002 (→ page 6).

Feser, F., M. Barcikowska, O. Krueger, F. Schenk, R. Weisse, et al. (2015). "Storminess over the North Atlantic and northwestern Europe—A review". In: *Quarterly Journal of the Royal Meteorological Society* 141.687, pp. 350–382 (→ page 21).

Feser, F., B. Rockel, H. von Storch, J. Winterfeldt, and M. Zahn (2011). "Regional climate models add value to global model data: a review and selected examples". In: *Bulletin of the American Meteorological Society* 92.9, pp. 1181–1192 (→ page 44).

Fink, A. H., S. Pohle, J. G. Pinto, and P. Knippertz (2012). "Diagnosing the influence of diabatic processes on the explosive deepening of extratropical cyclones". In: *Geophysical Research Letters* 39.7 (→ page 17).

Fischer, E. M. and R. Knutti (2015). "Anthropogenic contribution to global occurrence of heavy-precipitation and high-temperature extremes". In: *Nature climate change* 5.6, pp. 560–564 (→ page 4).

Flaounas, E., S. L. Gray, and F. Teubler (2021). "A process-based anatomy of Mediterranean cyclones: from baroclinic lows to tropical-like systems". In: *Weather and Climate Dynamics* 2.1, pp. 255–279. DOI: 10.5194/wcd-2-255-2021 (→ page 18).

Flaounas, E., L. Aragão, L. Bernini, S. Dafis, B. Doiteau, et al. (2023). "A composite approach to produce reference datasets for extratropical cyclone tracks: application to Mediterranean cyclones". In: *Weather and Climate Dynamics Discussions* 2023, pp. 1–32 (→ page 64).

Flaounas, E., S. Davolio, S. Raveh-Rubin, F. Pantillon, M. M. Miglietta, et al. (2022). "Mediterranean cyclones: Current knowledge and open questions on dynamics, prediction, climatology and impacts". In: *Weather and Climate Dynamics* 3.1, pp. 173–208 (→ pages 16, 17, 20, 58, 95).

Fraser-Baxter, S. E. (2023). *Italy's deadly floods can't be blamed on climate change, finds study.* Accessed on: January 30, 2024 (→ page 43).

Gao, Y., J. Lu, and L. R. Leung (2016). "Uncertainties in Projecting Future Changes in Atmospheric Rivers and Their Impacts on Heavy Precipitation over Europe". In: *Journal of Climate* 29.18, pp. 6711–6726. DOI: 10.1175/JCLI-D-16-0088.1 (→ page 174).

Ginesta, M., E. Flaounas, P. Yiou, and D. Faranda (2024). "Anthropogenic climate change will intensify European explosive storms similar to Alex, Eunice, and Xynthia in the future". In: *Journal of Climate*. under review (→ pages 62–67, 71, 97).

Ginesta, M., P. Yiou, G. Messori, and D. Faranda (2023). "A methodology for attributing severe extratropical cyclones to climate change based on reanalysis data: the case study of storm Alex 2020". In: *Climate Dynamics* 61, pp. 229–253. DOI: https://doi.org/10.1007/s00382-022-06565-x (→ pages 5, 28–30, 42, 44, 45, 95).

Giorgi, F., C. Jones, G. R. Asrar, et al. (2009). "Addressing climate information needs at the regional level: the CORDEX framework". In: *World Meteorological Organization (WMO) Bulletin* 58.3, p. 175 (→ page 44).

Gómara, I., B. Rodríguez-Fonseca, P. Zurita-Gotor, and J. G. Pinto (2014). "On the relation between explosive cyclones affecting Europe and the North Atlantic Oscillation". In: *Geophysical Research Letters* 41.6, pp. 2182–2190. DOI: https://doi.org/10.1002/2014GL059647 (→ page 15).

Grams, C. M., H. Wernli, M. Böttcher, J. Čampa, U. Corsmeier, et al. (2011). "The key role of diabatic processes in modifying the upper-tropospheric wave guide: a North Atlantic case-study". In: *Quarterly Journal of the Royal Meteorological Society* 137.661, pp. 2174–2193. DOI: https://doi.org/10.1002/qj.891 (→ page 18).

Gulev, S., P. Thorne, J. Ahn, F. Dentener, C. Domingues, et al. (2021). "Changing State of the Climate System. In Climate Change 2021: The Physical Science Basis. Contribution of Working Group I to the Sixth Assessment Report of the Intergovernmental Panel on Climate Change [Masson-Delmotte, V., P. Zhai, A. Pirani, S.L. Connors, C. Péan, S. Berger, N. Caud, Y. Chen, L. Goldfarb, M.I. Gomis, M. Huang, K. Leitzell, E. Lonnoy, J.B.R. Matthews, T.K. Maycock, T. Waterfield, O. Yelekçi, R. Yu, and B. Zhou (eds.)]. Cambridge University Press. In Press." In: Cambridge University Press (→ page 29).

Guo, Y., T. Shinoda, B. Guan, D. E. Waliser, and E. K. M. Chang (2020). "Statistical Relationship between Atmospheric Rivers and Extratropical Cyclones and Anticyclones". In: *Journal of Climate* 33.18, pp. 7817–7834. DOI: 10.1175/JCLI-D-19-0126.1 (→ page 173).

Haak, U. and U. Ulbrich (1996). "Verification of an objective cyclone climatology for the North Atlantic". In: *Meteorologische Zeitschrift* 5 (→ page 66).

Harrington, L. J., K. L. Ebi, D. J. Frame, and F. E. Otto (2022). "Integrating attribution with adaptation for unprecedented future heatwaves". In: *Climatic Change* 172.1-2, p. 2 (→ page 4).

Harvey, B., P. Cook, L. Shaffrey, and R. Schiemann (2020). "The response of the northern hemisphere storm tracks and jet streams to climate change in the CMIP3, CMIP5, and CMIP6 climate models". In: *Journal of Geophysical Research: Atmospheres* 125.23, e2020JD032701 (→ page 19).

Hawcroft, M. K., L. C. Shaffrey, K. I. Hodges, and H. F. Dacre (2012). "How much Northern Hemisphere precipitation is associated with extratropical cyclones?" In: *Geophysical Research Letters* 39.24. DOI: https://doi.org/10.1029/2012GL053866 (→ page 12).

Hawkins, E., G. P. Compo, and P. D. Sardeshmukh (2023). "ESD Ideas: Translating historical extreme weather events into a warmer world". In: *Earth System Dynamics* 14.5, pp. 1081–1084. DOI: 10.5194/esd-14-1081-2023 (→ page 22).

Hazeleger, W., B. J. van den Hurk, E. Min, G. J. van Oldenborgh, A. C. Petersen, et al. (2015). "Tales of future weather". In: *Nature Climate Change* 5.2, pp. 107–113 (→ page 4).

Herring, S. C., N. Christidis, A. Hoell, and P. A. Stott (2022). "Explaining Extreme Events of 2020 from a Climate Perspective". In: *Bulletin of the American Meteorological Society* 103.3, S1–S129. DOI: 10.1175/BAMS-ExplainingExtremeEvents2020.1 (→ page 2).

Hersbach, H., B. Bell, P. Berrisford, S. Hirahara, A. Horányi, et al. (2020). "The ERA5 global reanalysis". In: *Quarterly Journal of the Royal Meteorological Society* 146.730, pp. 1999–2049 (→ pages 19, 29, 44, 174).

Hinman, R. (1888). *Eclectic physical geography*. American Book Company (→ pages 13, 15).

Hodges, K. I., R. W. Lee, and L. Bengtsson (2011). "A Comparison of Extratropical Cyclones in Recent Reanalyses ERA-Interim, NASA MERRA, NCEP CFSR, and JRA-25". In: *Journal of Climate* 24.18, pp. 4888–4906. DOI: 10.1175/2011JCLI4097.1 (→ page 18).

Hodges, K. I., B. J. Hoskins, J. Boyle, and C. Thorncroft (2003). "A comparison of recent reanalysis datasets using objective feature tracking: Storm tracks and tropical easterly waves". In: *Monthly Weather Review* 131.9, pp. 2012–2037 (→ page 64).

Hoerling, M., A. Kumar, R. Dole, J. W. Nielsen-Gammon, J. Eischeid, et al. (2013). "Anatomy of an extreme event". In: *Journal of Climate* 26.9, pp. 2811–2832 (→ pages 5, 9).

Homar, V., A. Jansà, J. Campins, and C. Ramis (2006). "Towards a climatology of sensitivities of Mediterranean high impact weather x2212; first approach". In: *Advances in Geosciences* 7, pp. 259–267. DOI: 10.5194/adgeo-7-259-2006 (→ pages 17, 95).

Hoskins, B. J., M. E. McIntyre, and A. W. Robertson (1985). "On the use and significance of isentropic potential vorticity maps". In: *Quarterly Journal of the Royal Meteorological Society* 111.470, pp. 877–946. DOI: https://doi.org/10.1002/qj.49711147002 (→ page 17).

Hoskins, B. and K. Hodges (2019a). "The annual cycle of Northern Hemisphere storm tracks. Part I: Seasons". In: *Journal of Climate* 32.6, pp. 1743–1760 (→ page 15).

— (2019b). "The annual cycle of Northern Hemisphere storm tracks. Part II: Regional detail". In: *Journal of Climate* 32.6, pp. 1761–1775 (→ page 16).

Hoskins, B. J. and K. I. Hodges (2002). "New perspectives on the Northern Hemisphere winter storm tracks". In: *Journal of the Atmospheric Sciences* 59.6, pp. 1041–1061 (→ page 15).

Jacob, D., J. Petersen, B. Eggert, A. Alias, O. B. Christensen, et al. (2014). "EURO-CORDEX: new high-resolution climate change projections for European impact research". In: *Regional environmental change* 14, pp. 563–578 (→ pages 40, 55).

Jézéquel, A., J. Cattiaux, P. Naveau, S. Radanovics, A. Ribes, et al. (2018a). "Trends of atmospheric circulation during singular hot days in Europe". In: *Environmental Research Letters* 13.5, p. 054007 (→ pages 7, 95).

Jézéquel, A., V. Dépoues, H. Guillemot, A. Rajaud, M. Trolliet, et al. (2020). "Singular extreme events and their attribution to climate change: A climate service–centered analysis". In: *Weather, Climate, and Society* 12.1, pp. 89–101 (→ page 3).

Jézéquel, A., V. Dépoues, H. Guillemot, M. Trolliet, J.-P. Vanderlinden, et al. (2018b). "Behind the veil of extreme event attribution". In: *Climatic Change* 149, pp. 367–383 (→ pages 3, 5, 28).

Jézéquel, A., P. Yiou, and J.-P. Vanderlinden (2019). "Comparing scientists and delegates perspectives on the use of extreme event attribution for loss and damage". In: *Weather and Climate Extremes* 26, p. 100231. DOI: https://doi.org/10.1016/j.wace.2019.100231 (→ page 10).

Joos, H., M. Sprenger, H. Binder, U. Beyerle, and H. Wernli (2023). "Warm conveyor belts in present-day and future climate simulations-Part 1: Climatology and impacts". In: *Weather and Climate Dynamics* 4.1, pp. 133–155 (→ pages 19, 63).

Juliana v. United States (2016). *Case No. 6:15-cv-01517-TC, United States District Court, District of Oregon* (→ page 10).

— (2018). *Expert Report of Professor John P. Weyant, August 13, 2018 (Case 6:15-cv-01517-TC, Document 338-5)* (→ page 10).

Karwat, A., C. L. Franzke, and R. Blender (2022). "Long-Term Trends of Northern Hemispheric Winter Cyclones in the Extended ERA5 Reanalysis". In: *Journal of Geophysical Research: Atmospheres* 127.22, e2022JD036952 (→ pages 19, 20, 33, 34).

Kay, J. E., C. Deser, A. Phillips, A. Mai, C. Hannay, et al. (2015). "The Community Earth System Model (CESM) Large Ensemble Project: A Community Resource for Studying Climate Change in the Presence of Internal Climate Variability". In: *Bulletin of the American Meteorological Society* 96.8, pp. 1333–1349. DOI: 10.1175/BAMS-D-13-00255.1 (→ page 19).

King, A. D., M. R. Grose, J. Kimutai, I. Pinto, and L. J. Harrington (2023a). "Event attribution is not ready for a major role in loss and damage". In: *Nature Climate Change*, pp. 1–3 (→ page 10).

King, A. D., G. J. van Oldenborgh, D. J. Karoly, S. C. Lewis, and H. Cullen (2015). "Attribution of the record high Central England temperature of 2014 to anthropogenic influences". In: *Environmental Research Letters* 10.5, p. 054002 (→ page 8).

King, M. P., N. Keenlyside, and C. Li (2023b). "ENSO teleconnections in terms of non-NAO and NAO atmospheric variability". In: *Climate Dynamics*, pp. 1–17 (→ page 32).

Kluger, J. (2024). *Climate Gets Its Day in Court*. Accessed on: February 25, 2024 (→ page 10).

Kotlarski, S., K. Keuler, O. B. Christensen, A. Colette, M. Déqué, et al. (2014). "Regional climate modeling on European scales: a joint standard evaluation of the EURO-CORDEX RCM ensemble". In: *Geoscientific Model Development* 7.4, pp. 1297–1333 (→ page 49).

Kouroutzoglou, J., H. A. Flocas, K. Keay, I. Simmonds, and M. Hatzaki (2011). "Climatological aspects of explosive cyclones in the Mediterranean". In: *International Journal of Climatology* 31.12, pp. 1785–1802. DOI: https://doi.org/10.1002/joc.2203 (→ page 16).

Lackmann, G. M. (2015). "Hurricane Sandy before 1900 and after 2100". In: *Bulletin of the American Meteorological Society* 96.4, pp. 547–560. DOI: 10.1175/BAMS-D-14-00123.1 (→ page 9).

Lavers, D. A., R. P. Allan, G. Villarini, B. Lloyd-Hughes, D. J. Brayshaw, et al. (2013). "Future changes in atmospheric rivers and their implications for winter flooding in Britain". In: *Environmental Research Letters* 8.3, p. 034010 (→ page 174).

Leach, N. J., A. Weisheimer, M. R. Allen, and T. Palmer (2021). "Forecast-based attribution of a winter heatwave within the limit of predictability". In: *Proceedings of the National Academy of Sciences* 118.49, e2112087118 (→ pages 6, 7, 9, 22, 95).

Lewis, S. C., S. E. Perkins-Kirkpatrick, and A. D. King (2019). "Approaches to attribution of extreme temperature and precipitation events using multi-model and single-member ensembles of general circulation models". In: *Advances in Statistical Climatology, Meteorology and Oceanography* 5.2, pp. 133–146. DOI: 10.5194/ascmo-5-133-2019 (→ page 9).

Lewis, S. C. and D. J. Karoly (2013). "Anthropogenic contributions to Australia's record summer temperatures of 2013". In: *Geophysical Research Letters* 40.14, pp. 3705–3709. DOI: https://doi.org/10.1002/grl.50673 (→ page 9).

Little, A. S., M. D. Priestley, and J. L. Catto (2023). "Future increased risk from extratropical windstorms in northern Europe". In: *Nature Communications* 14.1, p. 4434 (→ page 21).

Litzow, M. A., M. J. Malick, A. A. Abookire, J. Duffy-Anderson, B. J. Laurel, et al. (2021). "Using a climate attribution statistic to inform judgments about changing fisheries sustainability". In: *Scientific Reports* 11.1, p. 23924 (→ page 4).

Liu, Z. and M. Alexander (2007). "Atmospheric bridge, oceanic tunnel, and global climatic teleconnections". In: *Reviews of Geophysics* 45.2 (→ page 32).

Lloyd, E. A. and T. G. Shepherd (2021). "Climate change attribution and legal contexts: evidence and the role of storylines". In: *Climatic Change* 167.3-4, p. 28 (→ page 10).

Lloyd, E. A. and N. Oreskes (2018). "Climate Change Attribution: When Is It Appropriate to Accept New Methods?" In: *Earth's Future* 6.3, pp. 311–325. DOI: https://doi.org/10.1002/2017EF000665 (→ page 6).

Lombroso, L. (2023). *Alluvione in Emilia-Romagna, i cambiamenti climatici hanno avuto un impatto limitato? Lo studio.* Accessed on: January 30, 2024 (→ page 43).

Ludwig, P., J. G. Pinto, M. Reyers, and S. L. Gray (2014). "The role of anomalous SST and surface fluxes over the southeastern North Atlantic in the explosive development of windstorm Xynthia". In: *Quarterly Journal of the Royal Meteorological Society* 140.682, pp. 1729–1741 (→ page 17).

Manabe, S. and R. T. Wetherald (1967). "Thermal Equilibrium of the Atmosphere with a Given Distribution of Relative Humidity". In: *Journal of Atmospheric Sciences* 24.3, pp. 241–259. DOI: 10.1175/1520-0469(1967)024<0241:TEOTAW>2.0.CO;2 (→ page 2).

Marjanac, S. and L. Patton (2018). "Extreme weather event attribution science and climate change litigation: an essential step in the causal chain?" In: *Journal of Energy & Natural Resources Law* 36.3, pp. 265–298 (→ page 10).

Martínez-Alvarado, O., L. H. Baker, S. L. Gray, J. Methven, and R. S. Plant (2014). "Distinguishing the Cold Conveyor Belt and Sting Jet Airstreams in an Intense Extratropical Cyclone". In: *Monthly Weather Review* 142.8, pp. 2571–2595. DOI: 10.1175/MWR-D-13-00348.1 (→ pages 13, 14, 95).

Massey, N., R. Jones, F. E. L. Otto, T. Aina, S. Wilson, et al. (2015). "weather@home—development and validation of a very large ensemble modelling system for probabilistic event attribution". In: *Quarterly Journal of the Royal Meteorological Society* 141.690, pp. 1528–1545. DOI: https://doi.org/10.1002/qj.2455 (→ page 9).

Meredith, E. P., V. A. Semenov, D. Maraun, W. Park, and A. V. Chernokulsky (2015). "Crucial role of Black Sea warming in amplifying the 2012 Krymsk precipitation extreme". In: *Nature Geoscience* 8.8, pp. 615–619 (→ page 6).

Mezzina, B., J. García-Serrano, I. Bladé, and F. Kucharski (2020). "Dynamics of the ENSO Teleconnection and NAO Variability in the North Atlantic–European Late Winter". In: *Journal of Climate* 33.3, pp. 907–923. DOI: 10.1175/JCLI-D-19-0192.1 (→ page 32).

Mitchell, D., C. Heaviside, S. Vardoulakis, C. Huntingford, G. Masato, et al. (2016). "Attributing human mortality during extreme heat waves to anthropogenic climate change". In: *Environmental Research Letters* 11.7, p. 074006 (→ pages 4, 8, 95).

MunichRe (2023). *Winter storms and blizzards - A risk to entire continents* (→ page 13).

Murray, R. J. and I. Simmonds (1991). "A numerical scheme for tracking cyclone centres from digital data". In: *Australian meteorological magazine* 39.3, pp. 155–166 (→ pages 68, 69).

Neu, U., M. G. Akperov, N. Bellenbaum, R. Benestad, R. Blender, et al. (2013). "IMILAST: A community effort to intercompare extratropical cyclone detection and tracking algorithms". In: *Bulletin of the American Meteorological Society* 94.4, pp. 529–547 (→ pages 15, 64–66, 68).

NOAA, N. C. f. E. I. (2023). *Monthly Global Climate Report for May 2023.* Accessed on: February 7, 2024 (→ page 43).

Nobel Prize Outreach AB (2024). *The Nobel Prize in Physics 2021*. https://www.nobelprize.org/prizes/physics/2021/popular-information/ (→ page 2).

Noy, I., M. Wehner, D. Stone, S. Rosier, D. Frame, et al. (2023). "Event attribution is ready to inform loss and damage negotiations". In: *Nature Climate Change* 13.12, pp. 1279–1281 (→ page 10).

Otto, F. E. L., S. Kew, S. Philip, P. Stott, and G. J. V. Oldenborgh (2022). "How to Provide Useful Attribution Statements: Lessons Learned from Operationalizing Event Attribution in Europe". In: *Bulletin of the American Meteorological Society* 103.3, S21–S25. DOI: 10.1175/BAMS-D-21-0267.1 (→ page 11).

Otto, F. E. (2017). "Attribution of weather and climate events". In: *Annual Review of Environment and Resources* 42, pp. 627–646 (→ page 5).

— (2023). "Attribution of Extreme Events to Climate Change". In: *Annual Review of Environment and Resources* 48, pp. 813–828 (→ pages 6, 8).

Otto, F. E., N. Massey, G. J. van Oldenborgh, R. G. Jones, and M. R. Allen (2012). "Reconciling two approaches to attribution of the 2010 Russian heat wave". In: *Geophysical Research Letters* 39.4 (→ page 6).

Otto, F. E., R. B. Skeie, J. S. Fuglestvedt, T. Berntsen, and M. R. Allen (2017). "Assigning historic responsibility for extreme weather events". In: *Nature Climate Change* 7.11, pp. 757–759 (→ page 10).

Otto, F. E., G. J. Van Oldenborgh, J. Eden, P. A. Stott, D. J. Karoly, et al. (2016). "The attribution question". In: *Nature Climate Change* 6.9, pp. 813–816 (→ page 6).

Pall, P., T. Aina, D. A. Stone, P. A. Stott, T. Nozawa, et al. (2011). "Anthropogenic greenhouse gas contribution to flood risk in England and Wales in autumn 2000". In: *Nature* 470, pp. 382–385. DOI: 10.1038/nature09762 (→ pages 4, 7, 95).

Pantillon, F., J.-P. Chaboureau, C. Lac, and P. Mascart (2013). "On the role of a Rossby wave train during the extratropical transition of hurricane Helene (2006)". In: *Quarterly Journal of the Royal Meteorological Society* 139.671, pp. 370–386. DOI: https://doi.org/10.1002/qj.1974 (→ page 18).

Pantillon, F., J.-P. Chaboureau, and E. Richard (2015). "Remote impact of North Atlantic hurricanes on the Mediterranean during episodes of intense rainfall in autumn 2012". In: *Quarterly Journal of the Royal Meteorological Society* 141.688, pp. 967–978 (→ page 18).

Patricola, C. M. and M. F. Wehner (2018). "Anthropogenic influences on major tropical cyclone events". In: *Nature* 563.7731, pp. 339–346 (→ page 22).

Payne, A. E., M.-E. Demory, L. R. Leung, A. M. Ramos, C. A. Shields, et al. (2020). "Responses and impacts of atmospheric rivers to climate change". In: *Nature Reviews Earth & Environment* 1.3, pp. 143–157 (→ page 174).

Perkins-Kirkpatrick, S. E., D. A. Stone, D. M. Mitchell, S. Rosier, A. D. King, et al. (2022). "On the attribution of the impacts of extreme weather events to anthropogenic climate change". In: *Environmental Research Letters* 17.2, p. 024009 (→ pages 4, 10).

Peterson, T. C., P. A. Stott, and S. Herring (2012). "Explaining Extreme Events of 2011 from a Climate Perspective". In: *Bulletin of the American Meteorological Society* 93.7, pp. 1041–1067. DOI: 10.1175/BAMS-D-12-00021.1 (→ page 2).

Petterssen, S. and S. J. Smebye (1971). "On the development of extratropical cyclones". In: *Quarterly Journal of the Royal Meteorological Society* 97.414, pp. 457–482. DOI: https://doi.org/10.1002/qj.49709741407 (→ page 18).

Petterssen, S. (1956). "Weather Analysis and Forecasting. A Textbook on Synoptic Meteorology". In: *McGraw-Hill* (→ page 15).

Pfahl, S., P. A. O'Gorman, and M. S. Singh (2015). "Extratropical Cyclones in Idealized Simulations of Changed Climates". In: *Journal of Climate* 28.23, pp. 9373–9392. DOI: 10.1175/JCLI-D-14-00816.1 (→ page 20).

Philip, S., S. Kew, G. J. van Oldenborgh, F. Otto, R. Vautard, et al. (2020). "A protocol for probabilistic extreme event attribution analyses". In: *Advances in Statistical Climatology, Meteorology and Oceanography* 6.2, pp. 177–203. DOI: 10.5194/ascmo-6-177-2020 (→ pages 3, 11).

Philip, S. Y., S. F. Kew, G. J. van Oldenborgh, F. S. Anslow, S. I. Seneviratne, et al. (2022). "Rapid attribution analysis of the extraordinary heat wave on the Pacific coast of the US and Canada in June 2021". In: *Earth System Dynamics* 13.4, pp. 1689–1713. DOI: 10.5194/esd-13-1689-2022 (→ page 9).

Philip, S., S. F. Kew, G. J. van Oldenborgh, E. Aalbers, R. Vautard, et al. (2018). "Validation of a Rapid Attribution of the May/June 2016 Flood-Inducing Precipitation in France to Climate Change". In: *Journal of Hydrometeorology* 19.11, pp. 1881–1898. DOI: 10.1175/JHM-D-18-0074.1 (→ page 22).

Pinto, J. G., I. Gómara, G. Masato, H. F. Dacre, T. Woollings, et al. (2014). "Large-scale dynamics associated with clustering of extratropical cyclones affecting Western Europe". In: *Journal of Geophysical Research: Atmospheres* 119.24, pp. 13–704 (→ page 43).

Pinto, J. G., M. K. Karremann, K. Born, P. M. Della-Marta, and M. Klawa (2012). "Loss potentials associated with European windstorms under future climate conditions". In: *Climate Research* 54.1, pp. 1–20 (→ page 13).

Pinto, J. G., T. Spangehl, U. Ulbrich, and P. Speth (2005). "Sensitivities of a cyclone detection and tracking algorithm: individual tracks and climatology". In: *Meteorologische Zeitschrift* 14.6, pp. 823–838 (→ pages 64, 68).

Pinto, J. G., S. Zacharias, A. H. Fink, G. C. Leckebusch, and U. Ulbrich (2009). "Factors contributing to the development of extreme North Atlantic cyclones and their relationship with the NAO". In: *Climate dynamics* 32, pp. 711–737 (→ page 15).

Portal, A., C. Pasquero, F. D'andrea, P. Davini, M. E. Hamouda, et al. (2022). "Influence of reduced winter land–sea contrast on the midlatitude atmospheric circulation". In: *Journal of Climate* 35.19, pp. 6237–6251 (→ page 20).

Priestley, M. D. K., D. B. Stephenson, A. A. Scaife, D. Bannister, C. J. T. Allen, et al. (2023). "Return levels of extreme European windstorms, their dependency on the North Atlantic Oscillation, and potential future risks". In: *Natural Hazards and Earth System Sciences* 23.12, pp. 3845–3861. DOI: 10.5194/nhess-23-3845-2023 (→ page 13).

Priestley, M. D. K., H. F. Dacre, L. C. Shaffrey, S. Schemm, and J. G. Pinto (2020a). "The role of secondary cyclones and cyclone families for the North Atlantic storm track and clustering over western Europe". In: *Quarterly Journal of the Royal Meteorological Society* 146.728, pp. 1184–1205. DOI: https://doi.org/10.1002/qj.3733 (→ page 18).

Priestley, M. D., D. Ackerley, J. L. Catto, K. I. Hodges, R. E. McDonald, et al. (2020b). "An overview of the extratropical storm tracks in CMIP6 historical simulations". In: *Journal of Climate* 33.15, pp. 6315–6343 (→ pages 19, 55).

Priestley, M. D. and J. L. Catto (2022). "Future changes in the extratropical storm tracks and cyclone intensity, wind speed, and structure". In: *Weather and Climate Dynamics* 3.1, pp. 337–360 (→ pages 21, 76, 81, 174).

Rahmstorf, S. and D. Coumou (2011). "Increase of extreme events in a warming world". In: *Proceedings of the National Academy of Sciences* 108.44, pp. 17905–17909 (→ page 6).

Raible, C. C., M. Messmer, F. Lehner, T. F. Stocker, and R. Blender (2018). "Extratropical cyclone statistics during the last millennium and the 21st century". In: *Climate of the Past* 14.10, pp. 1499–1514 (→ page 19).

Ralph, F. M., M. D. Dettinger, M. M. Cairns, T. J. Galarneau, and J. Eylander (2018). "Defining "atmospheric river": How the Glossary of Meteorology helped resolve a debate". In: *Bulletin of the American Meteorological Society* 99.4, pp. 837–839 (→ page 73).

Ramos, A. M., R. Tomé, R. M. Trigo, M. L. Liberato, and J. G. Pinto (2016). "Projected changes in atmospheric rivers affecting Europe in CMIP5 models". In: *Geophysical Research Letters* 43.17, pp. 9315–9323 (→ page 174).

Reale, M., W. D. Cabos Narvaez, L. Cavicchia, D. Conte, E. Coppola, et al. (2022). "Future projections of Mediterranean cyclone characteristics using the Med-CORDEX ensemble of coupled regional climate system models". In: *Climate dynamics*, pp. 1–24 (→ pages 20, 21).

Rinnovabili.it (2023). *Alluvione in Emilia Romagna, WWA: "Il climate change c'entra poco"*. Accessed on: January 30, 2024 (→ page 43).

Robine, J.-M., S. L. K. Cheung, S. Le Roy, H. Van Oyen, C. Griffiths, et al. (2008). "Death toll exceeded 70,000 in Europe during the summer of 2003". In: *Comptes rendus biologies* 331.2, pp. 171–178 (→ page 3).

Ruti, P. M., S. Somot, F. Giorgi, C. Dubois, E. Flaounas, et al. (2016). "MED-CORDEX initiative for Mediterranean climate studies". In: *Bulletin of the American Meteorological Society* 97.7, pp. 1187–1208 (→ page 21).

Sabelli, C. (2023). *Italy's deadly floods can't be blamed on climate change, finds study*. Accessed on: January 30, 2024 (→ page 43).

Sanders, F. and J. R. Gyakum (1980). "Synoptic-Dynamic Climatology of the "Bomb"". In: *Monthly Weather Review* 108.10, pp. 1589–1606. DOI: 10.1175/1520-0493(1980)108<1589:SDCOT>2.0.CO;2 (→ pages 13, 63, 175).

Schemm, S. (2023). "Toward Eliminating the Decades-Old "Too Zonal and Too Equatorward" Storm-Track Bias in Climate Models". In: *Journal of Advances in Modeling Earth Systems* 15.2. e2022MS003482 2022MS003482, e2022MS003482. DOI: https://doi.org/10.1029/2022MS003482 (→ page 17).

Schultz, D. M., L. F. Bosart, B. A. Colle, H. C. Davies, C. Dearden, et al. (2019). "Extratropical cyclones: A century of research on meteorology's centerpiece". In: *Meteorological monographs* 59, pp. 16–1 (→ page 13).

Schultz, D. M. and G. Vaughan (2011). "Occluded Fronts and the Occlusion Process: A Fresh Look at Conventional Wisdom". In: *Bulletin of the American Meteorological Society* 92.4, pp. 443–466. DOI: 10.1175/2010BAMS3057.1 (→ page 13).

Schulzweida, U., L. Kornblueh, and R. Quast (2019). *CDO user guide* (→ page 44).

Seiler, C. and F. W. Zwiers (2016). "How will climate change affect explosive cyclones in the extratropics of the Northern Hemisphere?" In: *Climate Dynamics* 46.11-12, pp. 3633–3644 (→ pages 21, 81, 174).

Seneviratne, S., X. Zhang, M. Adnan, W. Badi, C. Dereczynski, et al. (2021). "Weather and Climate Extreme Events in a Changing Climate. In Climate Change 2021: The Physical Science Basis. Contribution of Working Group I to the Sixth Assessment Report of the Intergovernmental Panel on Climate Change". In: (→ pages 20–22).

Shapiro, M. A. and D. Keyser (1990). *Fronts, jet streams and the tropopause*. Springer (→ page 13).

Shaw, T., M. Baldwin, E. A. Barnes, R. Caballero, C. Garfinkel, et al. (2016). "Storm track processes and the opposing influences of climate change". In: *Nature Geoscience* 9.9, pp. 656–664 (→ pages 15, 16, 20, 95).

Shepherd, T. G. (2014). "Atmospheric circulation as a source of uncertainty in climate change projections". In: *Nature Geoscience* 7.10, pp. 703–708 (→ pages 4, 174).

— (2016). "A common framework for approaches to extreme event attribution". In: *Current Climate Change Reports* 2.1, pp. 28–38 (→ page 5).

Sinclair, M. R. (1994). "An objective cyclone climatology for the Southern Hemisphere". In: *Monthly Weather Review* 122.10, pp. 2239–2256 (→ page 64).

Speranza, A., A. Buzzi, A. Trevisan, and P. Malguzzi (1985). "A theory of deep cyclogenesis in the lee of the Alps. Part I: Modifications of baroclinic instability by localized topography". In: *Journal of the atmospheric sciences* 42.14, pp. 1521–1535 (→ page 18).

Stendel, M., J. Francis, R. White, P. D. Williams, and T. Woollings (2021). "Chapter 15 - The jet stream and climate change". In: *Climate Change (Third Edition)*. Ed. by T. M. Letcher. Third Edition. Elsevier, pp. 327–357. DOI: https://doi.org/10.1016/B978-0-12-821575-3.00015-3 (→ page 20).

Stott, P. A., D. A. Stone, and M. R. Allen (2004). "Human contribution to the European heatwave of 2003". In: *Nature* 432.7017, pp. 610–614. DOI: 10.1038/Nature03089 (→ pages 3, 7, 8, 95).

Stott, P. A. and N. Christidis (2023). "Operational attribution of weather and climate extremes: what next?" In: *Environmental Research: Climate* 2.1, p. 013001 (→ page 11).

Tanaka, T., H. Kawase, Y. Imada, Y. Kawai, and S. Watanabe (2023). "Risk-based versus storyline approaches for global warming impact assessment on basin-averaged extreme rainfall: a case study for Typhoon Hagibis in eastern Japan". In: *Environmental Research Letters* 18.5, p. 054010 (→ page 6).

Terray, L. (2023). "A Storyline Approach to the June 2021 Northwestern North American Heatwave". In: *Geophysical Research Letters* 50.5. e2022GL101640 2022GL101640, e2022GL101640. DOI: https://doi.org/10.1029/2022GL101640 (→ page 8).

Tilinina, N., S. K. Gulev, I. Rudeva, and P. Koltermann (2013). "Comparing Cyclone Life Cycle Characteristics and Their Interannual Variability in Different Reanalyses". In: *Journal of Climate* 26.17, pp. 6419–6438. DOI: 10.1175/JCLI-D-12-00777.1 (→ pages 18, 20).

Tradowsky, J. S., S. Y. Philip, F. Kreienkamp, S. F. Kew, P. Lorenz, et al. (2023). "Attribution of the heavy rainfall events leading to severe flooding in Western Europe during July 2021". In: *Climatic Change* 176.7, p. 90 (→ pages 8, 22).

Trenberth, K. E., J. T. Fasullo, and T. G. Shepherd (2015). "Attribution of climate extreme events". In: *Nature Climate Change* 5.8, pp. 725–730 (→ pages 4, 6, 10).

Ulbrich, U., A. Fink, M. Klawa, and J. G. Pinto (2001). "Three extreme storms over Europe in December 1999". In: *Weather* 56.3, pp. 70–80 (→ page 12).

Ulbrich, U., G. C. Leckebusch, and J. G. Pinto (2009). "Extra-tropical cyclones in the present and future climate: a review". In: *Theoretical and applied climatology* 96, pp. 117–131 (→ page 21).

Ullrich, P. A., C. M. Zarzycki, E. E. McClenny, M. C. Pinheiro, A. M. Stansfield, et al. (2021). "TempestExtremes v2.1: A community framework for feature detection, tracking, and analysis in large datasets". In: *Geoscientific Model Development* 14.8, pp. 5023–5048 (→ pages 66, 175).

van Garderen, L., F. Feser, and T. G. Shepherd (2020). "A methodology for attributing the role of climate change in extreme events: a global spectrally nudged storyline". In: *Natural Hazards and Earth System Sciences Discussions* 2020, pp. 1–24 (→ page 5).

Van Oldenborgh, G. J., A. Van Urk, and M. Allen (2012). "The absence of a role of climate change in the 2011 Thailand floods". In: *Bull. Amer. Meteor. Soc* 93, pp. 1047–1049 (→ page 9).

Van Oldenborgh, G. (2007). "How unusual was autumn 2006 in Europe?" In: *Climate of the Past* 3.4, pp. 659–668 (→ page 3).

Vautard, R., P. Yiou, F. Otto, P. Stott, N. Christidis, et al. (2016). "Attribution of human-induced dynamical and thermodynamical contributions in extreme weather events". In: *Environmental Research Letters* 11.11, p. 114009. DOI: 10.1088/1748-9326/11/11/114009 (→ page 5).

Vautard, R., G. J. van Oldenborgh, F. E. L. Otto, P. Yiou, H. de Vries, et al. (2019). "Human influence on European winter wind storms such as those of January 2018". In: *Earth System Dynamics* 10.2, pp. 271–286. DOI: 10.5194/esd-10-271-2019 (→ page 22).

Vautard, R., J. Cattiaux, T. Happé, J. Singh, R. Bonnet, et al. (2023). "Heat extremes in Western Europe increasing faster than simulated due to atmospheric circulation trends". In: *Nature Communications* 14.1, p. 6803. DOI: 10.1038/s41467-023-42143-3 (→ page 5).

Visser, H., A. C. Petersen, and W. Ligtvoet (2014). "On the relation between weather-related disaster impacts, vulnerability and climate change". In: *Climatic change* 125, pp. 461–477 (→ pages 4, 82).

Wang, X. L., Y. Feng, R. Chan, and V. Isaac (2016). "Inter-comparison of extra-tropical cyclone activity in nine reanalysis datasets". In: *Atmospheric Research* 181, pp. 133–153. DOI: https://doi.org/10.1016/j.atmosres.2016.06.010 (→ page 18).

Watson, R. and the Core Writing Team (Eds.) (2001). "Climate Change 2001: Synthesis Report. A Contribution of Working Groups I, II, and III to the Third Assessment Report of the Intergovernmental Panel on Climate Change". In: *Cambridge University Press*, p. 398 (→ page 2).

Wernli, H. and H. C. Davies (1997). "A Lagrangian-based analysis of extratropical cyclones. I: The method and some applications". In: *Quarterly Journal of the Royal Meteorological Society* 123.538, pp. 467–489 (→ page 17).

Wernli, H. and C. Schwierz (2006). "Surface cyclones in the ERA-40 dataset (1958–2001). Part I: Novel identification method and global climatology". In: *Journal of the atmospheric sciences* 63.10, pp. 2486–2507 (→ page 65).

Wilks, D. S. (2016). ""The Stippling Shows Statistically Significant Grid Points": How Research Results are Routinely Overstated and Overinterpreted, and What to Do about It". In: *Bulletin of the American Meteorological Society* 97.12, pp. 2263–2273. DOI: 10.1175/BAMS-D-15-00267.1 (→ page 50).

Willison, J., W. A. Robinson, and G. M. Lackmann (2013). "The Importance of Resolving Mesoscale Latent Heating in the North Atlantic Storm Track". In: *Journal of the Atmospheric Sciences* 70.7, pp. 2234–2250. DOI: 10.1175/JAS-D-12-0226.1 (→ page 20).

Yettella, V. and J. E. Kay (2017). "How will precipitation change in extratropical cyclones as the planet warms? Insights from a large initial condition climate model ensemble". In: *Climate Dynamics* 49.5-6, pp. 1765–1781 (→ page 174).

Yiou, P., R. Vautard, P. Naveau, and C. Cassou (2007). "Inconsistency between atmospheric dynamics and temperatures during the exceptional 2006/2007 fall/winter and recent warming in Europe". In: *Geophys. Res. Lett.* 34.L21808, doi:10.1029/2007GL031981 (→ page 5).

Yiou, P. (2014). "AnaWEGE: a weather generator based on analogues of atmospheric circulation". In: *Geoscientific Model Development* 7.2, pp. 531–543. DOI: 10.5194/gmd-7-531-2014 (→ page 5).

Yiou, P., A. Jézéquel, P. Naveau, F. E. Otto, R. Vautard, et al. (2017). "A statistical framework for conditional extreme event attribution". In: *Advances in Statistical Climatology, Meteorology and Oceanography* 3.1, pp. 17–31 (→ page 5).

Zappa, G., M. K. Hawcroft, L. Shaffrey, E. Black, and D. J. Brayshaw (2015). "Extratropical cyclones and the projected decline of winter Mediterranean precipitation in the CMIP5 models". In: *Climate Dynamics* 45, pp. 1727–1738 (→ pages 20, 21).

Zappa, G., L. C. Shaffrey, K. I. Hodges, P. G. Sansom, and D. B. Stephenson (2013). "A multimodel assessment of future projections of North Atlantic and European extratropical cyclones in the CMIP5 climate models". In: *Journal of Climate* 26.16, pp. 5846–5862 (→ pages 20, 21, 76, 81).

Zhang, Z., F. M. Ralph, and M. Zheng (2019). "The relationship between extratropical cyclone strength and atmospheric river intensity and position". In: *Geophysical Research Letters* 46.3, pp. 1814–1823 (→ page 173).

Zhang, Z. and F. M. Ralph (2021). "The Influence of Antecedent Atmospheric River Conditions on Extratropical Cyclogenesis". In: *Monthly Weather Review* 149.5, pp. 1337–1357. DOI: 10.1175/MWR-D-20-0212.1 (→ page 174).

List of Figures

1.1 **Unconditional**: Stott et al. (2004) compared two climates, one with natural forcing (NAT) and a historical climate (HIST) considering anthropogenic forcing. Pall et al. (2011) used an atmospheric circulation model with prescribed sea surface temperature (SST) and sea ice depicting two different climates. **Conditional**: Faranda et al. (2022) used the analogues approach to identify changes in the magnitude of the events. Jézéquel et al. (2018a) compute the trends in the likelihood of the atmospheric circulation pattern that lead to a particular extreme event. Leach et al. (2021) is a forecast-based approach in which, by changing the lead time of the simulations, they are able to change the level of conditioning (the lead time closest to the time of the event is the most conditioned on the circulation). 7

1.2 Stott et al. (2004) defines an extreme event as a threshold in temperature. World Weather Attribution is an academic collaboration of rapid attribution studies using the unconditional approach, by defining events as exceedances of a threshold of, for example, temperature, precipitation, or wind speed. Faranda et al. (2022) defines an extreme event based on its atmospheric circulation pattern. Climameter is an academic collaboration of rapid attribution studies using the conditional approach, by defining events based on their synoptic pressure pattern. Climameter and WWA are further discussed in section 1.1.4. Mitchell et al. (2016) defines the event as the heat related mortality. 8

1.3 Source: statistics taken from Carbon Brief (2022). 12

1.4 Figure from Martínez-Alvarado et al. (2014). Structure of a Shapiro-Keyser type cyclone in the Northern Hemisphere (NH). 14

1.5 Winter storm tracks in the Northern Hemisphere (NH) (December–February, DJF) and Southern Hemisphere (SH) (June-August, JJA) using ERA-Interim reanalysis. Black contours show ETC track density. Blue lines show individual ETCs tracks for the top 0.5% most intense cyclones. Shading corresponds to the eddy kinetic energy. Figure from Shaw et al. (2016). 16

1.6 Number of intense cyclones over the 45 years of the ERA-40 period at mature stage. Figure from Homar et al. (2006), modified by Flaounas et al. (2022). 17

1.7 Schematic diagram summarizing future changes to ETCs in the NH. Figure from Catto et al. (2019). . 21

2.1 Factual minus counterfactual differences of sea level pressure (SLP, d) and geopotential height at 500hPa (Z500, h). Coloured contours show the differences while grey contours show the counterfactual absolute values. Shading shows statistically significant differences. In all panels, negative values are stippled. This figure corresponds to Figures 2(d) and 2(h) of Ginesta et al. (2023). 29

2.2 Difference between the composite of factual and counterfactual analogues for (d) 24-hour accumulated precipitation (PR) and (l) maximum 10m wind gust within 24 hours (WG). This figure corresponds to to Figures 7(d) and 7(l) of Ginesta et al. (2023). 30

2.3 a) Mean Euclidean distance between the sea level pressure map of Alex and its analogues as a function of the number of analogues. b) Slope of the mean Euclidean distance curve as a function of the number of analogues. 31

2.4 Factual minus counterfactual differences of sea level pressure (a, c) and Z500 (b, c) of the composites with 20 analogues (a, b) and 50 analogues (c, d). Colored contours indicate differences, while grey contours represent counterfactual absolute values. Shading shows statistically significant differences. Negative values in (a,c) are stippled. 31

2.5 Factual minus counterfactual differences of sea level pressure (a, c) and Z500 (b, d) of the analogues found with a smaller domain (a, b) and a larger domain (c, d). The domain used for analogue identification is depicted by the dashed black box. Colored contours indicate differences, while grey contours represent counterfactual absolute values. Shading shows statistically significant differences. 33

2.6 Counterfactual anomalies of sea level pressure (a, c) and Z500 (b, d) of the analogues found with the smaller domain (a, b) and the larger domain (c, d). 34

2.7 Boxplots for all analogues in both counterfactual and factual periods of the different internal variability indices: ENSO, AMO, and PDO. A Mann-Whitney test is used to identify statistical differences in both distributions, with the null hypothesis of no significant difference between the periods. The p-value is shown in the title. We use monthly indices produced by NOAA/ERSSTv5; for ENSO the index is Nino3.4. Dots show the values for Alex. 34

3.1 (a–c) ERA5 6–hourly sea level pressure (slp), total precipitation (pr), and Scirocco wind speed (ws) on the 4th November 1966 at 12 UTC. (d–f) Normalized fields of figure 3.1, using 1950-2022 as reference period. 41

3.2 Empirical Cumulative Distribution Function (ECDF) for a specific grid point [43.5°N 12°E] using ERA5 data from 1950 to 2022. The red dashed lines indicate the point or quantile to which the ECDF for the event on the 2nd of May 2023 at this specific grid point belongs. a) shows the ECDF for sea level pressure, b) for precipitaiton, and c) for wind speed. 46

3.3 (a–c) Sea level pressure (slp), precipitation (pr), and wind speed (ws) on the 2nd of May of 2023 using ERA5 daily data. (d–f) Normalized fields, representing the quantiles with respect to the ERA5 ECDF. 47

3.4 Histogram of the Euclidean distances between the event of the 2nd of May and all other timesteps in the ERA5 past period for slp (a), pr (b), and ws (c). 48

3.5 a) Timeseries of the spatially averaged total Euclidean Distance according to equation (3.5) for the present period to the event of the 2nd of May 2023. b,c,d) show the distances of the normalized fields of sea level pressure (slp), precipitation (pr), and wind speed (ws), each contributing equally to the total distance $d(t)$. Coloured crosses show the distances of the 20 analogues of the present period. 48

3.6 *Analogues quality* computed as the spatially averaged Euclidean distance between the pr of the events in ERA5 and the pr of the 20 analogues for each simulation over the regional domain. Each letter is a simulation, corresponding to table 3.1. 50

3.7 Sea level pressure (a), precipitation (e), and wind speed (i) on the 2nd of May 2023 using ERA5 data. slp composites of the 20 analogue storms for the past (b) and present (c) periods, and the corresponding pr (f,g) and ws (j,k) composites. Present minus past differences of slp, pr and ws are shown in (d,h,l). Shading in shows statistically significant differences. A bootstrap test was conducted with a confidence level of 95%. 51

3.8 Same as figure 3.7 but for the 10th of May 2023 51

3.9 Same as figure 3.7 but for the 16th of May 2023 52

3.10 Future minus present precipitation (pr) of the analogues over the regional domain (Fig. S1h dashed black box) for the event of the 2nd of May 2023. The mean is represented by a dot, and the confidence interval at a 90% confidence level is depicted by vertical bars, computed using a bootstrap test. Blue denotes positive significant change and brown negative. Each letter is a simulation, corresponding to table 3.1. 53

3.11 Same as figure S1 but for the 10th of May 2023 53

3.12 Same as figure S1 but for the 16th of May 2023 54

S1 Sea level pressure (a), precipitation (e), and wind speed (i) on the 2nd of May 2023 using ERA5 data. slp composites of the 20 analogue storms for the historical (b) and future (c) simulations using the EURO-CORDEX models, and the corresponding pr (f,g) and ws (j,k) composites. Future minus historical differences of slp, pr and ws are shown in (d,h,l). Shading in shows statistically significant differences. A bootstrap test was conducted with a confidence level of 95%. 56

S2 Same as figure S1 but for the 10th of May 2023 56

S3 Same as figure S1 but for the 16th of May 2023 57

4.1 24-hour track of the development stage of storm **Alex** (thick black line) and its analogues (thin grey lines), for ERA5 (a), CESM present (b), and CESM future (c). Explosive analogues' tracks are highlighted in red. The figure legend shows the number of analogues and explosive analogues. The tables beneath the figures depict the Normalized Deepening Rates. 95 % confidence intervals for CESM present and CESM future, determined using a bootstrap test, are denoted in brackets. This figure corresponds to figure 3 of Ginesta et al. (2024) included in Appendix B. 63

4.2 Shading: CESM future minus present differences in the composites of **explosive analogues** of storm **Alex** of (g) sea-level pressure, (c) horizontal gradient of equivalent potential temperature at 850 hPa, (h) hourly mean precipitation rate, and (i) hourly mean wind speed. Black contours show the CESM present composites, from 980 hPa and every 4 hPa for SLP, from 10 mm/day and every 5 mm/day for PR, and from 10 m/s and every 2 m/s for W. These figures correspond to figures 9g, 10c, 9h, 9i, of Ginesta et al. (2024) included in Appendix B, respectively. 65

4.3 24-hour track of the development stage of storm Alex (thick black line) and its analogues (thin grey lines) for ERA5 for storm Alex (a), Eunice (b), and Xynthia (c), using TE tracking method. Explosive analogues' tracks are highlighted in red. The dashed-line circle indicates the 300-km area used to identify mature stage storms. The figure legend shows the number of analogues and explosive analogues. The tables beneath the figures depict the Normalized Deepening Rate values. These plots would be the equivalent of figures 1a, 3a, and 5a, of the manuscript using M20 tracking method. 67

4.4 24-hour track of the development stage of storm Alex (thick black line) and its analogues (thin grey lines) for ERA5 for storm Alex for CESM present (a) and CESM future (b) periods using TE tracking method. Explosive analogues' tracks are highlighted in red. The dashed-line circle indicates the 300-km area used to identify mature stage storms. The figure legend shows the number of analogues and explosive analogues. The tables beneath depict the Normalized Deepening Rate values. These plots would be the equivalent of figures 1b,c of the manuscript, in which M20 tracking method was used. . . 68

4.5 Equivalent to figure 7 (d–i) of the manuscript but using TE tracking method to identify analogues. . . 69

4.6 24-hour track of the development stage of storm Alex (thick black line) and its analogues (thin grey lines) for ERA5 for storm Alex (a), Eunice (b), and Xynthia (c), using TE tracking method. Explosive analogues' tracks are highlighted in red. The dashed-line circle indicates the 300-km area used to identify mature stage storms. The figure legend shows the number of analogues and explosive analogues. The tables beneath the figures depict the Normalized Deepening Rate values. These plots would be the equivalent of figures 1a, 3a, and 5a of the manuscript, in which M20 tracking method was used. 70

4.7 Mean Euclidean distances between the 24–hour track of the development stage of storm Alex and its analogues for ERA5 using three tracking methods, M20, TE, and M02, for storm Alex (a), storm Eunice (b), and storm Xynthia (c). 70

4.8 Percentage change in the number of analogues for 16 CMIP6 runs under the SSP2-4.5 (a) and SSP5-8.5 (b) scenarios, computed with reference to the historical period [1986-2013]. The analysis covers two future periods: mid-century [2021-2060] and end of the century [2061-2100]. The black dashed line represents the percentage change in the end-of-century period [2091-2100] for the CESM large ensemble under the RCP8.5 scenario, as reported in the manuscript. 72

4.9 Detection and tracking of explosive storm Xynthia and its associated atmospheric river. Red indicates concurrent time steps with the atmospheric river and explosive development of the storm, in black the subsequent time steps. The shading represents the overlaying atmospheric river masks for each timestep, with darker colors indicating overlapping over timesteps. 73

4.10 a) Ratio (R) between the number of explosive storms with atmospheric river and the total number of explosive storms as a function of the time distance to the Maximum Deepening Point (MDP) for ERA5 and the historical period of CMIP6 models [1980–2009]. b) R for the CMIP6 models for the historical period and the future period [2070–2099] for the scenarios SSP1-2.6, SSP2-4.5, and SSP5-8.5. 75

4.11 a) Ratio (R) between the number of explosive storms with AR and the total number of explosive storms for the multi-model mean of CMIP6 historical period. b–d) Differences in R between the future scenarios and the historical period. Dots indicate the grid points where all six models agree on the sign. 75

List of Tables

3.1 List of RCM-GCM combinations with corresponding institutions. Last column shows the label for figures 3.6, 3.10,3.11,3.12. 45

4.1 List of General Circulation Models (GCM) and runs used with their respective nominal atmospheric resolutions. 71

Appendix A

Article "A methodology for attributing severe extratropical cyclones to climate change based on reanalysis data: the case study of storm Alex 2020"

A methodology for attributing severe extratropical cyclones to climate change based on reanalysis data: the case study of storm Alex 2020

Mireia Ginesta[1*], Pascal Yiou[1], Gabriele Messori[2,3] and Davide Faranda[1,4,5]

[1*]Laboratoire des Sciences du Climat et de l'Environnement, LSCE/IPSL, CEA-CNRS-UVSQ, Université Paris-Saclay, Gif-sur-Yvette, 91191, France.
[2]Department of Earth Sciences and Centre of Natural Hazards and Disaster Science (CNDS), Uppsala University, Uppsala, Sweden.
[3]Department of Meteorology and Bolin Centre for Climate Research, Stockholm University, Stockholm, Sweden.
[4]London Mathematical Laboratory, 8 Margravine Gardens London, W6 8RH, London, United Kingdom.
[5]LMD/IPSL, Ecole Normale Superieure, PSL research University, Paris, France.

*Corresponding author(s). E-mail(s): Mireia.Ginesta-Fernandez@lsce.ipsl.fr;
Contributing authors: pascal.yiou@lsce.ipsl.fr; gabriele.messori@geo.uu.se; davide.faranda@lsce.ipsl.fr;

Abstract

Extreme event attribution aims at evaluating the impact of climate change on specific extreme events. In this work, we present an attribution methodology for severe extratropical cyclones, and test it on storm Alex. Alex was an explosive extratropical cyclone that affected Southern France and Northern Italy at the beginning of October 2020. The methodology exploits mathematical properties of circulation analogues, and identifies changes in physical and statistical properties. We first

divide 6-hourly ERA5 data into two periods: a counterfactual period (1950–1984) and a factual period (1986–2021). We then identify the 30 cyclones in each period whose sea-level pressure maps are closest to Alex's map by selecting those with the lowest Euclidean distance from Alex. We term these "analogues" of Alex. We find that analogues in the factual period are more persistent than in the counterfactual period, which may favour severe impacts resulting from persistent strong winds and heavy precipitation, as was the case for Alex. This effect is compounded by the doubling in accumulated daily precipitation detected in Northern Italy between the counterfactual and factual analogues. In the factual period, the analogues display an increase in the eddy kinetic energy in their growth phase, with poleward-shifted backward tracks. We also identify a seasonal shift of the analogues, from spring to autumn. Finally, the analogues in the factual period are closer to Alex than in the counterfactual period. These changes collectively point to high-impact storms like Alex having become more common in a changing climate.

Keywords: Extratropical explosive cyclones, Extreme Event Attribution, Climate Change, Analogues

Acknowledgments

This work was supported by the European Union's Horizon 2020 research and innovation programme under the Marie Sklodowska-Curie grant agreement N° 956396 (European weather extremes: drivers, predictability and impacts (EDIPI) ITN). The authors wish to thank S Bourdin, J Riboldi, M Rodrigo, F Pons, S Thao and Y Robin for useful discussions, J Pinto for sharing the ERA5 tracks database, and two anonymous reviewers for their constructive comments.

1 Introduction

Under global warming, the atmosphere is experiencing dynamic and thermodynamic changes (Allan et al, 2021). Understanding and predicting such changes is an essential step in order to evaluate climate-related hazards today and in the future (Pörtner et al, 2022). A major effort in this direction has been achieved with extreme event attribution (EEA) (National Academies of Sciences, Engineering, and Medicine, 2016). EEA is an emerging field that originated in the early 2000s (e.g. Stott et al, 2004) whose objective is to estimate to what extent climate change influences the likelihood and severity of specific extreme climate events. Extreme event attribution combines statistical analyses and physical understanding (Stott et al, 2016), and has been applied to a broad range of extremes events, including droughts, cold spells, heatwaves or extreme rainfall events (e.g. Philip et al, 2018; Cattiaux et al, 2010; Stott et al, 2004; Jézéquel et al, 2018; Pall et al, 2011).

Some extreme event categories have nonetheless proved more difficult to analyse in an attribution framework than others. An example are extratropical cyclones (ETCs), whose location, frequency and intensity depend on a combination of large-scale, synoptic-scale and smaller dynamic and thermodynamic features (Shapiro et al, 1999). This makes it challenging to both understand recent trends in ETC occurrence and project future ones (e.g. Shaw et al, 2016). In the Northern Hemisphere (NH), the number of ETCs has likely increased in recent decades (Chang and Yau, 2016), while there is evidence of a decrease in the number of NH extreme cyclones in winter (Neu et al (2013), referred to as deep cyclones) and in summer (Chang et al (2016), referred to as strong cyclones). However, there is low confidence for such changes as they are subject to high internal variability and regional variations and they are sensitive to the choice of reanalysis (Tilinina et al, 2013) and cyclone detection and tracking methods (Neu et al, 2013). In future climate projections, the number of ETCs in the storm track regions is projected to decrease globally, while the number of extreme cyclones is likely to increase in NH winter (Priestley and Catto, 2022). As stated in the last IPCC report, the precipitation associated with ETCs over the NH (Seneviratne et al, 2021) and the number of ETCs associated with extreme precipitation (Lee et al, 2021) are projected to increase (high confidence). However, there is a less clear response regarding wind speed changes, which are expected to be small and subject to regional variations (Seneviratne et al, 2021).

These global or hemispheric-scale changes mask a number of important regional trends, although in many cases it may be difficult to determine to which extent these depend on long-term climatic changes or on low-frequency internal climate variability. For example, in the North Atlantic, there is evidence of an overall poleward shift of the storm track between 1979 and 2010 (Tilinina et al, 2013). The same authors state that very deep cyclones (<960 hPa) increased in frequency in the North Atlantic region from 1979 to 1990 in most reanalyses, and declined thereafter. However, such changes may be modulated by the interdecadal variability of the North Atlantic Oscillation (Feser et al, 2015). Simulations of future climates from the Coupled Model Intercomparison Project phases 5 and 6 (CMIP5 and CMIP6) project a tripolar anomaly pattern in winter North Atlantic storm track, with an extension of storm activity further into Europe and a decrease on the storm track's northern and southern flanks (Harvey et al, 2020; Zappa et al, 2013; Priestley and Catto, 2022). CMIP5 models and Regional Climate System Models from the Med-CORDEX initiative also show a weakening of the storm activity over the Mediterranean region (Zappa et al, 2015; Reale et al, 2022). However, according to the last IPCC report (Lee et al, 2021), there is low confidence in regional change projections in the NH and especially in the North Atlantic in winter due to "large natural internal variability, the competing effects of projected upper- and lower-tropospheric temperature gradient changes, and new evidence of weaknesses in simulating past variations in North Atlantic atmospheric circulation on seasonal-to-decadal timescales".

The uncertainty surrounding past and future regional trends in ETCs highlights the difficulty in attributing their occurrence to climate change. Here, we present an attribution methodology applicable to severe extratropical cyclones, and test it on storm Alex: an explosive cyclone that affected France and Italy in October 2020. We demonstrate that a combination of analogue analysis, dynamical systems theory and extreme value theory enables to attribute the characteristics and impacts of individual extratropical cyclones to the ongoing climatic changes.

The paper is organized as follows: section 2 describes the characteristics of Alex. Section 3 provides a detailed description of the data and methods used. It is followed by the presentation of the results in section 4 and a discussion and conclusion in section 5.

2 Alex: a high-impact explosive cyclone

Storm Alex was a powerful explosive cyclone (Sanders and Gyakum, 1980; Neu et al, 2013) that affected south-western Europe in October 2020. It formed as a small perturbation south of Greenland and was named by Météo-France on the 1st of October. Favoured by a very strong jet stream with core speeds of up to 100 m/s, Alex deepened rapidly and experienced explosive cyclogenesis between the 1st and the 2nd of October with a deepening rate of 1.62 Bergeron. The cyclone made landfall in Brittany on the night between the 1st–2nd October, with very intense surface winds of up to 140 km/h that caused widespread damage. On the 2nd of October in the early morning the cyclone reached its minimum pressure with values around 970 hPa (such as 969,6hPa in Vannes, France (Météo France, 2021)). The size of the cyclone was about $2x10^6$ km^2, with an effective radius of 810 km, computed using the area enclosed in the last closed isobar with 1 hPa step using the ERA5 reanalysis dataset (Hersbach et al, 2020). Alex then remained stationary over the English channel for a day. Southeasterly winds were induced in southern France and northern Italy, carrying warm, humid air from the Mediterranean and producing extremely heavy rainfall and strong winds. This phenomenon is known as a Mediterranean episode (WMO, 2020). On the 3rd of October the cyclone weakened and moved to Normandy. Finally, on the 4th of October, Alex headed northward to England and dissipated during the following days over the North Sea. Figure 1 shows Alex's backward and forward trajectories. It also shows the maximum wind gusts over land and the total accumulated precipitation over the domain between the 1st and the 4th of October at 06:00 UTC. As a caveat, it is possible that not all the precipitation and wind gusts displayed in Figure 1 are directly associated with storm Alex.

The persistence of storm Alex over the same region resulted in severe impacts, especially in southern France and northern Italy. The area located windward of the Alps received heavy and prolonged orographically-driven rainfall, leading to numerous record-breaking precipitation amounts registered in the Alpes-Maritimes, Var and Piedmont regions. Piedmont had the highest

rainfall since 1951, recording 630 mm in 24h in Sambughetto (European State of the Climate, 2020). Saint-Martin-Vésubie, a village in Alpes-Maritimes, recorded 501 mm of precipitation in 24 hours (Météo France, 2020a), which corresponds to more than three times the climatological October precipitation (Météo France, 2020b). Alex caused at least 23 fatalities (10 in France, 10 in Italy, 1 in Austria, 1 in Poland and 1 in the Czech Republic), more than 10 missing people and an estimated economic loss of about 2.7 billion euros (Météo France, 2021; Riviera 24, 2021; The Watchers, 2020; Aon, 2020).

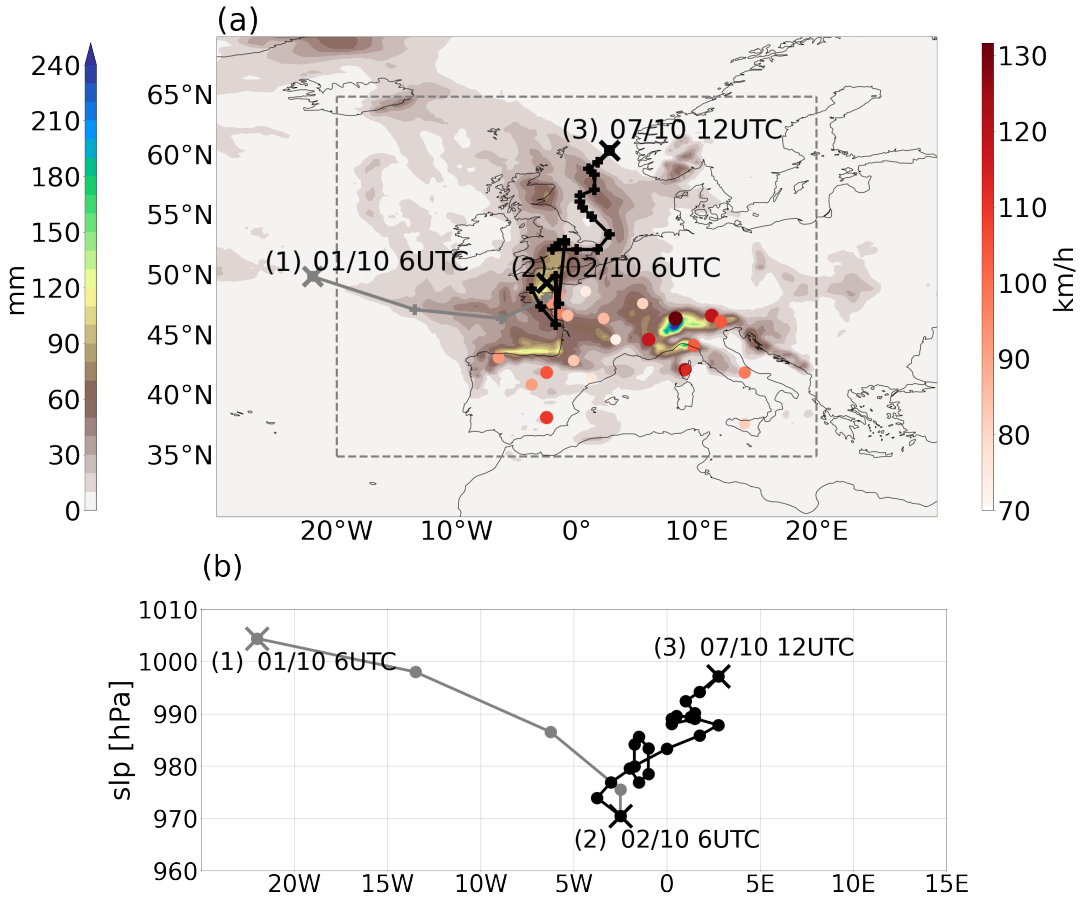

Fig. 1 (a) Backward (grey) and forward (black) trajectories of storm Alex relative to its point of maximum intensity. Total accumulated precipitation (shading) and maximum 10m wind gusts (coloured dots) between 01/10/2020 at 06:00 UTC and 04/10/2020 at 06:00 UTC, when Alex had its largest impacts. The numbers indicate when cyclogenesis occurred (1), when Alex reached its minimum sea-level pressure (2), and when it underwent cyclolysis (3). Dashed lines indicate the spatial domain used to find the analogues, covering (20W–20E, 35–65N). We use ERA5 6-hourly data to track the cyclone, and ERA5 hourly data to obtain the accumulated precipitation and maximum 10m wind gusts (see Section 3 for further details). The maximum 10m wind gusts were obtained for every region of France, Italy, and Spain, using spatial masks according to NUTS2 regions (Eurostat, 2021); here we only present some regions to have a general view of the storm's impacts. (b) The corresponding sea-level pressure evolution at the cyclone center as a function of time and longitude.

3 Methodology

We compute flow analogues (Yiou, 2014) to find pattern recurrences of Alex in mean sea-level pressure (SLP), and assess changes in the analogues within the ERA5 reanalysis dataset (Hersbach et al, 2020). We use 6-hourly data from 1950 to 2021, which we split into two 35-year periods: a factual period, from November 1986 to November 2021, and a counterfactual period, from January 1950 to December 1984. We refer to them as [1986-2021] and [1950-1984], respectively. The latter is meant to represent a climate only weakly affected by anthropogenic emissions, while the former presumably displays a stronger anthropogenic influence. This assumption is supported by a substantial change in the effective-radiative forcing from the 1980s onwards, as shown in Figure 2.10 of Chapter 2 in the last IPCC Sixth Assessment Report, (Gulev et al, 2021), and by a significant increase in the number of storms in the North Atlantic in the factual period with respect to the counterfactual (Fig. B1). The number of storms has been counted using the *TempestExtremes* software package (Ullrich et al, 2021; Ullrich and Zarzycki, 2017; Zarzycki and Ullrich, 2017). We pick 35-year periods as a balance between needing periods that are short enough to assume a relatively constant climate state, yet long enough to assume that interannual variability issued from periodic variations such as the El-Niño – Southern Oscillation averages out. Adopting two periods around 30-year long is a common practice in attribution studies (e.g. Luu et al, 2018; Vautard et al, 2019). We have tested that changing the periods slightly (e.g. [1950-1975] and [1995-2020]) do not alter qualitatively the results.

3.1 Analogue circulation patterns

We identify the 2nd of October 2020 at 6:00UTC as approximately when storm Alex reached its lowest central pressure (970.48hPa according to ERA5 data) while stalling over the English Channel. We term this time step *lag 0* date of Alex. We then use mean sea-level pressure to identify the best 30 analogue cyclones in the counterfactual and factual periods. To select the analogues, we compute the Euclidean distance between the sea-level pressure maps of the 2nd of October 2020 at 06:00UTC and all other time steps at each grid point of the spatial domain covering [20W–20E, 35–65N] (dashed-line box in Figure 1a). Then, we average the Euclidean distances for all grid boxes across the domain for each timestep, resulting in a time series of domain-averages Euclidean distances. The 30 analogues are the timesteps that display the 30 smallest Euclidean distances. To avoid counting several times the same cyclone, we impose a minimum 7-day separation between analogues. This is justified by the fact that 3 days is a typical timescale for the formation and decay of an extratropical cyclone (Moon et al, 2021), but that specific cyclones can last longer than this (e.g. Alex lasted 7 days). Since our main purpose is to find distinct storms similar to Alex in order to assess changes in their dynamical characteristics, we deem a 7-day separation appropriate. Changes in the spatial domain of up to 10 degrees do not alter the results in a significant manner.

Some quantitative changes are however expected when the domain is modified, as the analogues include information about all atmospheric structures within the chosen domain. The choice of 30 analogues is a balance between the needs to have a large enough sample size to make statistical inferences, and to have analogues that are suitably close to the reference event we are studying. Using 25 or 40 analogues rather than 30 does not change our results substantially. We have computed the average Euclidean distance of the closest 30 events for each sea-level pressure map of the two periods and found no significant differences in the probability distributions (Fig. B2). Hence, we conclude that 30 analogues is a robust choice.

Once we have obtained the *lag 0* dates of the 30 best analogues – namely the dates when the minimum Euclidean distance for each analogue is attained – we compute their composite maps for several variables of interest for each period, and the difference map between them. Figures B3 and B4 show the mean sea-level pressure patterns at the *lag 0* dates of the 30 analogues in the counterfactual and factual period, respectively. Additional variables of interest include geopotential height at 500 hPa (Z500), eddy kinetic energy at 500 hPa (EKE500), 24-hour accumulated precipitation (PR), 2m air temperature averaged over 24 hours (T2M), maximum 10m wind gust within 24 hours (WG), and deseasonalized 2m air temperature (T2Mdes). EKE500 is computed using a 24-hours difference filter (Wallace et al, 1988). WG is the maximum 3-second wind at 10 m height as defined by the World Meteorological Organization (WMO, 1987), where the gust is computed at every time step and the maximum is kept since the previous post-processing. To compute PR and WG, we use hourly data, and to evaluate T2M we use 6-hourly data. The start times to compute the accumulated values for PR, average values for T2M and maximum values for WG are the *lag 0* dates and end times are 24 hours after them, that is, at *lag +24* hours. To evaluate T2Mdes, we first compute a 31-day running-mean smoothed seasonal cycle for each period. We then subtract the smoothed seasonal cycle from the T2M data.

For each analogue, we compute 48 hours backward and forward cyclone trajectories with a 6-hours time step using a semi-objective Lagrangian approach. Cyclone centers are automatically identified by following the absolute minimum sea-level pressure. We have then checked and corrected each trajectory manually if needed, which induces some subjectiveness in our method. Some cyclones originate from secondary cyclogenesis, that is, from the trailing fronts of a 'primary cyclone' (Parker, 1998; Priestley et al, 2020). They are typically diagnosed by a trough in the sea-level pressure configuration of the primary cyclone. Here we detect them using a semi-objective method where troughs are detected visually but are required to have a minimum depth of 5hPa. We have compared factual cyclone tracks with those obtained following Pinto et al (2005), which corresponds to the method M02 from Neu et al (2013) of the Intercomparison of Mid Latitude Storm Diagnostics (IMILAST), without finding any qualitative differences. Hence, the tracking method used here is not expected to alter our results and conclusions.

We count the number of cyclones that experienced explosive cyclogenesis following the definition of Sanders and Gyakum (1980) as those with a Normalized Central Pressure Deepening Rate (NDR, Reale et al (2019)) greater than 1. We also count the number of cyclones entering the Mediterranean region as those that, after 24 hours or more, are located at latitudes south of 43°N and longitudes east of 3°E.

We finally assess the quality of analogues. We first compute *SLP anomalies* by subtracting Alex's SLP from the mean SLP of the analogues in the two periods. Second, we represent the probability distributions of the values of the SLP Euclidean distances between Alex and its analogues and we term it *analogues quality*.

3.2 Dynamical systems metrics

In order to characterise the dynamics of storm Alex and its analogues, we use local dimension and persistence metrics issued from dynamical systems theory. These metrics describe the local properties of a dynamical system (Lucarini et al, 2016), which for atmospheric data may be related to the characteristics of instantaneous regional atmospheric patterns (e.g. Messori et al, 2017; Faranda et al, 2017; Alvarez-Castro et al, 2018; Messori et al, 2021).

We follow the approach from Faranda et al (2017) and Lucarini et al (2016), who combine extreme value theory with dynamical systems theory to compute the local dimension d and persistence θ^{-1} of dynamical systems. Local dimension d describes the phase-space geometry of the trajectories in the neighbourhood of a certain state of the system. The higher d, the higher the number of possible evolutions to and from that state. The persistence θ^{-1} measures the average residence time around a given state, and is given by the inverse of the extremal index θ. θ has units of frequency (here 1/6 hours^{-1}, as we use 6-hourly data). Hence, to find the persistence in hours, we multiply θ^{-1} by a factor of 6. A detailed description of the procedure to compute d and θ^{-1} is provided in Appendix A.

3.3 Assessing statistical significance

To assess the statistical significance of the differences between the analogues' averages in the factual and counterfactual periods, we apply a bootstrap procedure with 1000 iterations (Wilks, 2005). Our null hypothesis is that both sets of analogues are drawn from distributions with the same mean. If the difference of the two original samples — factual minus counterfactual — has an absolute value larger than the 95th percentile of the bootstrap distribution, we reject the null hypothesis and conclude that the differences are statistically significant. To compute Confidence Intervals (CI) for statistical samples we again apply a bootstrap procedure with 1000 iterations, with a 95% confidence level, namely taking the 2.5th and 97.5th percentiles of the bootstrap distribution as the lower and upper bounds, respectively. To evaluate the CI of the local dimension d we resample the exceedances of the threshold $s(q)$ (see section A)

and compute d in each iteration. To calculate the CI of the extremal index θ we resample the inter-cluster and cluster sizes with equal probabilities (Süveges, 2007), and compute θ for each sampling iteration. Finally, the statistical significance of the differences between boxplots is assessed using a two-sample Kolmogorov-Smirnov test (Wilks, 2005), with a 5% significance level. The null hypothesis is that both data samples belong to the same, unknown distribution.

4 Results

4.1 Circulation patterns

Figure 2a–c shows the SLP map for the *lag 0* time step of Alex and the composite SLPs for analogues during the counterfactual and factual periods, respectively. Both sets of analogues capture the large-scale structure of Alex, albeit with a weaker magnitude as may be expected by the average of 30 events. Note that when computing the Euclidean distances to find the analogues we use the domain shown by the dashed-line box in Fig. 1, and so the North Atlantic large-scale atmospheric configuration might differ between analogues. The difference between the two analogue composites (Fig. 2d) displays an SLP dipole: high pressure anomalies over the North Atlantic and low pressure anomalies over North Africa. This northward (southward) extension of the high (low) pressure system yields an increase in the waviness of the pattern in the factual period. No significant differences are found at the cyclone center. In the middle troposphere (Z500), the analogues capture the low pressure structure over England that characterised Alex (Fig. 2e, f, g). The Z500 differences between the analogues in the two periods (Fig. 2h) partly resemble those in SLP: there is a northward extension and a strengthening of the Azores anticyclone, enhancing the waviness of the pressure field.

Fig. 3 shows Alex's SLP and Z500 and the composite SLP and Z500 of the analogues 12 hours after *lag 0* dates, that is, at *lag +12* hours. We find negative, albeit marginally significant, SLP anomalies over the cyclone core region. In the mid-troposphere, Z500 shows high-pressure anomalies over the North Atlantic. The pattern of the background flow is thus wavier in the factual period, as for *lag 0*, due to low-pressure anomalies in the cyclone region and upstream high-pressure anomalies.

We further analyse the EKE500 maps for Alex and its analogues (Figure 2i–l) 24 hours before *lag 0* dates, that is, at *lag -24h* hours. There is a clear difference between Alex's EKE500 and that of the analogues in both periods, which emphasizes that the analogue storms have different origins across the North Atlantic basin. Composite EKE500 analogue differences between the two periods (Fig. 2l) show a dipole of positive anomalies west of England and weaker negative anomalies at lower latitudes, representing a poleward shift in the factual period with respect to the counterfactual. In addition, EKE500 differences centered at 48 hours before Alex show this dipole but shifted about 10° to the west (Fig. B5). This pattern suggests a higher-latitude origin of the storms in the factual period, consistent with the increase in the waviness found

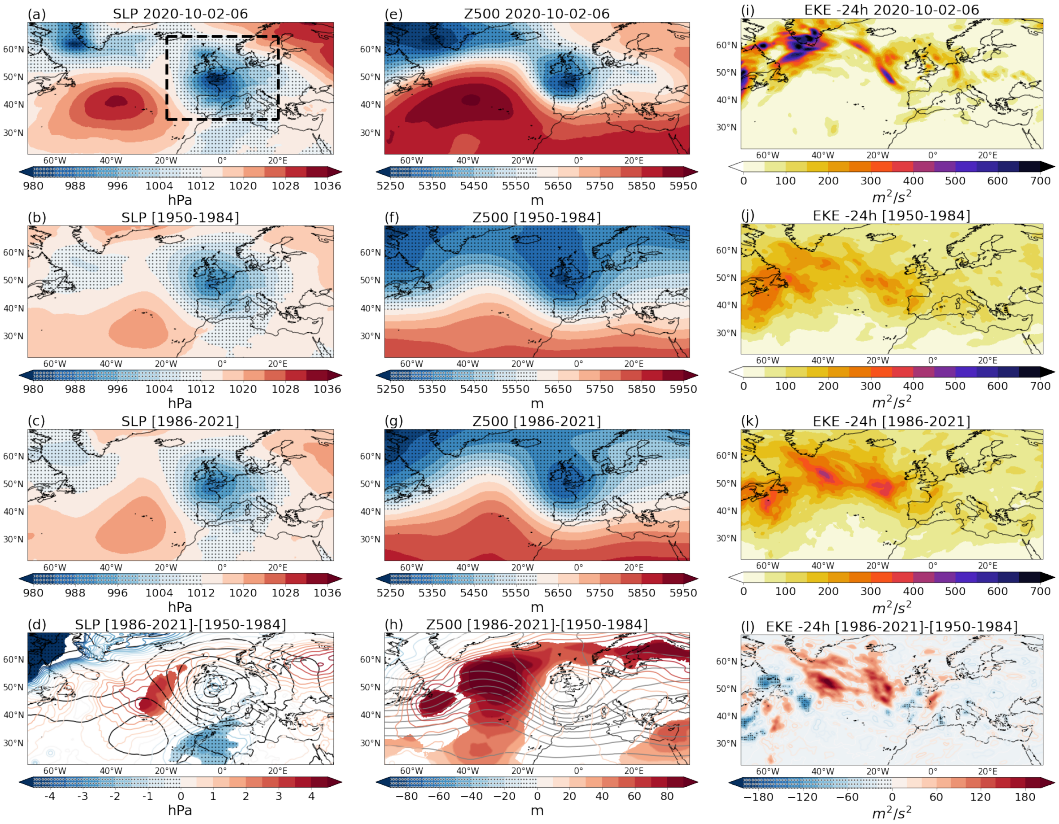

Fig. 2 Mean sea-level pressure (a) and geopotential height at 500hPa (e) at the *lag 0* date of storm Alex and 500 hPa eddy kinetic energy (i) 24 hours prior to the *lag 0*. SLP composites of the 30 analogue storms for the counterfactual (b) and factual (c) periods, and the corresponding Z500 (f,g) and EKE500 (j,k) composites. Factual minus counterfactual differences of SLP (d), Z500 (h) and EKE500 (l). Coloured contours in (d) and (h) show the differences while grey contours show the counterfactual absolute values. Shading in (d, h, l) shows statistically significant differences. In all panels, negative and low values are stippled

in the SLP and Z500 maps (Fig. 2d,h). Figure 2l also shows an increase of the maximum EKE500 over most of the North Atlantic, which implies that storms in the factual period are more energetic in their growth phase than those in the earlier period.

4.2 Cyclone tracking

To better assess changes in storm location, the tracks of the analogue cyclones are shown in Fig. 4. There is a clear latitudinal shift in the backward trajectories, that is, the trajectories of the cyclones up to 48 hours before the *lag 0* dates: in the factual period (solid red), the storms head towards Europe from higher latitudes than those in the counterfactual period (dashed blue). There is no overlap in the confidence intervals, which means that this shift is statistically significant. The forward trajectory response, that is, up to 48 hours after the *lag 0* dates, is less clear, as most storms dissipate not far upstream of the English Channel. The backward trajectory of Alex shows that

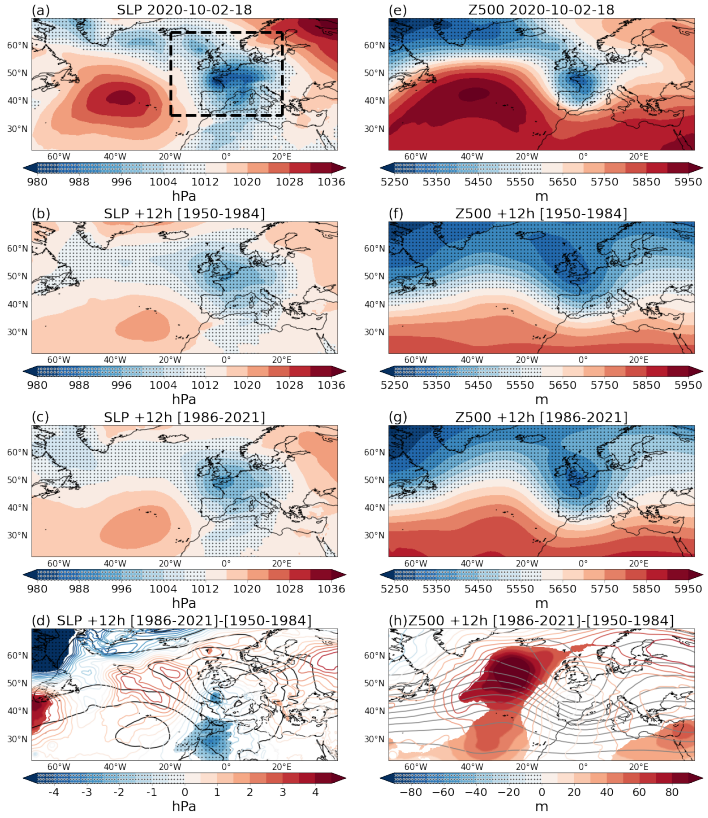

Fig. 3 Same Fig. 2a–h, but at *lag +12* dates.

the cyclone formed and grew at latitudes below 50°N (Fig. 4), indicating a higher resemblance with those in the counterfactual period.

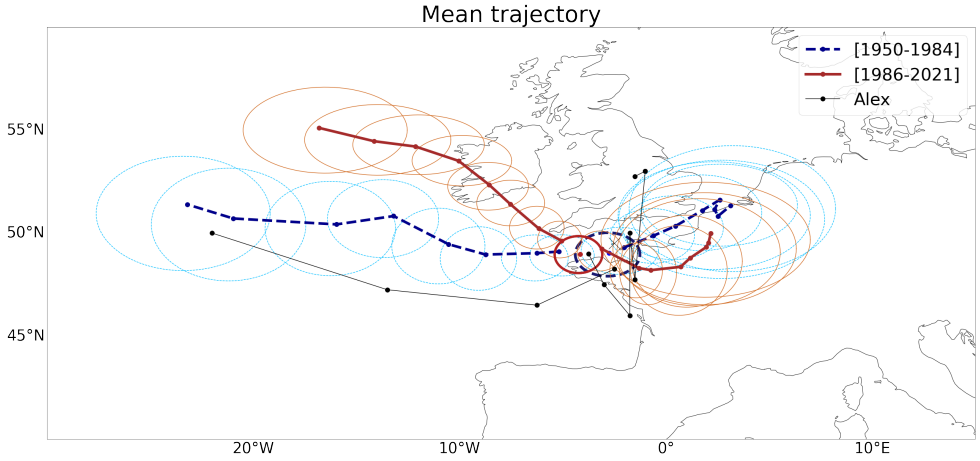

Fig. 4 Alex's track (black line) and average cyclone tracks for the factual (red solid line) and counterfactual (blue dashed line) periods. Dots represent cyclone locations on 6-hourly timesteps. Ellipses show the confidence interval, built using bootstrapping, for each timestep of factual (red thin solid lines) and counterfactual (blue thin dashed lines): the x-axis shows confidence intervals of longitudes and the y-axis of latitudes. Thick ellipses and dots show the confidence intervals and the average cyclone positions for the dates of the analogues, respectively.

A counting of explosive cyclones using the definition of Sanders and Gyakum (1980) has been performed for both periods. In the counterfactual period two analogue cyclones underwent explosive cyclogenesis, from 11/03/1976 at 6 AM to 12/03/1976 at 6 PM and from 03/10/1984 at 12 AM to 04/10/1984 at 12 PM. The latter corresponds to storm Hortense, which mainly affected Southwestern France (Météo France, 2019a). In the factual period, apart from Alex itself only one explosive cyclone has been found, from 04/11/2000 at 12 AM to 05/11/2000 at 18 PM. This is cyclone Rebekka, which had its greatest impact in Southern France (Météo France, 2019b). The NDRs of the two explosive cyclones in the counterfactual period (1.51 and 1.50, respectively) are larger than that of the single explosive cyclone in the factual period (1.20). Alex has the largest NDR of our cyclone sample (1.61). The results presented here only include a very small fraction of the North Atlantic cyclones, and the explosive cyclone analogues found take place over a short period of time, between the 1974 and 2000, which is not enough to attribute the decline (from 2 explosive cyclones to 1) to any specific factor. A counting of cyclones that ended in the Mediterranean region has also been done, and we find 3 in the counterfactual world and 5 in the factual. This increase in frequency may be linked to the increase in waviness seen previously, although the results found here are insufficient to draw conclusions on the tendency of the number of Atlantic cyclones reaching the Mediterranean.

4.3 Seasonality of analogues

Figure 5a,b shows that in the counterfactual period Alex-like storms were more common in spring while in factual conditions they occur chiefly in autumn. The number of analogues in winter and summer remains unchanged over the two periods.

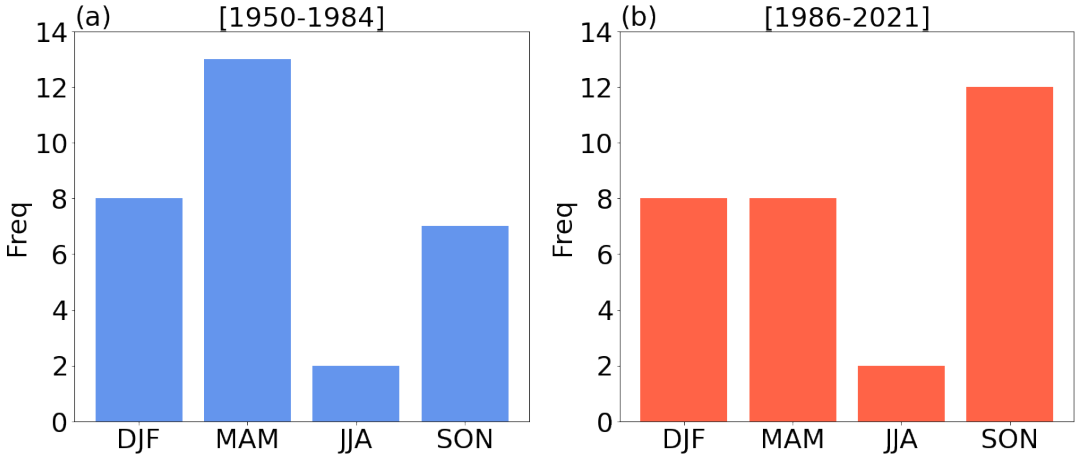

Fig. 5 Frequency of analogues per season, namely winter (DJF), spring (MAM), summer (JJA) and autumn (SON), for the counterfactual (a) and factual (b) periods.

The dynamical changes observed in figure 2d,h,l and 4, i.e., a wavier pressure pattern, a strengthening of the eddy activity, and a poleward shift of the backward trajectories, may be linked to either a direct or an indirect climate change signal. In the former, climate change would act to shift poleward and strengthen Alex's analogues directly. In the latter, climate change leads to a seasonal shift in the occurrence of analogue storms, and the observed changes correspond to the changes in the mean behavior of the cyclones according to the season of most frequent occurrence. The two effects are not exclusive, and changes may reflect a combination of direct and indirect signals. To help evaluate these two hypotheses, we search for 30 analogue storms in autumn (September-October-November) and 30 in spring (March-April-May) for each period and repeat the analysis of Sect. 4.1 and 4.2. Z500 field shows a wavier pattern, that is, a northward extension of the high pressure systems, in the factual period during autumn (Fig. B6), while in spring the pattern is less clear (Fig. B7). SLP maps show a deepening of the cyclone over France in autumn, and again a less clear pattern in spring. Hence, we attribute the wavier pattern and the increase in cyclone depth to: (i) a seasonal shift of the analogues from spring to autumn; and (ii) changes in autumn pressure patterns, when Alex occurred. This response could be then a combination of: (i) an indirect and (ii) a direct climate change signal, even though the proportion of (i) and (ii) is difficult to quantify. The mean tracking shows a clear poleward shift of backward and forward trajectories in spring, while in autumn the shift is weaker (Fig. B8).

4.4 Quality of Analogues

Figure 6a,b shows that composite SLP anomalies over the North Atlantic are smaller in the factual than in the counterfactual period. Figure 6c shows the distributions of the analogues quality. The set of factual cyclones provides better analogues than the cyclones from the counterfactual period. We also compute pressure anomalies and analogues quality for spring and autumn analogues separately (Fig. B9 and B10, respectively). Spring anomalies are larger over the North Atlantic compared to autumn ones in both periods. In the counterfactual period, analogues quality is better in spring than in autumn, which highlights the similarity of Alex with spring storms. In other words, Alex is more similar to analogue cyclones in spring in the counterfactual period, while the North Atlantic atmospheric circulation pattern associated with Alex is closer to that of the autumn analogues, consistent with the pressure field seasonality (Alex occurred in October). However, the quality of autumn analogues improves significantly in the factual world, while in spring there is almost no difference between the counterfactual and factual periods. We thus conclude that Alex was a "black swan" in autumn in the counterfactual period, and rather reflected the characteristics of spring cyclones. However, in the factual period the number of autumn analogues is rising (Fig. 5) and the quality is improving.

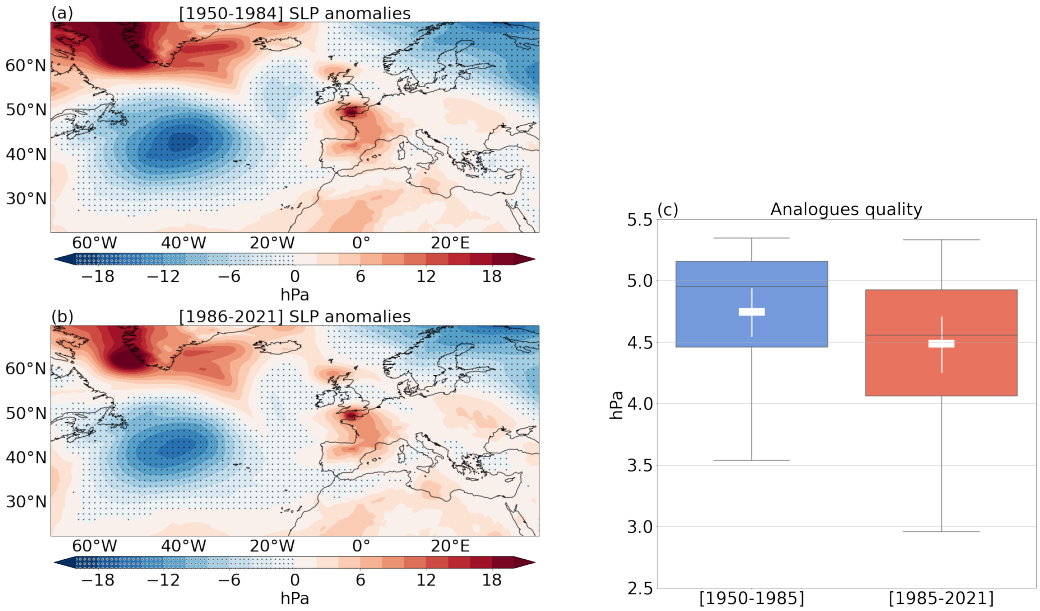

Fig. 6 Sea-level pressure anomalies of counterfactual (a) and factual (b) periods, and boxplots of analogues quality (c). The white horizontal lines show the means of each distribution and the white vertical lines the corresponding confidence intervals.

4.5 Impacts

In this section, we evaluate three surface fields to detect differences between factual and counterfactual impacts: PR, T2M and WG.

Alex generated heavy precipitation in southern and eastern France and northern Italy (Fig. 7a). The analogues averages (Fig. 7b,c) also show a significant amount of precipitation over this region in both periods, although much lower than storm Alex. There is also much weaker precipitation in southern England, central France and Northern Spain compared to Alex. This may be ascribed to a combination of weaker analogue cyclones and some variability in their position that leads to aliasing in the composite. Figure 7d shows a significant increase in precipitation between the counterfactual and factual analogues of more than 12 mm in 24 hours windward of the Alps, a region that suffered catastrophic consequences from Alex.

The increase in rainfall, probably linked to the Stau effect, is accompanied by a rise in 2m air temperature (Fig. 7h) leeward of the Alps, linked to the Foehn effect. In addition, there is a significant increase in temperature by more than 1.5 K over the eastern Mediterranean, the northeastern Atlantic Ocean, and the Baltic Sea. This increase can be due to a direct climate change signal, or it can reflect a shift in the seasonality of the analogues. To better assess these changes, we repeated the analysis on the deseasonalized T2M field (Fig. B11). We did not find significant changes between the counterfactual and factual periods, meaning that the T2M signal over the Alps and sea regions is mainly due to a shift in seasonality.

Figure 7l shows an increase of the 10m maximum wind gust in the Alps, Liguria and Provence of up to 5 m/s. Increasing accumulated precipitation

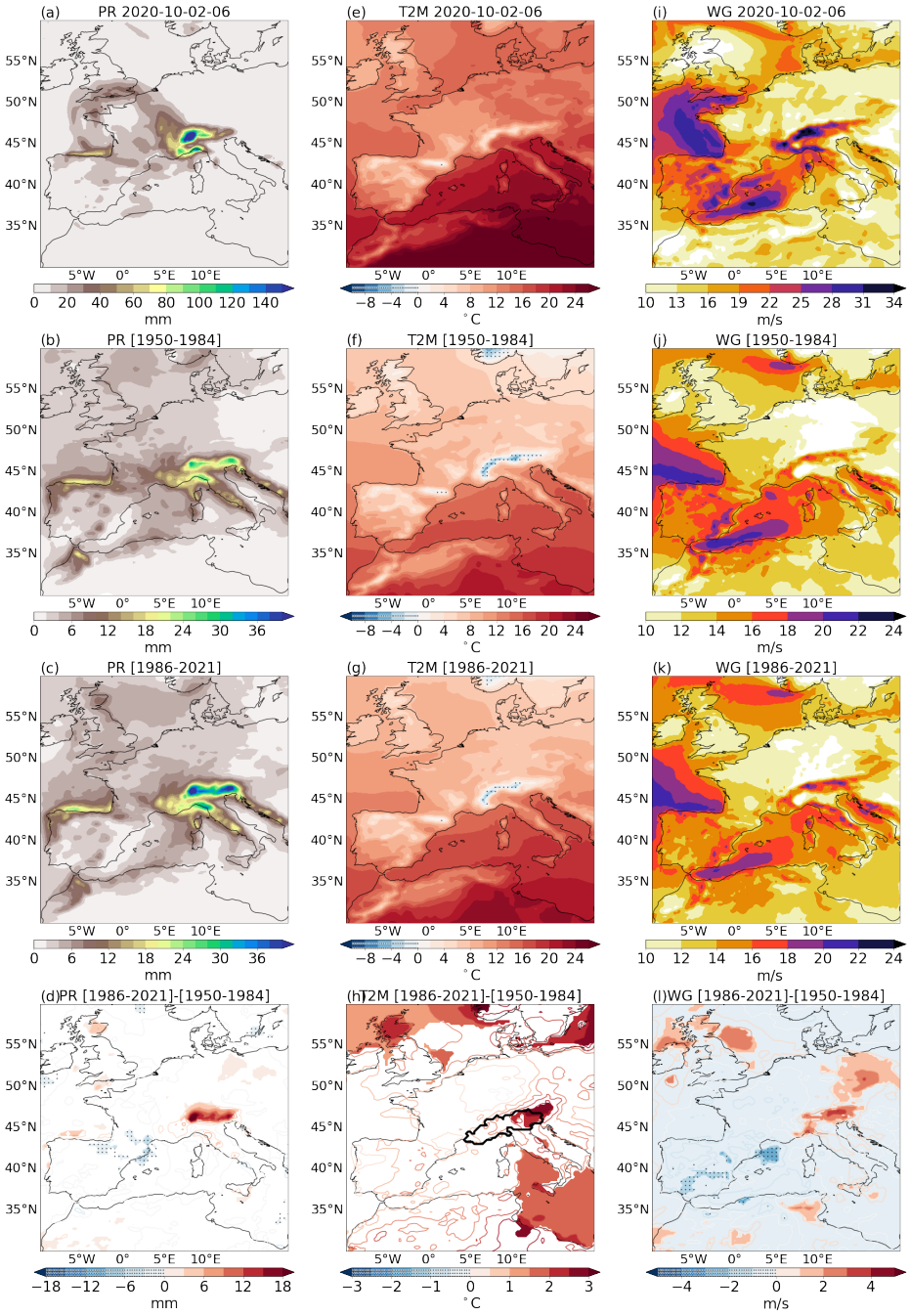

Fig. 7 24-hour accumulated precipitation for Alex (PR, a), counterfactual analogues (b), factual analogues (c), and difference between the two periods (d). Daily average of 6-hourly 2-meter air temperature for Alex (T2M, e), counterfactual analogues (f), factual analogues (g), and difference between the two periods (h). Maximum 10m wind gust within 24 hours for Alex (WG,i), counterfactual analogues (j), factual analogues (k), and difference between the two periods (l). Note that color bars in (a),(i) and (b,c),(j,k) are different. The thick black contour in (h) shows the spatial mask applied in the analysis of Fig. 8 and covers the *target region* formed by: Provence-Alpes-Côte d'Azur, Liguria, Piemonte, Lombardia, Valle d'Aoste, Provincia Autonoma di Bolzano, Veneto, Provincia Autonoma di Trento and Friuli-Venezia Giulia.

and maximum wind gust imply that factual cyclones are a greater hazard. 24-hour mean 10m meridional wind (Fig. B12) shows positive anomalies over the Ligurian Sea and the Gulf of Venice, which enhances the advection of warm, humid air from the Mediterranean to Northern Italy and Southeastern France (Fig. B12h). This increase in meridional wind, related to an increase in the meridional SLP gradient, can also yield the increase in precipitation seen previously (Fig. 7d, h).

To further quantify the observed increase in precipitation and temperature in northern Italy and southern France, we first apply a spatial mask (Fig. 7h) to limit the analysis to the regions of highest impacts for Alex and greater differences between the counterfactual and factual analogues. This delimited region is referred to as *target region* in the remaining text. For Alex's *lag 0* time step, we compute the 99th quantile of PR, T2M and WG over the *target region*. We then compute the (spatial) average values above this quantile in the *target region*. This procedure is also applied to the analogues. We term the (spatial) averages maximum precipitation (PRmax), maximum temperature (T2Mmax) and maximum wind gust (WGmax). Hence, we can determine the different probability distributions of PRmax, T2Mmax and WGmax, linked to an Alex-like storm, in the two periods (counterfactual and factual; Fig. 8). We find that PRmax during Alex is much higher than the rest of the analogues, reaching almost 250 mm. The means of PRmax for the analogues are around 50 mm in the counterfactual period and 80 mm in the factual period. In addition, in the factual period the 75% quantile of the boxplot exceeds 100 mm of rain, while it barely reaches 60 mm in the counterfactual. Hence, in the factual period there is an increase in maximum rainfall. T2Mmax during Alex is higher than that of most of its analogues. There is also a shift of the T2Mmax distribution towards higher maximum temperatures in factual conditions by about 2°C. WGmax during Alex is higher than that of the analogues in factual world but comparable with the counterfactual maximum. WGmax mean and median values increase from counterfactual to factual periods by about 2 m/s. PRmax distribution differences between the two periods are statistically significant, while the T2Mmax and WGmax differences are not. We repeated the analysis of Fig. 8 but for the full domain to find the analogues (dashed-line box in Fig. 1), and applying a land-sea mask for the wind gusts. We have found qualitatively different results for the wind gusts but similar for precipitation (not shown). In the case of wind gusts, the differences in the probability distributions are likely due to features of the synoptic circulation away from the *target region*. We found that 8 analogues in the counterfactual period and 12 in the factual have their highest wind gusts over the *target region*. Regarding the precipitation, the region of maximum precipitation of most of the analogues, that is, 22 in the counterfactual period and 25 in the factual, corresponds to the region of highest precipitation of Alex.

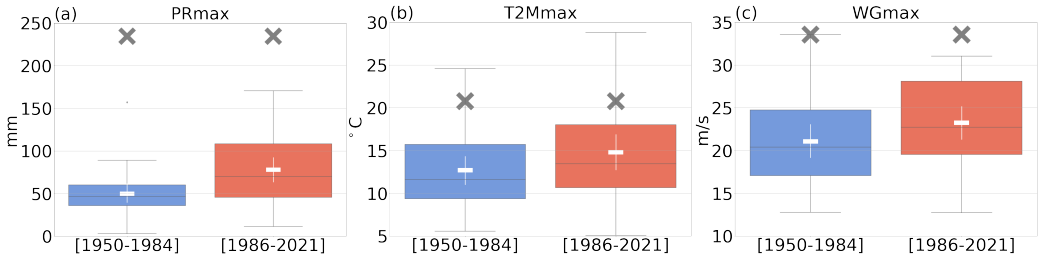

Fig. 8 Boxplot of the area-averaged values above the 99% quantile over the *target region* for PR (a), T2M (b) and WG (c). The white horizontal lines show the means of each distribution and the white vertical lines the corresponding confidence intervals. Grey crosses show the values of Alex.

4.6 Dynamical system metrics

Table 1 shows a decrease in d in the factual world with respect to the counterfactual, which means that the most recent climate has fewer possible evolutions than the counterfactual one. In addition, θ^{-1} shows that factual period storms are ∼4 hours more persistent than the counterfactual period ones (Table 1). Hence, the sea-level pressure pattern is more persistent in the factual period, increasing the stationarity of the cyclonic systems. The differences in d and θ^{-1} are both statistically significant. The decrease in d and the increase in θ^{-1} point to an increase in the intrinsic predictability, as low values of d and high of θ^{-1} are associated with high-predictability configurations (Messori et al, 2017; Faranda et al, 2017; Hochman et al, 2019). While this result is obtained specifically for severe cyclones, it is in line with the results found in Faranda et al (2019) and Scher and Messori (2019) who, using two independent approaches, argued for an increasing predictability of the midlatitude atmosphere.

	[1950-1984]	**[1986-2021]**	**Change %**
d	7.5 [6.6 8.3]	6.8 [6.1 7.6]	-8.5
θ^{-1}	20.8 [18.9 22.7]	24.1 [21.4 26.8]	15.7

Table 1 Local dimension d (unitless) and persistence θ^{-1} (hours) in the counterfactual (first column) and factual (second column) periods, and the relative changes in the factual with respect to the counterfactual period (third column). Values in brackets show confidence intervals.

5 Discussion and Conclusion

We have presented a methodology for the attribution of severe extratropical cyclones and their impacts to ongoing climate change. We specifically applied this to storm Alex, which struck southern and western Europe in October 2020. We based our analysis on 30 analogue storms (Yiou, 2014) for Alex in factual (with strong climate change) and counterfactual (with limited climate change) periods from ERA5, and their dynamical properties.

A comparison of the two sets of analogues evidences that the factual storms typically occur on the background of a wavier atmospheric pattern than the counterfactual storms. This stronger meridional component of the flow is likely linked to a slower-moving wave pattern (Screen and Simmonds, 2014), as also highlighted by a persistence index we computed using dynamical system theory. This shows an average 4h increase in the persistence of atmospheric patterns in the factual world. Previous studies also found an increase in persistent circulation regimes in recent years (Alvarez-Castro et al, 2018; Hoffmann, 2018), and some suggest a possible link with Arctic Amplification (Cohen et al, 2018; Yao et al, 2017; Kornhuber and Tamarin-Brodsky, 2021). The observed amplified low-level warming at high latitudes in the NH (Serreze et al, 2009) would act to weaken the zonal wind via the thermal wind relationship, resulting in an increase in amplitude of the polar jet meandering and slower wave propagation, and favouring the longer persistence of weather patterns that lead to extreme events. However, due to the complexity of the eddy-mean flow feedbacks, the underlying dynamics are not entirely clear (Hoskins and Woollings, 2015). In addition, a challenge arises in distinguishing the forced signal from the internal variability (Mann et al, 2017; Barnes and Screen, 2015), partly due to an incomplete knowledge of the influence of high-latitudes on mid-latitude weather as well as a lack of data (Cohen et al, 2014). Hence, according to the last IPCC report, "there is low to medium confidence in the exact role and quantitative effect of historical Arctic warming and sea-ice loss on mid-latitude atmospheric variability" (Doblas-Reyes et al, 2021). Further analysis linking sea-ice loss with the present work's findings could be performed, although the lack of reliable sea ice data before 1978 complicates the study.

We further find that, in the factual period, cyclones like Alex are more energetic in their growth phase, as seen by an increase in the eddy kinetic energy at *lag -24* hours. They also display lower pressures at *lag +12* hours during the decay phase of the storms. This interpretation assumes that *lag 0* corresponds also to the mature stage for the analogues of Alex. The analogues also tend to occur more frequently in autumn and less frequently in spring. However, this does not imply an a priori influence on storm intensity, as the two seasons are comparable in this respect (Hoskins and Hodges, 2019). When separating analogues according to season, autumn analogues have been found to undergo a large increase in cyclone intensity, which may be related to an increase in humidity leading to an increase in moist baroclinic instability and maximum EKE500 of baroclinic eddies (Gutowski Jr et al, 1992). Sinclair and Watterson (1999) also suggests that an enhancement in water vapor content and a localized increase in baroclinicity could increase regional storm activity. In addition, an increase of the land-sea contrast due to a faster warming over land than over the ocean (Jia et al, 2019) could enhance baroclinicity in summer and early autumn, yielding to an increase of the cyclones intensity. Further investigation using ad hoc numerical model simulations would be required to analyse this and discern the main sources of increased baroclinicity.

A poleward shift in the factual period of the eddy activity prior to the storms and of the backward trajectories has been found. According to Hoskins and Hodges (2019), in autumn the main North Atlantic storm track is located farther poleward than in spring. Hence, the poleward shift of the trajectories could be explained by a higher frequency of storms in autumn, as an indirect climate change signal. There is also a weak poleward shift of the backward trajectories in autumn, which acts as a direct climate change signal. However, we have also found that it is in spring when this poleward shift is greatest. In addition, the wavier pressure field configuration may act to deflect cyclones poleward over the North Atlantic. We thus deduce that the poleward shift is due to a combination of: (i) a direct climate change that shifts poleward the storms, especially in spring, probably due to a poleward shift of the region of maximum baroclinicity; (ii) an indirect signal, whereby analogues become more common in autumn when the cyclones are located further poleward; and (iii) wavier pressure patterns that deflect cyclones. Further analysis must be performed to evaluate each components' contribution to the observed poleward shift of the cyclones. A future pathway could be to create analogues based on the cyclone tracks.

Finally, an increase in precipitation in Northern Italy has been detected in the factual period, along with an increase in low-level temperature in the same region and wind gust over the Alps, Liguria and Provence. This result is in agreement with Reale et al (2022) and Zappa et al (2015), who, using climate models, found that the cyclone-related precipitation rate and wind speed will increase in the central Mediterranean region in a warmer climate. The increase in precipitation in Northern Italy could have a thermodynamic origin, linked to temperature by the Clausius Clapeyron relation, and a dynamic origin, related to the meridional wind and the orographically induced Stau effect. Deseasonalized temperature differences show that the temperature signal corresponds mainly to a seasonal shift of the analogues, which suggests that the increase in precipitation could be related to the shift from spring to autumn cyclones. Hence, in a warmer climate, hazardous Alex-like storms may become more likely, as they occur more frequently in the fall when the Mediterranean is warmer and the air is moister than in spring. The increase in southerly advection by 10m meridional wind has a dynamic origin, as storms have lower core pressures at *lag +12* dates in the factual climate. Southerly winds advect humid air from the Mediterranean, and together with the orographic forcing by the Alps, can increase precipitation. Hence, given the differences observed in the surface fields, more flooding could be triggered at the base of the Alps, the region that suffered the largest impacts during the Alex.

To summarize, our results show a more persistent atmospheric pattern for Alex-like cyclones in a warmer climate. Both signals indicate that the cyclones remain over the same region for longer, favouring extreme events that result from prolonged weather conditions. There is also an increase in the maximum eddy kinetic energy during their development and the cyclones display lower pressures during their decay phase. In addition, in the factual period,

Alex's analogues produce more precipitation in Northern Italy, and specifically along the southward flank of the Alps, which could trigger more severe flooding events. We emphasize that our findings do not explicitly demonstrate that the observed changes are entirely anthropogenically-driven, and they may also be influenced by the internal variability of the climate system. A large sample of model data would be required to adequately isolate the impact of anthropogenic radiative forcing.

The approach used in this work to attribute storm Alex and its impacts to climate change combines several techniques, including the analogues method (Yiou, 2014), dynamical systems theory (Faranda et al, 2017), and extreme event attribution (Stott et al, 2016), to provide a novel, complete toolkit for attribution studies. This toolkit may be applied with profit to other severe extra-tropical and tropical cyclones, and provide new insights on the influence of climate change on extreme weather phenomena.

Statements and declarations

- Funding: This project has received funding from the European Union's Horizon 2020 research and innovation programme under the Marie Sklodowska-Curie grant agreement N° 956396 (EDIPI project).
- Conflict of interest: The authors declare no conflict of interest.
- Ethics approval: Not applicable.
- Consent to participate: Not applicable.
- Consent for publication: Not applicable.
- Availability of data and materials: ERA5 data are available on the C3S Climate Data Store at https://cds.climate.copernicus.eu/#!/home.
- Code availability: The main results of this work were obtained using Python. The scripts are available upon request.
- Authors' contributions: MG performed the analysis. MG and DF co-designed the analyses. All authors participated to drafting and reviewing the manuscript.

References

Allan RP, Hawkins E, Bellouin N, et al (2021) IPCC, 2021: Summary for Policymakers. In Climate Change 2021: The physical science basis. Contribution of Working Group I to the Sixth Assessment Report of the Intergovernmental Panel on Climate Change [Masson-Delmotte, V., P. Zhai, A. Pirani, S.L. Connors, C. Péan, S. Berger, N. Caud, Y. Chen, L. Goldfarb, M.I. Gomis, M. Huang, K. Leitzell, E. Lonnoy, J.B.R. Matthews, T.K. Maycock, T. Waterfield, O. Yelekçi, R. Yu, and B. Zhou (eds.)]. Cambridge University Press. In Press.

Alvarez-Castro MC, Faranda D, Yiou P (2018) Atmospheric dynamics leading to West European summer hot temperatures since 1851. Complexity 2018:2494,509. https://doi.org/10.1155/2018/2494509

Aon (2020) Global Catastrophe Recap: October 2020. Available at: http://thoughtleadership.aon.com/documents/20201111_analytics-if-october-global-recap.pdf Accessed: October 202O

Barnes EA, Screen JA (2015) The impact of arctic warming onthe midlatitude jet-stream: Can it? has it? will it? WIREs Clim Change 6:277–286. https://doi.org/https://doi.org/10.1002/wcc.337

Cattiaux J, R. Vautard CC, Yiou P, et al (2010) Winter 2010 in europe: A cold extreme in a warming climate. Geophysical Research Letters 37. https://doi.org/https://doi.org/10.1029/2010GL044613

Chang E, Yau A (2016) Northern hemisphere winter storm track trends since 1959 derived from multiple reanalysis datasets. Climate Dynamics 47:1435–1454. https://doi.org/https://doi.org/10.1007/s00382-015-2911-8

Chang EKM, Ma CG, Zheng C, et al (2016) Observed and projected decrease in northern hemisphere extratropical cyclone activity in summer and its impacts on maximum temperature. Geophysical Research Letters 43:2200–2208

Cohen J, Screen JA, Furtado JC, et al (2014) Recent arctic amplification and extreme mid-latitude weather. Nature Geoscience 7:627–637. https://doi.org/https://doi.org/10.1038/ngeo2234

Cohen J, Zhang X, Francis J, et al (2018) Arctic change and possible influence on mid-latitude climate and weather: a us clivar white paper. US CLIVAR reports

Doblas-Reyes F, Sörensson A, Almazroui M, et al (2021) Linking global to regional climate change. In Climate Change 2021: The physical science basis. Contribution of Working Group I to the Sixth Assessment Report of the Intergovernmental Panel on Climate Change [Masson-Delmotte, V., P. Zhai, A. Pirani, S.L. Connors, C. Péan, S. Berger, N. Caud, Y. Chen, L. Goldfarb, M.I. Gomis, M. Huang, K. Leitzell, E. Lonnoy, J.B.R. Matthews, T.K. Maycock, T. Waterfield, O. Yelekçi, R. Yu, and B. Zhou (eds.)]. Cambridge University Press. In Press.

European State of the Climate (2020) Storm Alex. Available at https://climate.copernicus.eu/esotc/2020/storm-alex

Eurostat (2021) NUTS - Nomenclature of territorial units for statistics. https://ec.europa.eu/eurostat/web/nuts/background

Faranda D, Messori G, Yiou P (2017) Dynamical proxies of North Atlantic predictability and extremes. Scientific Reports https://doi.org/10.1038/srep41278, URL https://hal.archives-ouvertes.fr/hal-01340301

Faranda D, Alvarez-Castro M, Messori G, et al (2019) The hammam effect or how a warm ocean enhances large scale atmospheric predictability. Nat Commun 10:1316. https://doi.org/https://doi.org/10.1038/s41467-019-09305-8

Feser F, Barcikowska M, Krueger O, et al (2015) Storminess over the north atlantic and northwestern europe—a review. Quarterly Journal of the Royal Meteorological Society 141(687):350–382. https://doi.org/https://doi.org/10.1002/qj.2364, URL https://rmets.onlinelibrary.wiley.com/doi/abs/10.1002/qj.2364, https://arxiv.org/abs/https://rmets.onlinelibrary.wiley.com/doi/pdf/10.1002/qj.2364

Freitas ACM, Freitas JM, Todd M (2008) Hitting time statistics and extreme value theory. https://doi.org/10.48550/ARXIV.0804.2887

Gulev S, Thorne P, Ahn J, et al (2021) Changing state of the climate system. In Climate Change 2021: The physical science basis. Contribution of Working Group I to the Sixth Assessment Report of the Intergovernmental Panel on Climate Change [Masson-Delmotte, V., P. Zhai, A. Pirani, S.L. Connors, C. Péan, S. Berger, N. Caud, Y. Chen, L. Goldfarb, M.I. Gomis, M. Huang, K. Leitzell, E. Lonnoy, J.B.R. Matthews, T.K. Maycock, T. Waterfield, O. Yelekçi, R. Yu, and B. Zhou (eds.)]. Cambridge University Press. In Press.

Gutowski Jr WJ, Branscome LE, Stewart DA (1992) Life cycles of moist baroclinic eddies. Journal of Atmospheric Sciences 49:306–319

Harvey BJ, Cook P, Shaffrey L, et al (2020) The response of the Northern Hemisphere storm tracks and jet streams to climate change in the CMIP3, CMIP5, and CMIP6 climate models. Journal of Geophysical Research: Atmospheres 125. https://doi.org/https://doi.org/10.1029/2020JD032701

Hersbach H, Bell B, Berrisford P, et al (2020) The ERA5 global reanalysis. Quat J Roy Met Soc 146(730):1999–2049. https://doi.org/https://doi.org/10.1002/qj.3803, iSBN: 0035-9009 Publisher: Wiley Online Library

Hochman A, Alpert P, Harpaz T, et al (2019) A new dynamical systems perspective on atmospheric predictability: Eastern mediterranean weather regimes as a case study. Science advances 5(6):eaau0936

Hoffmann P (2018) Enhanced seasonal predictability of the summer mean temperature in central europe favored by new dominant weather patterns. Climate dynamics 50(7):2799–2812

Hoskins B, Woollings T (2015) Persistent extratropical regimes and climate extremes. Curr Clim Change Rep 1:115–124. https://doi.org/10.1007/s40641-015-0020-8

Hoskins BJ, Hodges KI (2019) The annual cycle of Northern Hemisphere storm tracks. Part II: Regional detail. Journal of Climate 32:1761–1775. https://doi.org/http://dx.doi.org/10.1175/jcli-d-17-0871.1

Jézéquel A, Yiou P, Radanovics S (2018) Role of circulation in european heatwaves using flow analogues. Climate dynamics 50(3):1145–1159

Jia G, Shevliakova E, Artaxo P, et al (2019) Land–climate interactions. In: Climate Change and Land: an IPCC special report on climate change, desertification, land degradation, sustainable land management, food security, and greenhouse gas fluxes in terrestrial ecosystems [P.R. Shukla, J. Skea, E. Calvo Buendia, V. Masson-Delmotte, H.-O. Pörtner, D.C. Roberts, P. Zhai, R. Slade, S. Connors, R. van Diemen, M. Ferrat, E. Haughey, S. Luz, S. Neogi, M. Pathak, J. Petzold, j. portugal pereira, P. Vyas, E. Huntley, K. Kissick, M. Belkacemi, J. Malley, (eds.)]. In press.

Kornhuber K, Tamarin-Brodsky T (2021) Future Changes in Northern Hemisphere Summer Weather Persistence Linked to Projected Arctic Warming. Geophysical Research Letters 48. https://doi.org/https://doi.org/10.1029/2020GL091603

Lee JY, Marotzke J, Bala G, et al (2021) Future global climate: Scenario-based projections and near-term information. In Climate Change 2021: The physical science basis. Contribution of Working Group I to the Sixth Assessment Report of the Intergovernmental Panel on Climate Change [Masson-Delmotte, V., P. Zhai, A. Pirani, S.L. Connors, C. Péan, S. Berger, N. Caud, Y. Chen, L. Goldfarb, M.I. Gomis, M. Huang, K. Leitzell, E. Lonnoy, J.B.R. Matthews, T.K. Maycock, T. Waterfield, O. Yelekçi, R. Yu, and B. Zhou (eds.)]. Cambridge University Press. In Press

Lucarini V, Faranda D, Wouters J (2012) Universal Behaviour of Extreme Value Statistics for Selected Observables of Dynamical Systems. https://doi.org/10.1007/s10955-012-0468-z

Lucarini V, Faranda D, Freitas ACM, et al (2016) Extremes and recurrence in dynamical systems. https://doi.org/https://doi.org/10.48550/arXiv.1605.07006, 1605.07006

Luu LN, Vautard R, Yiou P, et al (2018) Attribution of extreme rainfallevents in the South of France using EURO-CORDEX simulations. Geophysical Research Letters 45:6242–6250. https://doi.org/https://doi.org/10.1029/2018GL077807

Mann ME, Rahmstorf S, Kornhuber K, et al (2017) Influence of anthropogenic climate change on planetary wave resonance and extreme weather events. Scientific Reports 7. https://doi.org/10.1038/srep45242

Messori G, Caballero R, Faranda D (2017) A dynamical systems approach to studying midlatitude weather extremes. Geophysical Research Letters 44(7):3346–3354. https://doi.org/https://doi.org/10.1002/2017GL072879, URL https://agupubs.onlinelibrary.wiley.com/doi/abs/10.1002/2017GL072879, https://arxiv.org/abs/https://agupubs.onlinelibrary.wiley.com/doi/pdf/10.1002/2017GL072879

Messori G, Harnik N, Madonna E, et al (2021) A dynamical systems characterization of atmospheric jet regimes. Earth System Dynamics 12(1):233–251

Moon W, Manucharyan GE, Dijkstra HA (2021) Baroclinic instability and large-scale wave propagation in a planetary-scale atmosphere. https://doi.org/https://doi.org/10.1002/qj.4232

Météo France (2019a) Tempête Hortense du 4 octobre 1984. Available at http://tempetes.meteofrance.fr/IMG/anthemis_pdf/19841004.pdf

Météo France (2019b) Tempête Rebekka du 6 novembre 2000. Available at http://tempetes.meteo.fr/IMG/anthemis_pdf/20001106.pdf

Météo France (2020a) Bulletin climatique octobre 2020. Available at https://donneespubliques.meteofrance.fr/donnees_libres/bulletins/BCM/202010.pdf

Météo France (2020b) Tempête Alex: des intempéries exceptionnelles. Available at https://meteofrance.com/actualites-et-dossiers/climat/tempete-alex-des-intemperies-exceptionnelles

Météo France (2021) Tempête Alex du 2 octobre 2020. Available at http://tempetes.meteo.fr/IMG/anthemis_pdf/20201002.pdf

National Academies of Sciences, Engineering, and Medicine (2016) Attribution of Extreme Weather Events in the Context of Climate Change. The National Academies Press, Washington, DC, https://doi.org/10.17226/21852, URL https://www.nap.edu/catalog/21852/attribution-of-extreme-weather-events-in-the-context-of-climate-change

Neu U, Akperov MG, Bellenbaum N, et al (2013) IMILAST: A community effort to intercompare extratropical cyclone detection and tracking algorithms. Bulletin of the American Meteorological Society Bulletin of the American Meteorological Society 94:529–547. https://doi.org/https://doi.org/10.1175/BAMS-D-11-00154.1

Pall P, Aina T, Stone DA, et al (2011) Anthropogenic greenhouse gas contribution to flood risk in england and wales in autumn 2000. Nature 470:382–385. https://doi.org/10.1038/nature09762

Parker DJ (1998) Secondary frontal waves in the north atlantic region: A dynamical perspective of current ideas. Quarterly Journal of the Royal Meteorological Society 124(547):829–856. https://doi.org/https://doi.org/10.1002/qj.49712454709, URL https://rmets.onlinelibrary.wiley.com/doi/abs/10.1002/qj.49712454709, https://arxiv.org/abs/https://rmets.onlinelibrary.wiley.com/doi/pdf/10.1002/qj.49712454709

Philip S, Kew SF, van Oldenborgh GJ, et al (2018) Attribution analysis of the Ethiopian drought of 2015 p 2465–2486. https://doi.org/https://doi.org/10.1175/JCLI-D-17-0274.1

Pinto JG, Spangehl T, Ulbrich U, et al (2005) Sensitivities of a cyclone detection and tracking algorithm: individual tracks and climatology. Meteorologische Zeitschrift 14(6):823–838. https://doi.org/10.1127/0941-2948/2005/0068

Priestley MDK, Catto JL (2022) Future changes in the extratropical storm tracks and cyclone intensity, wind speed, and structure. Weather and Climate Dynamics 3(1):337–360. https://doi.org/10.5194/wcd-3-337-2022

Priestley MDK, Dacre HF, Shaffrey LC, et al (2020) The role of secondary cyclones and cyclone families for the north atlantic storm track and clustering over western europe. Quarterly Journal of the Royal Meteorological Society 146(728):1184–1205. https://doi.org/https://doi.org/10.1002/qj.3733, URL https://rmets.onlinelibrary.wiley.com/doi/abs/10.1002/qj.3733, https://arxiv.org/abs/https://rmets.onlinelibrary.wiley.com/doi/pdf/10.1002/qj.3733

Pörtner HO, Roberts D, Poloczanska E, et al (2022) IPCC, 2022: Summary for policymakers. In: Climate Change 2022: Impacts, Adaptation, and Vulnerability. Contribution of Working Group II to the Sixth Assessment Report of the Intergovernmental Panel on Climate Change

Reale M, Liberato ML, Lionello P, et al (2019) A global climatology of explosive cyclones using a multi-tracking approach. Tellus A: Dynamic Meteorology and Oceanography 71(1):1611,340. https://doi.org/10.1080/16000870.2019.1611340

Reale M, Narvaez WC, Cavicchia L, et al (2022) Future projections of mediterranean cyclone characteristics using the med-CORDEX ensemble of coupled regional climate system models. Climate dynamics 58:2501–2524. https://doi.org/https://doi.org/10.1007/s00382-021-06018-x

Riviera 24 (2021) A quattro mesi dalla tempesta Alex in Costa Azzurra si cercano ancora i corpi delle vittime. Available at: https://www.riviera24.it/2021/02/a-quattro-mesi-dalla-tempesta-alex-in-costa-azzurra-si-cercano-ancora-i-corpi-delle-vit

Appendix B

Article "Anthropogenic climate change will intensify European explosive storms similar to Alex, Eunice, and Xynthia in the future"

Anthropogenic climate change will intensify European explosive storms similar to Alex, Eunice, and Xynthia in the future

Mireia Ginesta,[a] Emmanouil Flaounas,[b] Pascal Yiou,[a] Davide Faranda,[a,c,d]

[a] *Laboratoire des Sciences du Climat et de l'Environnement, UMR 8212 CEA-CNRS-UVSQ, Univ. Paris-Saclay & IPSL, Orme des Merisiers, 91191 Gif-sur-Yvette, France*

[b] *Institute of Oceanography, Hellenic Center for Marine Research, Athens, Greece*

[c] *London Mathematical Laboratory, 8 Margravine Gardens, London, W6 8RH, UK*

[d] *LMD/IPSL, Ecole Normale Supérieure, PSL research University, 75005, Paris, France*

Corresponding author: Mireia Ginesta, Mireia.Ginesta-Fernandez@lsce.ipsl.fr

ABSTRACT: Extratropical storms, particularly explosive storms or 'weather bombs' with exceptionally high deepening rates, present substantial risks and are susceptible to climate change. Individual storms may exhibit a complex and hardly detectable response to human-driven climate change because of the atmosphere's chaotic nature and variability at regional level. It is thus essential to understand changes in specific storms for building local resilience and advancing our overall comprehension of storm trends. To address this challenge, this study performs future projections for three specific explosive storms, each impacting different European locations: Alex (October 2020), Eunice (January 2022), and Xynthia (February 2010). Using a dataset of 105 members from the Community Earth System Model version 1 (CESM1), we identify analogues —storms with a similar development stage— in two periods: the present-day climate (1991-2001) and a future climate scenario characterized by high anthropogenic greenhouse gas emissions (RCP8.5, 2091-2101).

We evaluate trends in the frequency of occurrence of the storms and intensity, as well as on meteorological hazards and the underlying dynamics. For all storms, our analysis reveals an increase in precipitation and wind speed in the analogues of the future climate, specially for the explosive ones. These findings underscore the potential consequences of explosive storms modified by climate change and their subsequent hazards on various regions of Europe, offering evidence that can be used to prepare and enhance adaptation processes.

SIGNIFICANCE STATEMENT: This study investigates the impact of climate change on explosive storms, or 'weather bombs,' and their potential consequences for European regions. We project future scenarios of three specific storms, Alex, Eunice, and Xynthia, using a state-of-the-art climate model. Our findings reveal a trend of increased precipitation and wind speed in these storms, emphasizing the heightened risks associated with climate change. The significance lies in understanding the local implications of explosive storms, aiding in the development of resilient strategies and adaptation measures.

1. Introduction

Weather variability in the mid-latitudes is controlled by atmospheric wave activity, consisting of propagating synoptic-scale cyclonic and anticyclonic circulation. Therein, extratropical storms play a key role in affecting the wave guide and producing the majority of high impact weather (Wallace and Hobbs 2006). They contribute substantially to total precipitation (Hawcroft et al. 2012) and are a source of wind energy (Liu et al. 2008; Rapella et al. 2023). Extratropical storms can also exhibit extreme behaviour, being associated with strong precipitation and flooding events (Hawcroft et al. 2018), strong and damaging winds (Roberts et al. 2014a), or a combination of both (Owen et al. 2021). Given their potential to be associated with meteorological hazards with significant socio-economic impacts (e.g., Liberato 2014; Jansa et al. 2001), understanding the evolution of their characteristics in a future climate is crucial.

Several studies have assessed the role of climate change in modifying the underlying dynamics of extratropical storms (e.g. Lehmann et al. 2014; Priestley and Catto 2022). Changes in frequency, position and intensity of the storm tracks, namely the preferred regions where storms travel through, are primary driven by changes in the horizontal temperature gradient in both lower and upper troposhere and in the vertical temperature profile (Catto et al. 2019). The Coupled Model Intercomparision Project (CMIP) phases 3, 5, and 6 generally agree on the spatial signature of the projected changes in storminess in the North Atlantic (Harvey et al. 2020). Specifically, models project a decrease in storm activity during summer, particularly in the southern regions, and produce a tripolar pattern in winter of an increase in storm activity in the British Isles and a decrease in the Mediterranean and Norwegian seas (Zappa et al. 2013; Priestley et al. 2020). Regarding extreme storms, the response consist of a decrease in frequency of ocurrence in the North

Atlantic basin, with a weak and local increase over the British Isles and the North Sea in winter (Zappa et al. 2013; Seiler and Zwiers 2016). Sources of uncertainty of climate projections stem from difficulties of isolating internal variability from the forced signal (Deser et al. 2012), as well scenario and model uncertainty (Hawkins and Sutton 2009; Sansom et al. 2013). In addition, low confidence still persists due to opposing thermodynamic processes that alter baroclinicity (Shaw et al. 2016), and challenges in resolving meso-scale and small scale features such as the diabatic processes (Schemm 2023).

While examining general trends in storm behaviour provides a fundamental understanding of the potential hazards of climate change, it is essential to recognize that specific storms may exhibit unique characteristics. This stems from the fact that specific storms are influenced by a combination of factors that may not be accurately captured in general trends, giving rise to a chaotic nature in the atmosphere and non-linear interactions. In addition, different regions may experience unique environmental conditions, such as local topography or oceanic currents, resulting in diverse storm behaviours in different areas. Hence, our study aims to bridge this gap by zooming in on the particular features of extreme storms in different regions. For this reason, we employ an approach within the field of Extreme Event Attribution (EEA) (Trenberth et al. 2015; Jézéquel et al. 2018), specifically designed to address these questions. This field allows us to delve into the domain of weather science to understand the specific meteorological conditions contributing to the event while simultaneously evaluating the role of climate change in shaping its occurrence and intensity (Shepherd 2016). We use a recent EEA approach that involves finding similar events, called *analogues*, in two different time periods and comparing their key variables (Faranda et al. 2022). Some studies have adapted this methodology to be more targeted for extratropical storms (Ginesta et al. 2022; Faranda et al. 2023).

In our study, we further adapt this EEA approach for the analysis of explosive storms. Explosive storms are characterized by a strong deepening rate in a short time period, and can produce widespread damage when they make landfall (Liberato et al. 2013; Fink et al. 2009). These storms were identified by Sanders and Gyakum (1980) as storms with a "Normalized central Deepening Rate" (NDR_c) greater than 1:

$$NDR_c = \frac{DR_{24h}}{24h} \frac{\sin(60^\circ)}{\sin(\varphi)}, \tag{1}$$

where DR_{24h} is the pressure difference over 24 hours measured at the storm center and φ is the latitude at its second time step. These storms, also known as "weather bombs", are mainly formed in regions of enhanced baroclinicity (Roebber 1984). In the North Atlantic, they primarily form during the boreal winter in the western part of the basin, where there is a strong horizontal temperature gradient linked to the Gulf Stream and land-sea contrast, large moisture availability and strong vertical wind shear (Reale et al. 2019; Brayshaw et al. 2009).

We focus on three explosive storms that hit different parts of Europe: Alex in October 2020, Eunice in January 2022, and Xynthia in February 2010. Unlike many EEA studies that compare the present climate with a pre-industrial climate (factual and counterfactual periods), our method uses present and future climate projections with the Community Earth System Model version 1 (CESM1). Our study aims to:

1. Evaluate how well CESM1 simulates storms with development stages similar to the three targeted storms.

2. Analyze future climate trends in the frequency of these storms and their deepening rates, considering the scenario with the highest greenhouse gases emissions, that is, the Representative Concentration Pathway 8.5 (RCP8.5).

3. Examine changes in the hazard levels of these events, quantified by measuring precipitation and wind speed.

4. Characterize the underlying dynamics contributing to these observed changes.

In the subsequent sections, we describe the data and methods used (Section 2), explore the characteristics of the storms (Section 3), analyze occurrence trends and intensity of storms (Section 5), and assess changes in climate drivers and underlying dynamics (Section 6). The conclusions of our study are presented in section 7.

2. Datasets and methods

a. Datasets

To address the above objectives, we use the Community Earth System Model version 1 (CESM1; Hurrell et al. (2013)), which is a global coupled climate model with a horizontal resolution of

about 1 degree. The radiative forcing applied in all simulations is the historical forcing until 2005 and the Representative Concentration Pathway 8.5 (RCP8.5) forcing from the CMIP5 project (Meinshausen et al. 2011) from 2005 onwards. We use a multimember initial condition ensemble CESM-LE (CESM-LE; Kay et al. (2015)), consisting of a 35-member ensemble of simulations from 1 January 1920 to 2100. To increase the number of members, two additional ensembles of 35 members each are performed. In both, 35 members are rerun from perturbations of $O(10^{-13})$ on the initial atmospheric temperature field of the first member of the CESM–LE, starting at 1980 and at 2081 (Röthlisberger et al. 2020). After a few years, due to the chaotic nature of the climate system, the members are in distinct states of their internal variability, and thus they are considered to be independent (Fischer et al. 2013). Hence, the experimental set–up of this study consists of 1050 years of a *present* climate, from 1991 to 2000, and 1050 years of a *future* climate, from 2091 to 2100. The radiative forcing is assumed to be relatively constant in a 10–year period. Kay et al. (2015) showed that the spread of the CESM-LE due to internal variability is comparable to CMIP5. In contrast to many CMIP5 models, CESM does not depict a too zonally oriented North Atlantic storm track (Dolores-Tesillos et al. 2022). According to Dolores-Tesillos et al. (2022), the model is able to reproduce fairly well storm frequencies and lifetimes, and most of the biases are associated to weak or short living storms. However, there is an underestimated number of storms over the ocean. At smaller scales, the model is able to represent the properties and structure of extratropical storms and their associated warm conveyor belts (Joos et al. 2023; Binder et al. 2023). The deepening rates of the weak and medium-strong storms in the NH in winter are also well captured by the model but there is an underestimation of the explosive ones (Binder et al. 2023).

In this study we also use ERA5 reanalysis data (Hersbach et al. 2020), covering the period from 1950 to 2020, as a validation of the CESM model performance. The ERA5 dataset has a horizontal resolution of 31 km.

The variables used from both reanalysis and CESM model are 6–hourly sea level pressure, hourly precipitation rate, and hourly wind speed at 10m. To better assess the drivers of the differences seen in CESM present and future periods we further analyze the following 6–hourly variables: equivalent potential temperature (θ_e) at 850hPa, horizontal gradient of θ_e ($\nabla\theta_e$) at 850hPa, distribution of the upper-tropospheric jet stream, and the low-level Eady Growth Rate (EGR) between 850hPa and 500hPa. The distribution of the upper-tropospheric jet stream is based on the methodology

outlined in Koch et al. (2006), where jet occurrence is identified by averaging wind speeds between 400 hPa and 100 hPa (to account for height variations) and exceeding a threshold of 30 m/s. EGR is computed as:

$$EGR = 0.31 \frac{f}{N} \sqrt{\frac{\delta(u,v)}{\delta z}} \tag{2}$$

where $f = 2\Omega sin\phi$ if the Coriolis parameter, $N = \sqrt{\frac{9.81}{\theta} \frac{\delta\theta}{\delta z}}$ is the Brunt-Väisälä frequency, and $\sqrt{\frac{\delta(u,v)}{\delta z}}$ is the vertical wind share. Ω is the angular velocity of the Earth ($7.29 \times 10^{-5} rad/s$), ϕ latitude, u and v zonal and meridional wind speeds, θ potential temperature, and z geopotential height.

b. Methods

We use the method of analogues (Yiou 2014), which has already been applied to the study of extratropical storms (Ginesta et al. 2022; Faranda et al. 2023), to find similar storms to Alex, Eunice, and Xynthia. In the context of this study, an analogue is defined as a storm with a similar development stage or a comparable track during its evolution. The full tracks of storms Alex, Eunice, and Xynthia are shown in figure A1 in the Appendix. We define the development stage of the storms as the 24h period before reaching their mature stage (figure A1 of the Appendix from points 0 to 1). First, we identify and track all storms in each dataset (ERA5, CESM present, CESM future). We use a Lagrangian approach where storms centers are defined and tracked as local minima in the sea-level pressure field (Wernli and Schwierz 2006). We then select the storms that have the most similar development stages to the targeted storms based on our definition of analogue. For that, we apply a two-step process:

- We first select all storms in the database that have a minimum sea level pressure lower than 1000 hPa and located within a circle of radius 300 km of the targeted storm center in its minimum sea level pressure point. This filter ensures that only storms in their mature stage are considered and that they have reached their minimum sea level pressure in the vicinity of the targeted storm's center region. We refer to these storms as *mature stage* storms, and the time when they reach their minimum sea level pressure is defined as *time 0*.

- We select the last five grid points of the development stage of the mature stage storms. As we use 6–hourly data, this corresponds to the tracks 24 hours before the time 0 dates. For each mature stage storm, we compute the averaged Euclidean distance between the track of the storm and the track of the targeted storm. We select the 20% mature stage storms with the lowest Euclidean distance from the targeted storm. This corresponds to the 20% most similar development stage tracks. We term these *analogues*. The decision to use 20% is a trade-off between finding tracks that resemble those of the targeted storms and having a sufficiently large sample size to draw meaningful statistical conclusions. We tested that altering the percentage to 10%, 15%, or 25% does not significantly impact our findings. We also select the analogues that undergo explosive cyclogenesis, that is, that have a NDR_c greater than 1 (Eq. 1). We term these *explosive analogues*.

3. Storm characteristics

In this section we contextualize the three storms and provide an overview of the associated impacts and meteorological drivers.

a. Storm Alex

Storm Alex occurred in early October 2020 and produced a devastating flood in the Alps region in 24 hours. Named by Météo-France on September 30, 2020, Alex caused record-breaking precipitation and hurricane-force winds, resulting in at least 15 fatalities and over 2.5 billion euros in economic losses (WMO 2020; European State of the Climate 2020; Météo France 2020; Aon 2020). The heavy precipitation associated with Alex in the Alps produced several record-breaking events, as high as 630 mm in a day recorded in Sambughetto (European State of the Climate 2020). The storm was also associated with hurricane-force winds, such as 186 km/h in Belle-Île - Le Talut (Météo France 2020).

The storm developed as a secondary cyclogenesis, that is, as a frontal-wave instability along of a synoptic front of a pre-existing storm. It deepen rapidly, enhanced by high upper level potential vorticity values. The pressure dropped more than 30 hPa in the first 24 hPa, and the NDR_c was about 1.6 B. It made landfall early 2 October when it reached its minimum sea level pressure on its core (around 970 hPa). On its southern flank, the strong pressure gradient favoured high quantities

of water vapour transport, and an atmospheric river was formed from the subtropical western North Atlantic to the vicinity of the storm core (Davolio et al. 2022). Storm Alex remained over France for a day, producing record-breaking heavy precipitation in the Mediterranean area in southern France and Northern Italy (Météo France 2020). In an EEA study based on reanalysis data Ginesta et al. (2022), the persistence of the storm, as well as the accumulated daily precipitation, increased in the present climate when compared to the recent past climate.

b. Storm Eunice

Eunice was the second and strongest storm of a cluster of winter storms (Met Office 2022) that lasted between the 16th – 20th of February 2022 and mainly affected western Europe. The storm, also known as Storm Zeynep or Storm Nora in Germany and Denmark, respectively, caused widespread damage, 17 fatalities, and insured losses estimated at 2.5–3.5 billion euros (NL Times 2022; Anadolu Agency 2022; Deutsche Welle 2022; BBC 2022; RTL Info 2022; The Irish Times 2022; RMS 2022).

Eunice formed from secondary cyclogenesis on February 17 in the North Atlantic. It deepened and moved rapidly northeast into England, experiencing explosive cyclogenesis with a central pressure drop of 30 hPa in 18 hours and an NDR of 1.6 B. On February 18 at around 6 am Eunice made landfall in Ireland and then crossed the UK in 12 hours. It produced widely spread damaging wind gusts in many coastal areas, especially in the south of the UK. A wind gust of 196 km/h was recorded in The Needles, Isle of Wight, the strongest ever recorded in England. On February 18 at around 6 pm the storm was located over the North Sea reaching a sea level pressure in its core below 970 hPa, the minimum of its lifetime. In the hours that followed, the storm swept across Western Europe with force, hitting in particular Germany, the Netherlands, and Belgium. On the February 19 at 6 am, Eunice was already located over the Baltic Sea, where it particularly affected Poland. It then continued moving eastwards, weakening and dissipating as it crossed inland Northeastern Europe.

c. Storm Xynthia

In winter 2009/2010, the general atmospheric circulation over Europe was characterized by an extreme and record-persistent negative phase of the North-Atlantic Oscillation (NAO) (Cattiaux

et al. 2010). This led to a low position of the jet stream, several severe cold spells, cold weather conditions and destructive storms. Xynthia was the strongest and most damaging extratropical storm to hit Europe in winter 2009/2010. This extreme storm, which occurred in late February/early March 2010, has raised interest in the scientific community due to its uncommon meteorological characteristics (e.g. Liberato et al. 2013) and impacts (e.g. Chadenas et al. 2014; Vinet et al. 2012). It followed an unusual SW-NE path, causing significant impacts in several western European countries, including more than 60 fatalities and insured losses of 1.5–3 billion euros (García-Pereda (NWC SAF/AEMET) 2010; Kolen et al. 2013; Worlwide 2010). At least 53 of the deaths occurred in France (Chauveau et al. 2011).

Xynthia began as a low-pressure system east of Bermuda on February 25, 2010, at around 30 degrees North in the subtropical Atlantic. Unlike most extratropical storms that intensify rapidly when they cross the polar jet stream (Uccellini 1990), Xynthia's intensification was primarily driven by the advection of low-level warm, humid air and associated with high values of equivalent potential temperature (θ_e) (Fink et al. 2012). The storm underwent explosive cyclogenesis between the 26th and the 27th while rapidly approaching to the Iberian Peninsula, with a maximum NDR of 1.9 B. On the 27th at 18:00 UTC it was already located west of the Bay of Biscay, reaching its minimum sea level pressure below 970 hPa. It then swept across western France, resulting in a powerful storm surge that locally exceeded 1.5 m and that produced most of the damages in France (Bertin et al. 2012). Xynthia continued its path northeastwards hitting specially Belgium, the Netherlands, Germany and Denmark. The storm dissipated around the 4 March over eastern Scandinavia.

4. Representation of explosive storms in CESM present-day climate

Figure 1 shows the number of mature stage storms every 10 years for ERA5 (a) and CESM present climate (b), as well as the counts for 100 years of those that are explosive (c,d). As noted by Dolores-Tesillos et al. (2022), there is an underestimation of storm numbers in the model compared to observations, particularly evident in the ocean. Furthermore, we observe an underestimation of mature stage storms west of Newfoundland, especially the explosive ones. In the regions studied, highlighted in red, we note a slight underestimation of both mature stage storms and explosive ones, especially in the North Sea. However, the bias is considerably smaller in these regions compared

to the ocean. Despite the relatively small proportion of storms assessed in this study compared to the overall North Atlantic basin, these three regions are highly susceptible to widespread damage when such storms make landfall.

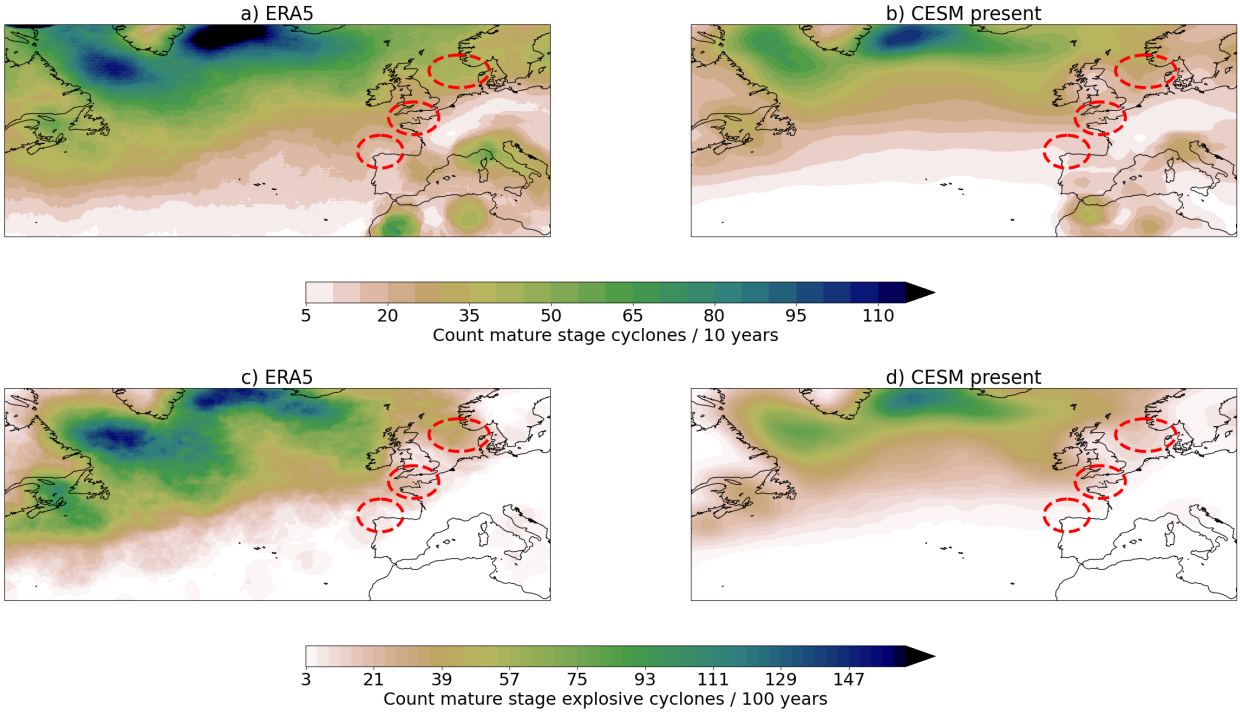

FIG. 1. Count of mature stage cyclones within 300 km for each grid point every 10 years for (a) ERA5 and (b) CESM present. (c,d) Count of those that are explosive, every 100 years.

Figure 2a shows the NDR_c of both ERA5 and CESM, similar as Binder et al. (2023) did for the Northern and Southern Hemispheres but focused on the North Atlantic. Figure 2b shows the differences between CESM present and ERA5. Consistent with their findings, we also identify a slight underestimation of the NDR_c of the most explosive storms in the basin, of up to around -0.2 in the most extreme cases. However, there is strong agreement across almost all percentiles.

This comparative analysis, together with assessments by Dolores-Tesillos et al. (2022) and Binder et al. (2023), gives confidence in the model's capability to simulate explosive storms making landfall on the western coast of Europe. Further exploration of the model's ability to simulate analogues of the storms will be conducted in the subsequent section.

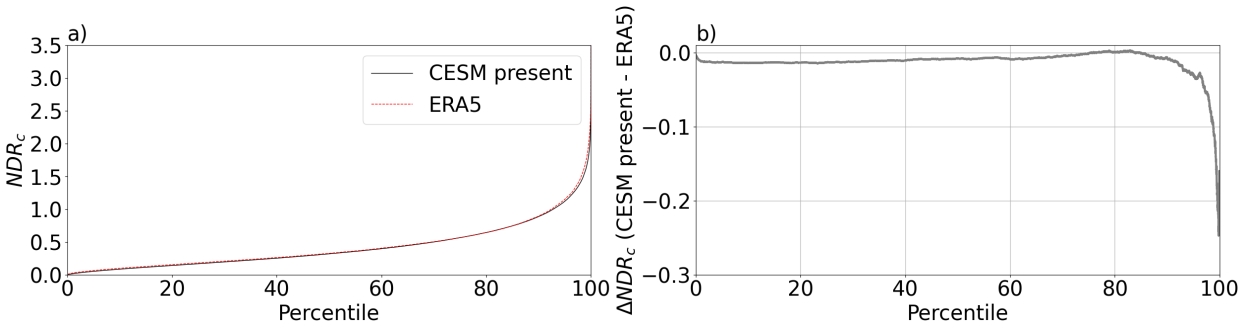

FIG. 2. a) Percentile curve of the Normalized central Deepening Rate (NDR_c) of storms in the North Atlantic for ERA5 and CESM present. b) Differences in the NDR_c between CESM present and ERA5.

5. Trends in frequency and intensity

In this section, we first validate the CESM model performance in simulating analogue storms of Alex, Eunice, and Xynthia, using ERA5 reanalysis data. Then, we assess future trends of frequency of occurrence and intensity, measured by the NDR, by comparing CESM present and future climates.

a. Storm Alex

Figure 3 shows the tracks during the development stage of the analogues and explosive analogues of Alex for each dataset. The legends also display the number of analogues and explosive analogues. In the ERA5 70-year period, 63 analogues have been identified, that is, around 9 analogues every 10 years. In contrast, fewer analogues are detected in the CESM present climate, with a frequency of almost 3 analogues every 10 years. This could be due to an underestimation of storm frequencies over the ocean (Dolores-Tesillos et al. 2022). In the ERA5 dataset, 10 of the 63 analogues are explosive, corresponding to a relative frequency of around 16% of the analogues. Three of these explosive analogues are known storms that made landfall in France (Table A1). The fraction of analogues that are explosive in the CESM present period is slightly lower than that of ERA5 (34 explosive analogues out of 299 analogues, that is, around 11%). The NDR_c, used here as a measure of the intensity, of the analogues and explosive analogues in CESM present is comparable to that of ERA5. We further measure the similarity of the analogues to the storm by computing the mean Euclidean distance between the 24-hour development stage tracks of the analogues and storm Alex. We term this *analogues quality* (Figs. 4a,c). The analogues quality distributions of CESM present

show comparable values with ERA5, as no analogue was more than 500 km apart and most of them differed by around 380 km. These distributions indicate the model's ability to simulate storms with development stage similar to Alex's. Figures 4b,d show the number of analogues per season. Most of the analogues occur in autumn season in both ERA5 and CESM present. However, in ERA5 the second most preferred season is spring, while in CESM present is winter. Few analogues are also detected in summer in both, ERA5 and CESM present.

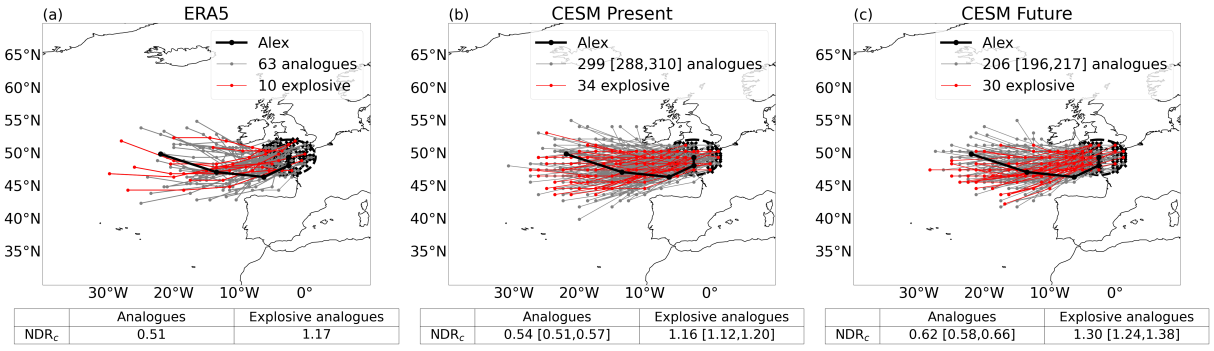

	Analogues	Explosive analogues
NDR_c	0.51	1.17

	Analogues	Explosive analogues
NDR_c	0.54 [0.51,0.57]	1.16 [1.12,1.20]

	Analogues	Explosive analogues
NDR_c	0.62 [0.58,0.66]	1.30 [1.24,1.38]

FIG. 3. 24-hour track of the development stage of storm **Alex** (thick black line) and its analogues (thin grey lines), for ERA5 (a), CESM present (b), and CESM future (c). Explosive analogues' tracks are highlighted in red. The dashed-line circle indicates the 300-km area used to identify mature stage storms. The figure legend shows the number of analogues and explosive analogues. The tables beneath the figures depict the Normalized Deepening Rate values, calculated using equation 1, for both analogues and explosive analogues. 95 % confidence intervals for CESM present and CESM future, determined using a bootstrap test, are denoted in brackets.

There is a statistically significant decrease in the number of analogues in the future climate with respect to the present from 299 to 206 (Fig. 3). This decrease is mainly seen in autumn and summer, but there is also a slight decrease in winter and spring (Fig. 4b). There is little change in the number of explosive analogues (34 to 30) (Fig. 3), with a decrease in frequency mainly in autumn (Fig. 4d). However, the relative frequency of explosive storms increases from present to future periods from 11% to 15%. Additionally, there is an increase in NDR_c of both analogues and explosive analogues in the future climate with respect to the present, which is considered statistically significant because the confidence intervals do not overlap. This suggests that the analogues and explosive analogues in the future climate will be associated with more intense deepening rates. Regarding the quality of the analogues, there is a statistically significant increase in the future period with respect to the present (Fig. 4a). This indicates that analogues in future

conditions resemble better Alex's development stage than in the present climate. In summary, anthropogenic radiative forcing is reducing the number of analogues of Alex, specially in autumn, but increasing their similarity to the storm as well as the deepening rates.

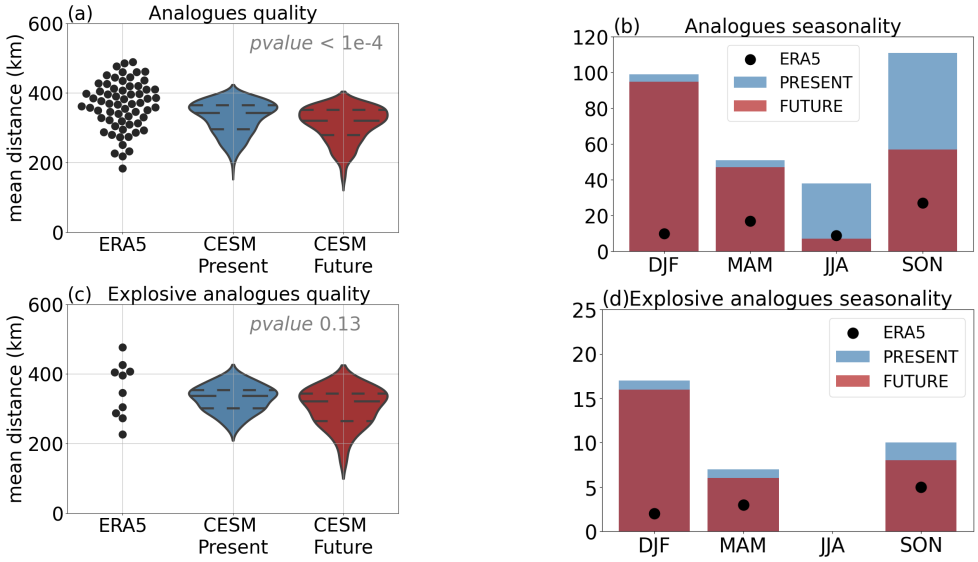

FIG. 4. (a,c) Mean Euclidean distances between the 24–hour track of the development stage of storm **Alex** and its **analogues** and explosive analogues for ERA5 (black dots), CESM present (blue probability distribution), and CESM future (red probability distribution). Dashed lines in violin plots show the quartiles 25%, 50%, and 75%. A Kolmogorov-Smirnov test was used to determine the statistically significant difference between CESM present and future distributions, with the resulting p-value indicated in the figure. (b,d) Number of analogues per season: SON (September, October, November), DJF (December, January, February), JJA (June, July, August), and MAM (March, April, May).

b. Storm Eunice

In ERA5 we found 126 analogues, that is, around 18 every 10 years (Fig. 5). However, CESM again underestimates the number of analogues, detecting 6–7 every 10 years in the present climate (696). 23 out of 126 analogues are explosive in the ERA5 dataset, of which 8 are documented storms that had an impact in Europe (Table A1). This corresponds to a relative frequency of explosive storms of 18.3%. The relative frequency of analogues that undergo explosive cyclogenesis in the CESM present is half of that of ERA5 (9.6%). In addition, the NDR_c of the analogues and explosive analogues is slightly lower in the model than in ERA5 for both present analogues and

explosive analogues. Regarding the quality of the analogues (Fig. 6a), the analogues detected by the model have lower mean Euclidean distances than those detected by ERA5. This indicates that the model is good at reproducing storms that resemble Eunice's development stage. In the ERA5 dataset, most of the analogues are found in autumn, while winter and summer have a similar frequency (Fig. 6b). In the CESM present, the number of analogues in winter is slightly higher than than in autumn.

Despite no significant changes in the number of analogues in the CESM future climate with respect to the present climate (Fig. 5b,c), there is a decrease in frequency in autumn, summer and spring, and an increase in winter (Fig. 6b). In the case of explosive storms, there is a significant increase in the number of explosive analogues (67 to 95), corresponding to an increase in the relative frequency of explosive cyclogenesis in a future climate. This increase is mainly seen in winter (Fig. 6d), and a decrease again in autumn. The NDR_c of the analogues increases in a future climate (Fig. 5b,c), but there are no significant changes in NDR_c of the explosive analogues. In the future climate, the analogues and explosive analogues quality is better than in the present, as evidenced by the statistically significant differences in probability distributions (Fig. 6a,c). As also seen in Figure 5, the spatial spread in the development stage tracks of the analogues is lower in the future climate, which means that future analogues represent Eunice's tracks better than those in the present. In summary, there is a significant increase in the frequency of explosive cyclogenesis in the future climate in winter. Additionally, the quality of analogues and explosive analogues improves significantly in the future. These changes collectively suggest an increased likelihood of Eunice-type storms in the future climate in winter.

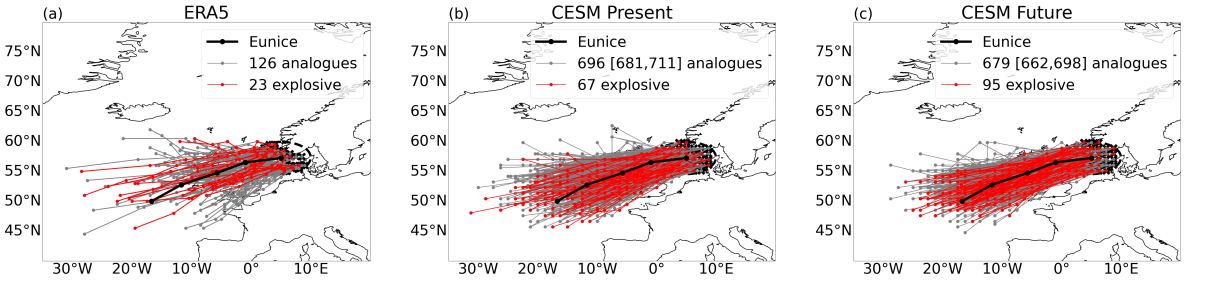

	Analogues	Explosive analogues
NDR_c	0.55	1.26

	Analogues	Explosive analogues
NDR_c	0.53 [0.51,0.55]	1.21 [1.18,1.24]

	Analogues	Explosive analogues
NDR_c	0.61 [0.58,0.63]	1.23 [1.20,1.27]

FIG. 5. Same as figure 3 but for storm **Eunice**.

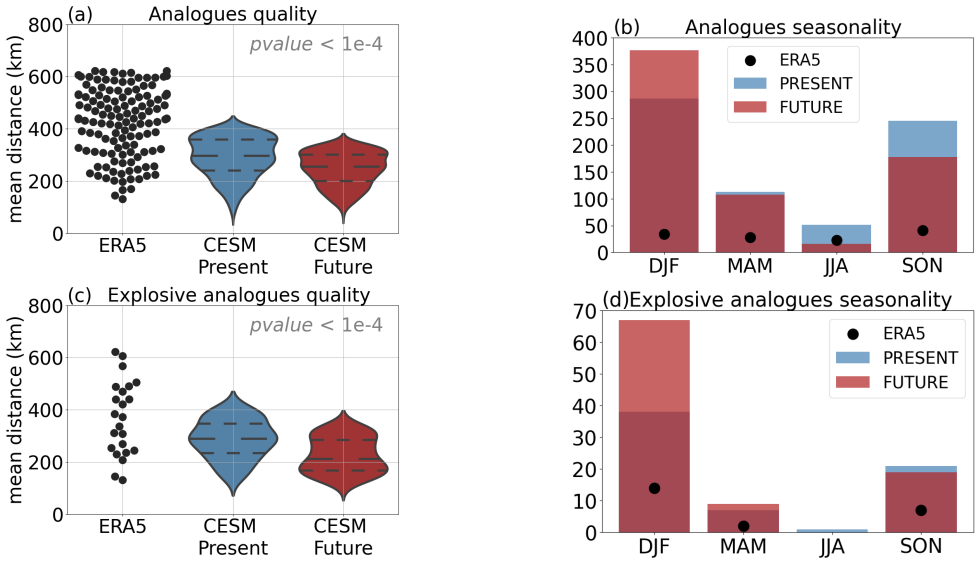

FIG. 6. Same as figure 4 but for storm **Eunice**.

c. Storm Xynthia

About 5 analogues every 10 years are detected in ERA5 and almost 1 every 10 years in the CESM present dataset (Fig. 7). This suggests that the CESM model underestimates the number of analogues that reach Galicia in their mature stage, linked to an underestimation of the storm frequency in that region shown by Dolores-Tesillos et al. (2022). In terms of explosive occurrence, 3 out of 38 analogues underwent explosive cyclogenesis in ERA5 period, that is, around 8% of the analogues. One of these is Miguel, a storm that affected western Europe in 2019 (Table A1). In the CESM present, the fraction of analogues that undergo explosive cyclogenesis is higher than in ERA5 (14 out of 101, that is, around 14%). In addition, the NDR_c of the analogues of the CESM present is higher than in ERA5. Despite the possible model biases, figures 8a,c show that the analogues and explosive analogues quality of the CESM dataset is comparable to that of the ERA5 period. In ERA5 the analogues occur more often in autumn, while in the CESM present dataset it is in spring (Fig. 8b).

In terms of the relative change between present and future climates, there is a significant decrease in the number of analogues in the future climate (101 to 68) (Fig. 7b,c). This decrease occur specially in spring, but also in autumn and summer (Fig. 8b). The number of explosive storms decreased slightly (from 14 to 11), with a decrease in spring and autumn but an increase in winter (Fig. 8d). Hence, there is an increase in the relative frequency of explosive storms, from around

14% to 16%. The NDR of the explosive analogues increases significantly under future climate conditions. However, due to the overlap in the confidence intervals, it is not possible to conclude that this increase is statistically significant, likely due to the insufficient sample size. No statistically significant changes are found in the analogues quality distributions between the two periods (Fig. 8a,c).

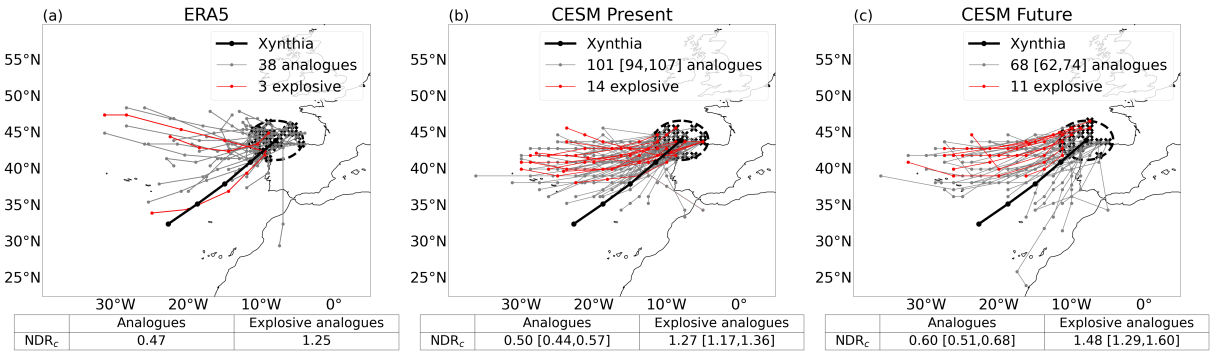

FIG. 7. Same as figure 3 but for storm **Xynthia**.

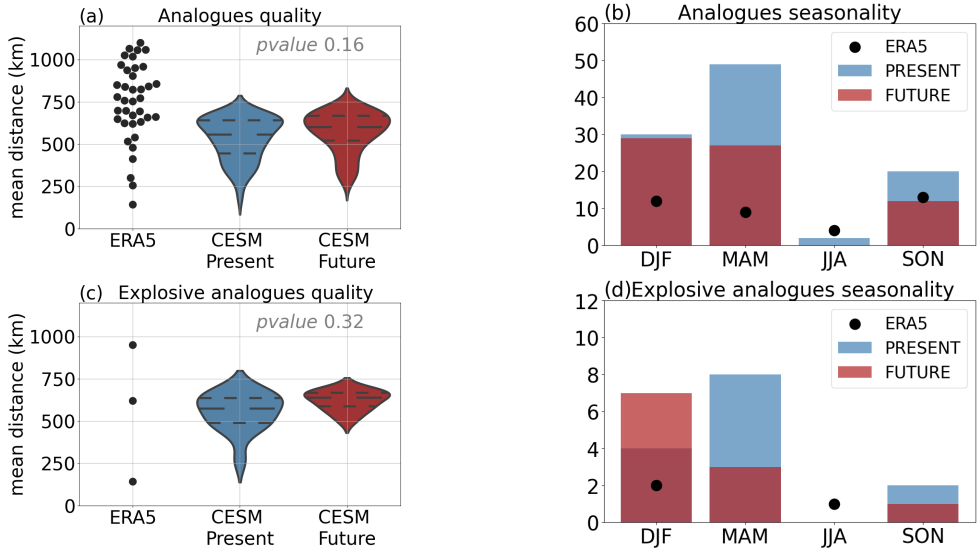

FIG. 8. Same as figure 4 but for storm **Xynthia**.

6. Meteorological hazards and Dynamics

In this section, we analyze trends in the fields of precipitation and wind speed at 10 m. To gain deeper insights into the evolving patterns of explosive analogues, we also assess the atmospheric dynamics contributing to these changes.

a. Storm Alex

Figures 9a,b,c show the sea–level pressure (SLP), precipitation rate (PR), and wind speed at 10 m (W) fields of storm Alex using ERA5 data at its time 0 date. The minimum SLP is around 970 hPa, and the storm center is squeezed over the English channel. Regarding PR, precipitation is primarily located along the storm's frontal structure, as well as over the Southeastern France coast and windward of the Alps. High wind speeds are predominantly observed in the southwestern section of the storm. The CESM present composites of analogues and explosive analogues for SLP, PR and W are shown in black contours in figures 9d–i as well as in figure A2 in the Appendix. As expected, the pressure gradient in the explosive analogues composites is higher than that in the analogues (higher and closer number of black contours in Fig. 9g,d, respectively), resulting in lower SLP values in the storm core. In addition, explosive analogues are associated to higher PR and W (black contours in Fig. 9h,i, respectively) than those of the analogues (Fig. 9e,f, respectively). SLP composites of both CESM present analogues and explosive analogues (Fig. 9d,g) depict a cyclonic structure with the center over the English channel, consistent with Alex. With respect to the PR pattern, this is predominantly located within the storm core and its southern region (fig. 9e,h). Due to the lack of precise alignment of storm fronts among the analogues, the PR pattern does not display a clearly defined frontal area. High values of W are located over the southern flank of the storm and over sea (Fig. 9f,i).

Shading in figures (Fig. 9d–f) show differences CESM future – minus – present of the analogues composites for sea–level pressure (SLP), precipitation rate (PR), and wind speed at 10 m (W), respectively. The analogues in the future period show positive anomalies of SLP northward of the Azores anticyclone as well as in the eastern Mediterranean (Fig. 9d). This contributes to increase the amplitude of the Rossby waves. In addition, there are SLP negative anomalies in the core of the analogues. This means that the analogues in the future period are associated to lower core pressures and to an increased pressure gradient. This, in turn, contributes to increase W in the

future period (Fig. 9f). In addition, PR increases, specially to the east of the storm core, in the future period (Fig. 9e). The SLP differences of the explosive analogues depict a similar structure to that of the analogues (Fig. 9g), with deeper storms in the future period and positive anomalies on the eastern Mediterranean and southern Scandinavia. Hence, there is an increase in the SLP gradient which is also reflected by an increase in W, specially to the east of the explosive analogues core (Fig. 9i). Figure 9h depicts an increase of PR in the northern flank analogues' core and a decrease, albeit smaller, southward.

The PR and W patterns of extratropical storms such as Alex and its analogues are mostly influenced by the position and intensity of weather fronts. To assess changes in the weather fronts, we evaluate the equivalent potential temperature at 850 hPa pattern (θ_e, figures 10a,b). We also compute the gradient of the θ_e field ($\nabla\theta_e$). The regions of the maximum $\nabla\theta_e$ are shown by white dashed lines in figures 10a,b, typically characterizing the presence of weather fronts. Figure 10c illustrates the future minus present differences in $\nabla\theta_e$, providing insights into the changes in front positions. In the CESM future, θ_e is overall higher than in the present, as a result of the expected increase in global temperatures and water vapour content in a changing climate (shading in Fig. 10a,b). Regarding the regions of maximum $\nabla\theta_e$ (white dashed line in Fig. 10a,b), we interpret that a cold front originates southwestern France and extends towards north of the Azores, as it is typically characterized by cold temperatures behind the warm sector. The other regions of maximum $\nabla\theta_e$ are over English Channel extending towards central western Europe, and they would be associated to the occluded and warm fronts, respectively. Regarding the future minus present differences in $\nabla\theta_e$, we see a noticeable increase and a slight southward shift along the position of the cold front (Fig. 10c). We also observe a northwestward shift in the warm front. These shifts lead to a relocation of weather fronts of the explosive analogues in the future climate compared to the present, potentially indicating a more rapid development of storms.

We also assess the upper-tropospheric jet stream distribution (figure 11) at the time 0 dates. Figures 11a and b show that the jet stream is situated in the southern flank and slightly westward of the low-level cyclone. Hence, the surface low is located at the left exit region of the jet streak. This configuration is typical of storms at their maximum intensity. In the future period, there is an extension and consequent intensification of the jet downstream and southward compared to the present composites. This downstream intensification may be associated with stronger upper-level

divergence, an increase in ascent airflow, and consequently, an increase in storm intensity and precipitation.

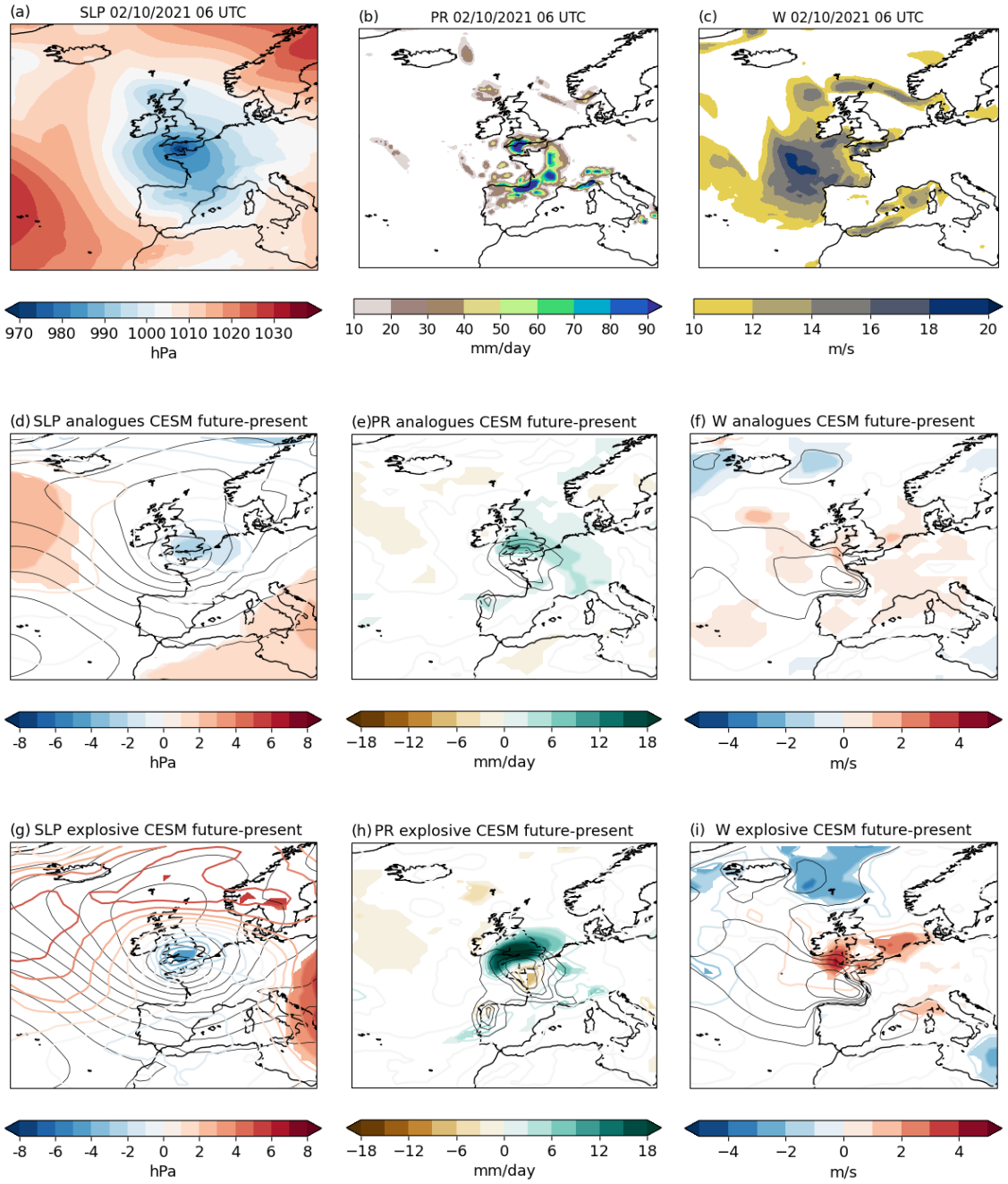

FIG. 9. (a) Sea level pressure (a), (b) precipitation rate, and (c) wind speed at 10 m for storm *Alex* at its time 0 using ERA5 data. (d–i) Black contours: Composites of the CESM present **analogues** and **explosive analogues** of storm **Alex** at their *time 0* dates of (d,g) sea-level pressure, at 4 hPa intervals, (e,h) hourly mean precipitation rate, from 10 mm/day and every 5 mm/day, and (f,i) hourly mean wind speed, from 10 m/s and every 2 m/s. Black contours are the same than shading in figure A2. Coloured contours: CESM future minus present differences of the composites of the analogues. Shading: CESM future minus present statistically significant differences.

To further link changes in PR and W of explosive analogues with the dynamics and possible drivers, we assess the changes in eady growth rate (EGR, equation 2), convective precipitation (PRECC), and large-scale precipitation (PRECL). We observe a slight increase in EGR 24 hours prior to the mature stage of the storms, indicating an enhanced baroclinicity in future explosive analogues compared to the present (Fig. 12a). This could be linked to an increase in the NDR (Fig. 3b,c) and in the intensity of storms in terms of wind speed (Fig. 9i). Furthermore, during the mature stage of the storms, we observe an overall increase in both PRECC and PRECL (Fig. 12b,c). Notably, PRECL contributes the most to the spatial changes observed in total precipitation (Fig. 9h). These changes in the PRECL pattern might be linked with the cyclonic shift of the weather fronts seen in figure 10c and changes in the stratiform precipitation produced by the warm conveyor belt.

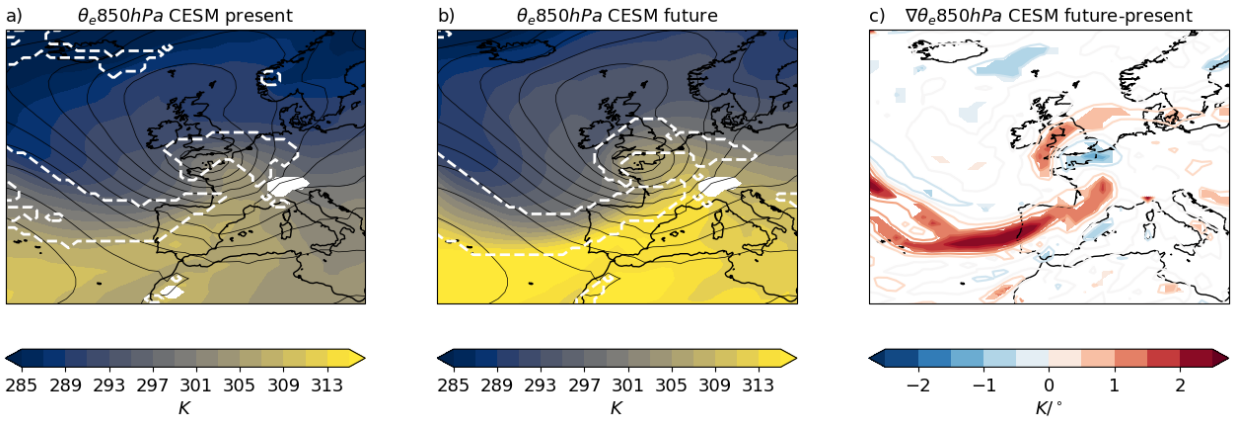

FIG. 10. (a,b) Shading: equivalent potential temperature at 850hPa for CESM (a) present and (b) future **explosive analogues** of **Alex** at their time 0 dates. White dashed lines: values exceeding the 80th percentile of the equivalent potential temperature gradient at 850 hPa. Black contours: composites of SLP at 4 hPa intervals (same as the shading in figure A2). (c) CESM future minus present differences in the composites of the horizontal gradient of equivalent potential temperature at 850 hPa.

b. Storm Eunice

Storm Eunice was situated over the North Sea during its mature stage (Fig. 13a). At that time, precipitation was relatively modest along a frontal line (Fig. 13b), while wind speeds were notably high, especially over the sea on the southern flank of the storm (Fig. 13c). The composites of

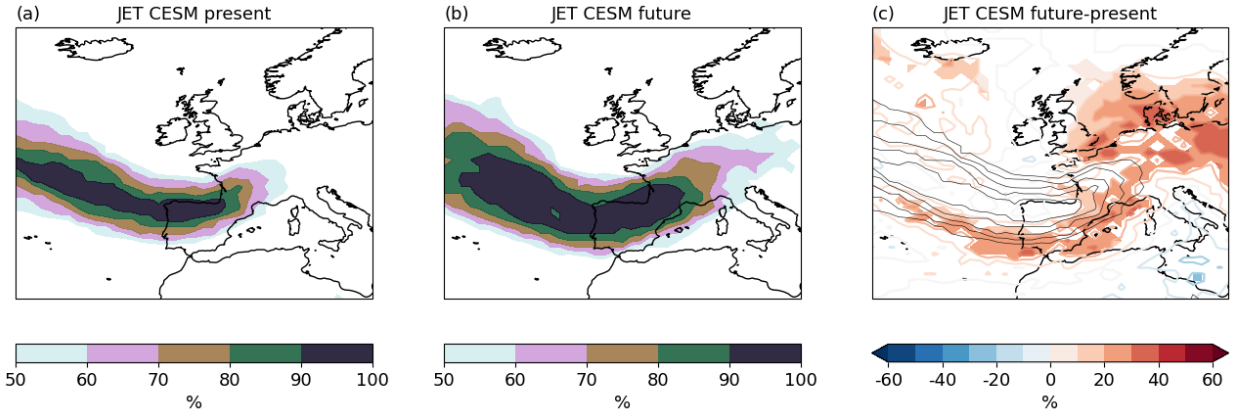

456 FIG. 11. Distribution of the jet events for CESM (a) present and (b) future **explosive analogues** of **Alex** at their
457 time 0 dates. (c) Shading: CESM future minus present differences in the distribution of the jet events. Black
458 contours: CESM present composite of the distribution of the jet events.

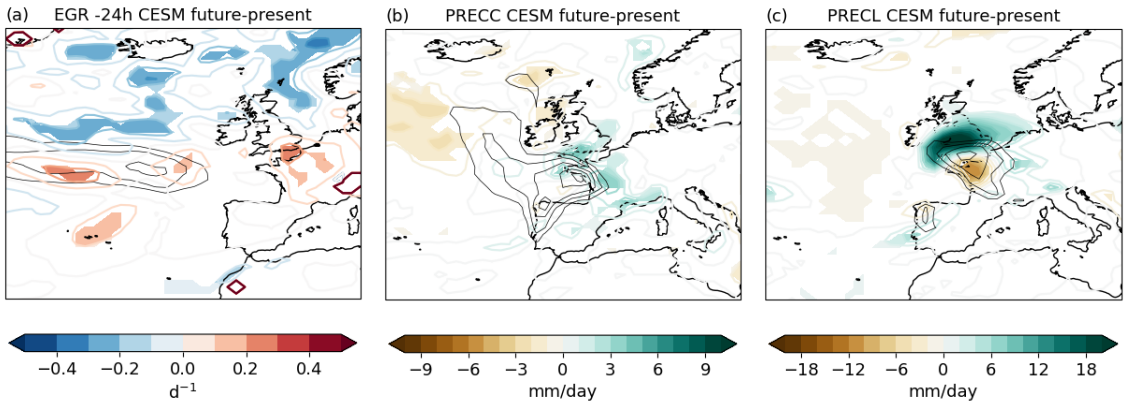

459 FIG. 12. Shading: CESM future minus present differences in the composites of **explosive analogues** of
460 (a) Eady growth rate 24 hours before the time 0 dates (EGR), (b) convective precipitation (PRECC), and (c)
461 large-scale precipitation (PRECL), respectively. Black contours: composites of CESM present of EGR, PRECC
462 and PRECL at intervals of 0.1 d^{-1} starting at 1 d^{-1}, 2 mm/day starting at 5 mm/day, and 5 mm/day starting at
463 10 mm/day, respectively (same as shadings in Figures A3).

468 analogues and explosive analogues exhibit similar patterns of SLP, represented by black contours
469 in figure 13d,g, respectively, and shading in figure A4a, d. In addition, the positions of highest PR
470 and W in both analogues and explosive analogues (A4e,f and A4h,i) coincide with those of storm

Eunice. Explosive analogues show, as expected, lower pressure at their core, and higher PR and W than the analogues.

The SLP pattern of the future analogues depicts lower pressures in the cyclonic structure and higher pressures in the anticyclonic with respect to the present analogues (Fig. 13d). This is linked to deeper analogues as well as an increase in the SLP gradient in their southern flank. The PR pattern depicts thus an increase in downstream of the analogues center and extended in western Europe (Fig. 13e). In terms of W, there is also an increase in the southern part of the analogues, that is, over the UK, the North Sea, and the Baltic Sea (Fig. 13f), which corresponds to the warm sector. The differences in the patterns of explosive analogues depict a similar pattern than the analogues: lower SLP, increase in PR, and stronger W specially over the sea (Fig. 13g,h,i).

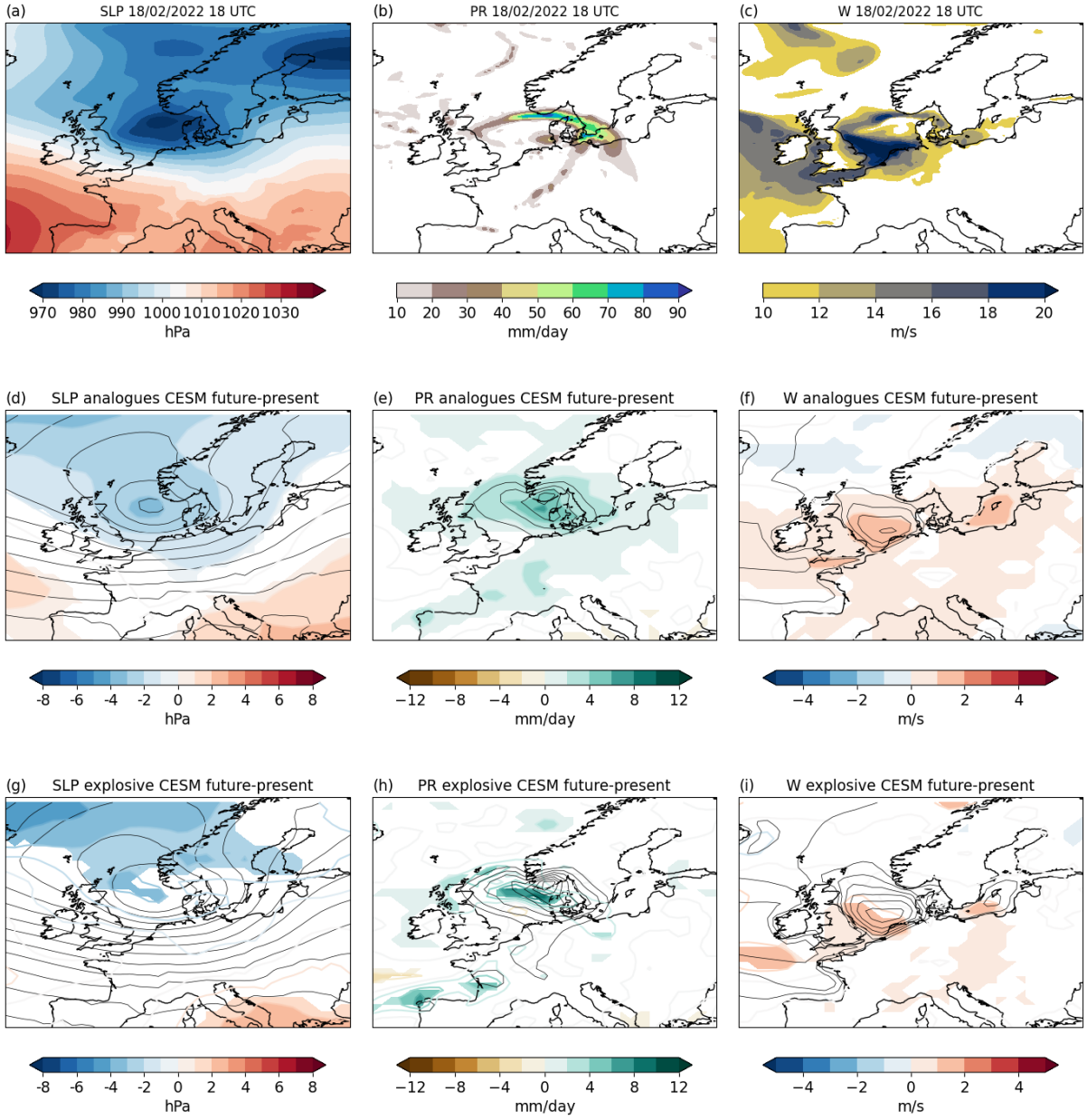

FIG. 13. Same as figure 9 but for **analogues of Eunice**.

Regarding the changes in $\nabla\theta_e$, figure 14c depicts an increase along a line starting in Germany and crossing central France and Bay of Biscay. This region corresponds to the southern flank of the cold front in the present climate, depicted in figure 14a in dashed white lines. Hence, the increase in $\nabla\theta_e$ can be interpreted as an intensification and a slight cyclonic shift of the cold front. This, in turn, might be linked to the increase in W in the cold sector seen in figure 13i and increase in PR over the cold front area (fig. 13h). On the contrary, a dipole pattern of $\nabla\theta_e$ over south Scandinavia suggests a deceleration of the warm front, shown in figure 14a as the tail of the comma-shape white dashed region.

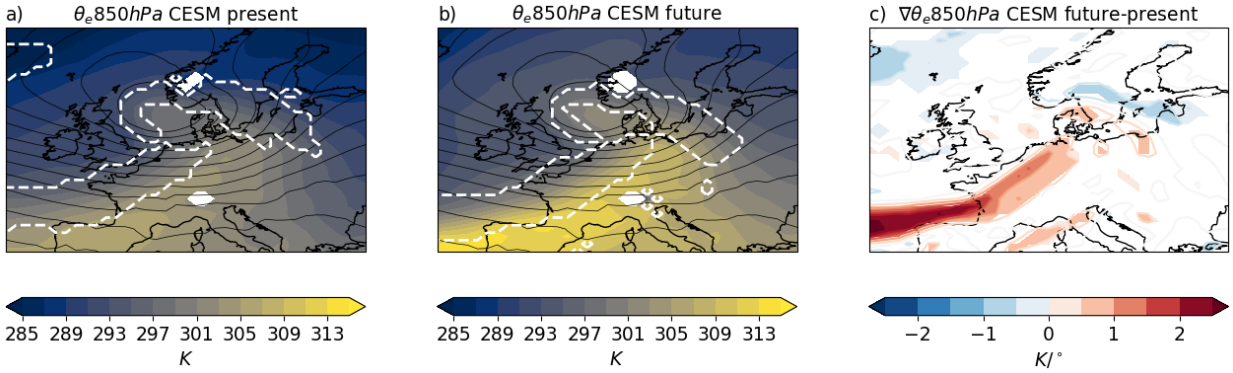

FIG. 14. Same as figure 10 but for storm **Eunice**

Figures 15a,b show that the jet stream is located southward and westward relative to the surface low. In the future period, the jet intensifies and extends further south. This suggests a localized increase in baroclinicity. Additionally, there is a slight increase in the northward flank exit region of the jet, which may be associated with an increase in upper-level divergence and ascent vertical motion.

Figure 16a shows a significant increase in the EGR 24 hours before the time 0 dates of the explosive analogues in a future period. This suggests that the changes in intensity and patterns of the explosive analogues are largely baroclinically-driven. Little changes are seen in PRECC and (Fig. 16b), with an increase in the cold sector of the storm. Regarding the PRECL pattern, figure 16c shows an increase over Bay of Biscay, probably linked to the increase in intensity of the cold front, as well as an increase over Denmark, where the warm front is located.

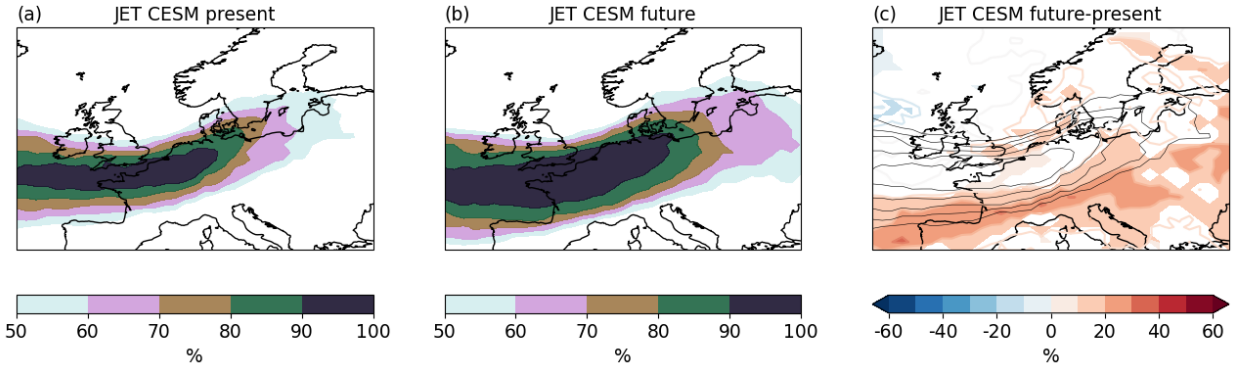

FIG. 15. Same as figure 11 but for storm **Eunice**

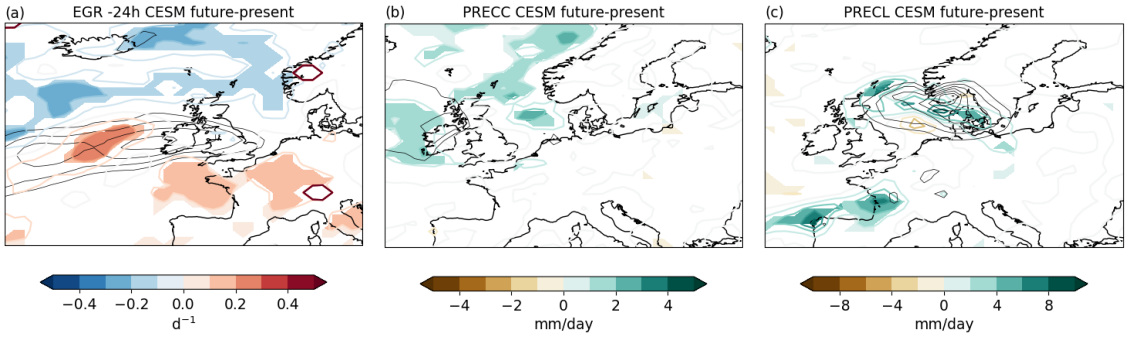

FIG. 16. Same as figure 12 but for storm **Eunice**

c. Storm Xynthia

The mature stage of storm Xynthia was situated over the Bay of Biscay (Fig. 17a). PR was primarily concentrated on the western flank of the storm (Fig. 17b), where the highest W was also observed (Fig. 17c). In this context, both analogues and explosive analogues successfully capture the mature stage's position (Fig. 17d,g). Regarding the patterns of PR and W (Fig. 17e,h and Fig. 17f,i), both are slightly shifted southwards, probably due to a misalignment between the storm fronts. Similar to storms Alex and Eunice, explosive analogues demonstrate lower SLP and higher PR and W.

Figure 17d depicts lower pressures in the north part of the core of the analogues. In addition, there are positive anomalies of SLP in both western and eastern of the cyclonic structure, which results in an increase in the waviness of the pressure pattern. In the case of PR and W, both show an increase in the analogues core and northeastern of the Iberian Peninsula (Fig. 17e,f). Figure 17g

shows that explosive analogues depict significant lower pressures in the future period, specially in their northern flank. This is linked with a significant increase in W (Fig. 17i). Similarly to Alex (Fig. 9h), PR depicts a significant increase in the northern flank of the explosive analogues' core, a slight decrease in the region of maximum PR in the present period, and a slight increase in their southern flank.

Figures 18a,b show a different spatial pattern of θ_e at 850hPa of present and future explosive analogues of Xynthia. In the present period, the warm sector of the storm does not overlap with the storm center. In contrast, in the future period the θ_e at 850hPa pattern has a T-bone structure, typical of the Shapiro–Keyser storms (Shapiro and Keyser 1990), and that could indicate a warm seclusion sector of the storms. In terms of changes in the gradient of θ_e, there is an overall increase of the gradient in the regions of the maximum gradient depicted by white dashed lines in 18a,b, which are the regions associated to the weather fronts. This is related to an increase in intensity of the weather fronts. A dipole with negative anomalies over the Bay of Biscay and positive anomalies northwestward suggest a cyclonic shift of the warm front position, even though the overall change is an increase in magnitude.

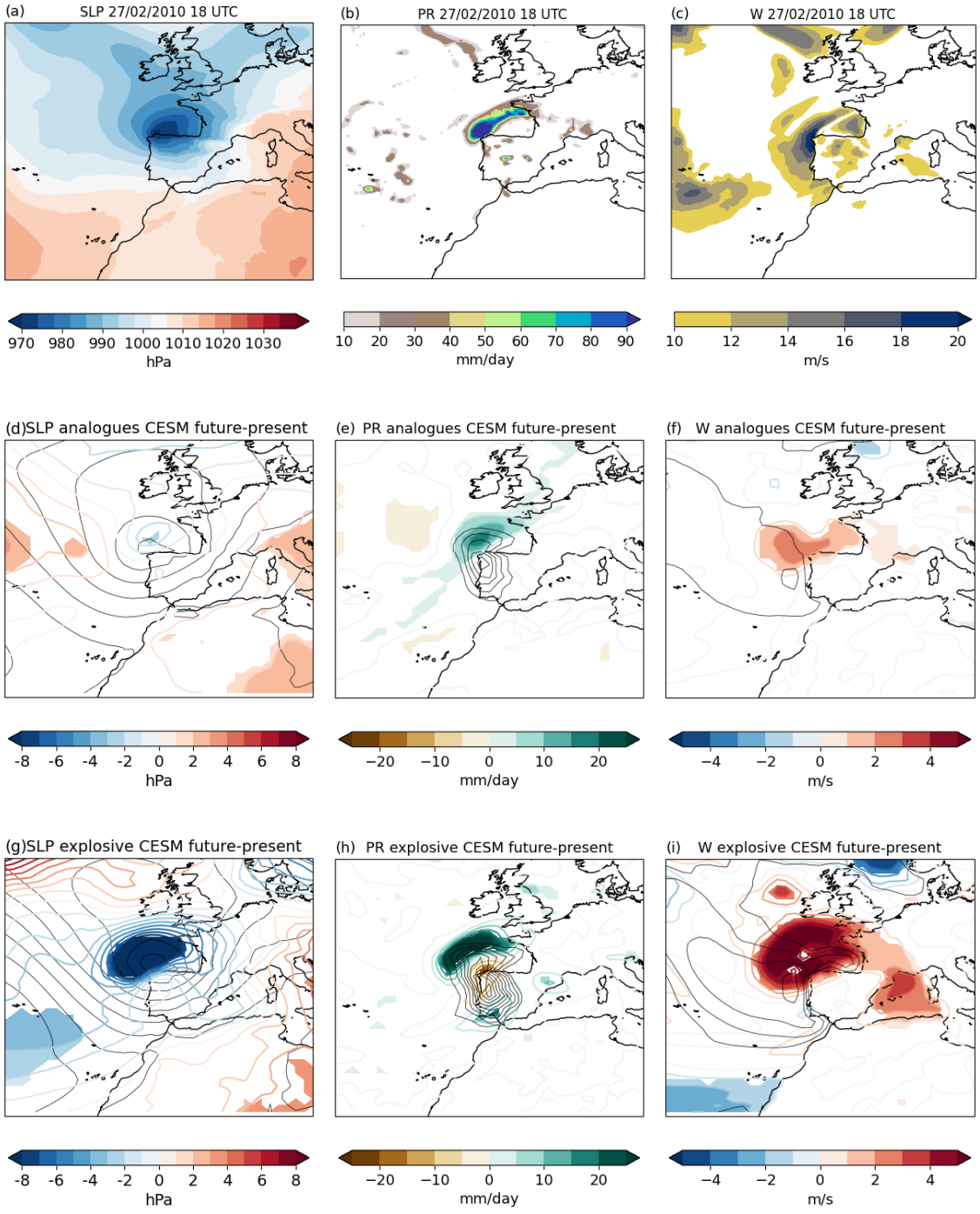

FIG. 17. Same as figure 9 but for **analogues of Xynthia**.

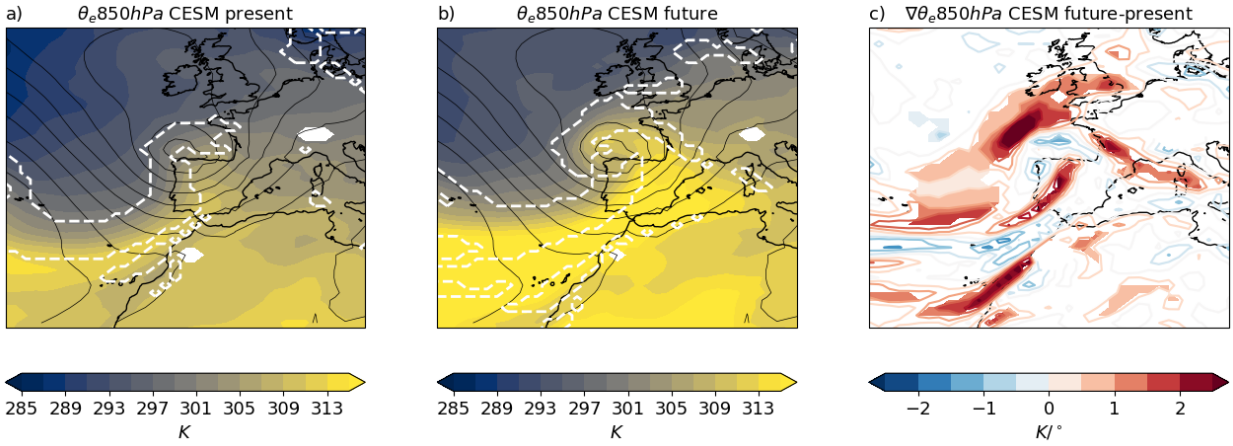

FIG. 18. Same as figure 10 but for storm **Xynthia**

Similar to storm Alex, Xynthia-like storms depict an extension downstream and southward of the jet stream in the future period. As previously discussed, this could lead to an increase in the vertical motion from the ageostrophic component of the wind and could be linked to the increase in precipitation and intensity of the storms. In addition, this position of the jet stream depicts a more advanced stage of the cyclone, and could be linked to the cyclonic relocation of the weather fronts.

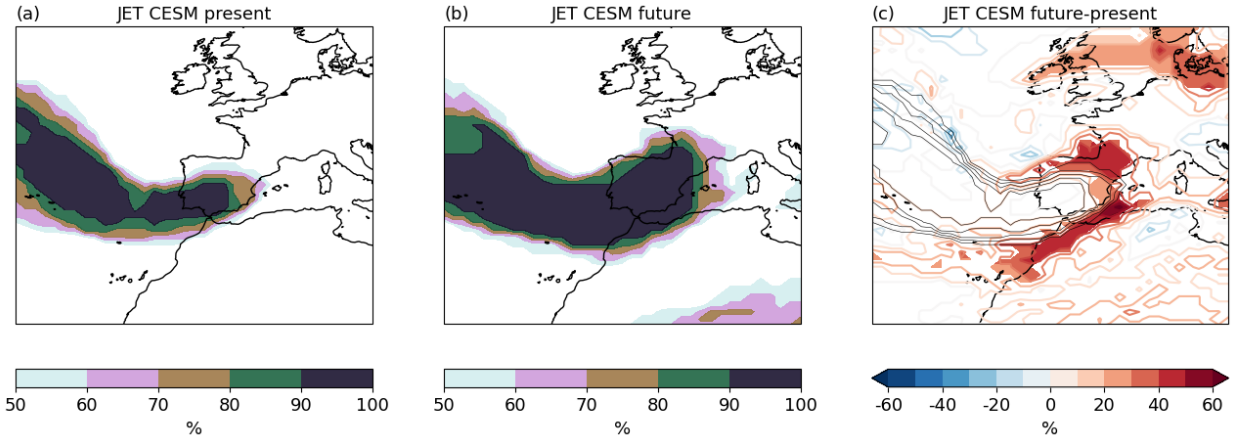

FIG. 19. Same as figure 11 but for storm **Xynthia**

Figure 20a depicts no change of the EGR in the region of its maximum, which means there are no changes in low-level baroclinicity 24 hours before the mature stage. Thus, changes assessed previously might be largely diabatically-driven. Regarding PRECC and PRECL (Fig. 20b,c)

spatial patterns, there is an overall increase in both types of precipitation. However, both show a tripolar pattern: a decrease in the core of the maximum precipitaiton area, and an increase in the southern and northern flanks. In the case of PRECL, this is linked to the cyclonic shift of the warm front and an intensification of both warm and cold fronts.

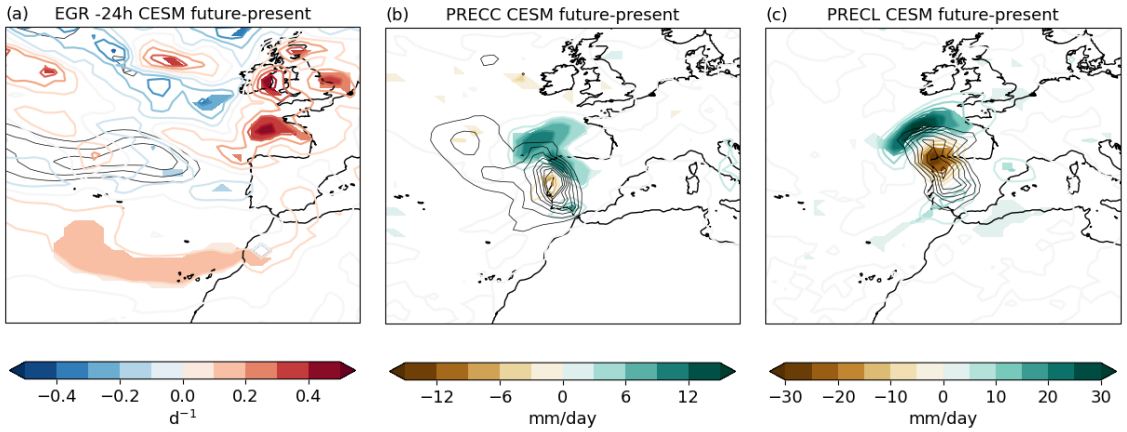

FIG. 20. Same as figure 12 but for storm **Xynthia**

7. Discussion and conclusions

We have conducted an analysis of three storms (Alex, Eunice, and Xynthia) under anthropogenic radiative forcing, using the CESM-Large Ensemble. We identified storms with a similar development stage to the three storms, and termed them *analogues*, in the present period (1991-2001) and in the future RCP8.5 period (2091-2100). We further selected those undergoing explosive cyclogenesis (*explosive analogues*). We found that the frequency and intensity of the analogue storms, as well as their associated meteorological hazards, will change in a future climate.

For storm Alex, a significant decrease in the number analogues has been observed, specially in autumn. However, there is an increase in the relative frequency of explosive analogues as well as in the normalized deepening rates. Furthermore, both analogues and explosive analogues will be associated with overall higher precipitation and stronger wind speeds. The large-scale precipitation pattern of the explosive analogues and the weather front disposition suggest a cyclonic shift of the mature stage of the storms. There is a small increase in the baroclinicity in the future explosive analogues, which makes changes in their characteristics both baroclinically and diabatically driven. These factors suggest that explosive Alex-like storms will not be less frequent in a future climate.

When they occur, they will deepen more rapidly and be associated with higher precipitation and wind speeds, indicating that storms like Alex could be a greater meteorological hazard in the future.

For storm Eunice, rather than a change in the number of analogues, there is a seasonal shift towards more analogues in winter and fewer elsewhere. However, we found a significant increase in the number of analogues that undergo explosive cyclogenesis. The quality of both analogues and explosive analogues also increases in a future climate. Additionally, there will be an increase in precipitation rate and wind speed of the analogues and explosive analogues. These changes in the characteristics of explosive analogues are, at least partially, baroclinically-driven. Therefore, explosive Eunice-like storms will not only be more frequent but also more severe in a warmer climate.

We found it difficult to identify good analogues of storm Xynthia in both reanalysis and climate models. Hence, we can claim that storm Xynthia was an unusual event, and that a caveat of this study is the quality of its analogues. We observed a decrease in the number of analogues, specially in spring, but a slight increase in the relative frequency of explosive cyclogenesis. Xynthia-like storms are expected to have higher precipitation rates and wind speeds in a future climate. The explosive analogues depict an overall significant increase in precipitation and wind speed, with a cyclonic shift in their mature stage. Changes in the patterns of explosive analogues are likely to be largely diabatically-driven, as there is no change in low-level baroclinicity previous to the mature stage of the storms. Therefore, Xynthia-like storms are becoming less probable but more severe, especially those that are explosive, in a warmer climate.

Trends in the number of analogues, including explosive ones, depend on the specific storm under consideration. Eunice-like explosive storms are expected to be more frequent, in line with previous studies that project a slight increase in explosive frequency close to the British Isles and on the North Sea (Seiler and Zwiers 2016; Zappa et al. 2013). The relative frequency of explosive storms like Alex and Xynthia is also expected to increase with respect to the non explosive storms. The increase in precipitation associated with storms in a future climate is consistent with other studies (Hawcroft et al. 2018; Zhang and Colle 2017; Michaelis et al. 2017). For the explosive analogues of Alex and Xynthia, we found a similar precipitation changes to Sinclair et al. (2020). Sinclair et al. (2020) found, using aquaplanet simulations, a poleward displacement of the region of maximum precipitation, mainly due to changes in the large-scale precipitation pattern, in a future

climate. There is less confidence in future projections regarding the dynamical intensity, such as wind speed, associated to the storms (Seneviratne et al. 2021; Catto et al. 2019). However, our study reveals that, across all the storms analysed, surface winds are expected to increase, specially for the explosive analogues. For Eunice, the increase is located over the warm sector of the storms, as consistent with previous studies (Priestley and Catto 2022; Dolores-Tesillos et al. 2022). The drivers behind the changes in the pattern of the storms, whether they are baroclinically-driven or diabatically-driven, vary depending on the storm. However, as found by Dolores-Tesillos et al. (2022), Binder et al. (2023), and Joos et al. (2023), diabatic effects play a key role in increasing the wind speed, the deepening rates, and the intensity of the strongest storms. For the case of Xynthia, Ludwig et al. (2014) found that the storm intensification was mainly led by anomalously high sea surface temperatures and diabatic processes, and also suggested that Xynthia-like storms could be more frequent in a warmer climate. We note that we found no changes in low-level baroclinicity for Xynthia-like storms during the development stage. Hence, we suggest that diabatic processes contribute to the increase in wind and precipitation for Xynthia-like explosive storms in a future climate, as well as a relative increase of the explosive frequency, consistent with the prediction by Ludwig et al. (2014). In addition Sinclair et al. (2020), found, using an aquaplanet model, that storms in a warmer climate are more diabatically-driven. To better understand the potential influence of diabatic effects on storm intensification, a comprehensive study on the role of warm conveyor belts in storm intensification (Binder et al. 2023) could be conducted. Our study thus identifies both similarities and differences when compared to previous research on various behaviors of extratropical and explosive storms in the North Atlantic under climate change. These findings not only emphasize the differences in regional trends but also suggest that storms may exhibit distinct behaviors compared to the overall changes, potentially yielding different responses to anthropogenic radiative forcing.

Our approach has limitations that should be acknowledged. First, our analysis is based on a single model, the CESM model version 1, which was chosen for its availability as a large ensemble dataset of more than 100 members with 6-hourly data. While CESM has been shown to simulate the characteristics of storms fairly well (Dolores-Tesillos et al. 2022; Joos et al. 2023; Binder et al. 2023) and to have a spread due to internal variability comparable to the CMIP5 multi-model spread (Kay et al. 2015), a multi-model study would better assess model uncertainty. Second, we use a

single scenario, the worst-case scenario (RCP8.5), due to its availability. This scenario represents an extreme case assuming high greenhouse gas emissions throughout the 21st century. Although this extreme scenario proves valuable in detecting the anthropogenic radiative forcing signal, it may not encompass the entire range of future climate projections. Therefore, our findings may not be generalized to other scenarios. Future studies should explore the robustness of our results using multiple models and scenarios. Finally, we use a single tracking scheme. However, we filter out the weakest storms, and so the dependence on the tracking scheme is considered minor (Neu et al. 2013).

The analogues are considered recurrences in the atmospheric patterns of to the storms, and so our results can also be applied to the explosive analogues found in the ERA5 dataset, some of them being known high-impact storms in the region (Table A1). In conclusion, we found that all of the storms analyzed in this study are expected to become more severe and impactful with climate change. As suggested by Shepherd (2016), demonstrating that certain extreme events can occur again and result in even worse consequences with climate change, as shown in this study, can help advocate for investment in protective measures against hypothetical risks. Hence, these storms can serve as reference points for building resilience and preparing for future events.

Acknowledgments. This work was supported by the European Union's Horizon 2020 research and innovation programme under the Marie Sklodowska-Curie grant agreement N° 956396 (European weather extremes: drivers, predictability and impacts (EDIPI) ITN). The authors would like to express special thanks to H. Wernli and his Atmospheric Dynamics group at ETH Zurich, particularly M. Sprenger, M. Röthlisberger, H. Binder, J. Riboldi, and U. Beyerle, for their valuable discussions and assistance in accessing the CESM data.

Data availability statement. The ERA5 data are publicly available online at https://cds.climate.copernicus.eu/. We acknowledge the Atmospheric Dynamics and Climate Physics groups at ETH Zurich for providing access to CESM data.

APPENDIX

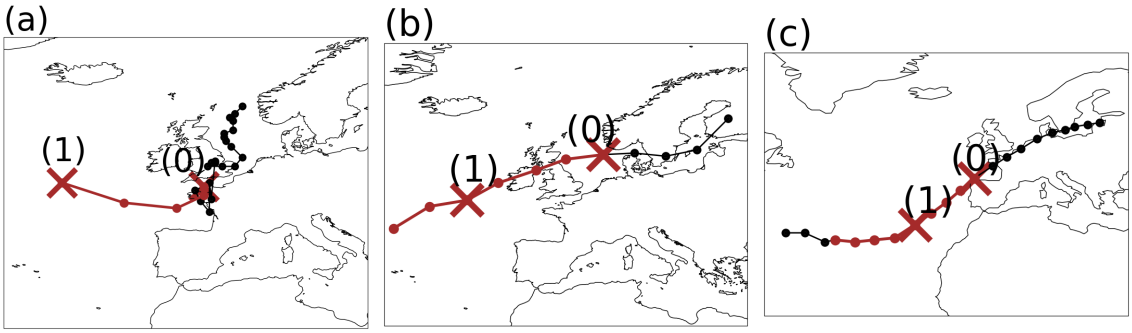

FIG. A1. 6–hourly tracks of storms Alex (a), Eunice (b), and Xynthia (c). (0) depicts the minimum sea level pressure point, and (1) the position of the storm 24 hours before (0). The brown line indicates when the storm underwent explosive cyclogenesis.

Alex			
Storm Angus	20 November 2016	United Kingdom, France	Also known as storm Nanette in France. The event left 2 fatalities and wind gusts up to 170 km/h (Sky News 2016; Met Office 2016; The telegraph 2016).
Storm Norberto	5 March 2020	France, Spain	Wind gusts around 100 km/h and up to 140 km/h were recorded (The European Forecaster 2021; AEMET 2021)
Storm Katie	28 March 2016	France, United Kingdom	The highest windgust recorded was 170 km/h in Isle of Wight (The European Forecaster 2021; AEMET 2021)
Eunice			
"Adolph Bermpohl" storm	23 February 1967	North Sea	The Adolph Bermpohl was a sea rescue cruiser on which its crew died due to the severity of the storm in the North Sea. Other boats also sank in the same storm (The Wreck Site 2017).
October storm	17 October 1967	Norway, Sweden	Hurricane-force winds of up to 144 km/h were recorded in some parts of southern Sweden (SMHI and Institute 2021).
Storm Capella	3 January 1976	Ireland, United Kingdom, Belgium, France, Denmark, Germany, Netherlands	Also known as Ruisbroek flood in Belgium. The storm resulted in severe wind damage across western and central Europe and coastal flooding. One of the strongest windgusts recorded during the event was 215 km/h at Lowther Hills (Met Office 1976). It left at least 82 fatalities (Berz 1988).
Burns' Day storm	25 January 1990	Ireland, United Kingdom, France, Belgium, Netherlands, Germany, Denmark	Also known as Storm Daria. Hurricane-force wind gust were recorded, such as 167 km/h at Abertporth (McCallum 1990) and 176 km/h at Pointe du Raz (Météo France 2019). The storm left at least 95 fatalities across Europe, being one of the deathliest storms in Europe (Météo France 2019).
Storm Oratia	30 October 2000	France, Germany, Netherlands and United Kingdom	Storm Oratia (Tora in Norway) (Extreme Wind Storms Catalogue n.d.) was probably the worst storm to hit United Kindgom after the Great Storm of 1987 (NASA Earth Observatory 2017). The storm brought heavy rainfall and strong winds to many areas of southern Britain, with wind gusts up to 150 km/h.
Storm Ulli	3 January 2012	United Kingdom, Ireland, Netherlands, Scandinavia	Storm Emil in Norway (The Nordic Page Norway n.d.). The damages were estimated at 0.2 billion USD (Koks and Haer 2020; Roberts et al. 2014b)
Storm Bronagh	21 September 2018	United Kingdom	Wind gusts up to 125 km/h recorded in the Isle of Wight (Met Office 2018).
Storm Christoph	21 January 2021	United Kingdom	The event was characterized by heavy precipitation above 100 mm. This was one of the wettest 3–day periods on record in the western and northwestern part of England and Wales (Met Office 2021).
Xynthia			
Storm Miguel	6 June 2019	Spain, France, Belgium, Luxemburg, Netherlands	The storm brought high winds and heavy precipitation to western Europe, with wind gusts up to 150 km/h (AEMET 2020; EUMETSAT 2019). It caused at least three deaths.

TABLE A1. Explosive analogues of each storm detected with ERA5, which are also known storms that had an impact across Europe. The first column corresponds to the storm name, the second column shows the date of minimum sea level pressure, the third column lists the regions affected, and the fourth column provides notes on some meaningful aspects.

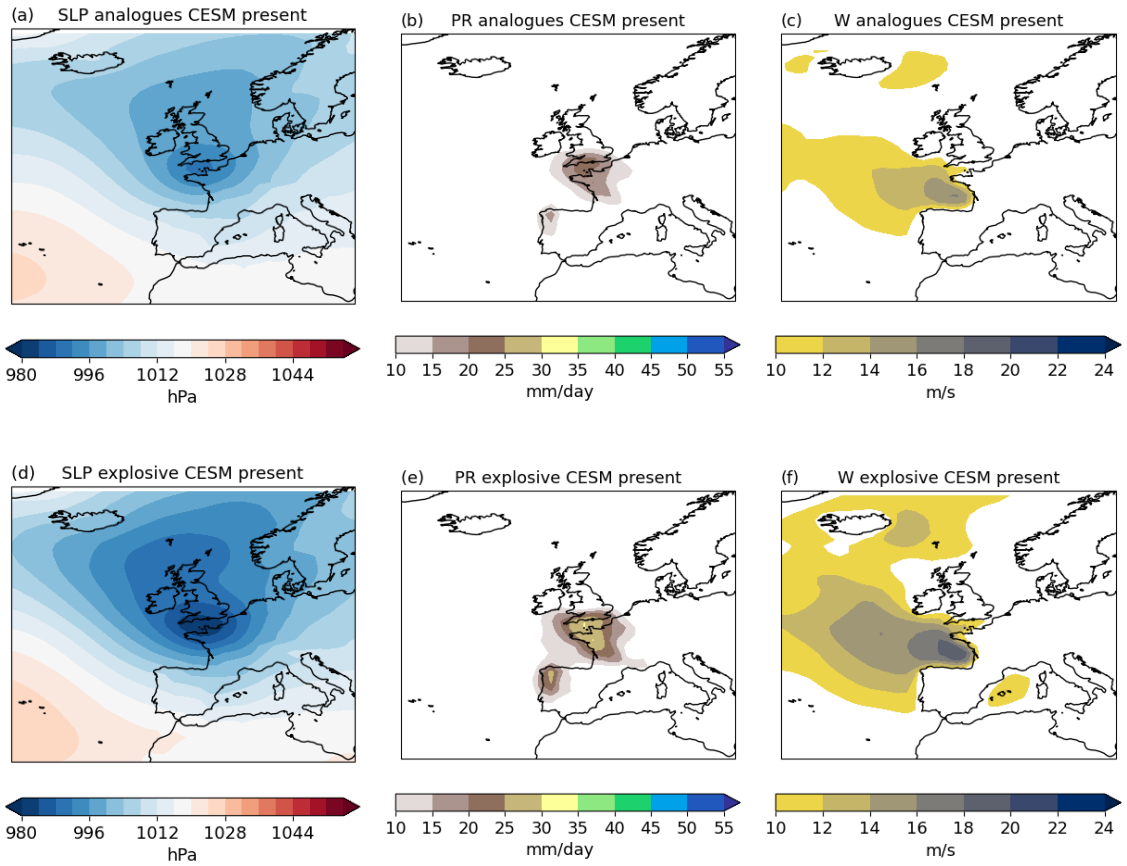

FIG. A2. Composites of the CESM present **analogues** and **explosive analogues** of **Alex** at their *time 0* dates of (a,d) sea-level pressure, (b,e) hourly mean precipitation rate, and (c,f) hourly mean wind speed.

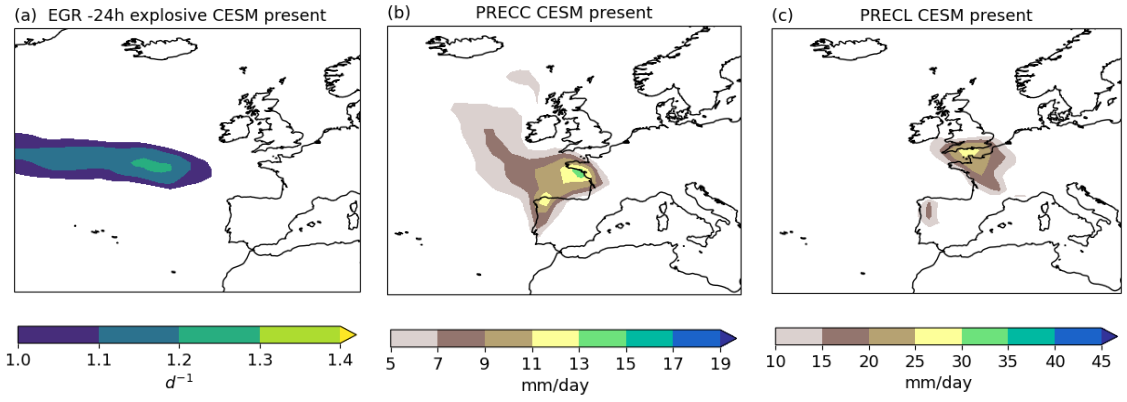

FIG. A3. Composites of the CESM present **explosive analogues** of **Alex** at their *time 0* dates of (a) eady growth rate, (b) hourly mean convective precipitation, and (c) hourly mean large-scale precipitation rate.

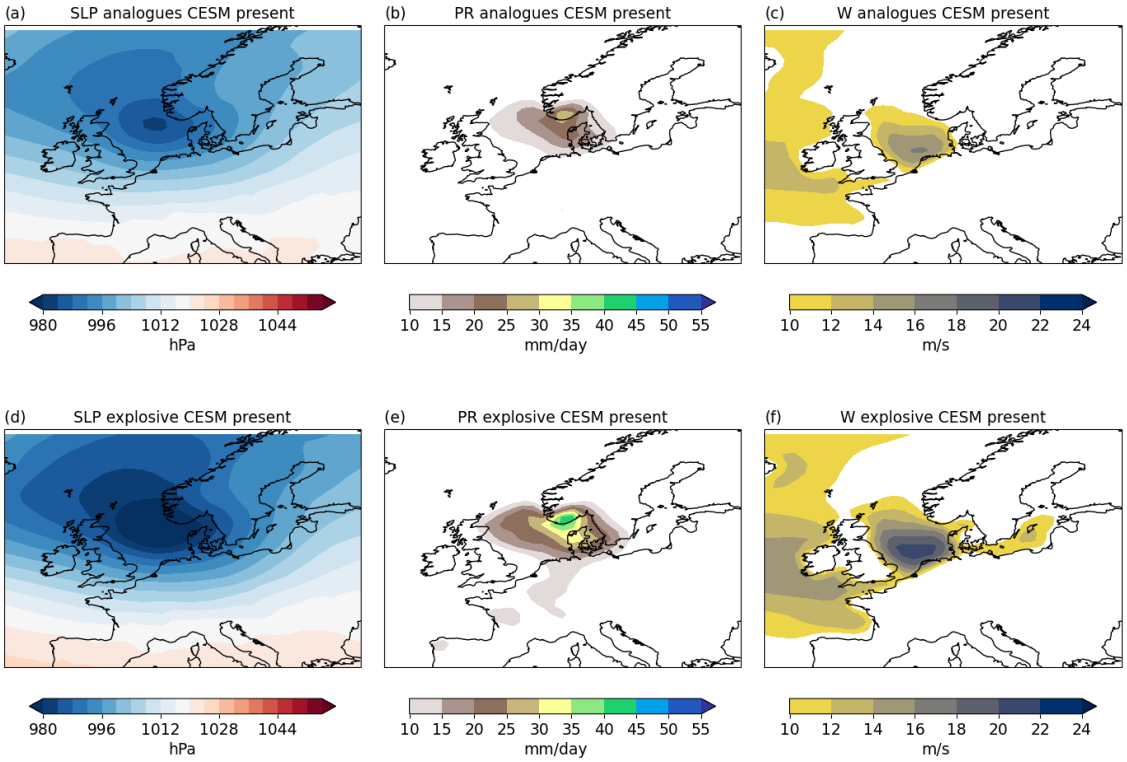

FIG. A4. Same as figure A2 but for **analogues of Eunice**.

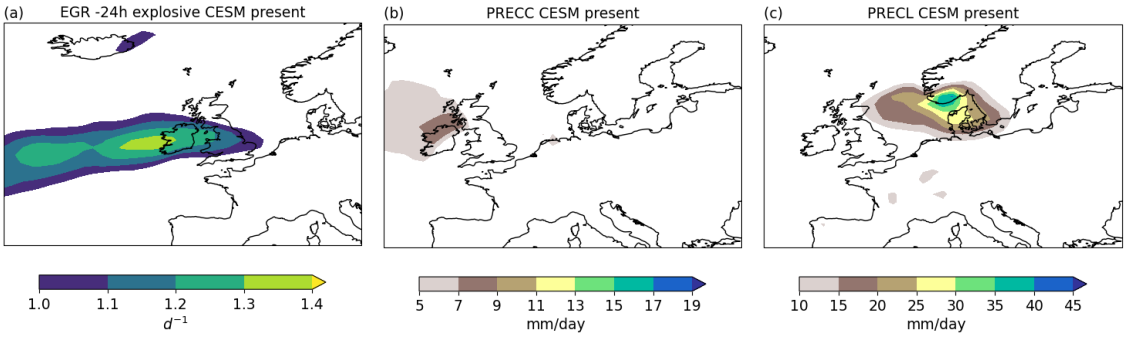

FIG. A5. Same as figure A3 but for **explosive analogues** of **Eunice**

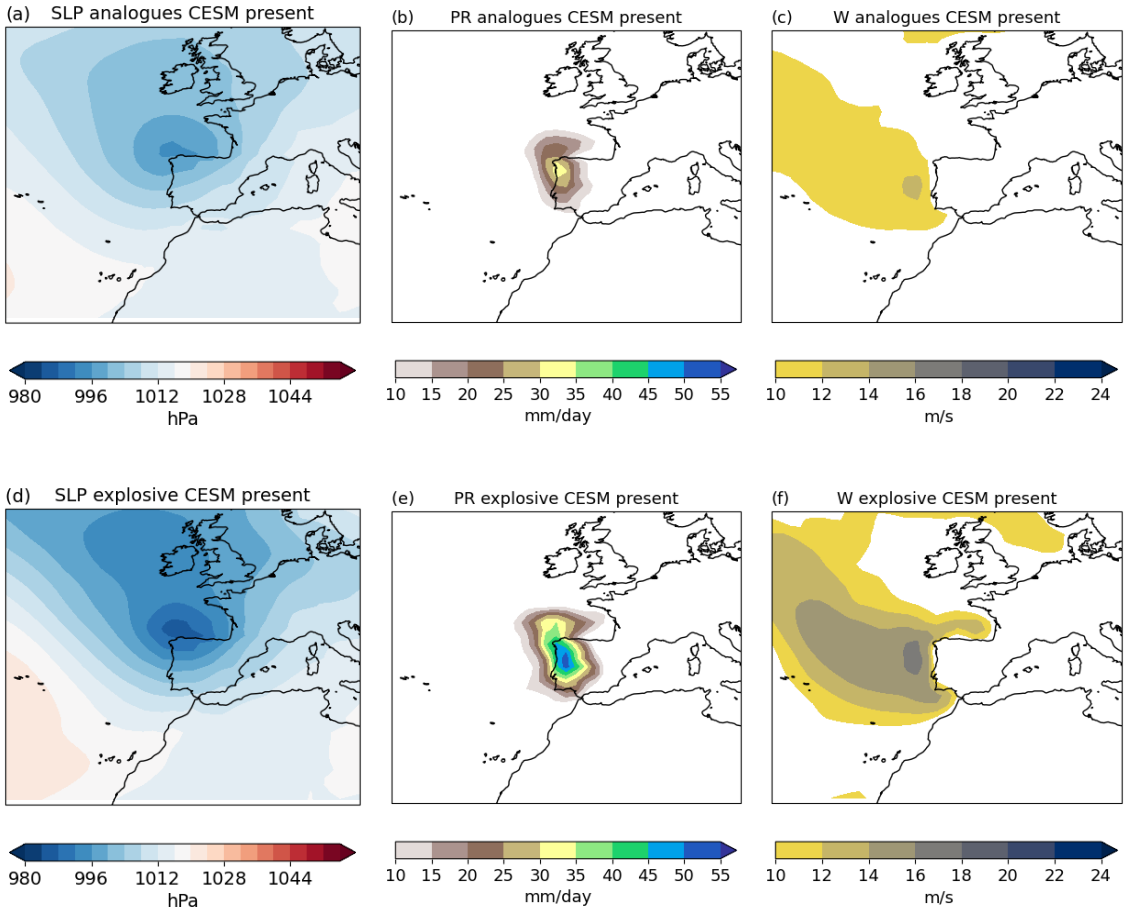

FIG. A6. Same as figure A2 but for **analogues of Xynthia**.

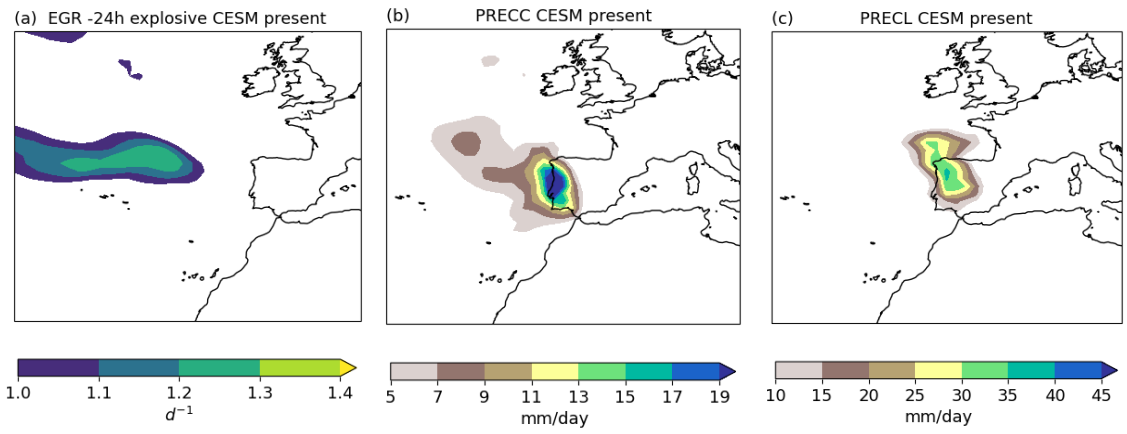

FIG. A7. Same as figure A3 but for **explosive analogues** of **Xynthia**

References

AEMET, 2020: Spanish state meteorological agency: Borrasca Miguel. Accessed: 2023-03-06, https://www.aemet.es/ca/conocermas/borrascas/2018-2019/estudios_e_impactos/miguel.

AEMET, 2021: Spanish state meteorological agency: Borrasca Norberto. Accessed: 2023-03-06, https://www.aemet.es/ca/conocermas/borrascas/2019-2020/estudios_e_impactos/norberto.

Anadolu Agency, 2022: Storm Eunice leaves 4 dead, over 400,000 homes without power in Poland. Accessed: 2023-01-11, https://www.aa.com.tr/en/europe/storm-eunice-leaves-4-dead-over-400-000-homes-without-power-in-poland/2507945.

Aon, 2020: Global Catastrophe Recap: October 2020. Available at: http://thoughtleadership.aon.com/documents/20201111_analytics-if-october-global-recap.pdf Accessed: October 202O.

BBC, 2022: Storm Eunice: Three people killed as strong winds sweep across UK. Accessed: 2023-01-11, https://www.bbc.com/news/uk-60439651.

Bertin, X., N. Bruneau, J.-F. Breilh, A. B. Fortunato, and M. Karpytchev, 2012: Importance of wave age and resonance in storm surges: The case xynthia, bay of biscay. *Ocean Modelling*, **42**, 16–30, https://doi.org/https://doi.org/10.1016/j.ocemod.2011.11.001, URL https://www.sciencedirect.com/science/article/pii/S1463500311001776.

Berz, G., 1988: List of major natural disasters, 1960–1987. *Natural Hazards*, **1 (1)**, 97–99.

Binder, H., H. Joos, M. Sprenger, and H. Wernli, 2023: Warm conveyor belts in present-day and future climate simulations–part 2: Role of potential vorticity production for cyclone intensification. *Weather and Climate Dynamics*, **4 (1)**, 19–37.

Brayshaw, D. J., B. Hoskins, , and M. Blackburn, 2009: The basic ingredients of the North Atlantic storm track. Part I: Land–sea contrast and orography. *Journal of Atmospheric Sciences*, **66**, 2539–2558, https://doi.org/0.1175/2009JAS3078.1.

Cattiaux, J., R. Vautard, C. Cassou, P. Yiou, V. Masson-Delmotte, and F. Codron, 2010: Winter 2010 in europe: A cold extreme in a warming climate. *Geophysical Research Letters*, **37 (20)**.

Catto, J. L., and Coauthors, 2019: The future of midlatitude cyclones. *Current Climate Change Reports*, **5**, 407–420.

Chadenas, C., A. Creach, and D. Mercier, 2014: The impact of storm xynthia in 2010 on coastal flood prevention policy in france. *Journal of Coastal Conservation*, **18 (5)**, 529–538.

Chauveau, E., and Coauthors, 2011: Xynthia: leçons d'une catastrophe. *Cybergeo: European Journal of Geography*.

Davolio, S., M. Vercellino, M. M. Miglietta, L. D. Pitura, S. Laviola, and V. Levizzani, 2022: The influence of an atmospheric river on a heavy precipitation event over the western alps. *Weather and Climate Extremes*, 100542.

Deser, C., A. Phillips, V. Bourdette, and H. Teng, 2012: Uncertainty in climate change projections: the role of internal variability. *Climate dynamics*, **38 (3)**, 527–546.

Deutsche Welle, 2022: Europe reckons with cost of Storm Zeynep. Accessed: 2023-01-11, https://www.dw.com/en/europe-reckons-with-cost-of-storm-zeynep/a-60823280.

Dolores-Tesillos, E., F. Teubler, and S. Pfahl, 2022: Future changes in north atlantic winter cyclones in cesm-le–part 1: Cyclone intensity, potential vorticity anomalies, and horizontal wind speed. *Weather and Climate Dynamics*, **3 (2)**, 429–448.

EUMETSAT, 2019: Storm Miguel batters parts of Europe. Accessed: 2023-03-06, https://www.eumetsat.int/storm-miguel-batters-parts-europe.

European State of the Climate, 2020: Storm Alex. Accessed: 2023-03-06, https://climate.copernicus.eu/esotc/2020/storm-alex.

Extreme Wind Storms Catalogue, n.d.: Oratia (Tora). Accessed: 2023-03-06, http://www.europeanwindstorms.org/cgi-bin/storms/storms.cgi?storm1=Oratia_Tora.

Faranda, D., S. Bourdin, M. Ginesta, M. Krouma, G. Messori, R. Noyelle, F. Pons, and P. Yiou, 2022: A climate-change attribution retrospective of some impactful weather extremes of 2021.

Faranda, D., M. Ginesta, T. Alberti, E. Coppola, and M. Anzidei, 2023: Attributing venice acqua alta events to a changing climate and evaluating the efficacy of mose adaptation strategy. *npj Climate and Atmospheric Science*, **6 (1)**, 181.

Fink, A. H., T. Brücher, V. Ermert, A. Krüger, and J. G. Pinto, 2009: The european storm kyrill in january 2007: synoptic evolution, meteorological impacts and some considerations with respect

to climate change. *Natural Hazards and Earth System Sciences*, **9 (2)**, 405–423, https://doi.org/10.5194/nhess-9-405-2009.

Fink, A. H., S. Pohle, J. G. Pinto, and P. Knippertz, 2012: Diagnosing the influence of diabatic processes on the explosive deepening of extratropical cyclones. *Geophysical Research Letters*, **39 (7)**.

Fischer, E. M., U. Beyerle, and R. Knutti, 2013: Robust spatially aggregated projections of climate extremes. *Nature Climate Change*, **3 (12)**, 1033–1038.

García-Pereda (NWC SAF/AEMET), J., 2010: Storm Xynthia. URL https://www.eumetsat.int/storm-xynthia.

Ginesta, M., P. Yiou, G. Messori, and D. Faranda, 2022: A methodology for attributing severe extratropical cyclones to climate change based on reanalysis data: the case study of storm alex 2020. *Climate Dynamics*, 1–25.

Harvey, B., P. Cook, L. Shaffrey, and R. Schiemann, 2020: The response of the northern hemisphere storm tracks and jet streams to climate change in the cmip3, cmip5, and cmip6 climate models. *Journal of Geophysical Research: Atmospheres*, **125 (23)**, e2020JD032 701.

Hawcroft, M., E. Walsh, K. Hodges, and G. Zappa, 2018: Significantly increased extreme precipitation expected in europe and north america from extratropical cyclones. *Environmental Research Letters*, **13 (12)**, 124 006, https://doi.org/10.1088/1748-9326/aaed59, URL https://doi.org/10.1088/1748-9326/aaed59.

Hawcroft, M. K., L. C. Shaffrey, K. I. Hodges, and H. F. Dacre, 2012: How much northern hemisphere precipitation is associated with extratropical cyclones? *Geophysical Research Letters*, **39 (24)**, https://doi.org/https://doi.org/10.1029/2012GL053866, URL https://agupubs.onlinelibrary.wiley.com/doi/abs/10.1029/2012GL053866, https://agupubs.onlinelibrary.wiley.com/doi/pdf/10.1029/2012GL053866.

Hawkins, E., and R. Sutton, 2009: The potential to narrow uncertainty in regional climate predictions. *Bulletin of the American Meteorological Society*, **90 (8)**, 1095 – 1108, https://doi.org/https://doi.org/10.1175/2009BAMS2607.1, URL https://journals.ametsoc.org/view/journals/bams/90/8/2009bams2607_1.xml.

Hersbach, H., and Coauthors, 2020: The era5 global reanalysis. *Quarterly Journal of the Royal Meteorological Society*, **146 (730)**, 1999–2049, https://doi.org/https://doi.org/10.1002/qj.3803, URL https://rmets.onlinelibrary.wiley.com/doi/abs/10.1002/qj.3803, https://rmets.onlinelibrary.wiley.com/doi/pdf/10.1002/qj.3803.

Hurrell, J. W., and Coauthors, 2013: The community earth system model: a framework for collaborative research. *Bulletin of the American Meteorological Society*, **94 (9)**, 1339–1360.

Jansa, A., P. Alpert, A. Buzzi, and P. Arbogast, 2001: Medex, cyclones that produce high impact weather in the mediterranean. *Avalaible at http://medex. aemet. uib. es*.

Jézéquel, A., V. Dépoues, H. Guillemot, M. Trolliet, J.-P. Vanderlinden, and P. Yiou, 2018: Behind the veil of extreme event attribution. *Climatic Change*, **149**, 367–383.

Joos, H., M. Sprenger, H. Binder, U. Beyerle, and H. Wernli, 2023: Warm conveyor belts in present-day and future climate simulations-part 1: Climatology and impacts. *Weather and Climate Dynamics*, **4 (1)**, 133–155.

Kay, J. E., and Coauthors, 2015: The community earth system model (cesm) large ensemble project: A community resource for studying climate change in the presence of internal climate variability. *Bulletin of the American Meteorological Society*, **96 (8)**, 1333–1349.

Koch, P., H. Wernli, and H. C. Davies, 2006: An event-based jet-stream climatology and typology. *International Journal of Climatology: A Journal of the Royal Meteorological Society*, **26 (3)**, 283–301.

Koks, E., and T. Haer, 2020: A high-resolution wind damage model for europe. *Scientific Reports*, **10**, 6866, https://doi.org/10.1038/s41598-020-63580-w.

Kolen, B., R. Slomp, and S. Jonkman, 2013: The impacts of storm xynthia february 27–28, 2010 in france: lessons for flood risk management. *Journal of Flood Risk Management*, **6 (3)**, 261–278, https://doi.org/https://doi.org/10.1111/jfr3.12011, URL https://onlinelibrary.wiley.com/doi/abs/10.1111/jfr3.12011, https://onlinelibrary.wiley.com/doi/pdf/10.1111/jfr3.12011.

Lehmann, J., D. Coumou, K. Frieler, A. V. Eliseev, and A. Levermann, 2014: Future changes in extratropical storm tracks and baroclinicity under climate change. *Environmental Research Letters*, **9 (8)**, 084 002.

Liberato, M., J. Pinto, R. Trigo, P. Ludwig, P. Ordóñez, D. Yuen, and I. Trigo, 2013: Explosive development of winter storm xynthia over the subtropical north atlantic ocean. *Natural Hazards and Earth System Sciences*, **13 (9)**, 2239–2251.

Liberato, M. L., 2014: The 19 january 2013 windstorm over the north atlantic: large-scale dynamics and impacts on iberia. *Weather and Climate Extremes*, **5-6**, 16–28, https://doi.org/https://doi.org/10.1016/j.wace.2014.06.002, URL https://www.sciencedirect.com/science/article/pii/S2212094714000620.

Liu, W. T., W. Tang, and X. Xie, 2008: Wind power distribution over the ocean. *Geophysical Research Letters*, **35 (13)**, https://doi.org/https://doi.org/10.1029/2008GL034172, URL https://agupubs.onlinelibrary.wiley.com/doi/abs/10.1029/2008GL034172, https://agupubs.onlinelibrary.wiley.com/doi/pdf/10.1029/2008GL034172.

Ludwig, P., J. G. Pinto, M. Reyers, and S. L. Gray, 2014: The role of anomalous sst and surface fluxes over the southeastern north atlantic in the explosive development of windstorm xynthia. *Quarterly Journal of the Royal Meteorological Society*, **140 (682)**, 1729–1741.

McCallum, E., 1990: The burns' day storm, 25 january 1990. *Weather*, **45 (5)**, 166–173.

Meinshausen, M., and Coauthors, 2011: The rcp greenhouse gas concentrations and their extensions from 1765 to 2300. *Climatic change*, **109 (1)**, 213–241.

Met Office, 1976: Monthly weather report: January 1976. Available at https://web.archive.org/web/20121023103203/http://www.metoffice.gov.uk/media/pdf/m/r/Jan1976.pdf.

Met Office, 2016: Storm angus. Available at https://www.metoffice.gov.uk/weather/warnings-and-advice/uk-storm-centre/storm-angus.

Met Office, 2018: Storm bronagh. Accessed: 2023-03-06, https://www.metoffice.gov.uk/weather/warnings-and-advice/uk-storm-centre/storm-bronagh.

Met Office, 2021: Storm Christoph 18 to 20 January 2021. Accessed: 2023-03-06, https://www.metoffice.gov.uk/binaries/content/assets/metofficegovuk/pdf/weather/learn-about/uk-past-events/interesting/2021/2021_01_storm_christoph.pdf.

Met Office, 2022: Storms dudley, eunice and franklin, february 2022. Available at: https://www.metoffice.gov.uk/binaries/content/assets/metofficegovuk/pdf/weather/learn-about/uk-past-events/interesting/2022/2022_01_storms_dudley_eunice_franklin_r1.pdf Accessed: March 2023.

Michaelis, A. C., J. Willison, G. M. Lackmann, and W. A. Robinson, 2017: Changes in winter north atlantic extratropical cyclones in high-resolution regional pseudo–global warming simulations. *Journal of Climate*, **30 (17)**, 6905 – 6925, https://doi.org/https://doi.org/10.1175/JCLI-D-16-0697.1, URL https://journals.ametsoc.org/view/journals/clim/30/17/jcli-d-16-0697.1.xml.

Météo France, 2019: Tempête DARIA du 25 janvier 1990. Available at http://tempetes.meteo.fr/IMG/anthemis_pdf/19900125.pdf.

Météo France, 2020: Tempête Alex: des intempéries exceptionnelles. Available at https://meteofrance.com/actualites-et-dossiers/climat/tempete-alex-des-intemperies-exceptionnelles.

NASA Earth Observatory, 2017: Superstorm Sweeps Over England. Accessed: 2023-03-06, https://wrecksite.eu/wreck.aspx?258019.

Neu, U., and Coauthors, 2013: Imilast: A community effort to intercompare extratropical cyclone detection and tracking algorithms. *Bulletin of the American Meteorological Society*, **94 (4)**, 529–547.

NL Times, 2022: Fourth death confirmed in Netherlands as Storm Eunice heads north. Accessed: 2023-01-11, https://nltimes.nl/2022/02/18/fourth-death-confirmed-netherlands-storm-eunice-heads-north.

Owen, L. E., J. L. Catto, D. B. Stephenson, and N. J. Dunstone, 2021: Compound precipitation and wind extremes over europe and their relationship to extratropical cyclones. *Weather and Climate Extremes*, **33**, 100 342, https://doi.org/https://doi.org/10.1016/j.wace.2021.100342, URL https://www.sciencedirect.com/science/article/pii/S2212094721000384.

Priestley, M. D. K., D. Ackerley, J. L. Catto, K. I. Hodges, R. E. McDonald, and R. W. Lee, 2020: An overview of the extratropical storm tracks in cmip6 historical simulations. *Journal of Climate*,

Appendix C

Manuscript in preparation "Future projections of the concurrences of atmospheric rivers and explosive cyclones in the North Atlantic"

In this chapter, I provide a brief overview of the scientific background, data, and methods that support figures 4.10 and 4.11, forming the basis of the manuscript in preparation that I am co-leading with Ferran Lopez Marti, PhD student from Uppsala University.

C.1 Scientific background

Atmospheric rivers (ARs) are long and narrow atmospheric corridors that transport high levels of water vapour in the lower troposphere. When they make landfall, they can cause severe impacts such as flooding or intense rainfall. Extratropical cyclones (ETCs), when coupled with atmospheric rivers, play a role in driving extreme weather events in the mid-latitudes.

Guo et al., 2020 showed, through composite analysis, that ARs tend to be situated in the warm sector of cyclones, with an anticyclone downstream and equatorward of the cyclone strengthening the pressure gradient, potentially intensifying the AR (Eiras-Barca et al., 2018). Eiras-Barca et al., 2018 suggested that ARs may play a crucial role in the explosive deepening of cyclones; in the North Atlantic, approximately 75% of explosive cyclones are associated with an AR, compared to only around 40% of non-explosive cyclones. Zhang et al., 2019 showed that about 80% of ARs are linked to ETCs in the western North Pacific, while approximately 45% of ETCs are associated with

ARs. They further observed that ETCs associated with strong ARs exhibit significantly greater intensification. Additionally, Zhang and Ralph, 2021 identified the significant role of water vapor inflow from ARs in intensifying rapid cyclogenesis in the North Pacific.

Numerous studies have investigated the impact of anthropogenic radiative forcing on ETCs and ARs individually. The thermodynamic response of ARs to climate change is characterized by an increase in Integrated Water Vapor Transport (IVT). This increase is driven by the Clausius-Clapeyron relation, which implies a rise in moisture content in a warmer atmosphere. Moreover, the vertically integrated water vapor content undergoes further amplification compared to surface water vapor (Payne et al., 2020). This thermodynamic signal would act to increase the number of ARs detected in a warmer climate. Similarly, the thermodynamic response acts to increase the precipitation within ETCs (Yettella and Kay, 2017). The dynamics response to climate change, such as changes in the atmospheric circulation patterns, is less certain (Shepherd, 2014). Several studies point out to an increase in both frequency and or intensity in central northern western Europe of both AR and ETCs (Espinoza et al., 2018; Gao et al., 2016; Lavers et al., 2013; Priestley and Catto, 2022; Ramos et al., 2016; Seiler and Zwiers, 2016).

Acknowledging the potential hazards posed by explosive cyclones and atmospheric rivers in the North Atlantic, particularly along the western coast of Europe, highlights the significance of evaluating their projected trends in a future climate. Uncertainties persist regarding the evolving relationship between these two phenomena in a warmer climate. The objective of this study is to assess future trend projections of the interplay between explosive cyclones and atmospheric rivers using state-of-the-art CMIP6 data.

C.2 Data and methods

We use ERA5 reanalysis data Hersbach et al., 2020 with a horizontal resolution of $0.25^{o} \times 0.25^{o}$ as our current climate observational reference and for validating the General Circulation Models (GMCs).

In addition, we use six GCMs from the CMIP6 dataset (MPI-ESM1-2-LR, MPI-ESM1-2-HR, NorESM2-MM, EC-Earth3, CMCC-ESM2, MIROC6) Eyring et al., 2016 for two periods: the current climate (1980-2009) using historical simulation, and the future climate at the end of the XXI century (2070-2099), with three simulations following the SSP1-2.6; SSP2-4.5; and SSP5-8.5 forcing scenarios. The selection of GCMs is constrained by the availability of 6-hourly instantaneous variables in vertical model levels required for AR analysis.

All datasets consist of 6-hourly data during the extended-winter period (November to March) over the North Atlantic region [22.5N – 70N, 80W – 50E]. ARs detection and tracking is based on the vertical integral of northward and eastward water vapor flux, that is, the integrated water vapor transport (IVT), and cyclone detection and tracking is based on sea level pressure (SLP).

C.2.1 Extratropical cyclone tracking

We use the TempestExtremes algorithm developed by Ullrich et al., 2021. To detect ETCs, we use the executable *DetectNodes*, which recognizes candidate "nodes" corresponding to local minima in the SLP field. Candidate points within a 6° great circle distance (GCD) are merged. Subsequently, we use *StitchNodes* to connect these candidate nodes into tracks. The criteria for tracking include: the distance between consecutive detections should not exceed 6 GCD, the tracks must persist for a minimum of 24 hours, the maximum duration between two detections is set at 6 hours, and the cyclones must have moved at least 12 GDP to filter out stationary lows, such as the Icelandic Low.

Extratropical cyclones are classified as explosive cyclones if their Normalized Deepening Rate (NDR) (Sanders and Gyakum, 1980) is equal to or higher than 1: $NDR_c = \frac{DR_{24h}}{24h}\frac{\sin(60°)}{\sin(\varphi)}$, where DR_{24h} is the pressure difference over 24 hours measured at the storm center and φ is the latitude at its second time step.

C.2.2 Atmospheric river tracking

We detect and track ARs based on the IVT using the TempestExtremes algorithm. The IVT is defined pointwise as:

$$IVT = \frac{1}{g}\sqrt{(\int_{p_0}^{300hPa} qUdp)^2 + (\int_{p_0}^{300hPa} qVdp)^2}$$

where q is the specific humidity, V is the wind vector and g is the gravitation acceleration. We separately compute the eastward IVT_E and northward IVT_N integrated vapor transport, using the zonal and meridional winds respectively. For the detection of ARs we use the executable *DetectBlobs*. We find potential candidates by detecting ridges in the IVT field. Ridges are defined as points where the Laplacian of the IVT is below $-4 \times 10^4 \mathrm{kgm^{-2}s^{-1}rad^{-2}}$, as this operator identifies elongated areas and regions of local maxima. In addition, the IVT should be higher than $250\mathrm{kgm^{-1}s^{-1}}$. Each candidate should have an area larger than $4 \times 10^5 \mathrm{km^{-2}}$. To connect candidates or "blobs" we use *StitchBlobs*. The detected candidates are concatenated if at least one grid point is detected as AR in sequential timesteps. In addition, they should last 60 hours.

C.2.3 Concurrences

For each extratropical cyclone and the subset of explosive cyclones, we compute the Maximum Deepening Rate (MDP), which is the difference in sea level pressure between two consecutive 6-hourly timesteps, following (Eiras-Barca et al., 2018). This metric allows us to evaluate the influence of atmospheric rivers on the development of the cyclone. We then assess the presence of an atmospheric river before and after this point of MDP. Subsequently, we determine whether a specific timestep of an extratropical cyclone, as well as for the subset of explosive cyclones, is linked to an atmospheric river by detecting the presence of an atmospheric river within a 1500 km distance.

Appendix D

Coauthored articles

I coauthored the following articles, which are attached below:

- Faranda, D., S. Bourdin, M. Ginesta, M. Krouma, R. Noyelle, et al. (2022). “A climate-change attribution retrospective of some impactful weather extremes of 2021”. In: *Weather and Climate Dynamics*: I analyzed and wrote the section 4.1 on Winter Storm Filomena.
- Faranda, D., M. Ginesta, T. Alberti, E. Coppola, and M. Anzidei (2023). “Attributing Venice Acqua Alta events to a changing climate and evaluating the efficacy of MoSE adaptation strategy”. In: *npj climate and atmospheric science*: I modified the methodology to find analogues with respect to the first version and perform the analysis on the analogues (figure 2).
- Rapella, L., Faranda, D., and Gaetani, M., and Drobinski, P., and Ginesta, M. (2023) "Climate change on extreme winds already affects off-shore wind power availability in Europe". In: *Environmental Research Letters*. I helped with the coding to perform the analysis, helped interpreting the results, and revised the manuscript.

Weather Clim. Dynam., 3, 1311–1340, 2022
https://doi.org/10.5194/wcd-3-1311-2022

Weather and Climate Dynamics
Open Access
EGU

A climate-change attribution retrospective of some impactful weather extremes of 2021

Davide Faranda[1,2,3], **Stella Bourdin**[1], **Mireia Ginesta**[1], **Meriem Krouma**[1], **Robin Noyelle**[1], **Flavio Pons**[1], **Pascal Yiou**[1], **and Gabriele Messori**[4,5,6,7]

[1]Laboratoire des Sciences du Climat et de l'Environnement, UMR 8212 CEA-CNRS-UVSQ, Université Paris-Saclay, IPSL, 91191 Gif-sur-Yvette, France
[2]London Mathematical Laboratory, 8 Margravine Gardens London, London W6 8RH, UK
[3]LMD/IPSL, École Normale Supérieure, PSL Research University, Paris, France
[4]Department of Earth Sciences, Uppsala University, Uppsala, Sweden
[5]Centre of Natural Hazards and Disaster Science (CNDS), Uppsala, Sweden
[6]Department of Meteorology, Stockholm University, Stockholm, Sweden
[7]Bolin Centre for Climate Research, Stockholm, Sweden

Correspondence: Davide Faranda (davide.faranda@cea.fr)

Received: 4 February 2022 – Discussion started: 17 February 2022
Revised: 30 September 2022 – Accepted: 5 October 2022 – Published: 17 November 2022

Abstract. The IPCC AR6 report outlines a general consensus that anthropogenic climate change is modifying the frequency and intensity of extreme events such as cold spells, heat waves, storms or floods. A pertinent question is then whether climate change may have affected the characteristics of a specific extreme event or whether such event would have even been possible in the absence of climate change. Here, we address this question by performing an attribution of some major extreme events that occurred in 2021 over Europe and North America: the Winter Storm Filomena, the French spring cold spell, the Westphalia floods, the Mediterranean summer heat wave, Hurricane Ida, the Po Valley tornado outbreak, Medicane Apollo and the late-autumn Scandinavian cold spell. We focus on the role of the atmospheric circulation associated with the events and its typicality in present (factual world) and past climate conditions (counterfactual world) – defined using the ERA5 dataset 1950 to present. We first identify the most similar sea-level pressure patterns to the extreme events of interest in the factual and counterfactual worlds – so-called analogues. We then compute significant shifts in the spatial characteristics, persistence, predictability, seasonality and other characteristics of these analogues. We also diagnose whether in the present climate the analogues of the studied events lead to warmer/-cooler or dryer/wetter conditions than in the past. Finally we verify whether the El Niño–Southern Oscillation and the Atlantic Multidecadal Oscillation may explain interdecadal changes in the analogues' characteristics. We find that most of the extreme events we investigate are significantly modified in the present climate with respect to the past, because of changes in the location, persistence and/or seasonality of cyclonic/anticyclonic patterns in the sea-level pressure analogues. One of the events, Medicane Apollo, appears to be a black swan of the atmospheric circulation, with poor-quality analogues. Our approach, complementary to the statistical extreme-event attribution methods in the literature, points to the potentially important role of the atmospheric circulation in attribution studies.

1 Introduction

One of the main novelties of the latest IPCC AR6 report (IPCC, 2021) with respect to previous IPCC documents is the increased confidence that anthropogenic climate change is critically affecting weather extremes. As stated by the IPCC AR6,

> a warmer climate will intensify very wet and very dry weather and climate events and seasons, with implications for flooding or drought (high confi-

> dence), but the location and frequency of these events depend on projected changes in regional atmospheric circulation, including monsoons and mid-latitude storm tracks.

Similarly, the already very clear statements of the previous reports on changes in temperature extremes are confirmed and strengthened:

> In all continental regions [...] and at the continental scale, it is very likely that the intensity and frequency of hot extremes will increase and the intensity and frequency of cold extremes will decrease.

Other studies underline that we are already observing prolonged periods of extremely warm conditions (Horton et al., 2016) with increased droughts leading to forest fires (Flannigan et al., 2000), species extinctions (Román-Palacios and Wiens, 2020) and health issues for vulnerable populations (Mitchell et al., 2016). Recent scientific literature points to the need of understanding the role of dynamical drivers of changes in weather extremes: in winter, increased persistence of cyclonic and anticyclonic structures can lead to extremely wet or dry periods (Berkovic and Raveh-Rubin, 2022) on the eastern Mediterranean. Further changes in persistence of synoptic structures are also expected under continued global warming in the Northern Hemisphere summer (see, e.g., Kornhuber and Tamarin-Brodsky, 2021). Under global warming, Gordon et al. (2005), Bala et al. (2010) and Pendergrass et al. (2017) suggest that, in the shoulder seasons, we observe a large variability of rains associated with both tropical and extratropical storms and convective events, leading to an alteration of the hydrological cycle.

While these assessments are meaningful when considering (relatively) large ensembles of extreme events with similar characteristics, it is also important to evaluate whether the probability of occurrence or physical characteristics of single extreme events have been influenced by anthropogenic climate change. This knowledge builds awareness of the consequences of greenhouse gas emissions in the general public and allows stakeholders to evaluate specific impacts induced by climate change. For these reasons, attributing a single extreme event to climate change has given rise to a wealth of studies – an entire field named attribution (Shepherd, 2016; Knutson et al., 2017; Jézéquel et al., 2018b; Naveau et al., 2020; van Oldenborgh et al., 2021).

Studies in extreme-event attribution are conventionally grounded in extreme value theory (Trenberth et al., 2015), which they use to estimate return times of threshold exceedances of particular observables (e.g., temperatures above or below a target value for a certain number of consecutive days for heat waves or cold spells). The main drawback of such statistical attribution is that it does not take into account the physical processes leading to the extreme events. Climate change is likely associated with complex dynamical changes in the atmosphere (e.g., Kennedy et al., 2016; Sharmila and Walsh, 2018; Stendel et al., 2021), yet the conventional extreme value approach overlooks these entirely. This brought Shepherd (2014) to argue that the atmospheric circulation is a key element of the uncertainty in attribution studies and in parallel stimulated attempts to incorporate knowledge of the atmospheric circulation into an attribution framework (Shepherd, 2016; Yiou et al., 2017).

Here, we build upon this line of work by performing an attribution of some notable extremes occurring during the 2021 calendar year, based on large-scale atmospheric drivers. In particular, we analyze (i) the Winter Storm Filomena, which caused, in January, heavy snowfall and extremely cold conditions in Spain; (ii) the late winter cold spell that occurred in April 2021 in France with large impacts on vegetation and agriculture; (iii) the July floods in Westphalia, Germany, responsible for the destruction of entire villages, destruction of infrastructure and heavy loss of lives; (iv) the record-breaking temperatures during the August Mediterranean heat wave and the associated wildfires in Greece and Italy; (v) the September Po Valley tornado outbreak; (vi) Hurricane Ida, which caused extensive damage in Louisiana and New York city; (vii) Medicane (Mediterranean hurricane) Apollo, which caused heavy flooding in Sicily in October; and (viii) the November Scandinavian cold spell, which led to record-low temperatures for the season.

In order to attribute these events to climate change, we study the associated atmospheric circulation patterns and we search for pattern recurrences – which we term analogues – in the far (1950–1979) and recent past (1992–2021). Our working hypothesis is that the far past acts as a counterfactual world where the Earth's climate was less heavily influenced by anthropogenic forcing when compared to the recent past (the factual world). Here, we assume that 30 years is a long enough period to average out high-frequency interannual variability of the atmospheric motions. However, it is necessary to control for the effect of lower-frequency and inter-decadal variability, such as that caused, for example, by the Atlantic Multidecadal Oscillation or by low-frequency modulations of the El Niño–Southern Oscillation. If a direct influence of such low-frequency variability is excluded, then changes in analogues between the two periods we consider are attributed to the climate-change signal. We present in Sect. 2 the methodological aspects of this work, introducing in Sect. 3 the relevant assessment metrics. Section 4 contains, for each event, (i) a meteorological description of the event, (ii) a summary of the known impacts of climate change on that event class and (iii) our attribution analyses. Our conclusions are presented in Sect. 5.

2 A method for attributing extreme events to climate change which takes into account changes in atmospheric circulation

We study changes in weather patterns associated with extreme events by leveraging the framework of weather analogues (Yiou et al., 2003). We first identify the peak day of each extreme event. We then perform a semi-objective detection of the concurrent large-scale weather pattern using daily average sea-level pressure (slp) from the ERA5 reanalysis database over 1950–2021 (Hersbach et al., 2020). The choice of using slp is motivated by (i) the fact that in the ERA5 reanalysis, this quantity is closely constrained from station observations; (ii) its capability to track and identify extratropical cyclones (Walker et al., 2020); and (iii) the absence of long-term trends in its values but also in the dynamical systems metrics computed on it (Faranda et al., 2019a; see Sect. 3). The semi-objectivity lies in the exact choice of geographical domain over which the pattern is identified. For cyclones, the domain of the analysis can be easily identified as the low-pressure area associated with the storm. For cold spells and heat waves, we follow Stefanon et al. (2012), who have shown that these events have a large-scale dynamical footprint spanning the size of the European continent. For all cases, we have tested that our method is qualitatively insensitive to modest changes in the domain size. We split the ERA5 dataset into two periods: 1950–1979 and 1992–2021. We take the first period to represent a counterfactual world with a weaker anthropogenic influence on climate than the second period, which represents our factual world affected by anthropogenic climate change. To take into account the possible influence of low-frequency modes of natural variability in explaining differences between the two periods, we also consider the possible roles of the El Niño–Southern Oscillation (ENSO) and the Atlantic Multidecadal Oscillation (AMO).

For each period, we scan all the daily average slp geographical maps and select the best 33 analogues, namely the maps minimizing the Euclidean distance with respect to the map of the event itself. The number of 33 corresponds approximately to the smallest 3‰ of Euclidean distances in each subset of our data. We have tested extracting between 25 and 50 analogue maps, without finding any qualitatively large differences in our results. For the factual period, as is common practice in attribution studies, the event itself is removed. Furthermore, we forbid the analogue search in a window of a week centered around the date of the event. We restrict the analogue search to the extended season during which each event occurs (DJFM, MAMJ, JJAS or SOND) or to the seasons relevant for the occurrence of specific extreme events such as hurricanes or tornadoes. This allows us to identify possible seasonality shifts between the counterfactual and factual periods yet prevents conflating the different physical processes which may contribute to a given class of extremes during the warm versus cold seasons. We then compute the average slp map for all analogues in each of the two periods and take the difference between the two averages (Δslp). To determine significant changes between the analogue maps of the two periods, we adopt a bootstrap procedure which consists of pooling the dates from the two periods together, randomly extracting 33 dates from this pool 1000 times, creating the corresponding difference maps and marking as significant only grid point changes more than 2 standard deviations above or below the mean of the bootstrap sample. We also plot the 2 m temperature (t2m) and daily precipitation rate fields (tp) on the dates of the closest slp analogues, repeating the same bootstrap procedure to identify significant changes. We additionally plot the distributions of several evaluation metrics in the two periods (see Sect. 3). We finally consider the seasonality of the analogues within the relevant season and their association with ENSO and AMO. We conduct the latter analysis using monthly indices computed from the NOAA/ERSSTv5 data and retrieved from KNMI's climate explorer. In particular, the ENSO index is the 3.4 version as defined by Huang et al. (2017), and the AMO index is computed as described in Trenberth and Shea (2006). When the ENSO 3.4 index is positive, it corresponds to El Niño, and when it is negative, it corresponds to La Niña. To assess the significance of changes in factual vs. counterfactual distributions, we conduct in all cases a two-sided Cramér–von Mises test at the 0.05 significance level. If the p value is smaller than 0.05, the null hypothesis ($H = 0$) that the two samples come from the same distribution can be rejected (Anderson, 1962). All relevant figure panels display the p value (pval) and the result of the test H in the title.

3 Evaluation metrics

Following Faranda et al. (2020), we define some quantities that support our interpretation of the analogue-based attribution. All of these may then be compared between the counterfactual and factual periods.

- *Analogue quality* Q. Q is the average Euclidean distance of a given day from its closest 33 analogues (Faranda et al., 2020). One can then compare Q for the peak day of the extreme event to Q for each analogue of the extreme event. If the value of Q for the extreme event belongs to the same distribution as, or is smaller than, the values of Q for the analogues, then the extreme event has good analogues, and attribution can be performed. If instead the Q for the extreme event is larger than that of the analogue days, then this indicates a highly unusual slp configuration, and the results of the attribution analysis must be interpreted with care. Differences between the counterfactual and factual periods in the value of Q for the peak day of the extreme event indicate whether the atmosphere is visiting states (analogues) that are more or less similar to the map associated with the extreme. Differences in the distribu-

tion of Q for the 33 analogues indicate whether those states are in turn becoming more or less typical of the atmospheric variability. In order to test the homogeneity of the analogues in the two periods, we have computed Q for all days in the factual and counterfactual periods on a wide North Atlantic domain [80° W–50° E and 22.5–70° N] and applied the two-sided Cramér–von Mises test at the 0.05 significance level. The p value found (0.1995) implies that the null hypothesis that the two samples come from the same distribution cannot be rejected, hence supporting our claim of homogeneity.

- *Predictability index D*. Using dynamical systems theory (Freitas et al., 2011, 2016; Lucarini et al., 2016), we can compute the local dimension D of each daily slp map (Faranda et al., 2017, 2019b; see Appendix A). The local dimension is a proxy for the number of degrees of freedom of the field, meaning that the higher D, the more unpredictable the temporal evolution of the slp maps will be (Faranda et al., 2017; Messori et al., 2017; Hochman et al., 2019). If the dimension D of the peak day of the extreme event is higher or lower than that of its analogues, then the extreme will be respectively less or more predictable than the closest dynamical situations identified in the data. We compute two values of D for the event, one using the data in the counterfactual period and one using the data in the factual period. As for Q, we also compute the distributions of D for all the analogues in each period. This informs on how predictable the extreme event is with respect to its analogues.

- *Persistence index Θ*. Another quantity derived from the dynamical systems theory is the persistence Θ of a given configuration (Faranda et al., 2017; see Appendix A). The persistence estimates for how many days we are likely to observe a map that is an analogue of the one considered (Moloney et al., 2019). As for Q and D, we compute the two values of the persistence for the extreme event in the factual and counterfactual worlds and the corresponding distributions of persistence for the analogues.

- *Seasonality of analogues*. We can count the number of analogues in each month to detect whether there has been a shift of the circulation towards earlier or later months of the season. This can have strong thermodynamic implications, for example, if a circulation leading to large positive temperature anomalies in early spring becomes more common later in the season, when average temperatures are much higher.

- *Association with ENSO and AMO*. To account for the effect of natural interdecadal variability, we analyze the distributions of the ENSO and AMO indices corresponding to analogues of each event in the factual and counterfactual periods. If the null hypothesis that the two distributions do not differ between the two periods is rejected, it is not possible to exclude that thermodynamic or dynamic differences in the analogues are partly due to these modes of natural variability rather than anthropogenic forcing. On the other hand, if it is not possible to reject the null hypothesis of equal distributions, observed changes in analogues are attributed to human activity. It is worth noting that such null hypothesis of no influence of natural variability is coherent with the view of Trenberth (2011), who argued that

> Past attribution studies of climate change have assumed a null hypothesis of no role of human activities [...] I argue that because global warming is "unequivocal" and "very likely" caused by human activities, the reverse should now be the case. The task, then, could be to prove there is no anthropogenic component to a particular observed change in climate.

See also the discussion in Lloyd and Oreskes (2018) for support of Trenberth's position.

4 Results

Our list of 2021 extreme events is not intended to be exhaustive. We cover Europe and North America, and we try to select events that differ in impacts, season and genesis in order to provide a rich overview of the attribution capabilities of our approach but also of its implementation difficulties. We provide in Table 1 the list of the events studied, with the peak day of each extreme used for the analogue search, affected countries, longitude–latitude boxes used for the analogue search, and months used for the analogue search. A graphical representation of the events is provided in Fig. 1.

4.1 Winter Storm Filomena

In early January 2021 the weather regime over the Euro-Atlantic sector was characterized by a negative phase of the North Atlantic Oscillation (NAO), with cold air from the Arctic being advected over southern Europe and frontal activity favored over the Azores. Filomena was associated with an extratropical cyclone that moved from the Azores to the Canary Islands and the Iberian Peninsula on 6 and 7 January respectively, resulting in strong precipitation and hurricane-force winds. It triggered historic snowfalls in the inland regions of the peninsula and a 14 d long cold spell. This exceptional event caused four casualties between 9 and 16 January and economic losses of up to EUR 2 billion (Aon, 2021). The cyclone formed on 1 January in the northeastern inland of the United States. On 3 January it entered the North Atlantic, and it began a sharp displacement southeastward forced by a high-pressure system in the central North Atlantic and

Table 1. List of the events presented in this study, with the peak day of each extreme used for the analogue search, affected countries, longitude–latitude boxes used for the analogue search, and months used for the analogue search.

Event	Date (dd-mm-yyyy)	Countries	Analogue box	Analogue months
Winter Storm Filomena	09-01-2021	Spain	[15° W, 10° E, 30° N, 46° N]	DJFM
French spring cold spell	06-04-2021	France	[10° W, 30° E, 30° N, 70° N]	MAMJ
Westphalia floods	14-07-2021	Benelux/Germany	[5° W, 23° E, 41° N, 59° N]	JJAS
Mediterranean heat wave	11-08-2021	Spain/France/Italy	[10° W, 25° E, 30° N, 45° N]	JJAS
Hurricane Ida	02-09-2021	USA	[80° W, 55° W, 35° N, 55° N]	ASON
Po Valley tornado outbreak	19-09-2021	Italy	[10° W, 20° E, 35° N, 50° N]	MJJASO
Medicane Apollo	29-10-2021	Italy	[10° E, 20° E, 34° N, 40° N]	SOND
Scandinavian cold spell	28-11-2021	Sweden/Norway	[10° W, 30° E, 35° N, 75° N]	SOND

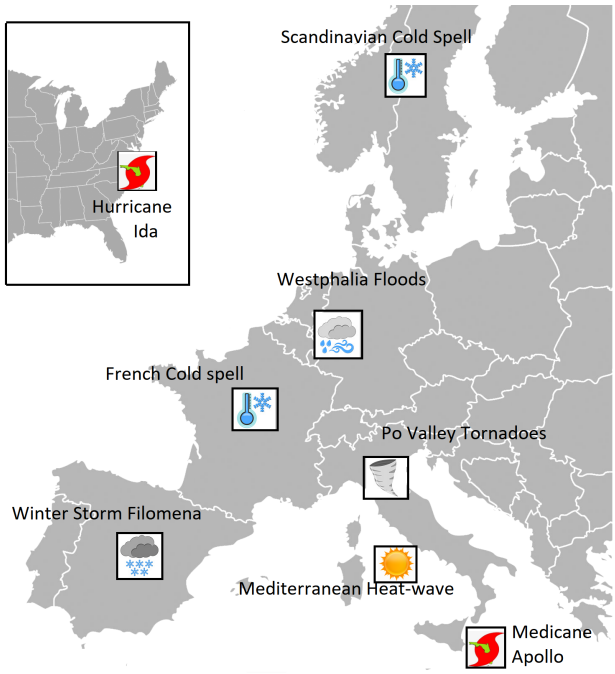

Figure 1. Graphical representation of the events studied in this work.

pushed by a polar jet with a strong meridional component. When it arrived west of the Azores on 5 January in somewhat weakened form, it was named Filomena by the Spanish State Meteorological Agency (AEMET), which emitted a severe weather warning for Canary Islands and Spain for the 2 following days. On 6 and 7 January, Filomena strengthened as it moved southeast towards the Canary Islands. The cyclone then traveled northeastward towards the Iberian Peninsula on 7 January, bringing relatively warm, humid air for the winter season. At this time, southern Europe was experiencing cold temperature anomalies because of an anticyclone located west of the UK, resulting in temperature minimums below 0 °C in almost the entire Iberian Peninsula. Hence, when the storm arrived in the Gulf of Cádiz on 8 January, its warm front blew over the preexisting cold air, allowing precipitation in the form of snow or sleet throughout most of the Iberian Peninsula, except for some parts of southern Spain. The precipitation lasted for 3 d, until Filomena dissipated in the Mediterranean Sea on 11 January. The most affected regions were central and northeastern Spain, which accumulated an average of 30 to 50 cm of snow (AEMET, 2021b). The accumulated snow favored the persistence of low temperatures in the following days, triggering a cold spell that lasted for about 2 weeks, from 5 to 17 January, with a temperature average of 2 °C in the Iberian Peninsula and an anomaly of −3.8° with respect to the 1981–2010 climatology, as recorded by the AEMET (2021b).

4.1.1 Extratropical winter storms and climate change

The IPCC report (Lee et al., 2021) highlights that

> the number of extratropical cyclones (ETC) composing the storm tracks is projected to weakly decline in future projections, but by no more than a few percent change

and that

> the reduction is mostly located on the equatorward flank of the storm tracks.

However, it also states that

> substantial uncertainty and thus low confidence remain in projecting regional changes in Northern Hemisphere jet streams and storm tracks, especially for the North Atlantic basin in winter.

Nonetheless, as stated in chap. 11 of the IPCC AR6 (Seneviratne et al., 2021),

> despite small changes in the dynamical intensity of ETCs, there is high confidence that the precipitation associated with ETCs will increase in the future.

In addition, there is

> high confidence that snowfall associated with winter ETCs will decrease in the future, because increases in tropospheric temperatures lead to a lower proportion of precipitation falling as snow.

Besides the IPCC report, numerous studies have addressed the influence of climate change on extratropical cyclones (ETCs) due to their impacts on many regions of the planet (e.g., Zappa et al., 2013; Ulbrich et al., 2009; Priestley and Catto, 2022). Hence, there is a priori mixed evidence for the anthropogenic contribution to dynamical changes in Filomena-like storms.

4.1.2 Attribution of Filomena to climate change

We now use the ERA5 data to perform the attribution of the cyclonic circulation associated with Filomena for 9 January 2021 in the past and present climates (Fig. 2). We find a significant increase in the slp up to 3 hPa in the factual period (Fig. 2a–d). Figure 2e–g shows that Filomena was an unusually cold event compared to its analogues even in the counterfactual period. In the factual period analogue temperatures over Iberia are significantly warmer than in the counterfactual period (Fig. 2h), by up to 4 °C. This can likely be related to the long-term surface temperature warming signal in recent years. Precipitation for the factual analogues compared to the counterfactual ones is significantly larger in the center and center-east of the Iberian Peninsula, where Filomena had its highest impact, and in the southeast of the peninsula (Fig. 2l). On the other hand, precipitation is significantly lower in the Gulf of Lion and southwestern Mediterranean Sea.

The analogue quality Q for Filomena is in the upper tail of the distribution, indicating moderate quality, and is poorer in the factual period (Fig. 2m) . There is little change in the event's predictability index D (Fig. 2n) with respect to the atmospheric circulation in the two periods. Still, the analogue distributions in the two periods are statistically different, with the factual period showing a shift towards higher D values. On the contrary, the persistence Θ of the event with respect to the circulation decreases (Fig. 2o), while no significant change is found in the Θ of the analogues. Figure 2p shows only modest changes in seasonality, with a slight increase in January and February analogues. Although Filomena occurred during a negative ENSO phase, there is a significant change in the ENSO distribution for the analogues, with the factual period showing more positive values (Fig. 2q). This means that the results may be modulated by ENSO. The distributions of the AMO phases do not evidence any significant influence of this mode on the analogues (Fig. 2r).

Filomena-like storms in the factual period display higher slp yet cause more precipitation in central Spain, the region that suffered the highest impacts from the storm. Even though there are slightly more analogues in the coldest months, that is, January and February, there is a significant increase in the 2 m temperature, making the snow at low altitudes less probable in a warmer climate. Given the reasonable quality of analogues, we can state that the results are in line with the expected climate-change trends discussed in the previous section. However, since there is a shift in the distributions of ENSO conditioned to the analogues, we cannot reject the hypothesis that ENSO variability has some influence on the analogues of Filomena.

4.2 French spring cold spell

A frost event took place from 6 to 8 April 2021 in France. It was exceptional, with daily minimum temperatures below −5 °C recorded in several locations. Grapevines and fruit trees were damaged especially in the Loire and Rhône valleys, as frost management strategies (e.g., heating from braziers) could not be implemented in time. The temperatures broke record lows at many French weather stations. This cold event happened 1 week after an episode of high temperatures in March, which was also record-breaking at many locations in France (LaChaineMeteo, 2021) and western Europe. This sequence (or compound event, according to the definition proposed by Zscheischler et al., 2020) led the growing season to start early, with bud burst occurring in March and the new leaves and flowers left exposed to the deep frost episode that followed in early April. The April cold spell was associated with an advection of cold air from the Arctic into France on 5–6 April 2021, facilitated by a deep low pressure based over Scandinavia and anticyclonic conditions overs Iceland. This created the low-temperature anomaly in the subsequent days.

4.2.1 Cold spells and climate change

The IPCC AR6 describes as "virtually certain" that there have been warmer and/or rarer cold spells over most land areas since the 1950s, that this trend is due to anthropogenic climate change, and that it is set to continue in the future (IPCC, 2021). As stated in chap. 11 of the IPCC AR6 (Seneviratne et al., 2021),

> a decrease in the number of cold spell days has been observed over nearly all land surface areas (Easterling et al., 2016) and in the northern mid-latitudes in particular (Van Oldenborgh et al., 2019).

While a rapid warming, in general, lowers the probability of cold spell occurrence, projected changes in the temperature distribution imply that regional changes in cold spell frequency and/or intensity may not match changes in the mean temperature (Tamarin-Brodsky et al., 2019). Similarly, Kodra et al. (2011) have shown that long-lasting periods where temperatures drop below an absolute threshold (e.g., frost days) may still be produced locally and occasionally even in future, warmer climates. There has also been a lively debate in

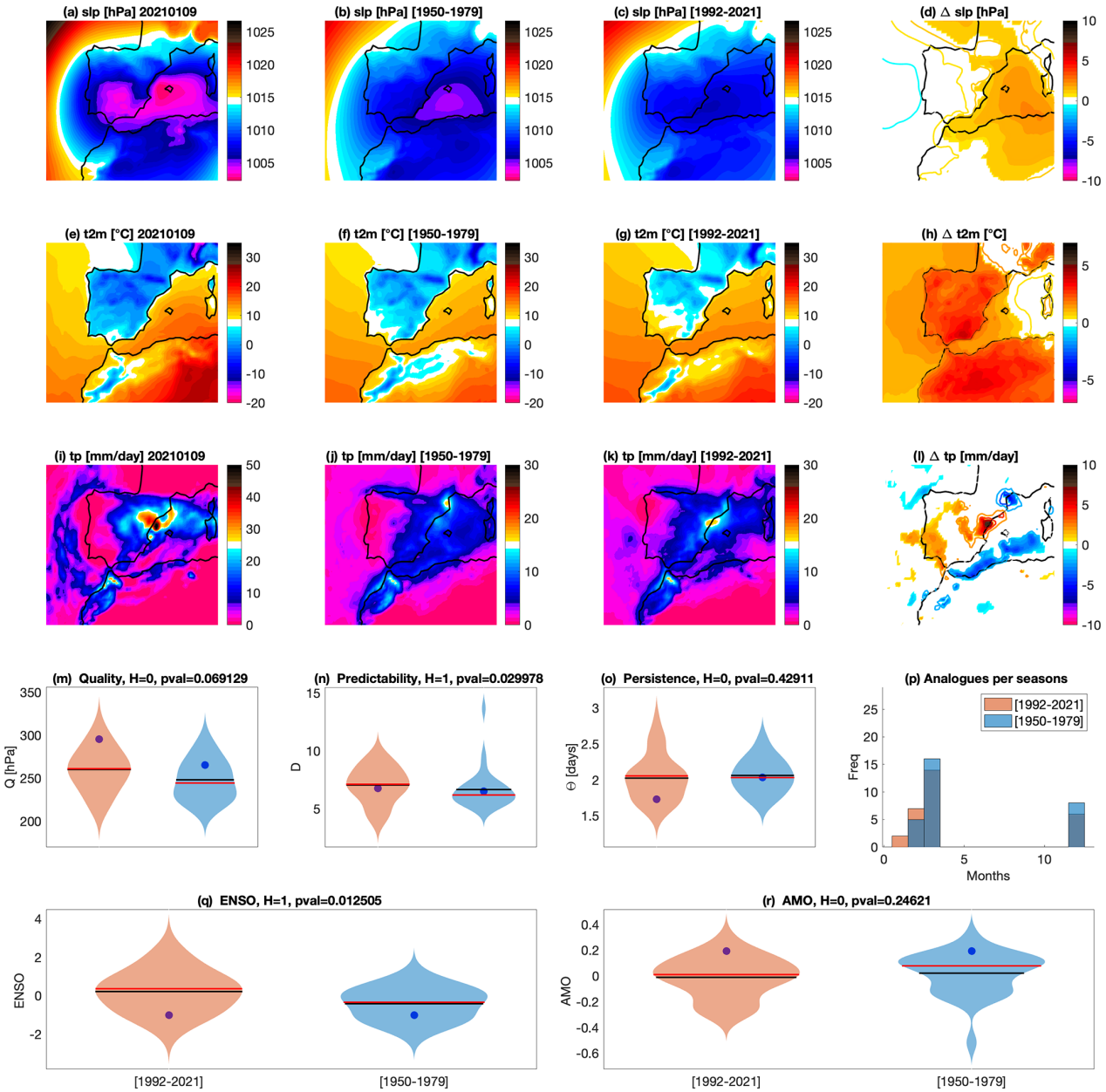

Figure 2. Attribution for Storm Filomena on 9 January 2021. Daily mean sea-level pressure slp **(a)**, 2 m temperatures t2m **(e)** and total precipitation tp **(i)** on the day of the event. Average of the 33 sea-level pressure analogues found for the counterfactual [1950–1979] **(b)** and factual [1992–2021] **(c)** periods and corresponding 2 m temperatures **(f, g)** and daily precipitation rate **(j, k)**. Δslp **(d)**, Δt2m **(h)** and Δtp **(l)** between factual and counterfactual periods: colored–filled areas show significant anomalies with respect to the bootstrap procedure. Violin plots for counterfactual (blue) and factual (orange) periods for the analogue quality Q **(m)**, the predictability index D **(n)**, the persistence index Θ **(o)** and the distribution of analogues in each month **(p)**. Violin plots for counterfactual (blue) and factual (orange) periods for ENSO **(q)** and AMO **(r)**. Values for the peak day of the extreme event are marked by a color-filled circle.

the literature on whether dynamical changes associated with climate change may act to partly counter the thermodynamic changes and favor cold spell occurrence. Faranda (2020) and D'Errico et al. (2022) argued that circulation patterns associated with cold spells over Europe have been increasing in frequency in the present climate and will continue to do so under future climate change. Several authors have also argued for or against a link between Arctic amplification and an increased occurrence of cold spells in some mid-latitude regions (Mori et al., 2014; Cohen et al., 2018; Blackport and Screen, 2020; Ye and Messori, 2020; Jolly et al., 2021).

Cold spells continue to have large detrimental socioeconomic effects, with several high-impact events occurring in recent winters, notably during the 2018–2019 and 2020–2021 winters in North America (Lee and Butler, 2020; BBC, 2022; Lillo et al., 2021; Doss-Gollin et al., 2021; Miller, 2022) and the 2017–2018 winter in Europe (Kautz et al., 2020; LeMonde, 2018). Moreover, even if the absolute severity of cold spells decreases, rapid temperature swings are a hazard in their own right (Kral-O'Brien et al., 2019; Casson et al., 2019).

4.2.2 Attribution of the French spring cold spell to climate change

A statistical analysis of the temperatures during the French cold spell of 2021 was proposed by a team of the World Weather Attribution (Vautard et al., 2021). This report concluded that while climate change has raised the absolute temperatures during cold spells, it has also led to an intensification of growing-period frosts due to earlier bud burst. The 2021 cold outbreak occurred right after a specific weather pattern called the "Atlantic Ridge", identified as one of the four main weather regimes in the North Atlantic region (Michelangeli et al., 1995). The goal of this section is to analyze how the features of this weather pattern have evolved with climate change using the ERA5 reanalyses (Fig. 3). This analysis complements the report of Vautard et al. (2021) by examining the atmospheric circulation. We focus on the date of 6 April 2021, the day where the circulation particularly favored the advection of cold air into France. For this day the slp pattern (Fig. 3a) consisted of a ridge of high pressure over the Atlantic and a large cyclonic structure over Scandinavia, with cold air advection from northern latitudes into France. The analogues associated with this circulation in the counterfactual (Fig. 3b) and factual (Fig. 3c) periods exhibit the same zonal pressure gradient, and their difference (Fig. 3d) shows that the gradient is amplified in factual world, leading to stronger cold advection towards France. The t2m for 6 April 2021 (Fig. 3e) shows cold conditions over northern and western Europe, while the analogues are milder (Fig. 3f, g), and Δt2m is mostly greater than 0 °C everywhere. If we focus over France, we can conclude that this cold spell would have led to temperatures 2–4 °C colder without anthropogenic forcing. Looking at the precipitation maps (Fig. 3i, j, k) and the Δtp (Fig. 3l) we see that the cold spell atmospheric pattern corresponds to dry conditions over France. There is no change in precipitation patterns over France between the factual and counterfactual conditions (Fig. 3l). However, the reinforcement of the zonal pressure gradient in the factual period leads to an increase in the precipitation over continental Europe and a decrease on the Mediterranean Sea. The values of Q (Fig. 3m) suggest that the pattern under examination is rare compared to its analogues. The distribution of the predictability index D (Fig. 3n) shifts towards lower values in the factual period, although there are no significant changes relative to the counterfactual distribution. Similarly, there are not significant shifts in the distribution of the persistence Θ (Fig. 3o). Nonetheless, the extreme itself becomes markedly more persistent relative to the atmospheric circulation in the factual period. The monthly distribution of the analogues (Fig. 3p) suggests that there is a shift of this circulation pattern towards April and June months and that its occurrence in March is decreasing in recent times.

Figure 3q suggests a significant change in the ENSO phases associated with the analogues in the two periods, while no significant role of the AMO is detected with this analysis (Fig. 3r). Therefore the attribution of this event to climate change comes with the caveat of a potential role of ENSO on the associated pattern of atmospheric circulation.

To conclude, our analysis suggests, in line with the literature on cold spells and climate change cited in Sect. 4.2.1, that the French spring cold spell event is becoming rare in the month of March in the current climate and that it would have led to cooler temperatures in a world without climate change.

4.3 Westphalia floods

On 11 July 2021 the synoptic situation over western Europe was characterized by a ridge situated west of Ireland. As this low-pressure system – named "Bernd" by the German Meteorological Service (DWD; see Junghänel et al., 2021) – gradually moved eastward, it was isolated from the usually westerly large-scale flow by a strong anticyclonic system that built up over the eastern part of the Atlantic and deviated the jet stream north of Scotland. By 13 July, Bernd was completely cut from the main flow and remained stationary over western and central Europe until 16 July, before being gradually pushed east. Hot and moist surface air from northern Europe and the Mediterranean was advected by the cyclonic movement around the cutoff, which led from 12 to 15 July to recurrent and persistent heavy rains first over mountain ranges due to orographic and dynamic uplift and then over the entire region of Belgium, Luxembourg, western Germany and eastern France. The maximum precipitations over the region were centered on the west of Belgium with some locations receiving more than 250 mm of rain in 48 h (e.g., in Jalhay, Belgium, according to what reported

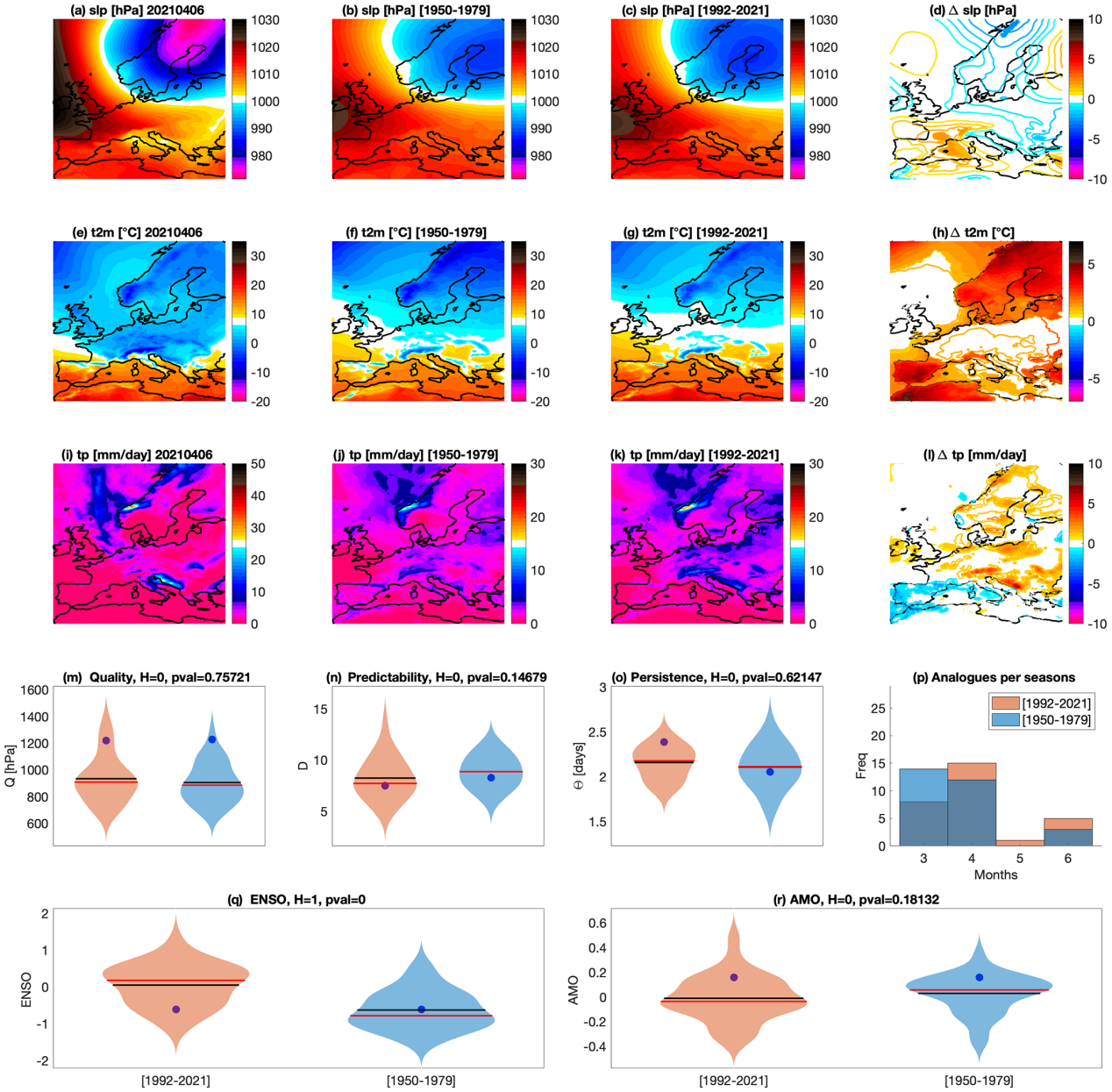

Figure 3. Attribution for the French cold spell on 6 April 2021. Daily mean sea-level pressure slp **(a)**, 2 m temperatures t2m **(e)** and total precipitation tp **(i)** on the day of the event. Average of the 33 sea-level pressure analogues found for the counterfactual [1950–1979] **(b)** and factual [1992–2021] **(c)** periods and corresponding 2 m temperatures **(f, g)** and daily precipitation rate **(j, k)**. Δslp **(d)**, Δt2m **(h)** and Δtp **(l)** between factual and counterfactual periods: colored–filled areas show significant anomalies with respect to the bootstrap procedure. Violin plots for counterfactual (blue) and factual (orange) periods for the analogue quality Q **(m)**, the predictability index D **(n)**, the persistence index Θ **(o)** and the distribution of analogues in each month **(p)**. Violin plots for counterfactual (blue) and factual (orange) periods for ENSO **(q)** and AMO **(r)** indices. Values for the peak day of the extreme event are marked by a blue dot. Horizontal bars in panels **(m)**–**(r)** correspond to the mean (black) and median (red) of the distributions.

by Kreienkamp et al., 2021). The soils, already humid due to recurring precipitation events during the preceding 3 weeks, were incapable of absorbing more water, which led to runoff and overflow of small watercourses and flash floods. Afterwards, larger rivers such as the Ruhr and the Meuse also overflowed, causing massive casualties mainly in Germany (196 people, according to DieWelt, 2021) and Belgium (42 casualties, according to Het Laatste Nieuws, 2021). In addition to the terrible fatalities, the floods severely damaged goods and infrastructure, with a total cost estimated around EUR 10 billion (Business Insurance, 2022) for Belgium. It was afterwards found using hydrological data that the flood in the regions affected was significantly higher than any flood since the beginning of the systematic records (Kreienkamp et al., 2021).

4.3.1 Floods and climate change

Rapidly after the event, the potential link between the event and climate change was highlighted by activists and journalists. Indeed, as the atmosphere warms up, it can contain more water – 7 % K^{-1} of warming according to the Clausius–Clapeyron relationship – therefore allowing more intense extreme precipitation events. Several studies (Madsen et al., 2014; Kundzewicz et al., 2018, 2019) investigated the link between climate variability, extreme precipitation, and hydrological floods globally and in Europe. As stated in the last IPCC report (IPCC, 2021), there is high confidence that

> a warmer climate will intensify very wet and very dry weather and climate events and seasons, but the location and frequency of these events depend on projected changes in regional atmospheric circulation.

Especially for Europe, there is medium confidence that at 1.5 °C of warming,

> heavy precipitation and associated flooding are projected to intensify and be more frequent.

This result highly depends on the type of water basins, especially if the peak flow is snowmelt-dominated. More generally, heavy precipitations are strongly entangled with natural variability of the climate system. Ultimately, although flooding usually depends strongly on the local characteristics of the hydrological system – especially artificialization of soils and containment of rivers – more intense flooding can be linked to climate change via the increased intensity of heavy rains.

4.3.2 Attribution of Westphalia floods to climate change

An attribution study of the Westphalia floods has already been published by the World Weather Attribution network, which investigated the influence of climate change on heavy precipitations over a broad region of western Europe (Kreienkamp et al., 2021). The authors of the study concluded that a climate warming of 1.2 °C (current climate) led to an increase in the likelihood of such an event by a factor between 1.2 and 9 with respect to the pre-industrial period. Here, we condition the attribution results on the atmospheric dynamics leading to the occurrence of similar events. Results of our attribution analysis are displayed in Fig. 4. We found no significant decrease in the slp of the cutoff low over Germany between the factual and counterfactual periods (Fig. 4a–d) and only moderate increases in t2m over the regions of interest (Fig. 4e–h). We found also a large and significant increase in precipitation (up to 5 mm d^{-1}) over southwest Germany, eastern France and the western Alps (Fig. 4i–l). This increase is consistent with the increasing amount of water vapor that a warmer atmosphere can carry.

Overall, the analogue quality (Fig. 4m) is good in both periods. It allows us to emphasize that, even if intense precipitation events due to cutoff lows over western Europe in summer are not unusual, this event was particularly intense and climate change likely made it more intense via an increased quantity of water vapor in the atmosphere. No significant changes are observed in the distributions of predictability D (Fig. 4n) and persistence Θ (Fig. 4o) or in the predictability or persistence of the event itself relative to the circulation in the two periods. In the factual period, events tend to happen slightly more frequently in the month of July (Fig. 4p), a favorable month for the development of large convective systems in the area, but overall changes in seasonality are small. When investigating the link between the event and low-frequency variability of the climate system, Fig. 4q shows no significant difference in the ENSO distributions during analogue occurrences between the factual and counterfactual periods, even though the distribution in the counterfactual period is broader. Figure 4r, however, displays a significant change between the AMO distributions, with the analogues in the factual period being found in warmer phases of the AMO than in the counterfactual period. This suggests that attributing this event to climate change requires disentangling the possible role of AMO versus global warming.

In summary, the Westphalia floods occurred after an intense rain event caused by a cutoff lows stagnating over the region of Belgium, Luxembourg, western Germany and eastern France. They caused massive casualties and severely damaged property and infrastructure. Our analysis is coherent with the existing literature which shows that a warmer atmosphere leads to an intensification of extreme rain events which in turn can exacerbate the intensity of floods. It should nonetheless be emphasized that attributing this event requires taking into account the role of low-frequency climate variability in the results.

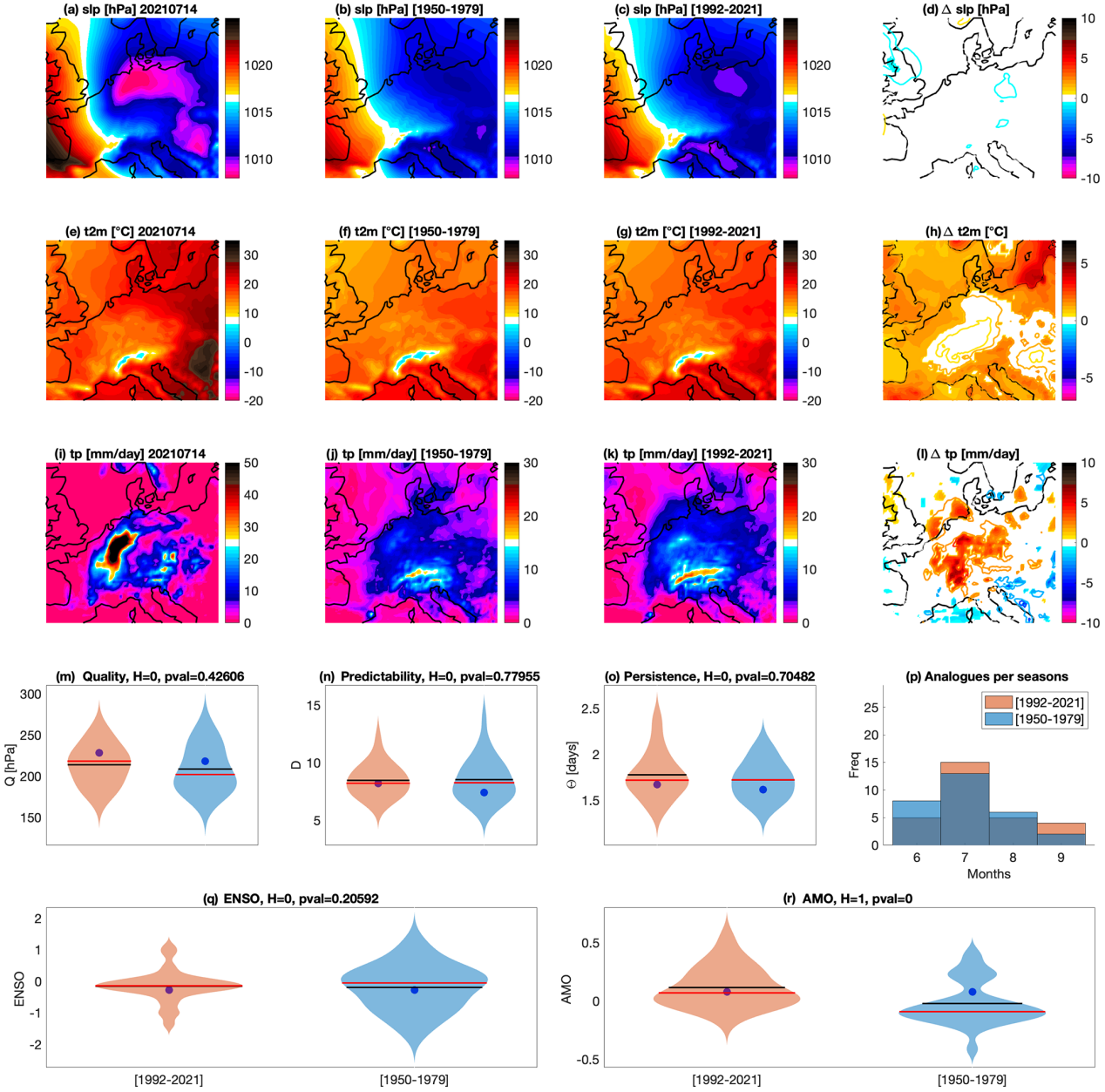

Figure 4. Attribution for the Westphalia floods on 14 July 2021. Daily mean sea-level pressure slp **(a)**, 2 m temperatures t2m **(e)** and total precipitation tp **(i)** on the day of the event. Average of the 33 sea-level pressure analogues found for the counterfactual [1950–1979] **(b)** and factual [1992–2021] **(c)** periods and corresponding 2 m temperatures **(f, g)** and daily precipitation rate **(j, k)**. Δslp **(d)**, Δt2m **(h)** and Δtp **(l)** between factual and counterfactual periods: colored–filled areas show significant anomalies with respect to the bootstrap procedure. Violin plots for counterfactual (blue) and factual (orange) periods for the analogue quality Q **(m)**, the predictability index D **(n)**, the persistence index Θ **(o)** and the distribution of analogues in each month **(p)**. Violin plots for counterfactual (blue) and factual (orange) periods for ENSO **(q)** and AMO **(r)**. Values for the peak day of the extreme event are marked by a blue dot. Horizontal bars in panels **(m)**–**(r)** correspond to the mean (black) and median (red) of the distributions.

4.4 Mediterranean heat wave

During the month of August, an area of high pressure in the upper troposphere affected a large part of the Mediterranean basin. The upper-lever high-pressure system caused atmospheric subsidence which simultaneously compressed the air and warmed it, a phenomenon known as "heat dome". This atmospheric configuration induced a severe heat wave over the Mediterranean region from 10 to 15 August: southern Italy, France, Spain and north Africa were most affected, with extensive wildfires and high temperatures. On 11 August, record-breaking temperatures were recorded at several locations in Italy. The town of Santa Maria Capua Vetere in Campania reached 42.2 °C, 44.5 °C was recorded at Bova in Calabria and 43.6 °C was recorded at Ballao in Sardinia (Mazzoleni, 2021). The highest temperature was recorded in eastern Sicily with a peak of 48.8 °C recorded in Floridia in the province of Syracuse (SIAS, 2021). This is the current European temperature record. From 12 August, the heat dome moved towards Spain. There, the heat peak was reached on 14 August, establishing a new national temperature record of 47.4 °C in Montoro, Andalusia (AEMET, 2021a). The heat wave also reached southeastern France, where 40.9 °C was recorded in Varages in the Var, and 41.2 °C was recorded in Trets, Bouches-du-Rhône. Some records were broken also in Tunisia, with 47 °C in Tunis and 50.3 °C in Kairouan (WMO, 2021). The heat wave additionally triggered extensive wildfires in Italy, Spain, France and Greece. During the night of 11 to 12 August, more than 500 fires were recorded in Italy, causing four casualties (CEMS, 2021c). Spain faced fires in the area of Navalacruz and Riofrío. A fire of 90 km of perimeter devastated 12 000 ha of vegetation and led to the evacuation of 1000 inhabitants (CEMS, 2021a). Similarly in the Var (France) wildfires burned 6300 ha and resulted in the evacuation of 7000 people and the death of 2 people (CEMS, 2021b).

4.4.1 Mediterranean heat waves and climate change

The IPCC AR6 (Ali et al., 2022) clearly highlights the major changes in heat wave characteristics in the Mediterranean region brought about by climate change. The report states that

> Surface temperature in the Mediterranean region is now 1.5 °C above the pre-industrial level, with a corresponding increase in high-temperature extreme events (high confidence)

and that

> A growing number of observed impacts across the entire basin are now being attributed to climate change, along with major roles of other forcing of environmental change (high confidence). These impacts include multiple consequences of longer and/or more intensive heat waves.

Finally, the report states that

> During the 21st century, climate change is projected to intensify throughout the [Mediterranean] region. Air and sea temperature and their extremes (notably heat waves) are likely to continue to increase more than the global average (high confidence).

Several studies in the literature have investigated the changes related to climatic factors in the Mediterranean, coming to similar conclusions concerning the generalized increase in heat wave frequency and intensity expected in the region (e.g., Guerreiro et al., 2018; Molina et al., 2020), and also highlighting that this may be accompanied by a drying trend (Spinoni et al., 2020; Grillakis, 2019).

4.4.2 Attribution of the Mediterranean heat wave to climate change

We use ERA5 to perform the attribution of the anticyclonic circulation associated with the Mediterranean heat wave in past and present climates. We note that we will select the analogues independently of the extratropical or tropical nature of the depression that produced them. Figure 5 shows the results for the 11 August 2021, when the heat wave peaked over southern Italy. We do not detect a significant change in the slp for the factual period compared to the counterfactual period (Fig. 5a–d). However, we do observe a significant warming in t2m in the factual analogues compared to the counterfactual ones (Fig. 5h), with positive Δt2m anomalies of 2–3 °C over much of the land areas in the western Mediterranean basin. Nonetheless, the factual analogues are still cooler than the observed extremely warm conditions on 11 August 2021 (Fig. 5e, g). The warming in the factual period is associated with a significant decrease in tp in southern continental Europe and over Sicily, which could be explained by the high temperatures and stability which suppress convection (Fig. 5i–l). The Q values (Fig. 5m) suggest a reasonably good analogue quality in both periods. Again in both periods, the extreme-event predictability index D is close to the maximum of the analogue distributions (Fig. 5n), despite the fact that the two distributions are significantly different. This means that the slp pattern for the observed heat wave was unpredictable relative to its analogues. Moreover, the event's D is higher when calculated on the factual period data than on the counterfactual period data. Persistence Θ shows no significant changes in the analogues' distribution or large changes in the event's Θ as computed from the data in the two periods (Fig. 5o). Only minor changes in seasonality are observed (Fig. 5p). We finally looked at the possible influence of the low-frequency variability (ENSO and AMO) on the analogues (Fig. 5q, r). We cannot dismiss the impact of ENSO and AMO variability as the distributions of both indices conditioned on the analogues change significantly between the factual and counterfactual periods. Specifically, the

ENSO distribution shifts from weakly negative to neutral values, while the AMO distribution shifts from weakly negative to positive values.

In summary, our analysis is in line with the existing literature cited in Sect. 4.4.1, as it shows the predominance of the thermodynamic effects of climate change on the heat wave, with a clear warming signal in the analogues, which is higher than that of the global average. This signal is associated with dryer conditions over land. We nonetheless reiterate the possible influence of low-frequency climate variability on our results.

4.5 Hurricane Ida

Hurricane Ida was a tropical and post-tropical cyclone that occurred in the North Atlantic basin (Caribbean Sea and mainland USA) in August 2021. Besides being the most intense tropical cyclone (TC) to make landfall in the USA in that season, it had a very damaging post-tropical stage. Hurricane Ida (track shown in Fig. 6) was first detected as a tropical wave on 23 August. It was named as a tropical storm on 26 August, and it became a Category 1 hurricane on the day it made a first landfall over Cuba on 27 August. This landfall did not weaken it, and it underwent rapid intensification as it approached Louisiana's coast, where it made landfall again as a Category 4 hurricane (NHC/NOAA, 2021). At its peak intensity, 1 min sustained winds reached 240 km h^{-1} and the minimum central pressure was 929 hPa. Notably, it did not rapidly weaken because of the "brown ocean effect", where flat and moist land conditions allow a TC to retain its intensity for a longer period of time. Ida finally dropped below hurricane strength on 30 August.

While it was still a tropical wave, Ida triggered floods in Venezuela with 20 casualties. In Cuba, the material damage was important, but no casualties were reported. In Louisiana and Mississippi there were a total of 38 deaths, among which 23 were indirect, mostly from carbon monoxide poisoning (Hanchey et al., 2021). A large power outage left more than 1 million experiencing a blackout. Heavy infrastructural damage is estimated around USD 15 billion (NCDC/NOAA, 2021). These figures can be compared to Katrina's – the costliest hurricane to date, which made landfall on the same date and the same place 16 years before – 1838 deaths and USD 125 billion in damages (NHC/NOAA, 2018).

While Ida was weakening into an extratropical low, it combined with a frontal zone, regaining tropical-storm force winds and unleashing large amounts of rainfall over the northeastern USA. The casualties in this region were greater than those for Ida's tropical stage, with 42 deaths mostly due to flash floods. Finally, Ida ended its course over eastern Canada, dissipating in the Gulf of St. Lawrence.

4.5.1 Hurricanes and climate change

Of all extreme events, tropical cyclones (TC) are among those for which the impacts of climate change are the most uncertain. The reason for this is threefold: (i) the lack of a satisfying theory for cyclogenesis, (ii) the short span of reliable observations, and (iii) the difficulty to simulate TCs in state-of-the-art global models, because of their too coarse resolution. Despite the relatively short span of available observations, some conclusions can still be drawn from the past record (Knutson et al., 2019).

Notably, the IPCC's AR6 report (IPCC, 2021) states that

> it is very likely that heavy precipitation events will intensify and become more frequent in most regions with additional global warming. At the global scale, extreme daily precipitation events are projected to intensify by about 7 % for each 1 °C of global warming (high confidence). The proportion of intense tropical cyclones (categories 4–5) and peak wind speeds of the most intense tropical cyclones are projected to increase at the global scale with increasing global warming (high confidence). (SPM, B2.4)

Modeling studies using different methodologies (large-scale indicators vs. direct TC tracking) disagree on the sign of future global TC frequency trends. There is nonetheless some confidence in trends of TC-related risks. Knutson et al. (2020) highlight these in order of decreasing certainty: (1) because of sea-level rise, storms surges will become more important; (2) TC precipitation rates will increase; (3) the proportion of intense TCs among all TCs will continue to rise, and the maximum surface wind speed will increase of about 5 %.

There is also growing concern about the increase in windstorm risks associated with post-tropical cyclones (Haarsma, 2021). Indeed, studies in reanalyses showed that despite representing a small number of extratropical storms, post-tropical cyclones are among the most intense ones to reach North America and Europe (Baker et al., 2021; Sainsbury et al., 2020). A global climate-change projection shows that more tropical cyclones are likely to undergo post-tropical transition in the future, especially in the North Atlantic basin (Michaelis and Lackmann, 2019).

4.5.2 Attribution of Hurricane Ida to climate change

We now focus on the day Ida produced heavy precipitation in New York City, namely 2 September 2021, and apply the analogue methodology to perform an attribution. We note that we select analogues independently of the extratropical or tropical nature of the depression that has produced them. Figure 7a shows the daily slp associated with Ida on the chosen date, and Fig. 7b and c show the analogue average for the counterfactual and the factual periods. We find a signifi-

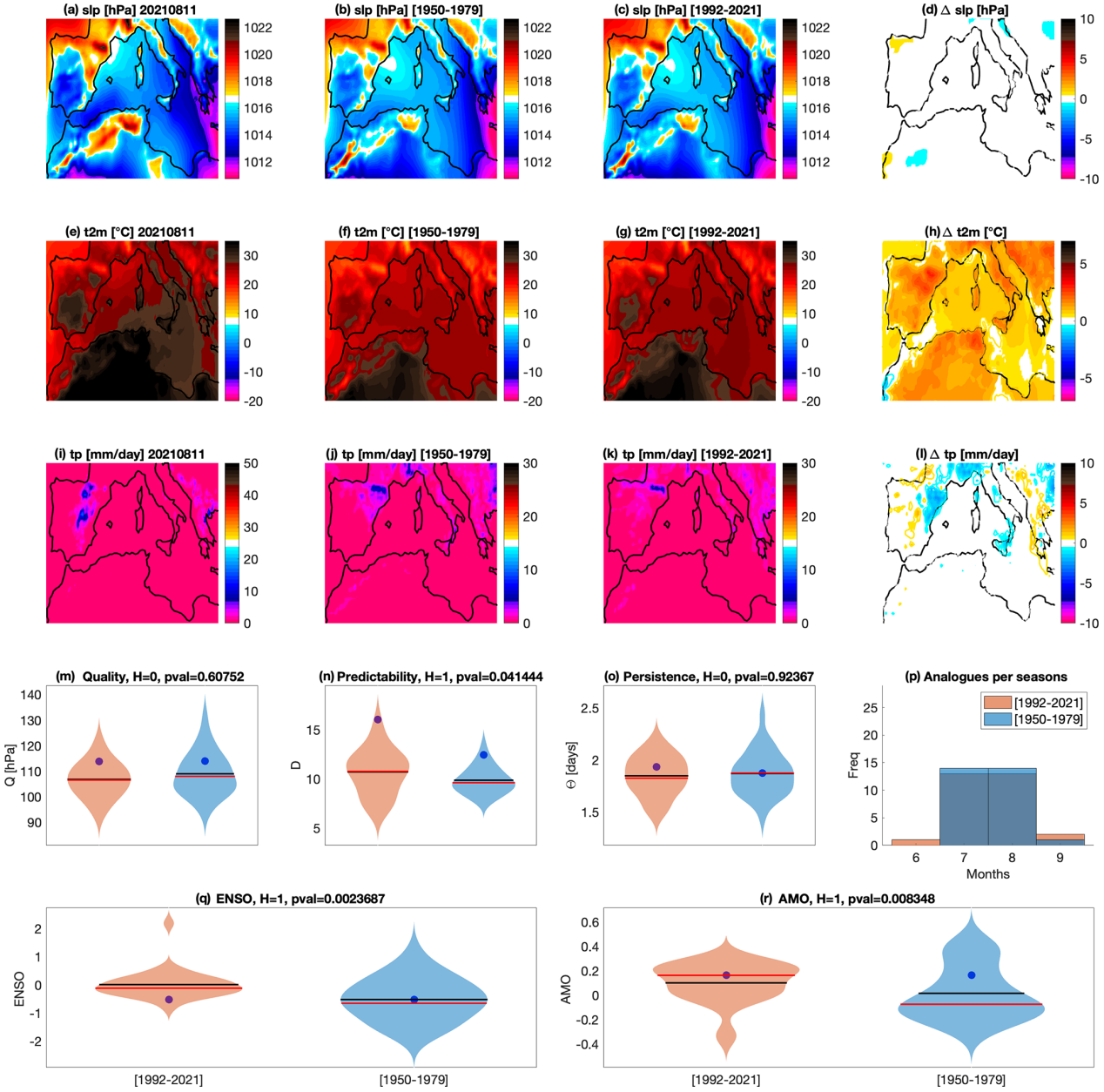

Figure 5. Attribution for the Mediterranean heat peak on 11 August 2021. Daily mean sea-level pressure slp **(a)**, 2 m temperatures t2m **(e)** and total precipitation tp **(i)** on the day of the event. Average of the 33 sea-level pressure analogues found for the counterfactual [1950–1979] **(b)** and factual [1992–2021] **(c)** periods and corresponding 2 m temperatures **(f, g)** and daily precipitation rate **(j, k)**. Δslp **(d)**, Δt2m **(h)** and Δtp **(l)** between factual and counterfactual periods: colored–filled areas show significant anomalies with respect to the bootstrap procedure. Violin plots for counterfactual (blue) and factual (orange) periods for the analogue quality Q **(m)**, the predictability index D **(n)**, the persistence index Θ **(o)** and the distribution of analogues in each month **(p)**. Violin plots for counterfactual (blue) and factual (orange) periods for ENSO **(q)** and AMO **(r)**. Values for the peak day of the extreme event are marked by a blue dot. Horizontal bars in panels **(m)**–**(r)** correspond to the mean (black) and median (red) of the distributions.

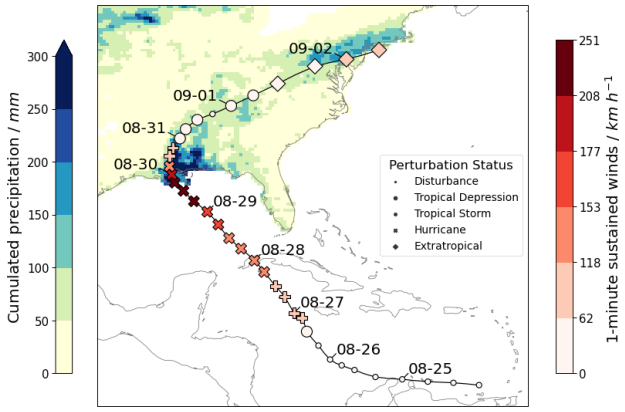

Figure 6. Track and associated precipitation for Hurricane Ida. The 6-hourly track positions from the IBTrACS (Knapp et al., 2010; Knapp et al., 2018) database are provided with their wind speed and status from the NHC report. Cumulated daily precipitation between 28 August and 3 September 2021 from the NCEP/CPC (2022) US Unified Precipitation is displayed. White indicates no data.

cant weakening of the slp depression (i.e., an increase in the minimum slp) for the factual with respect to the counterfactual period (Fig. 7d). Furthermore, we observe that temperatures (Fig. 7e–g) are significantly warmer (Fig. 7h) in the factual period. The signal of changes in analogues' precipitation between the two periods is mixed, and both sets of analogues additionally display relatively different precipitation patterns from that observed for Ida (Fig. 7i–l). We have confidence in these results because the quality of the analogues Q for the event is well within (albeit in the upper tails of) the distributions of Q for its analogues in both factual and counterfactual periods (Fig. 7m). The distribution of analogue quality changes significantly between the two periods, and we observe that the distribution is narrower and shifted towards lower values in the factual period, meaning that the event is becoming more typical (Fig. 7m). There is also a significant change in predictability of the analogue distribution, with a shift towards lower D (and hence higher predictability, Fig. 7n), but not in persistence (Fig. 7o). We see an increase in analogues in the months of August/September in the factual period (Fig. 7p): these months are in the tropical cyclone season in the North Atlantic, and therefore it is likely that more events in the factual period correspond to post-tropical cyclones. This is in line with the significant change in the AMO distribution between the two sets of analogues, with a shift towards more positive (warmer) values in the factual period (Fig. 7r). Indeed, a warmer phase of the AMO favors cyclonic activity and hence post-cyclonic activity. There is no significant change in the distribution of ENSO between the two sets of analogues (Fig. 7q).

Ida was already a rare extreme event as a Category 4 hurricane, but it will leave a mark especially because of its impactful post-tropical stage. As discussed in Sect. 4.5.1, very intense hurricanes are likely to become more frequent with climate change, and they will be more likely to undergo post-tropical transition. What is particular for Ida, however, is that this transition occurred inland. What allowed the storm to remain intense in between a very strong tropical cyclone stage and the encounter with an extratropical perturbation could be the wet and warm conditions allowing for the brown ocean effect. However, we are aware of no formal study of such inland post-tropical cyclones in the literature. An important caveat of our analysis is that it does not take into account the post-tropical or extratropical nature of the analogue storms but only their slp footprints, so that it is hard to disentangle changes in the type of events that would occur in the area and the impact of climate change on each type of event. Our results nonetheless highlight a potential increase in autumn storm risk over northeastern North America and a possible AMO-driven modulation in the observed signal.

4.6 Po Valley tornado outbreak

On 19 September 2021, an outbreak of seven tornadoes affected the central Po Valley, in northern Italy. In particular, six of these formed in Lombardy and one, the most intense and damaging, hit a small airport near Carpi, Emilia-Romagna. Both mesocyclonic and non-mesocyclonic vortices were observed during the event, one the most impressive tornado outbreaks on record for the region. While tornadoes and waterspouts do occur regularly in Italy, they are on average much less frequent and less intense than in areas such as the midwestern and southeastern USA. However, the structure and location of the Po Valley can lead to the insurgence of environmental conditions conducive for occasionally intense phenomena, including tornadoes reaching EF4+ intensity on the Enhanced Fujita scale (Doswell et al., 2009). During the summer, the Po Valley can persistently host hot and humid air. The presence of the Adriatic Sea to the southeast provides an additional source of moisture, which can be advected to the region by the low-level jet preceding low-pressure systems approaching from the northwest. Moreover, the presence of the Apennines mountain range can encourage the formation of dry lines in the event of southwesterly flow due to foehn effect, contributing to supercell development (Alberoni et al., 1996). On 19 September, a high-pressure system extended from the central Mediterranean Sea to Scandinavia, while a high-level low pressure approached the Po Valley from France, connected to a trough located over northwestern Europe. During the afternoon, the region was affected by a dynamic and thermodynamic setup favorable to tornado development: a hot and humid low-level jet from the east, a strong wind shear with winds from the southwest at 500 hPa, a jet stream from the west at 200 hPa, and an approaching upper-level low characterized by relatively cold air and by the entrainment of stratospheric dry air. This led to the formation of strong thunderstorms associated with six tornadoes over Lombardy, roughly arranged

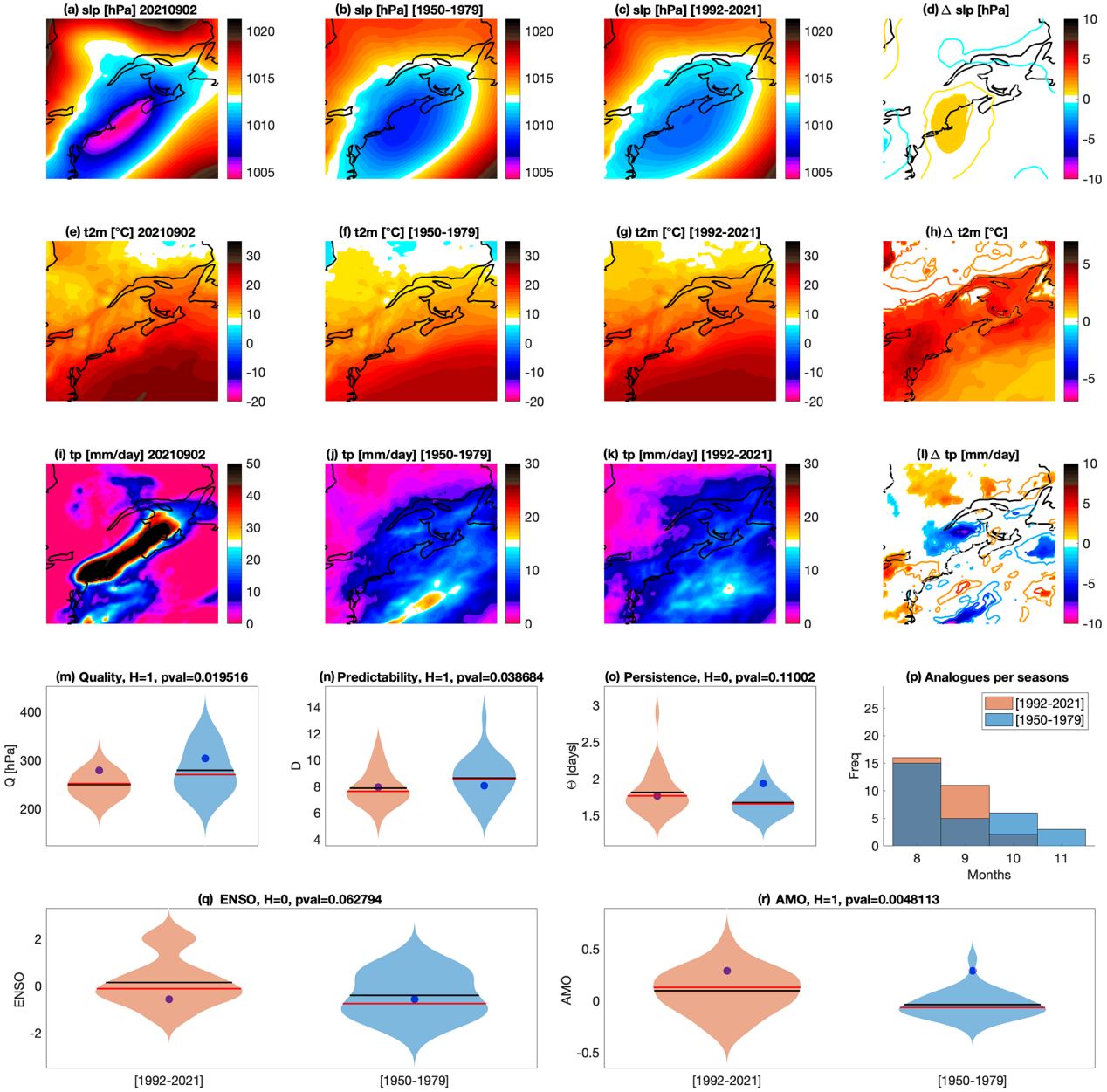

Figure 7. Attribution for the Hurricane Ida passage over the New York City area on 2 September 2021. Daily mean sea-level pressure slp **(a)**, 2 m temperatures t2m **(e)** and total precipitation tp **(i)** on the day of the event. Average of the 33 sea-level pressure analogues found for the counterfactual [1950–1979] **(b)** and factual [1992–2021] **(c)** periods and corresponding 2 m temperatures **(f, g)** and daily precipitation rate **(j, k)**. Δslp **(d)**, Δt2m **(h)** and Δtp **(l)** between factual and counterfactual periods: colored–filled areas show significant anomalies with respect to the bootstrap procedure. Violin plots for counterfactual (blue) and factual (orange) periods for the analogue quality Q **(m)**, the predictability index D **(n)**, the persistence index Θ **(o)** and the distribution of analogues in each month **(p)**. Violin plots for counterfactual (blue) and factual (orange) periods for ENSO **(q)** and AMO **(r)**. Values for the peak day of the extreme event are marked by a blue dot. Horizontal bars in panels **(m)**–**(r)** correspond to the mean (black) and median (red) of the distributions.

along a line between the cities of Milan and Brescia. Around 17:00 CEST (UTC+2), an isolated thunderstorm formed to the southeast of this area, closer to the Apennines range, and assumed markedly supercellular features, with a hook-echo reflectivity signature, a Doppler velocity couplet and a deviation to the right with respect to the mid-level flow: all clear signs of a strong rotating updraft. This supercell produced a well-documented tornado which hit a local airport, resulting in possible EF3 damage (Poli and Stanzani, 2022).

4.6.1 Tornadoes and climate change

The IPCC AR6, chap. 11 (Seneviratne et al., 2021), states that past trends in tornado occurrence are not robust due to short observation time series and that

> There is medium confidence that the mean annual number of tornadoes in the USA has remained relatively constant, but their variability of occurrence has increased since the 1970s, particularly over the 2000s, with a decrease in the number of days per year, and an increase in the number of tornadoes on these days (high confidence). Detected tornadoes have also increased in Europe, but the trend depends on the density of observations.

Moreover, even though high confidence is given to an increase in CAPE over the tropics and subtropics, over the USA, the increase in CAPE could be associated with a decrease in the vertical wind shear. This according to the IPCC suggests

> favourable conditions for an increase in severe convective storms in the future, but the interpretation of how tornadoes or hail will change is an open question because of the strong dependence on shear.

Finally, the IPCC report (Seneviratne et al., 2021) concludes that it is

> extremely difficult to detect and attribute changes in severe convective storms.

Most studies are focused on the USA, pointing to an increased variability, efficiency and possibly intensity of tornado outbreaks in the last decades (Brooks et al., 2014; Elsner et al., 2015, 2019). However, tornadoes in Europe remain an underestimated threat (Antonescu et al., 2017), even though they can affect very densely populated areas, as in the case described in this article.

4.6.2 Attribution of the Po Valley tornado outbreaks to climate change

Figure 8 shows the results for the attribution of the synoptic configuration associated with the Po Valley tornado outbreak episode. We do not observe significant differences in the pressure field over the Po Valley and only a marginally weaker low-pressure area in the Genoa Gulf (Fig. 8a–d) for the factual with respect to the counterfactual analogues. Instead, we observe that temperatures are significantly warmer (Fig. 8h) in the recent period, especially over land, including the Po Valley, and the Adriatic sea. This provides an increased amount of convective potential energy, through the transport of hot and humid air within the low-level jet. The factual period atmospheric configuration is further associated with higher precipitation over the Alps and central Europe and slightly lower precipitation over the Italian Peninsula (Fig. 8i–l), which is coherent with a more intense transport of warm and humid air from the southeast.

The analogue quality shows that this circulation pattern is relatively common compared to the rest of the analogues. We do not detect visible changes in the predictability D (Fig. 8n) and persistence Θ (Fig. 8o) of the analogues between the two periods. However, the predictability of the event itself is lower (higher D) when computed using data from the factual period. The seasonal occurrence of analogues (Fig. 8p) is quite consistent with the months of occurrence of tornadoes in northern Italy, with a maximum during summer; however, we do observe a general shift towards analogues occurring earlier in the season during the factual period, with the largest increase in July, when land-surface temperatures reach the annual maximum and the probability of low-pressure areas entering the Mediterranean basin is higher than in May or June, offering more energy and occasions for convective instability. Finally, changes in the distributions of ENSO (Fig. 8q) and AMO between the two periods (Fig. 8r) are at the very margin of statistical significance, suggesting that no strong conclusion can be drawn on the influence or lack thereof of these modes of decadal and inter-decadal variability.

Our analysis of the Po Valley tornado outbreak shows a clear increase in temperature of the analogues of this event in the factual period. This is compatible with the occurrence of more favorable environments for tornadoes due to climate change as mentioned in Sect. 4.6.1. However, the small spatiotemporal scale of the phenomenon requires caution in the interpretation of the attribution results.

4.7 Medicane Apollo

When the relatively cold atmospheric air coming from polar latitudes meets the warm surface of the Mediterranean Sea, extratropical cyclones change their characteristics into near-tropical depressions. These hybrids – termed "medicanes" (portmanteau of the words Mediterranean and hurricanes) – can be very damaging because of the strong winds and the intense convective precipitations (thunderstorms) originating around the eye of the storm.

Medicane Apollo (named by a consortium of European meteorological services; see Meteoweb, 2021) formed on 28 October in the Ionian Sea, offshore of Sicily, from a very

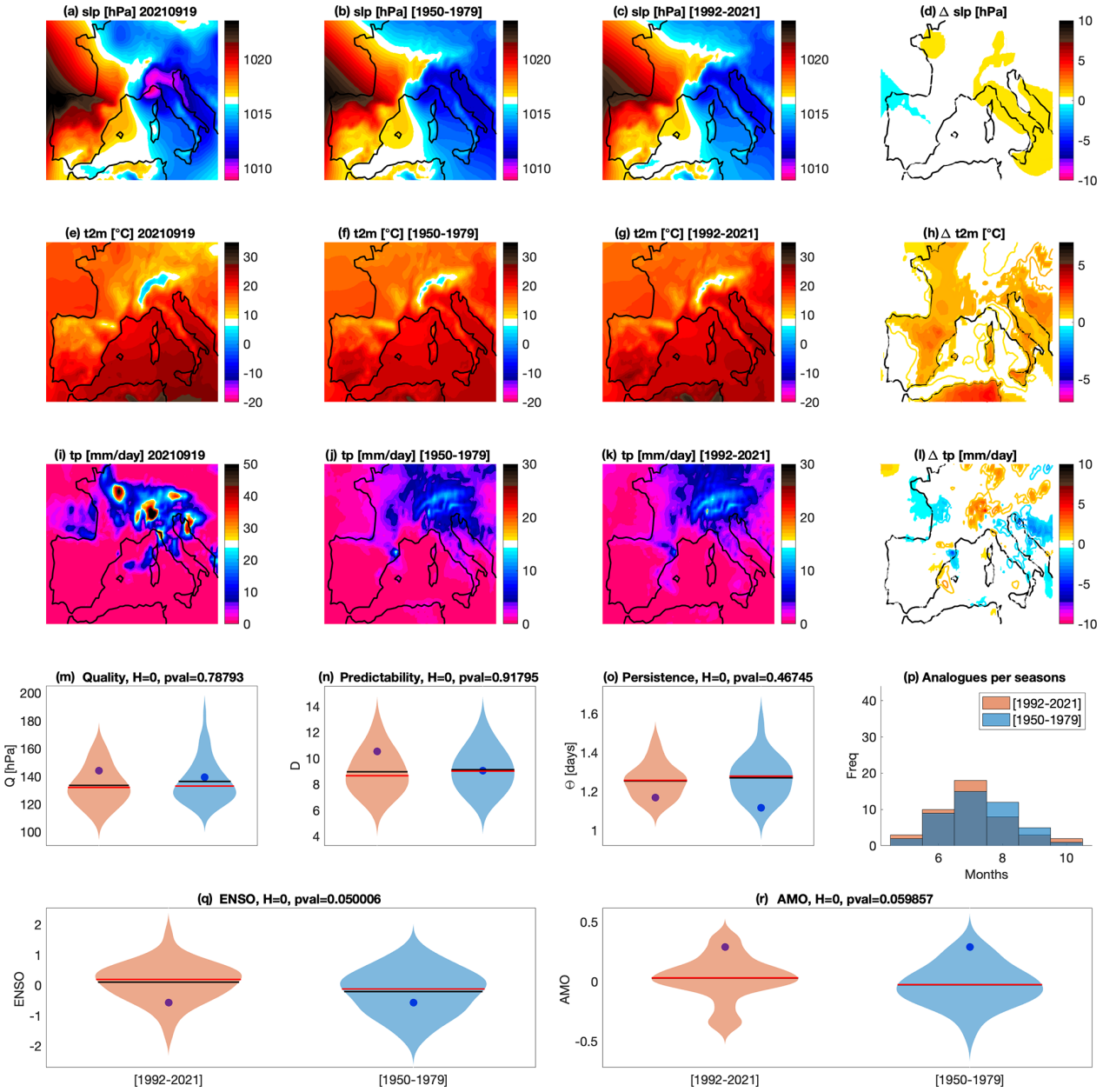

Figure 8. Attribution for the Po Valley tornado outbreak on 19 September 2021. Daily mean sea-level pressure slp **(a)**, 2 m temperatures t2m **(e)** and total precipitation tp **(i)** on the day of the event. Average of the 33 sea-level pressure analogues found for the counterfactual [1950–1979] **(b)** and factual [1992–2021] **(c)** periods and corresponding 2 m temperatures **(f, g)** and daily precipitation rate **(j, k)**. Δslp **(d)**, Δt2m **(h)** and Δtp **(l)** between factual and counterfactual periods: colored–filled areas show significant anomalies with respect to the bootstrap procedure. Violin plots for counterfactual (blue) and factual (orange) periods for the analogue quality Q **(m)**, the predictability index D **(n)**, the persistence index Θ **(o)** and the distribution of analogues in each month **(p)**. Violin plots for counterfactual (blue) and factual (orange) periods for ENSO **(q)** and AMO **(r)**. Values for the peak day of the extreme event are marked by a blue dot. Horizontal bars in panels **(m)**–**(r)** correspond to the mean (black) and median (red) of the distributions.

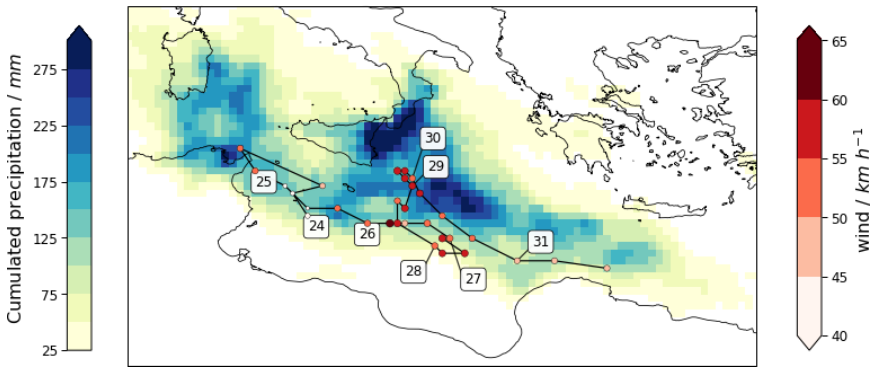

Figure 9. Track and associated precipitation for Apollo. Data from ERA5: track position is retrieved as the local minimum of slp, wind is the maximum wind speed in a 1.5° great-circle distance (GCD) radius of the slp center, precipitation is cumulated between 00:00 UTC on 24 October 2021 and 16:00 UTC on 31 October 2021. Time stamps indicate the first point for each day whose number is indicated.

active low-pressure disturbance. This low-pressure system was isolated near the Balearic Islands around 22 October and then moved to the central Mediterranean Sea, producing self-regenerating thunderstorms in the area of Catania on 24 October. These thunderstorms, which occurred before the extratropical cyclone became a medicane, already resulted in extremely heavy rain and floods in Catania (>400 mm rain in 48 h, estimated by SIAS, 2021). Figure 9 displays the track of the cyclone along its life cycle. During the tropical phase of Apollo, according to the latest report available, at least 10 people were killed by the storm in Sicily, Malta, Algeria and Tunisia (jbarisk, 2021). The highest wind gusts were measured on 29 October ($104\,\mathrm{km\,h^{-1}}$), and the minimum pressure was estimated at 999 hPa. The Sicilian meteorological service (SIAS) measured >200 mm convective precipitation associated with Apollo in the area of Syracuse on the same date. Apollo started to weaken on 30 October 2021 and made landfall near Bayda, Libya, a few days later.

4.7.1 Medicanes and climate change

It is difficult to study trends in frequency and intensity of medicanes under climate change. First of all, our knowledge of historical medicanes is very limited before the satellite era, and they are rare events with an estimated frequency of between 1 and 2 events per year (Cavicchia et al., 2014a). Medicane genesis is favored when an extratropical depression gets isolated from the polar jet stream. This cutoff becomes quasi-stationary on the Mediterranean Sea and can use the large availability of heat and humidity from the sea to produce organized convection. Recent studies of medicanes under climate change have therefore considered two elements: the precursors, namely the cutoff low, and the potential for organized convection once the first condition is met (Cavicchia et al., 2014b; Romero and Emanuel, 2017; Tous et al., 2016). On one hand, a recent study suggests that the jet stream will shift northward (Stendel et al., 2021) and therefore cutoff lows on the Mediterranean Sea may become slightly less frequent. On the other hand, the Mediterranean Sea is warming faster than the larger oceans, increasing the potential for convection once a depression system is present in the area. We then expect to see fewer medicanes but more intense ones (González-Alemán et al., 2019).

4.7.2 Attribution of Medicane Apollo to climate change

We now use the ERA5 dataset to perform the attribution of the cyclonic circulation associated with Apollo in the past and present climates (Fig. 10). We note that we will select analogues independently of the extratropical or tropical nature of the depression that has produced them. The analogue average slp values for both the factual and counterfactual periods (Fig. 10b, c) do not reach slp minima comparable to that of Apollo (Fig. 10a), although this may partly be an effect of averaging maps with cyclones at slightly different locations. The Δslp (Fig. 10d) displays a weak yet significant positive anomaly over the northern part of the domain, indicating that factual analogue cyclones are less deep or southward-shifted relative to counterfactual ones. Furthermore, we observe that temperatures are significantly warmer in the factual world, especially on the island of Sicily and on the southern Mediterranean basin (Fig. 10e–h). This warming is associated with a significant increase in precipitation in the factual period, likely due to the larger availability of heat and humidity from the sea (Fig. 10i–l). These results must be interpreted with care because the analogue quality clearly shows that Apollo's circulation pattern is extremely rare compared with the rest of its analogues (Fig. 10m). Apollo thus appears to be a black swan event. We do not detect remarkable changes in the distributions of the predictability index D (Fig. 10n) or the persistence Θ (Fig. 10o). However, the event itself displays a lower D and higher Θ when these are computed using factual data rather than counterfactual data. This could also have contributed to enhancing the persistence

of precipitation on the same areas. We do see a clear increase in analogues in the month of September in the factual period (Fig. 10p): this is the warmest month for the Mediterranean Sea, hence the most favorable for the development of deep convection in association with cyclonic depressions. This factor can greatly enhance precipitation, especially on the mountain ranges exposed to the winds, as in the case of Apollo, for the Etna and the Peloritani mountain ranges in Sicily. Finally, no significant differences in ENSO (Fig. 10q) and AMO (Fig. 10r) distributions conditioned to analogues have been found between the factual and counterfactual periods.

In keeping with the general trends reported in Sect. 4.7.1, our analysis highlights the potential intensification of precipitation associated with cyclones around the island of Sicily, supported both by higher temperatures and increased occurrence of cyclones in the month of September, the warmest for the Mediterranean Sea. However, we point to the black swan nature of this storm compared to its analogues and therefore to a careful interpretation of the attribution results obtained above.

4.8 Scandinavian cold spell

During late November 2021, Scandinavia experienced record-low temperatures for the season. On 28 November, the Nikkaluokta weather station in Sweden recorded −37.4 °C, which was the lowest November temperature recorded in the country since 1980. Other stations in northern Sweden recorded their lowest November temperatures since the 1950s (SMHI, 2022a). Comparable records occurred in the first days of December. In Norway, the −36.7 °C recorded in Kautokeino was the lowest November reading since 2002 (SMHI, 2022b). These frigid temperatures were part of a broader area of below-average temperatures, peaking in the last week of November and first days of December, and stretching from northwestern Russia all the way to Spain (which recorded one of the top 10 coldest November months on record, AEMET, 2022). The cold spell impacted transports, including suspension of entire train lines (SVT, 2022) and an unusually large number of road accidents in southern Sweden (SVD, 2022).

The cold spell was associated with a large ridge forming over the North Atlantic starting from 23 November and drawing cold Arctic and Siberian air over the continent. A pressure dipole with a high over Scandinavia and a low over central Europe further favored cold air advection. The Atlantic Ridge persisted until early December, after which a more zonal circulation occurred, bringing warmer air masses over large parts of Europe.

4.8.1 Scandinavian cold spells and climate change

As discussed in Sect. 4.2.1, it is virtually certain that there has been a decrease in severity and/or frequency of cold spells in the last several decades, and the consensus is that at a global level this decrease will continue in the future. Scandinavia fits this trend and has shown a significant decrease in wintertime cold days in recent decades (Matthes et al., 2015). In the future, the decrease in wintertime cold days is expected to be stronger than in several other European regions (Dosio, 2016), as is the increase in yearly minimum daily-mean temperature (Bernes, 2017, p. 102).

4.8.2 Attribution of the Scandinavian cold spell to climate change

Figure 11 shows the results of our attribution analysis for the Scandinavian cold spell. The slp analogues suggest that the pressure dipole over Europe seen during the cold spell is quite an unusual configuration and that such a dipole has typically become weaker in the factual period (Fig. 11a–d). The weaker dipole in the analogues during both periods corresponds to warmer t2m compared to the event, but there is only a weak increase in the temperatures of the analogues between the two periods over Scandinavia. The only exceptions are the coastal areas in western and northern Norway (Fig. 11h). There is additionally a strong increase in temperatures over the Norwegian and Greenland seas and northeastern Europe, in keeping with the lower pressure to the north of Scandinavia in the factual period compared to the counterfactual period (Fig. 11d). The lack of a significant warming signal across Scandinavia is coupled to modest changes in the seasonality of the analogues (Fig. 11p) and in precipitation and the associated cloudiness (Fig. 11l). We hypothesize that the cold Siberian air masses contributing to the low Scandinavian temperatures during these events may not have warmed significantly (Cohen et al., 2013).

The quality of the analogues is good and shows little change when moving from the counterfactual to the factual world (Fig. 11m), as does their predictability (Fig. 11n). Interestingly, the unusualness of the slp dipole configuration highlighted in Fig. 11a–c thus does not translate to an unusually poor analogue quality for the event in question. The persistence Θ of the analogue patterns shows a weak increase in the factual period, albeit with no significant change in the distribution; the persistence of the event itself computed on the factual data instead increases sharply relative to that computed on the counterfactual data (Fig. 11o). This provides an alternative hypothesis to explain the weak change in Scandinavian temperatures between the two periods, in addition to the above-discussed weak warming of Siberian air masses. Indeed the longer persistence of the slp pattern – and hence of the cold advection – in the factual period could partly compensate for the effect of warmer air being advected over the region. The increased persistence may be compared to the findings of Matthes et al. (2015), who find no shifts from longer to shorter cold spells in the northern high latitudes, except for a decrease in only the longest episodes.

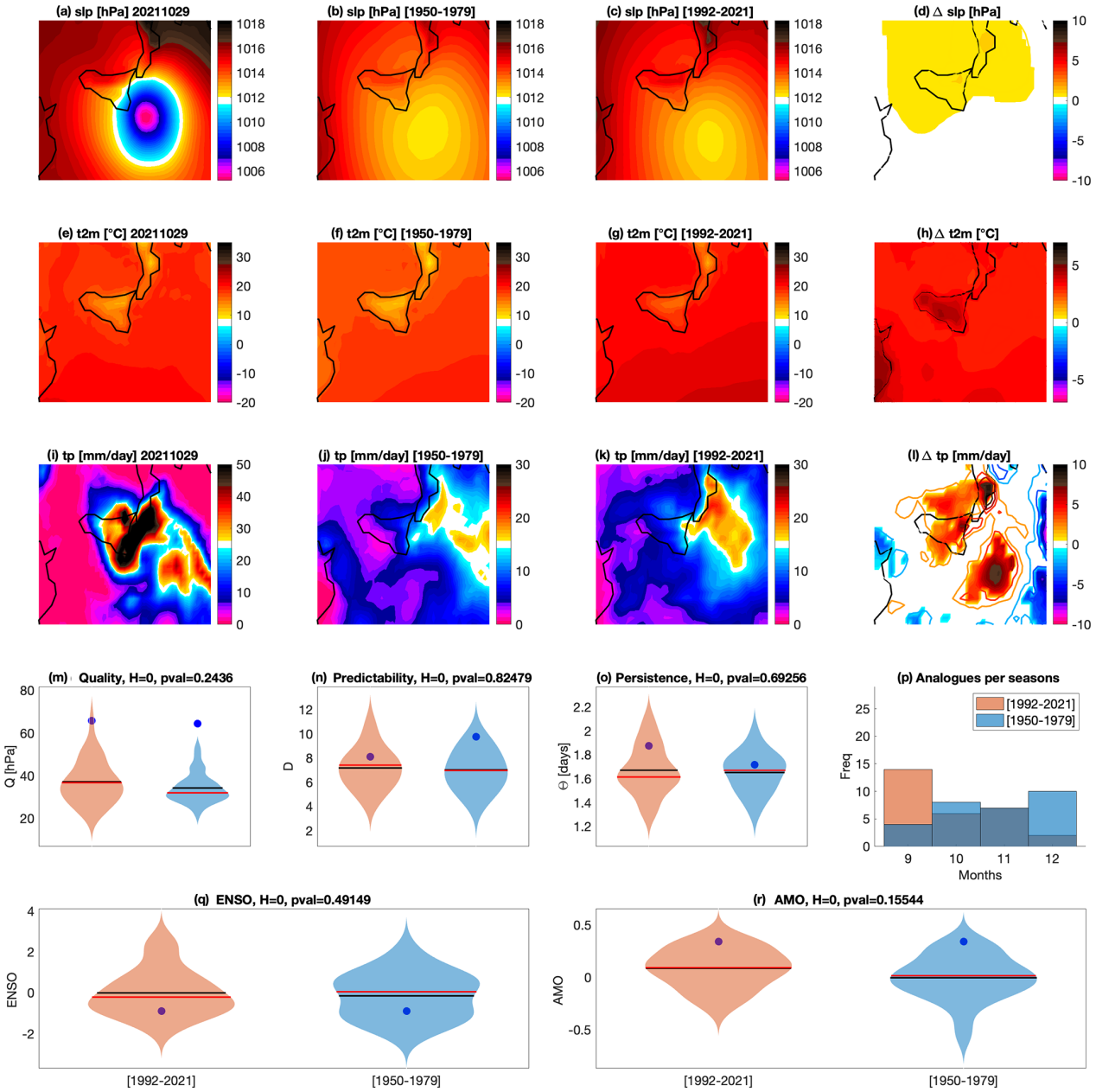

Figure 10. Attribution for the Medicane Apollo on 29 October 2021. Daily mean sea-level pressure slp **(a)**, 2 m temperatures t2m **(e)** and total precipitation tp **(i)** on the day of the event. Average of the 33 sea-level pressure analogues found for the counterfactual [1950–1979] **(b)** and factual [1992–2021] **(c)** periods and corresponding 2 m temperatures **(f, g)** and daily precipitation rate **(j, k)**. Δslp **(d)**, Δt2m **(h)** and Δtp **(l)** between factual and counterfactual periods: colored–filled areas show significant anomalies with respect to the bootstrap procedure. Violin plots for counterfactual (blue) and factual (orange) periods for the analogue quality Q **(m)**, the predictability index D **(n)**, the persistence index Θ **(o)** and the distribution of analogues in each month **(p)**. Violin plots for counterfactual (blue) and factual (orange) periods for ENSO **(q)** and AMO **(r)**. Values for the peak day of the extreme event are marked by a blue dot. Horizontal bars in panels **(m)**–**(r)** correspond to the mean (black) and median (red) of the distributions.

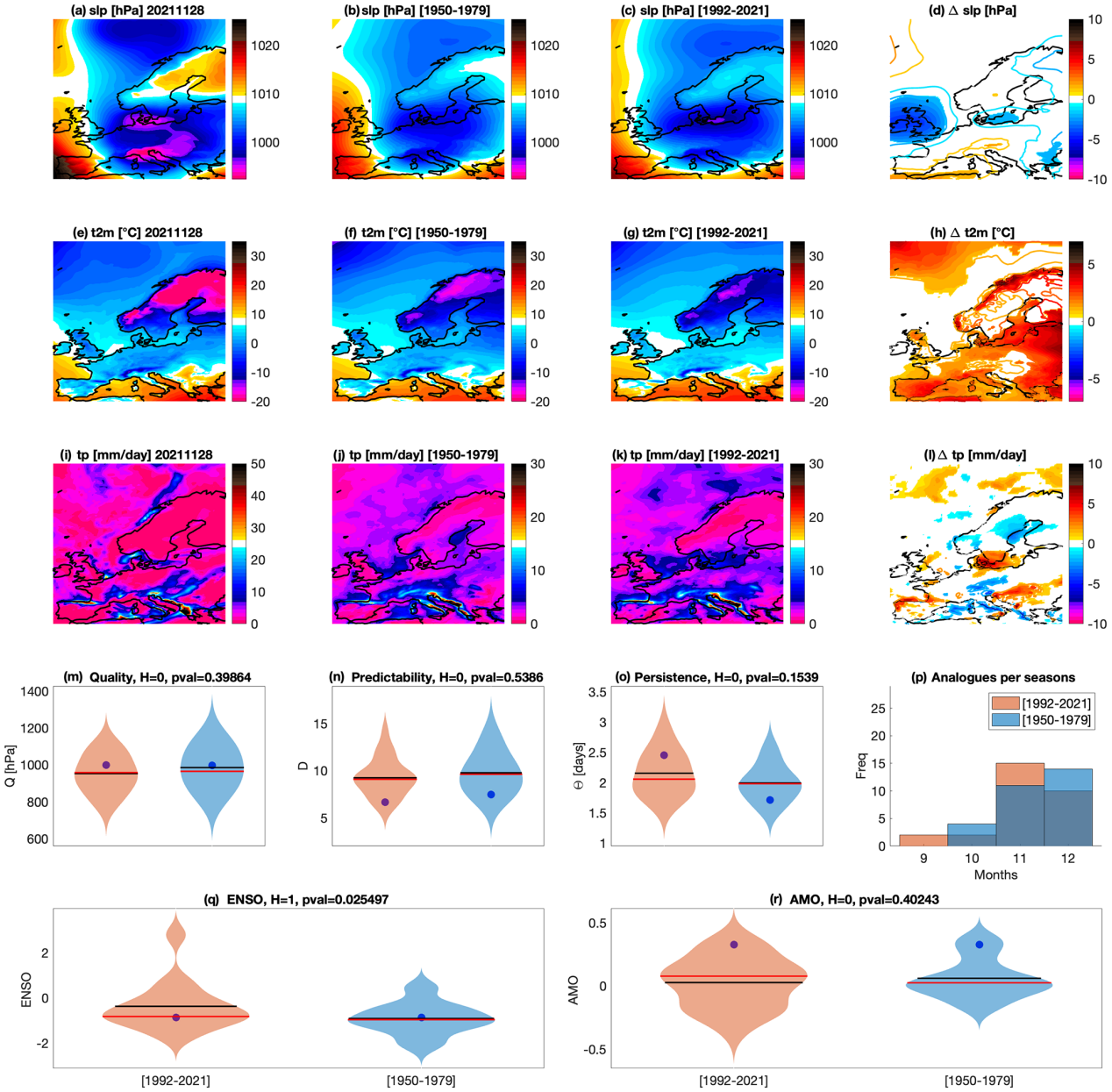

Figure 11. Attribution for the Scandinavian cold spell on 28 November 2021. Daily mean sea-level pressure slp **(a)**, 2 m temperatures t2m **(e)** and total precipitation tp **(i)** on the day of the event. Average of the 33 sea-level pressure analogues found for the counterfactual [1950–1979] **(b)** and factual [1992–2021] **(c)** periods and corresponding 2 m temperatures **(f, g)** and daily precipitation rate **(j, k)**. Δslp **(d)**, Δt2m **(h)** and Δtp **(l)** between factual and counterfactual periods: colored–filled areas show significant anomalies with respect to the bootstrap procedure. Violin plots for counterfactual (blue) and factual (orange) periods for the analogue quality Q **(m)**, the predictability index D **(n)**, the persistence index Θ **(o)** and the distribution of analogues in each month **(p)**. Violin plots for counterfactual (blue) and factual (orange) periods for ENSO **(q)** and AMO **(r)**. Values for the peak day of the extreme event are marked by a blue dot. Horizontal bars in panels **(m)**–**(r)** correspond to the mean (black) and median (red) of the distributions.

Finally, the analogues show a significant change in ENSO distribution, with a weak shift towards more positive ENSO phases in the factual period (Fig. 11q). There is an association between positive ENSO and more severe European winters (e.g., Fraedrich, 1990, 1994), which may provide a further explanation for the lack of significant warming in the factual period analogues. The changes in AMO distribution associated with the analogues in the two periods are inconclusive (Fig. 11r).

Based on the above, we conclude that the atmospheric configuration driving cold spells such as the November 2021 episode has not become more unusual with climate change and that the intensity of the cold spells engendered by similar atmospheric configurations has not weakened significantly, contrary to the decreasing trends observed in data and model simulations for cold days in Scandinavia (Sect. 4.8.1). ENSO may provide some modulation of the cold spell characteristics between the two periods, but based on the moderate changes observed in its association with the cold spell analogues, we deem it unlikely to be the main physical driver of our results. We thus interpret the November 2021 event as a persistent cold extreme in a warming climate.

5 Conclusions

We have analyzed the atmospheric circulation associated with a selection of high-impact extreme events occurring in 2021 from an attribution perspective. Specifically, we have performed a semi-objective selection of a representative circulation pattern for each extreme and have then identified two sets of analogues: the first in the 1950–1979 period, which approximates a counterfactual world; the second in the 1992–2021 period, which approximates a factual world. Regardless the specificity of each event, our analysis evidences the relevant role of atmospheric circulation changes under anthropogenic climate change in controlling the characteristics of many of these events, which is a conclusion of relevance to the broader field of extreme-event attribution.

A second important outcome of this study is to include, in the attribution framework, the systematic use of the dynamical indicators of persistence and predictability. Persistence is of particular interest, since there has been a lively scientific debate on changes in atmospheric persistence and how these may affect extreme events (Coumou and Rahmstorf, 2012; Hoskins and Woollings, 2015; Wehrli et al., 2020).

Finally, we have studied the quality of the analogues – namely the typicality of the analogues relative to the atmospheric variability – and their changes over time. This brings a third relevant outcome, namely the ability to understand whether both a given circulation and its analogues are becoming more or less typical (i.e., have better or worse analogues). The two do not always vary in tandem, meaning that the quality of the analogues for a given extreme may remain unchanged while the analogues of the analogues become better. While not immediate to interpret, this provides some subtle insights into how the configurations conducive to an extreme relate to the broader atmospheric variability typical of a given climate. In the case of Medicane Apollo, the lack of good-quality analogues directly points to the unprecedented nature of this event, making it a black swan among the weather patterns in Europe. It is therefore questionable to attempt any attribution statements in this case. This finding is also a warning that weather extreme events do not necessarily belong to the sample of weather situations observed in the last several decades.

The main limitations of our framework include the somewhat arbitrary choice of the region used to define the analogues, the timescale for the selection of the analogues and the number of analogues retained for analysis. Moreover, only for two of the events – the Po Valley tornado outbreak and Medicane Apollo – is it possible to statistically exclude a role of natural inter-decadal variability of ENSO and AMO in explaining differences in the analogues. We are well aware of these limitations and have designed the study to minimize their impact. The main advantage of working with analogues of sea-level pressure is the possibility of applying expert judgment to select a region that includes the large-scale cyclonic/anticyclonic structures concurring with the event. The use of daily means allows us to average out the daily cycle. Longer timescales have been tested, but they produce worse analogues due to the fact that the synoptic structures move too much and lead to aliased atmospheric patterns. We nonetheless believe that longer timescales could be used to study long-lasting extreme events such as droughts. Furthermore, at daily time resolution information about the stationarity or lack thereof of the patterns is retained in the persistence metric. We have tested the dependence of our results on the number of analogues used and found that numbers between 25 and 50 analogues provide a good balance between having meaningful statistics and selecting good-quality analogues. Finally, we highlight that conventional extreme value attribution shares many of the same limitations, including the choice of the region, thresholds and timescale.

Our approach does not want to substitute extreme-event attributions based on the statistical fitting of extreme value distributions: those approaches can be used to inform stakeholders of changes in return times of extreme events in factual versus counterfactual worlds, and they have been successfully used by the attribution community in a large number of instances (Trenberth et al., 2015; Van Oldenborgh and Van Ulden, 2003; Vautard and Yiou, 2012; Van Oldenborgh et al., 2012; Trenberth et al., 2015; Vautard et al., 2016, 2018). We rather see our analysis as complementing statistical approaches by providing insights on the possible changes over time of the dynamics underlying specific extreme events, as described by National Academies of Sciences, Engineering, and Medicine (2016). Further development of this methodology can include the use of analogues to flag populations of events that share the same dynamical

origin, on the line of research proposed by Jézéquel et al. (2018b) and Shepherd (2019). This would allow us to use the tools of statistical attribution with an additional conditioning from the analogues and to release an automated package that produces these analyses in a matter of minutes as soon as the ERA5 data are available. Other possible extensions include searching for analogues of different observables such as geopotential height, temperature on pressure levels, winds and more. Although valuable, these options must be evaluated with extreme care in the context of attribution because of the non-linear trends already introduced by the anthropogenic forcing on the average of these quantities (Jézéquel et al., 2018a).

To conclude, the analogue approach to extreme-event attribution shows that many extreme events are significantly modified in the present climate with respect to the past, because of changes in the position, persistence and seasonality of cyclonic/anticyclonic patterns. Our approach, complementary to the statistical methods already available in the attribution community, underscores the importance of considering changes in the atmospheric circulation when performing attribution studies.

Appendix A: Predictability and persistence indices

The attractor of a dynamical system is a geometric object defined in the space hosting all the possible states of the system (phase space). Each point ζ on the attractor can be characterized by two dynamical indicators: the local dimension D, which indicates the number of degrees of freedom active locally around ζ, and the persistence Θ, a measure of the mean residence time of the system around ζ (Faranda et al., 2017). To determine D, we exploit recent results from the application of extreme value theory to Poincaré recurrences in dynamical systems. This approach considers long trajectories of a system – in our case successions of daily slp latitude–longitude maps – corresponding to a sequence of states on the attractor. For a given point ζ in phase space (e.g., a given slp map), we compute the probability that the system returns within a ball of radius ϵ centered on the point ζ. The Freitas et al. (2010) theorem, modified by Lucarini et al. (2012), states that logarithmic returns,

$$g(x(t)) = -\log(\mathrm{dist}(x(t), \zeta)), \tag{A1}$$

yield a probability distribution such that

$$\Pr(z > s(q)) \simeq \exp\left[-\vartheta(\zeta)\left(\frac{z-\mu(\zeta)}{\sigma(\zeta)}\right)\right], \tag{A2}$$

where $z = g(x(t))$ and s is a high threshold associated with a quantile q of the series $g(x(t))$. Requiring that the orbit falls within a ball of radius ϵ around the point ζ is equivalent to asking that the series $g(x(t))$ is over the threshold s; therefore, the ball radius ϵ is simply $e^{-s(q)}$. The resulting distribution is the exponential member of the generalized Pareto distribution family. The parameters μ and σ, namely the location and the scale parameter of the distribution, depend on the point ζ in phase space. $\mu(\zeta)$ corresponds to the threshold $s(q)$, while the local dimension $D(\zeta)$ can be obtained via the relation $\sigma = 1/D(\zeta)$. This is the metric of predictability introduced in Sect. 3.

When $x(t)$ contains all the variables of the system, the estimation of D based on extreme value theory has a number of advantages over traditional methods (e.g., the box counting algorithm, Liebovitch and Toth, 1989; Sarkar and Chaudhuri, 1994). First, it does not require us to estimate the volume of different sets in scale space: the selection of $s(q)$ based on the quantile provides a selection of different scales s which depends on the recurrence rate around the point ζ. Moreover, it does not require the a priori selection of the maximum embedding dimension as the observable g is always a univariate time series.

The persistence of the state ζ is measured via the extremal index $0 < \vartheta(\zeta) < 1$, a dimensionless parameter, from which we extract $\Theta(\zeta) = \Delta t/\vartheta(\zeta)$. Here, Δt is the time step of the dataset being analyzed. $\Theta(\zeta)$ is therefore the average residence time of trajectories around ζ, namely the metric of persistence introduced in Sect. 3, and it has units of time (in this study days). If ζ is a fixed point of the attractor, then $\Theta(\zeta) = \infty$. For a trajectory that leaves the neighborhood of ζ at the next time iteration, $\Theta = 1$. To estimate ϑ, we adopt the Süveges estimator (Süveges, 2007). For further details on the extremal index, see Moloney et al. (2019).

Code availability. The code to compute the dynamical indicators of predictability D and persistence θ is available at https://fr.mathworks.com/matlabcentral/fileexchange/95768-attractor-local-dimension-and-local-persistence-computation (last access: 25 October 2022; Faranda, 2022).

Data availability. ERA5 reanalysis is available from the Copernicus Climate Change Service Climate Data Store (https://doi.org/10.24381/cds.bd0915c6, Hersbach et al., 2018).

Author contributions. DF conceived the study, performed the attribution analysis for all events and wrote the section on the Medicane Apollo. SB wrote the section on Hurricane Ida and performed cyclone tracking analyses. MG wrote the section about storm Filomena. MK wrote the section about the Mediterranean heat wave. RN wrote the section about the Westphalia floods. FP wrote the section about the Po Valley tornado outbreak. PY wrote the section about the French spring cold spell. GM wrote the section about the Scandinavian cold spell and contributed to the final drafting of the manuscript. All the authors contributed to writing and reviewing the introduction, methods, and conclusions of the article.

Competing interests. The contact author has declared that none of the authors has any competing interests.

Disclaimer. Publisher's note: Copernicus Publications remains neutral with regard to jurisdictional claims in published maps and institutional affiliations.

Acknowledgements. The authors wish to thank Maria del Carmen Alvarez-Castro, Jacopo Riboldi, Melinda Galfi, Mathieu Vrac, Andreia Hisi, Erika Coppola, Robert Vautard and the two anonymous reviewers for useful discussions and inputs.

Financial support. This research has been supported by the Agence Nationale de la Recherche (grant nos. ANR-19-ERC7-0003 (BOREAS) and ANR-20-CE01-0008-01 (SAMPRACE)), the Centre National de la Recherche Scientifique (MANU project DINCLIC), and the European Union's Horizon 2020 research and innovation program (grant no. 101003469 (XAIDA), European Research Council (ERC) grant no. 948309 (CENÆ), and Marie Skłodowska-Curie grant no. 956396 (EDIPI)).

Review statement. This paper was edited by Peter Knippertz and reviewed by two anonymous referees.

References

AEMET: La ola de calor del puente de agosto'21 y los récords de temperaturas en España, Spanish State Meteorological Agency, https://aemetblog.es/2021/08/18/la-ola-de-calor-del-puente-de-agosto21-y-los-records-de-temperaturas-en-espana/ (last access: 27 January 2022), 2021a.

AEMET: Informe sobre la borrasca Filomena y la ola de frio, Spanish State Meteorological Agency, http://www.aemet.es/documentos/es/conocermas/recursos_en_linea/publicaciones_y_estudios/estudios/Informe_episodio_filomena.pdf (last access: 21 October 2022), 2021b.

AEMET: Noviembre de 2021, un mes muy frío, Spanish State Meteorological Agency https://www.aemet.es/es/noticias/2021/12/resumen_clima_noviembre_2021, last access: 14 January 2022.

Alberoni, P., Nanni, S., Crespi, M., and Monai, M.: The supercell thunderstorm on 8 June 1990: mesoscale analysis and radar observations, Meteorol. Atmos. Phys., 58, 123–138, 1996.

Ali, E., Cramer, W., Carnicer, J., Georgopoulou, E., Hilmi, N., Cozannet, G. L., and P. Lionello, P.: Cross-Chapter Paper 4: Mediterranean Region, in: Climate Change 2022: Impacts, Adaptation and Vulnerability, Contribution of Working Group II to the Sixth Assessment Report of the Intergovernmental Panel on Climate Change, Cambridge University Press Cambridge, UK and New York, NY, USA, 2233–2272, 2022.

Anderson, T. W.: On the distribution of the two-sample Cramer-von Mises criterion, Ann. Math. Stat., 33, 1148–1159, 1962.

Antonescu, B., Schultz, D. M., Holzer, A., and Groenemeijer, P.: Tornadoes in Europe: An underestimated threat, B. Am. Meteorol. Soc., 98, 713–728, 2017.

Aon: Global Catastrophe Recap, http://thoughtleadership.aon.com/documents/20210209_analytics-if-january-global-recap.pdf, last access: 20 January 2021.

Baker, A. J., Hodges, K. I., Schiemann, R. K., and Vidale, P. L.: Historical variability and lifecycles of North Atlantic midlatitude cyclones originating in the tropics, J. Geophys. Res.-Atmos., 126, e2020JD033924, https://doi.org/10.1029/2020JD033924, 2021.

Bala, G., Caldeira, K., and Nemani, R.: Fast versus slow response in climate change: implications for the global hydrological cycle, Clim. Dynam., 35, 423–434, 2010.

BBC: Polar vortex death toll rises to 21 as US cold snap continues, https://www.bbc.com/news/world-us-canada-47088684, last access: 14 January 2022.

Berkovic, S. and Raveh-Rubin, S.: Persistent warm and dry extremes over the eastern Mediterranean during winter: The role of North Atlantic blocking and central Mediterranean cyclones, Q. J. Roy. Meteor. Soc., 148, 2384–2409, 2022.

Bernes, C.: En varmare värld: Växthuseffekten och klimatets förändringar – Tredje upplagan, NATURVÅRDSVERKET, Stockholm, 184 pp., ISBN: 978-91-620-1300-4, 2017.

Blackport, R. and Screen, J. A.: Weakened evidence for mid-latitude impacts of Arctic warming, Nat. Clim. Change, 10, 1065–1066, 2020.

Brooks, H. E., Carbin, G. W., and Marsh, P. T.: Increased variability of tornado occurrence in the United States, Science, 346, 349–352, 2014.

Business Insurance: Recent floods cause nearly $12 billion damage in Belgium, https://www.businessinsurance.com/article/00010101/STORY/912343432/Recent-floods-cause-nearly-$12-billion-damage-in-Belgium, last access: 27 January 2022.

Casson, N. J., Contosta, A. R., Burakowski, E. A., Campbell, J. L., Crandall, M. S., Creed, I. F., Eimers, M. C., Garlick, S., Lutz, D. A., Morison, M. Q., Morzillo, A. T., and Nelson, S. J.: Winter weather whiplash: Impacts of meteorological events misaligned with natural and human Systems in Seasonally Snow-Covered Regions, Earth's Future, 7, 1434–1450, 2019.

Cavicchia, L., von Storch, H., and Gualdi, S.: A long-term climatology of medicanes, Clim. Dynam., 43, 1183–1195, 2014a.

Cavicchia, L., von Storch, H., and Gualdi, S.: Mediterranean tropical-like cyclones in present and future climate, J. Climate, 27, 7493–7501, 2014b.

CEMS: Fire in Castilla y Leon, Spain, COPERNICUS Emergency Management Service, https://emergency.copernicus.eu/mapping/list-of-components/EMSR538 (last access: 31 January 2022), 2021a.

CEMS: Fire in Var, France, COPERNICUS Emergency Management Service, https://emergency.copernicus.eu/mapping/list-of-components/EMSR541 (last access: 31 January 2022), 2021b.

CEMS: The Copernicus Emergency Management Service monitors fire events in the Mediterranean region, COPERNICUS Emergency Management Service, https://emergency.copernicus.eu/mapping/ems/copernicus-emergency-management-service-monitors-fire-events-mediterranean-region (last access: 31 January 2022), 2021c.

Cohen, J., Jones, J., Furtado, J. C., and Tziperman, E.: Warm Arctic, cold continents: A common pattern related to Arctic sea ice melt, snow advance, and extreme winter weather, Oceanography, 26, 150–160, 2013.

Cohen, J., Zhang, X., Francis, J., Jung, T., Kwok, R., Overland, J., Tayler, P. C., Lee, S., Laliberte, F., and Feldstein, S.: Arctic change and possible influence on mid-latitude climate and weather: a US CLIVAR White Paper, US CLIVAR, https://doi.org/10.5065/d6th8kgw, 2018.

Coumou, D. and Rahmstorf, S.: A decade of weather extremes, Nat. Clim. Change, 2, 491–496, 2012.

D'Errico, M., Pons, F., Yiou, P., Tao, S., Nardini, C., Lunkeit, F., and Faranda, D.: Present and future synoptic circulation patterns associated with cold and snowy spells over Italy, Earth Syst. Dynam., 13, 961–992, https://doi.org/10.5194/esd-13-961-2022, 2022.

DieWelt: Hochwasser aktuell: Zahl der Toten in Rheinland-Pfalz steigt auf 135 – Mindestens 184 Opfer durch Flut in Deutschland, https://www.welt.de/vermischtes/article232577293/Hochwasser-Mindestens-166-Tote-in-NRW-Rheinland-Pfalz-und-Bayern.html, last access: 22 July 2021.

Dosio, A.: Projections of climate change indices of temperature and precipitation from an ensemble of bias-adjusted high-resolution EURO-CORDEX regional climate models, J. Geophys. Res.-Atmos., 121, 5488–5511, 2016.

Doss-Gollin, J., Farnham, D. J., Lall, U., and Modi, V.: How unprecedented was the February 2021 Texas cold snap?, Environ. Res. Lett., 16, 064056, https://doi.org/10.1088/1748-9326/ac0278, 2021.

Doswell III, C. A., Brooks, H. E., and Dotzek, N.: On the implementation of the enhanced Fujita scale in the USA, Atmos. Res., 93, 554–563, 2009.

Easterling, D. R., Kunkel, K. E., Wehner, M. F., and Sun, L.: Detection and attribution of climate extremes in the observed record, Weather and Climate Extremes, 11, 17–27, 2016.

Elsner, J. B., Elsner, S. C., and Jagger, T. H.: The increasing efficiency of tornado days in the United States, Clim. Dynam., 45, 651–659, 2015.

Elsner, J. B., Fricker, T., and Schroder, Z.: Increasingly powerful tornadoes in the United States, Geophys. Res. Lett., 46, 392–398, 2019.

Faranda, D.: An attempt to explain recent changes in European snowfall extremes, Weather Clim. Dynam., 1, 445–458, https://doi.org/10.5194/wcd-1-445-2020, 2020.

Faranda, D.: Attractor Local Dimension and Local Persistence computation, version 1.0.0, Matlab © matlab central fileexchange [code], https://fr.mathworks.com/matlabcentral/fileexchange/95768-attractor-local-dimension-and-local-persistence-computation, last access: 25 October 2022.

Faranda, D., Messori, G., and Yiou, P.: Dynamical proxies of North Atlantic predictability and extremes, Sci. Rep., 7, 41278, https://doi.org/10.1038/srep41278, 2017.

Faranda, D., Alvarez-Castro, M. C., Messori, G., Rodrigues, D., and Yiou, P.: The hammam effect or how a warm ocean enhances large scale atmospheric predictability, Nat. Commun., 10, 1–7, 2019a.

Faranda, D., Messori, G., and Vannitsem, S.: Attractor dimension of time-averaged climate observables: insights from a low-order ocean-atmosphere model, Tellus A, 71, 1–11, 2019b.

Faranda, D., Vrac, M., Yiou, P., Jézéquel, A., and Thao, S.: Changes in future synoptic circulation patterns: consequences for extreme event attribution, Geophys. Res. Lett., 47, e2020GL088002, https://doi.org/10.1029/2020GL088002, 2020.

Flannigan, M. D., Stocks, B. J., and Wotton, B. M.: Climate change and forest fires, Sci. Total Environ., 262, 221–229, 2000.

Fraedrich, K.: European grosswetter during the warm and cold extremes of the El Niñco/Southern Oscillation, Int. J. Climatol., 10, 21–31, 1990.

Fraedrich, K.: An ENSO impact on Europe?, Tellus A, 46, 541–552, 1994.

Freitas, A. C. M., Freitas, J. M., and Todd, M.: Hitting time statistics and extreme value theory, Probab. Theory Rel., 147, 675–710, 2010.

Freitas, A. C. M., Freitas, J. M., and Todd, M.: Extreme value laws in dynamical systems for non-smooth observations, J. Stat. Phys., 142, 108–126, 2011.

Freitas, A. C. M., Freitas, J. M., and Vaienti, S.: Extreme Value Laws for sequences of intermittent maps, arXiv [preprint], https://doi.org/10.48550/arXiv.1605.06287, 20 May 2016.

González-Alemán, J. J., Pascale, S., Gutierrez-Fernandez, J., Murakami, H., Gaertner, M. A., and Vecchi, G. A.: Potential increase in hazard from Mediterranean hurricane activity with global warming, Geophys. Res. Lett., 46, 1754–1764, 2019.

Gordon, L. J., Steffen, W., Jönsson, B. F., Folke, C., Falkenmark, M., and Johannessen, Å.: Human modification of global water vapor flows from the land surface, P. Natl. Acad. Sci. USA, 102, 7612–7617, 2005.

Grillakis, M. G.: Increase in severe and extreme soil moisture droughts for Europe under climate change, Sci. Total Environ., 660, 1245–1255, 2019.

Guerreiro, S. B., Dawson, R. J., Kilsby, C., Lewis, E., and Ford, A.: Future heat-waves, droughts and floods in 571 European cities, Environ. Res. Lett., 13, 034009, https://doi.org/10.1088/1748-9326/aaaad3, 2018.

Haarsma, R.: European Windstorm Risk of Post-Tropical Cyclones and the Impact of Climate Change, Geophys. Res. Lett., 48, e2020GL091483, https://doi.org/10.1029/2020GL091483, 2021.

Hanchey, A., Schnall, A., Bayleyegn, T., et al.: Notes from the Field: Deaths Related to Hurricane Ida Reported by Media – Nine States, August 29–September 9, 2021, MMWR Morb Mortal Wkly Rep, 70, 1385–1386, https://doi.org/10.15585/mmwr.mm7039a3, 2021.

Hersbach, H., Bell, B., Berrisford, P., Biavati, G., Horányi, A., Muñoz Sabater, J., Nicolas, J., Peubey, C., Radu, R., Rozum, I., Schepers, D., Simmons, A., Soci, C., Dee, D., and Thépaut, J.-N.: ERA5 hourly data on pressure levels from 1959 to present, Copernicus Climate Change Service (C3S) Climate Data Store (CDS) [data set], https://doi.org/10.24381/cds.bd0915c6, 2018.

Hersbach, H., Bell, B., Berrisford, P., Hirahara, S., Horányi, A., Muñoz-Sabater, J., Nicolas, J., Peubey, C., Radu, R., and Schepers, D.: The ERA5 global reanalysis, Q. J. Roy. Meteor. Soc., 146, 1999–2049, 2020.

Het Laatste Nieuws: Een van de twee laatste vermiste personen na overstromingen in ons land teruggevonden, https://www.hln.be/binnenland/een-van-de-twee-laatste-

vermiste-personen-na-overstromingen-in-ons-land-teruggevonden~a4a4c681/, last access: 29 July 2021.

Hochman, A., Alpert, P., Harpaz, T., Saaroni, H., and Messori, G.: A new dynamical systems perspective on atmospheric predictability: Eastern Mediterranean weather regimes as a case study, Science Advances, 5, eaau0936, https://doi.org/10.1126/sciadv.aau0936, 2019.

Horton, R. M., Mankin, J. S., Lesk, C., Coffel, E., and Raymond, C.: A review of recent advances in research on extreme heat events, Current Climate Change Reports, 2, 242–259, 2016.

Hoskins, B. and Woollings, T.: Persistent extratropical regimes and climate extremes, Current Climate Change Reports, 1, 115–124, 2015.

Huang, B., Thorne, P. W., Banzon, V. F., Boyer, T., Chepurin, G., Lawrimore, J. H., Menne, M. J., Smith, T. M., Vose, R. S., and Zhang, H.-M.: Extended reconstructed sea surface temperature, version 5 (ERSSTv5): upgrades, validations, and intercomparisons, J. Climate, 30, 8179–8205, 2017.

IPCC: Summary for Policymakers, in: Climate Change 2021: The Physical Science Basis. Contribution of Working Group I to the Sixth Assessment Report of the Intergovernmental Panel on Climate Change, edited by: Masson-Delmotte, V., Zhai, P., Pirani, A., Connors, S. L., Péan, C., Berger, S., Caud, N., Chen, Y., Goldfarb, L., Gomis, M. I., Huang, M., Leitzell, K., Lonnoy, E., Matthews, J. B. R., Maycock, T. K., Waterfield, T., Yelekçi, O., Yu, R., and Zhou, B., Cambridge University Press, Cambridge, United Kingdom and New York, NY, USA, 3–32, 2021.

jbarisk: Hurricane-like storm causes flooding in the Mediterranean, October 2021, https://www.jbarisk.com/flood-services/event-response/medicane-apollo (last access: 1 February 2022), 2021.

Jézéquel, A., Cattiaux, J., Naveau, P., Radanovics, S., Ribes, A., Vautard, R., Vrac, M., and Yiou, P.: Trends of atmospheric circulation during singular hot days in Europe, Environ. Res. Lett., 13, 054007, https://doi.org/10.1088/1748-9326/aab5da, 2018a.

Jézéquel, A., Dépoues, V., Guillemot, H., Trolliet, M., Vanderlinden, J.-P., and Yiou, P.: Behind the veil of extreme event attribution, Climatic Change, 149, 367–383, https://doi.org/10.1007/s10584-018-2252-9, 2018b.

Jolly, E., D'Andrea, F., Rivière, G., and Fromang, S.: Linking warm Arctic winters, Rossby waves and Cold Spells: an idealized numerical study, J. Atmos. Sci., 78, 2783–2799, https://doi.org/10.1175/JAS-D-20-0088.1, 2021.

Junghänel, T., Bissolli, P., Daßler, J., Fleckenstein, R., Imbery, F., Janssen, W., Kaspar, F., Lengfeld, K., Leppelt, T., Rauthe, M., Dietze, M., Bell, R., Ozturk, U., Cook, K. L., Andermann, C., Beer, A. R., Damm, B., Lucia, A., Fauer, F. S., Nissen, K. M., Sieg, T., and Thieken, A. H: Hydro-klimatologische Einordnung der Stark-und Dauerniederschläge in Teilen Deutschlands im Zusammenhang mit dem Tiefdruckgebiet "Bernd" vom 12. bis 19. Juli 2021, Deutscher Wetterdienst, https://www.dwd.de/DE/leistungen/besondereereignisse/niederschlag/20210721_bericht_starkniederschlaege_tief_bernd.pdf (last access: 25 October 2022), 2021.

Kautz, L.-A., Polichtchouk, I., Birner, T., Garny, H., and Pinto, J. G.: Enhanced extended-range predictability of the 2018 late-winter Eurasian cold spell due to the stratosphere, Q. J. Roy. Meteor. Soc., 146, 1040–1055, 2020.

Kennedy, D., Parker, T., Woollings, T., Harvey, B., and Shaffrey, L.: The response of high-impact blocking weather systems to climate change, Geophys. Res. Lett., 43, 7250–7258, 2016.

Knapp, K. R., Kruk, M. C., Levinson, D. H., Diamond, H. J., and Neumann, C. J.: The international best track archive for climate stewardship (IBTrACS) unifying tropical cyclone data, B. Am. Meteorol. Soc., 91, 363–376, 2010.

Knapp, K. R., Diamond, H. J., Kossin, J. P., Kruk, M. C., and Schreck III, C. J.: International Best Track Archive for Climate Stewardship (IBTrACS) Project, Version 4, NOAA National Centers for Environmental Information, https://doi.org/10.25921/82ty-9e16, 2018.

Knutson, T., Kossin, J., Mears, C., Perlwitz, J., and Wehner, M.: Detection and attribution of climate change, in: Climate Science Special Report: A Sustained Assessment Activity of the U.S. Global Change Research Program, edited by: Wuebbles, D. J., Fahey, D. W., Hibbard, K. A., Dokken, D. J., Stewart, B. C., and Maycock, T. K., U.S. Global Change Research Program, Washington, DC, USA, 160–185, 2017.

Knutson, T., Camargo, S. J., Chan, J. C., Emanuel, K., Ho, C.-H., Kossin, J., Mohapatra, M., Satoh, M., Sugi, M., Walsh, K., and Wu, L.: Tropical cyclones and climate change assessment: Part I: Detection and attribution, B. Am. Meteorol. Soc., 100, 1987–2007, 2019.

Knutson, T., Camargo, S. J., Chan, J. C., Emanuel, K., Ho, C.-H., Kossin, J., Mohapatra, M., Satoh, M., Sugi, M., Walsh, K., and Wu, L.: Tropical cyclones and climate change assessment: Part II: Projected response to anthropogenic warming, B. Am. Meteorol. Soc., 101, E303–E322, 2020.

Kodra, E., Steinhaeuser, K., and Ganguly, A. R.: Persisting cold extremes under 21st-century warming scenarios, Geophys. Res. Lett., 38, L08705, https://doi.org/10.1029/2011GL047103, 2011.

Kornhuber, K. and Tamarin-Brodsky, T.: Future changes in Northern Hemisphere summer weather persistence linked to projected Arctic warming, Geophys. Res. Lett., 48, e2020GL091603, https://doi.org/10.1029/2020GL091603, 2021.

Kral-O'Brien, K. C., O'Brien, P. L., and Harmon, J. P.: Need for false spring research in the Northern Great Plains, USA, Agricultural & Environmental Letters, 4, 190025, https://doi.org/10.2134/ael2019.07.0025, 2019.

Kreienkamp, F., Philip, S. Y., Tradowsky, J. S., Kew, S. F., Lorenz, P., Arrighi, J., Belleflamme, A., Bettmann, T., Caluwaerts, S., Chan, S. C., Ciavarella, A., De Cruz, L., De Vries, H., Demuth, N., Ferrone, A., Fischer, E. M., Fowler, H. J., Görgen, K., Heinrich, D., Henrichs, Y., Lenderink, G., Kaspar, F., Nilson, E., Otto, F. E. L., Ragone, F., Seneviratne, S. I., Singh, R. K., Skålevåg, A., Termonia, P., Thalheimer, L., Van Aalst, M., Van den Bergh, J., Van de Vyver, H., Vannitsem, S., Van Oldenborgh, G. J., Van Schaeybroeck, B., Vautard, R., Vonk, D., and Wanders, N.: Rapid attribution of heavy rainfall events leading to the severe flooding in Western Europe during July 2021, World Weather Atribution, 1–51, https://www.worldweatherattribution.org/wp-content/uploads/Scientific-report-Western-Europe-floods-2021-attribution.pdf (last access: 25 October 2022), 2021.

Kundzewicz, Z. W., Pińskwar, I., and Brakenridge, G. R.: Changes in river flood hazard in Europe: a review, Hydrol. Res., 49, 294–302, 2018.

Kundzewicz, Z. W., Szwed, M., and Pińskwar, I.: Climate variability and floods – A global review, Water, 11, 1399, https://doi.org/10.3390/w11071399, 2019.

LaChaineMeteo: Bilan climatique d'avril 2021: entre sécheresse et records de froid, https://actualite.lachainemeteo.com/actualite-meteo/2021-05-05/bilan-climatique-d-avril-2021-entre-secheresse-et-records-de-froid-59270 (last access: 1 February 2022), 2021.

Lee, J.-Y., Marotzke, J., Bala, G., Cao, L., Corti, S., Dunne, J., Engelbrecht, F., Fischer, E., Fyfe, J., Jones, C., Maycock, A., Mutemi, J., Ndiaye, O., Panickal, S., and Zhou, T.: Future Global Climate: Scenario-Based Projections and Near-Term Information, in: Climate Change 2021: The Physical Science Basis. Contribution of Working Group I to the Sixth Assessment Report of the Intergovernmental Panel on Climate Change, edited by: Masson-Delmotte, V., Zhai, P., Pirani, A., Connors, S. L., Péan, C., Berger, S., Caud, N., Chen, Y., Goldfarb, L., Gomis, M. I., Huang, M., Leitzell, K., Lonnoy, E., Matthews, J. B. R., Maycock, T. K., Waterfield, T., Yelekçi, O., Yu, R., and Zhou, B., Cambridge University Press, Cambridge, United Kingdom and New York, NY, USA, 553–672, 2021.

Lee, S. H. and Butler, A. H.: The 2018–2019 Arctic stratospheric polar vortex, Weather, 75, 52–57, 2020.

LeMonde: La vague de froid se poursuit en Europe et fait des dizaines de morts, https://www.lemonde.fr/climat/article/2018/02/28/la-vague-de-froid-se-poursuit-en-europe-et-fait-des-dizaines-de-morts_5263856_1652612.html (last access: 14 January 2022), 2018.

Liebovitch, L. S. and Toth, T.: A fast algorithm to determine fractal dimensions by box counting, Phys. Lett. A, 141, 386–390, 1989.

Lillo, S. P., Cavallo, S. M., Parsons, D. B., and Riedel, C.: The Role of a Tropopause Polar Vortex in the Generation of the January 2019 Extreme Arctic Outbreak, J. Atmos. Sci., 78, 2801–2821, 2021.

Lloyd, E. A. and Oreskes, N.: Climate Change Attribution: When Is It Appropriate to Accept New Methods?, Earth's Future, 6, 311–325, 2018.

Lucarini, V., Faranda, D., and Wouters, J.: Universal behaviour of extreme value statistics for selected observables of dynamical systems, J. Stat. Phys., 147, 63–73, 2012.

Lucarini, V., Faranda, D., Freitas, A. C. M., Freitas, J. M., Holland, M., Kuna, T., Nicol, M., Todd, M., and Vaienti, S.: Extremes and recurrence in dynamical systems, John Wiley & Sons, ISBN 978-1-118-63219-2, 2016.

Madsen, H., Lawrence, D., Lang, M., Martinkova, M., and Kjeldsen, T.: Review of trend analysis and climate change projections of extreme precipitation and floods in Europe, J. Hydrol., 519, 3634–3650, 2014.

Matthes, H., Rinke, A., and Dethloff, K.: Recent changes in Arctic temperature extremes: warm and cold spells during winter and summer, Environ. Res. Lett., 10, 114020, https://doi.org/10.1088/1748-9326/10/11/114020, 2015.

Mazzoleni, M.: Cronaca meteo 3Bmeteo – Caldo storico in Sicilia, raggiunti i 49 °C: è il nuovo record Europeo, https://www.3bmeteo.com/giornale-meteo/cronaca-meteo—caldo-storico-in-sicilia–raggiunti-i-49-c—-il-nuovo-record-europeo-504610 (last access: 21 October 2022), 2021.

Messori, G., Caballero, R., and Faranda, D.: A dynamical systems approach to studying midlatitude weather extremes, Geophys. Res. Lett., 44, 3346–3354, 2017.

Meteoweb: Medicane Apollo, Aeronautica: per la prima volta un consorzio di Paesi europei ha dato un nome ufficiale ad un evento meteorologico, https://www.meteoweb.eu/2021/10/medicane-apollo-per-la-prima-volta-un-nome-ufficiale/1734332/ (last access: 27 January 2022), 2021.

Michaelis, A. C. and Lackmann, G. M.: Climatological changes in the extratropical transition of tropical cyclones in high-resolution global simulations, J. Climate, 32, 8733–8753, 2019.

Michelangeli, P.-A., Vautard, R., and Legras, B.: Weather regimes: Recurrence and quasi stationarity, J. Atmos. Sci., 52, 1237–1256, 1995.

Miller, B.: These US cities had the coldest morning in decades – with some reaching all-time record lows, CNN, https://edition.cnn.com/2021/02/16/us/record-cold-weather-us-trnd/index.html, last access: 14 January 2022.

Mitchell, D., Heaviside, C., Vardoulakis, S., Huntingford, C., Masato, G., Guillod, B. P., Frumhoff, P., Bowery, A., Wallom, D., and Allen, M.: Attributing human mortality during extreme heat waves to anthropogenic climate change, Environ. Res. Lett., 11, 074006, https://doi.org/10.1088/1748-9326/11/7/074006, 2016.

Molina, M., Sánchez, E., and Gutiérrez, C.: Future heat waves over the Mediterranean from an Euro-CORDEX regional climate model ensemble, Sci. Rep., 10, 1–10, 2020.

Moloney, N. R., Faranda, D., and Sato, Y.: An overview of the extremal index, Chaos, 29, 022101, https://doi.org/10.1063/1.5079656, 2019.

Mori, M., Watanabe, M., Shiogama, H., Inoue, J., and Kimoto, M.: Robust Arctic sea-ice influence on the frequent Eurasian cold winters in past decades, Nat. Geosci., 7, 869–873, 2014.

National Academies of Sciences, Engineering, and Medicine: Attribution of Extreme Weather Events in the Context of Climate Change, The National Academies Press, Washington, DC, https://doi.org/10.17226/21852, 2016.

Naveau, P., Hannart, A., and Ribes, A.: Statistical methods for extreme event attribution in climate science, Annu. Rev. Stat. Appl., 7, 89–110, 2020.

NCDC/NOAA: Billion-Dollar Weather and Climate Disasters, https://www.ncdc.noaa.gov/billions/events/US/2021 (last access: 31 January 2022), 2021.

NCEP/CPC: PSL Data: CPC Unified Gauge-Based Analysis of Daily Precipitation over CONUS RT: NOAA Physical Sciences Laboratory, https://psl.noaa.gov/data/gridded/data.unified.daily.conus.html, last access: 25 January 2022.

NHC/NOAA: Costliest U.S. tropical cyclones tables updated, https://www.nhc.noaa.gov/news/UpdatedCostliest.pdf (last access: 31 January 2022), 2018.

NHC/NOAA: National Hurricane Center – Hurricane IDA Advisory Archive, https://www.nhc.noaa.gov/archive/2021/IDA.shtml (last access: 31 January 2022), 2021.

Pendergrass, A. G., Knutti, R., Lehner, F., Deser, C., and Sanderson, B. M.: Precipitation variability increases in a warmer climate, Sci. Rep., 7, 1–9, 2017.

Poli, V. and Stanzani, R.: Rapporto dell'evento meteorologico del 19 e 20 settembre 2021, Arpae Emilia-Romagna – Struttura Idro-Meteo-Clima, https://allertameteo.regione.emilia-romagna.it/documents/20181/437770/Evento+19-20+settembre+2021.pdf/

ff3ed88f-773d-06e9-eb02-d0a306ae9121?t=1633503536867, last access: 26 January 2022.

Priestley, M. D. K. and Catto, J. L.: Future changes in the extratropical storm tracks and cyclone intensity, wind speed, and structure, Weather Clim. Dynam., 3, 337–360, https://doi.org/10.5194/wcd-3-337-2022, 2022.

Román-Palacios, C. and Wiens, J. J.: Recent responses to climate change reveal the drivers of species extinction and survival, P. Natl. Acad. Sci. USA, 117, 4211–4217, 2020.

Romero, R. and Emanuel, K.: Climate change and Hurricane-like extratropical cyclones: Projections for North Atlantic polar lows and medicanes based on CMIP5 models, J. Climate, 30, 279–299, 2017.

Sainsbury, E. M., Schiemann, R. K., Hodges, K. I., Shaffrey, L. C., Baker, A. J., and Bhatia, K. T.: How important are post-tropical cyclones for European windstorm risk?, Geophys. Res. Lett., 47, e2020GL089853, https://doi.org/10.1029/2020GL089853, 2020.

Sarkar, N. and Chaudhuri, B. B.: An efficient differential box-counting approach to compute fractal dimension of image, IEEE T. syst. man cyb., 24, 115–120, 1994.

Seneviratne, S., Zhang, X., Adnan, M., Badi, W., Dereczynski, C., Luca, A. D., Ghosh, S., Iskandar, I., Kossin, J., Lewis, S., Otto, F., Pinto, I., Satoh, M., Vicente-Serrano, S., Wehner, M., and Zhou, B.: Weather and Climate Extreme Events in a Changing Climate., in: Climate Change 2021: The Physical Science Basis. Contribution of Working Group I to the Sixth Assessment Report of the Intergovernmental Panel on Climate Change, edited by: Masson-Delmotte, V., Zhai, P., Pirani, A., Connors, S. L., Péan, C., Berger, S., Caud, N., Chen, Y., Goldfarb, L., Gomis, M. I., Huang, M., Leitzell, K., Lonnoy, E., Matthews, J. B. R., Maycock, T. K., Waterfield, T., Yelekçi, O., Yu, R., and Zhou, B., Cambridge University Press, Cambridge, United Kingdom and New York, NY, USA, 1513–1766, 2021.

Sharmila, S. and Walsh, K.: Recent poleward shift of tropical cyclone formation linked to Hadley cell expansion, Nat. Clim. Change, 8, 730–736, 2018.

Shepherd, T. G.: Atmospheric circulation as a source of uncertainty in climate change projections, Nat. Geosci., 7, 703–708, https://doi.org/10.1038/ngeo2253, 2014.

Shepherd, T. G.: A Common Framework for Approaches to Extreme Event Attribution, Current Climate Change Reports, 2, 28–38, https://doi.org/10.1007/s40641-016-0033-y, 2016.

Shepherd, T. G.: Storyline approach to the construction of regional climate change information, P. Roy. Soc. A, 475, 20190013, https://doi.org/10.1098/rspa.2019.0013, 2019.

SIAS: SMI: Italian meteorological society: 11 Agosto 2021: 48,8 °C presso Siracusa, possibile nuovo record di caldo italiano ed Europeo, Servizio Informativo Agrometeorologico Siciliano, http://www.sias.regione.sicilia.it/frameset_dati.htm (last access: 27 January 2022), 2021.

SMHI: November 2021 – Nästan rekordkall avslutning, https://www.smhi.se/klimat/klimatet-da-och-nu/manadens-vader-och-vatten-sverige/manadens-vader-i-sverige/november-2021-nastan-rekordkall-avslutning-1.176606, last access: 14 January 2022a.

SMHI: November 2021 – La Niña bidrog till översvämningar i sydvästra Kanada, https://www.smhi.se/klimat/klimatet-da-och-nu/manadens-vader-i-varlden/november-2021-la-nina-bidrog-till-oversvamningar-i-sydvastra-kanada-1.176603, last access: 14 January 2022b.

Spinoni, J., Barbosa, P., Bucchignani, E., Cassano, J., Cavazos, T., Christensen, J. H., Christensen, O. B., Coppola, E., Evans, J., Geyer, B., Giorgi, F., Hadjinicolaou, P., Jacob, D., Katzfey, J., Koenigk, T., Laprise, R., Lennard, C. J., Kurnaz, M. L., Li, D., Llopart, M., McCormick, N., Naumann, G., Nikulin, G., Ozturk, T., Panitz, H.-J., da Rocha, R. P., Rockel, B., Solman, S. A., Syktus, J., Tangang, F., Teichmann, C., Vautard, R., Vogt, J. V., Winger, K., Zittis, G., and Dosio, A.: Future Global Meteorological Drought Hot Spots: A Study Based on CORDEX Data, J. Climate, 33, 3635–3661, https://doi.org/10.1175/JCLI-D-19-0084.1, 2020.

Stefanon, M., D'Andrea, F., and Drobinski, P.: Heatwave classification over Europe and the Mediterranean region, Environ. Res. Lett., 7, 014023, https://doi.org/10.1088/1748-9326/7/1/014023, 2012.

Stendel, M., Francis, J., White, R., Williams, P. D., and Woollings, T.: The jet stream and climate change, in: Climate Change, Elsevier, 327–357, https://doi.org/10.1016/B978-0-12-821575-3.00015-3, 2021.

Süveges, M.: Likelihood estimation of the extremal index, Extremes, 10, 41–55, 2007.

SVD: Oväder drar österut – flera trafikolyckor, https://www.svd.se/fortsatta-snoproblem-i-soder, last access: 14 January 2022.

SVT: Tågtrafik i Norrbotten ställs in – för kallt att köra, https://www.svt.se/nyheter/lokalt/norrbotten/tagtrafik-i-norrbotten-stalls-in-for-kallt-att-kora, last access: 14 January 2022.

Tamarin-Brodsky, T., Hodges, K., Hoskins, B. J., and Shepherd, T. G.: A Dynamical Perspective on Atmospheric Temperature Variability and Its Response to Climate Change, J. Climate, 32, 1707–1724, 2019.

Tous, M., Zappa, G., Romero, R., Shaffrey, L., and Vidale, P. L.: Projected changes in medicanes in the HadGEM3 N512 high-resolution global climate model, Clim. Dynam., 47, 1913–1924, 2016.

Trenberth, K. E.: Attribution of climate variations and trends to human influences and natural variability, Wiley Interdisciplinary Reviews: Climate Change, 2, 925–930, 2011.

Trenberth, K. E., and Shea, D. J.: Atlantic hurricanes and natural variability in 2005, Geophys. Res. Lett., 33, L12704, https://doi.org/10.1029/2006GL026894, 2006.

Trenberth, K. E., Fasullo, J. T., and Shepherd, T. G.: Attribution of climate extreme events, Nature Clim. Change, 5, 725–730, https://doi.org/10.1038/nclimate2657, 2015.

Ulbrich, U., Leckebusch, G. C., and Pinto, J. G.: Extra-tropical cyclones in the present and future climate: a review, Theor. Appl. Climatol., 96, 117–131, 2009.

Van Oldenborgh, G. J. and Van Ulden, A.: On the relationship between global warming, local warming in the Netherlands and changes in circulation in the 20th century, Int. J. Climatol., 23, 1711–1724, 2003.

Van Oldenborgh, G. J., Van Urk, A., and Allen, M.: The absence of a role of climate change in the 2011 Thailand floods, B. Am. Meteorol. Soc, 93, 1047–1049, 2012.

Van Oldenborgh, G. J., Mitchell-Larson, E., Vecchi, G. A., De Vries, H., Vautard, R., and Otto, F.: Cold waves are get-

ting milder in the northern midlatitudes, Environ. Res. Lett., 14, 114004, https://doi.org/10.1088/1748-9326/ab4867, 2019.

van Oldenborgh, G. J., van der Wiel, K., Kew, S., Philip, S., Otto, F., Vautard, R., King, A., Lott, F., Arrighi, J., Singh, R., and van Aalst, M.: Pathways and pitfalls in extreme event attribution, Climatic Change, 166, 1–27, 2021.

Vautard, R. and Yiou, P.: ATTRIBUTION Robustness of warming attribution, Nat. Clim. Change, 2, 26–27, 2012.

Vautard, R., Yiou, P., Otto, F., Stott, P., Christidis, N., Oldenborgh, G. J. V., and Schaller, N.: Attribution of human-induced dynamical and thermodynamical contributions in extreme weather events, Environ. Res. Lett., 11, 114009, https://doi.org/10.1088/1748-9326/11/11/114009, 2016.

Vautard, R., Colette, A., Van Meijgaard, E., Meleux, F., van Oldenborgh, G. J., Otto, F., Tobin, I., and Yiou, P.: Attribution of Wintertime Anticyclonic Stagnation Contributing to Air Pollution in Western Europe, B. Am. Meteorol. Soc., 99, S70–S75, 2018.

Vautard, R., van Oldenborg, G., Bonnet, R., Li, S., Robin, Y., Kew, S., Philip, S., Soubeyroux, J., Dubuisson, B., N, V., Riechstein, M., and Otto, F.: Human influence on growing period frosts like the early april 2021 in Central France, World Weather Attribution, https://www.worldweatherattribution.org/wp-content/uploads/GrowingPeriodFrost2021.pdf (last access: 31 January 2022), 2021.

Walker, E., Mitchell, D., and Seviour, W.: The numerous approaches to tracking extratropical cyclones and the challenges they present, Weather, 75, 336–341, 2020.

Wehrli, K., Hauser, M., and Seneviratne, S. I.: Storylines of the 2018 Northern Hemisphere heatwave at pre-industrial and higher global warming levels, Earth Syst. Dynam., 11, 855–873, https://doi.org/10.5194/esd-11-855-2020, 2020.

WMO: État du climat en 2021: des phénomènes météorologiques extrêmes et de lourdes conséquences, World Meteorological Organisation [data set], https://public.wmo.int/fr/medias/communiques-de-presse/etat-du-climat-en-2021-des-phenomenes-meteorologiques-extremes-et-de (last access: 27 January 2022), 2021.

Ye, K. and Messori, G.: Two leading modes of wintertime atmospheric circulation drive the recent warm Arctic–cold Eurasia temperature pattern, J. Climate, 33, 5565–5587, 2020.

Yiou, P., Jézéquel, A., Naveau, P., Otto, F. E. L., Vautard, R., and Vrac, M.: A statistical framework for conditional extreme event attribution, Adv. Stat. Clim. Meteorol. Oceanogr., 3, 17–31, https://doi.org/10.5194/ascmo-3-17-2017, 2017.

Yiou, S., Balembois, F., Schaffers, K., and Georges, P.: Efficient laser operation of an Yb:S-FAP crystal at 985 nm, Appl. Optics, 42, 4883–4886, 2003.

Zappa, G., Shaffrey, L. C., Hodges, K. I., Sansom, P. G., and Stephenson, D. B.: A Multimodel Assessment of Future Projections of North Atlantic and European Extratropical Cyclones in the CMIP5 Climate Models, J. Climate, 26, 5846–5862, 2013.

Zscheischler, J., Martius, O., Westra, S., Bevacqua, E., Raymond, C., Horton, R. M., van den Hurk, B., AghaKouchak, A., Jézéquel, A., and Mahecha, M. D.: A typology of compound weather and climate events, Nat. Rev. Earth Environ., 1, 333–347, https://doi.org/10.1038/s43017-020-0060-z, 2020.

npj | climate and atmospheric science

www.nature.com/npjclimatsci

ARTICLE OPEN

Check for updates

Attributing Venice Acqua Alta events to a changing climate and evaluating the efficacy of MoSE adaptation strategy

Davide Faranda[1,2,3]✉, Mireia Ginesta[1], Tommaso Alberti[4], Erika Coppola[5] and Marco Anzidei[4]

We use analogues of atmospheric patterns to investigate changes in four devastating Acqua Alta (flooding) events in the lagoon of Venice associated with intense Mediterranean cyclones occurred in 1966, 2008, 2018 and 2019. Our results provide evidence that changes in atmospheric circulation, although not necessarily only anthropogenically driven, are linked to the severity of these events. We also evaluate the cost and benefit of the MoSE system, which was designed to protect against flooding. Our analysis shows that the MoSE has already provided protection against analogues of the most extreme event, which occurred in 1966. These findings have significant implications for the future of Venice and other coastal cities facing similar challenges from rising sea levels due to extreme events. This study also provides a pathway to evaluate the effectiveness of adaptation in a scenario more frequent and intense extreme events if higher global warming levels will be reached.

npj Climate and Atmospheric Science (2023)6:181; https://doi.org/10.1038/s41612-023-00513-0

INTRODUCTION

The Acqua Alta events in Venice have caused significant damage to the cultural and economic heritage of the city over the years[1]. These events, which involve the flooding of the city's streets and buildings, have become increasingly frequent and severe in recent decades[2,3]. The three most devastating Acqua Alta events in terms of costs and damages occurred on 04/11/1966, 29/10/2018, and 12/11/2019, and have particularly impacted the city's cultural and economic heritage[4] and a forth one from a comparable sea levels high but less devastating occurred on 01/12/2008. The 1966 event[5], also known as the "Great Flood of Venice", caused widespread damage to buildings and artworks, including the historic St. Mark's Basilica. The 2018 and 2019 events, which occurred within a year of each other, caused significant damage to the city's cultural landmarks and businesses, including the iconic Caffè Florian and many of the city's historic shops[6]. Figure 1 provides a schematic representation of the hazards faced by the Venice lagoon due to rising sea levels. It shows the relationship between sea level, flooded area, and estimated damages. An empirical approach has been used to estimate the relation between the sea level reached within the lagoon and the economic damages based on data available for the four most devastating events. An analytical function was designed using an exponential law to link economic damage and observed sea level change. The parameters of the fit were estimated using the Levenberg-Marquardt algorithm and assessed for robustness using the Least Absolute Residuals method (see Methods). Figure 1 also highlights significant flooding levels, such as the level at which foodbridges are needed to walk across St. Mark's square and the level at which water enters the St. Mark's Basilica.

Acqua Alta events in Venice result from a complex interplay of various factors, as documented in literature[7,8]. These events involve high tides, which are influenced by natural phenomena such as the moon's position and phases, as well as the gravitational forces exerted by other celestial bodies. However, when strong winds blow across the Adriatic Sea towards the Venetian Lagoon, they can cause an increase in the water level, known as storm surge. This is because the winds push the water towards the city and the narrow entrance of the lagoon limits its ability to escape. The synoptic weather situation that causes these strong winds is typically a low-pressure system over the Tyrrhenian Sea, known as Genoa Low. If combined with high-pressure systems over central and northern Europe, this creates a strong pressure gradient and thus strong winds blowing towards Venice, causing potentially hazardous conditions. The impacts of the Genoa Low system as well as Mediterranean cyclones have been widely documented in literature[9–13], emphasising the importance of understanding this synoptic weather pattern in leading extreme events[14,15].

Climate change is widely considered to be a major contributing factor to the increased frequency and severity of extreme weather events, including storm surges and flooding[16]. The Intergovernmental Panel on Climate Change (IPCC) has stated that the increasing frequency and severity of extreme weather events are very likely caused by human activities, including the burning of fossil fuels and the resultant emissions of greenhouse gases[17]. These activities have led to changes in the Earth's climate, which have in turn altered storm patterns, increased sea levels, and caused more frequent and severe weather events[17]. Coastal zones, such as the historical city of Venice and its lagoon in the Northern Adriatic Sea, are particularly vulnerable to extreme sea levels, requiring a realistic approach to assess the risks and future projections of flooding, claiming for attribution studies of extreme weather events to climate change[18–24].

Given the peculiar landscape, Venice is expected to be particularly vulnerable to climate change. Sea levels in Venice have risen by approximately 26 centimeters over the past century, with projections indicating a change in extreme total water level between 20 and 40 cm for RCP4.5 (2100) and RCP8.5 (2050) and up to 80 cm for the RPC8.5 (2100)[25]. Nevertheless, the complexity of the climate system and the challenges of climate change make

[1]Laboratoire des Sciences du Climat et de l'Environnement, CEA Saclay l'Orme des Merisiers, UMR 8212 CEA-CNRS-UVSQ, 91191 Gif-sur-Yvette, France. [2]London Mathematical Laboratory, 8 Margravine Gardens, London W6 8RH, UK. [3]Laboratoire de Météorologie Dynamique/IPSL, École Normale Supérieure, PSL Research University, Sorbonne Université, 75005 Paris, France. [4]Istituto Nazionale di Geofisica e Vulcanologia, via di Vigna Murata 605, Rome 00143, Italy. [5]International Centre for Theoretical Physics, Strada Costiera 11, Trieste 34100, Italy. ✉email: davide.faranda@lsce.ipsl.fr

Published in partnership with CECCR at King Abdulaziz University

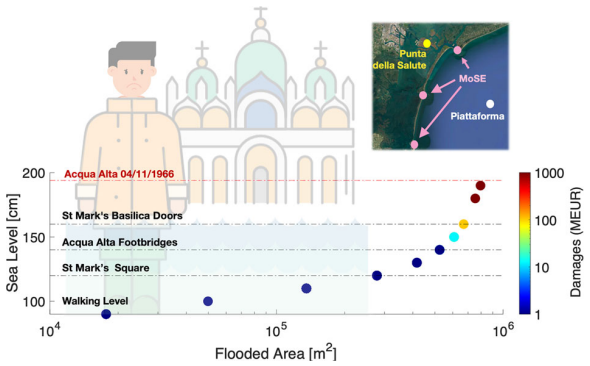

Fig. 1 Schematic representation of hazards for Venice lagoon. The relation between the sea level and the flooded area as a function of the estimated damages (filled coloured circles). The horizontal dashed-dotted black lines mark significant flooding levels corresponding to the sea level flooding St. Mark's square (120 cm), the level at which foodbridges are needed to walk across the square (140 cm), and the level at which water will enter the St. Mark's Basilica (160 cm). The red dashed-dotted line marks the level reached by the 04/11/1966 event known as "Great Flood of Venice" and studied in this work. The inset shows the location of the two tide gauge stations used to evaluate the sea levels within the lagoon (Punta della Salute, yellow circle) and outside (Piattaforma, white circle). The pink circles mark instead the position of the MoSE barriers at the three inlets (Diga Nord, Malamocco, and Diga Sud). Adapted from https://www.comune.venezia.it/it/content/venezia-e-lacqua-alta under the Creative Commons Licence 3.0 for non-commercial purposes.

difficult to evaluate the role of synoptic pattern changes in leading to Acqua Alta extreme events[2,4]. In the context of coastal floods in the city of Venice, there is a notable lack of studies that have attempted to attribute changes in atmospheric circulation over the Mediterranean region to specific causes. The complex and dynamic nature of the Mediterranean climate system in relation to Venice, affected by factors as local topography, ocean currents, and large-scale weather patterns, presents significant challenges in identifying and understanding the underlying mechanisms driving changes in atmospheric circulation. Despite the limited research in this area, it is widely acknowledged that changes in atmospheric circulation patterns can have significant impacts on the frequency and intensity of coastal floods in Venice, as well as on the city's infrastructure and economy[26].

Despite these difficulties, the Italian government has invested about 6.2 billion euros in the Experimental Electromechanical Module (MoSE) project, which includes a series of mobile barriers located in the three main channels that connect the lagoon with the north Adriatic Sea[27–29]. The MoSE project has faced some delays and controversies, but the barriers were successfully tested in 2020 and are expected to become fully operational soon. However, the issue of Acqua Alta in Venice is complex and multifaceted, requiring a coordinated and sustained effort to address. The MoSE project represents an important step forward, but further action is needed to mitigate the impacts of climate change and protect this unique and valuable cultural heritage site. The inset in Fig. 1 shows the location of the two tide gauge stations used to evaluate sea levels in this article (Punta della Salute and Piattaforma), while the pink circles indicate the position of the MoSE barriers at the three inlets.

In this paper, we employ a methodology that combines the use of analogue atmospheric patterns and statistical analysis [e.g. [30]] to attribute the increasing frequency and severity of Acqua Alta events in Venice to climate change. Specifically, we use atmospheric circulation patterns from the three most devastating Acqua Alta events in the lagoon (04/11/1966 - 194 cm; 29/10/2018 - 156 cm; and 12/11/2019 - 187 cm) and from a comparable (in terms of sea levels) but less devastating one (01/12/2008 - 156 cm) to identify analogues of these patterns in the recent past. By comparing the frequency of these analogues to the historical record, we assess the likelihood that the observed increase in Acqua Alta events is due to natural variability or climate change. To evaluate the effectiveness of MoSE (Experimental Electromechanical Module) protection, we analyse the analogues of the most extreme events and estimate the potential flood damage that would have occurred without MoSE activation. Finally, we perform a cost-benefit analysis to evaluate the economic implications of MoSE activation during Acqua Alta events.

RESULTS

Attribution of the 1966 event

We compare sea level pressure (slp), 2 meter temperature (t2m), total precipitation (pr), and the 10 m wind speed Scirocco-component (w) fields during Acqua Alta events in Venice from 1993 to 2022 (Factual Present) to the fields from 1950-1979 (Counterfactual Past), when human-driven climate change was just beginning. The choice of the variables is justified by the need of reflecting the airflows and weather conditions that characterise extreme events beyond floods. The method (see details below) ensures that comparisons are relevant, unlike purely statistical modeling techniques, which aim to simply analyse meteorological variables without tracing them back to the phenomena that produce them.

On November 4th, 1966, Venice experienced the highest Acqua Alta ever recorded since systematic measurements began. This was due to strong Scirocco winds, a strong depression, and a disastrous storm surge that breached the Murazzi (a hydraulic defense structure) in multiple locations. The high water persisted for 22 h above 110 cm and about 40 h above 50 cm, causing significant damage to the city, including power and gas outages, flooded streets and buildings, and destroyed boats and businesses. The island of Sant'Erasmo disappeared under waves up to 4 meters high, and Murano's glass factories were almost entirely destroyed (https://nuovavenezia.gelocal.it/venezia/cronaca/2016/10/17/news/la-cronaca-dell-aqua-granda-a-venezia-4-novembre-1966-1.14265973).

The meteorological contribution to the Acqua Alta was impressive, reaching 185 cm, while the maximum coincided with an astronomical tide of only 9 cm. The Scirocco winds prevented the outflow of water from the lagoon to the sea, and the minimum subsequent high tide was 116 cm. At 06:00 pm, the tide gauge at Punta della Salute reached 194 cm, the highest value ever recorded. Although other Italian cities were also severely affected by the storm, Venice was one of the most severely affected, and the city remained isolated for days.

Figure 2 displays the results of the attribution analysis for the 1966 Acqua Alta event in Venice. The study used the sea level pressure (slp), total precipitation (pr) and Scirocco 10m wind field (W) of the event (Fig. 2a) to search for analogues for both counterfactual (Fig. 2b) and factual (Fig. 2c) periods in the domain 10°E–15°E 42°N–47°N (Table 2). The slp field of the event consists of a deep Genoa Low depression. The analysis found that the slp field depicts negative anomalies on the southern flank of the cyclonic pattern in the factual period with respect to the counterfactual one (Fig. 2d). The temperature field does not depict significant changes between the two periods (Fig. 2e–h). The atmospheric pattern of the factual period is associated with higher precipitation over Lombardy and Veneto, which can enhance the contribution to Acqua Alta coming from the Adige and the Po Rivers (Fig. 2i–l). The maximum Scirocco winds were stronger over the Adriatic sea as well as over Veneto, which might contribute to an increase in storm surge (Fig. 2m–p).

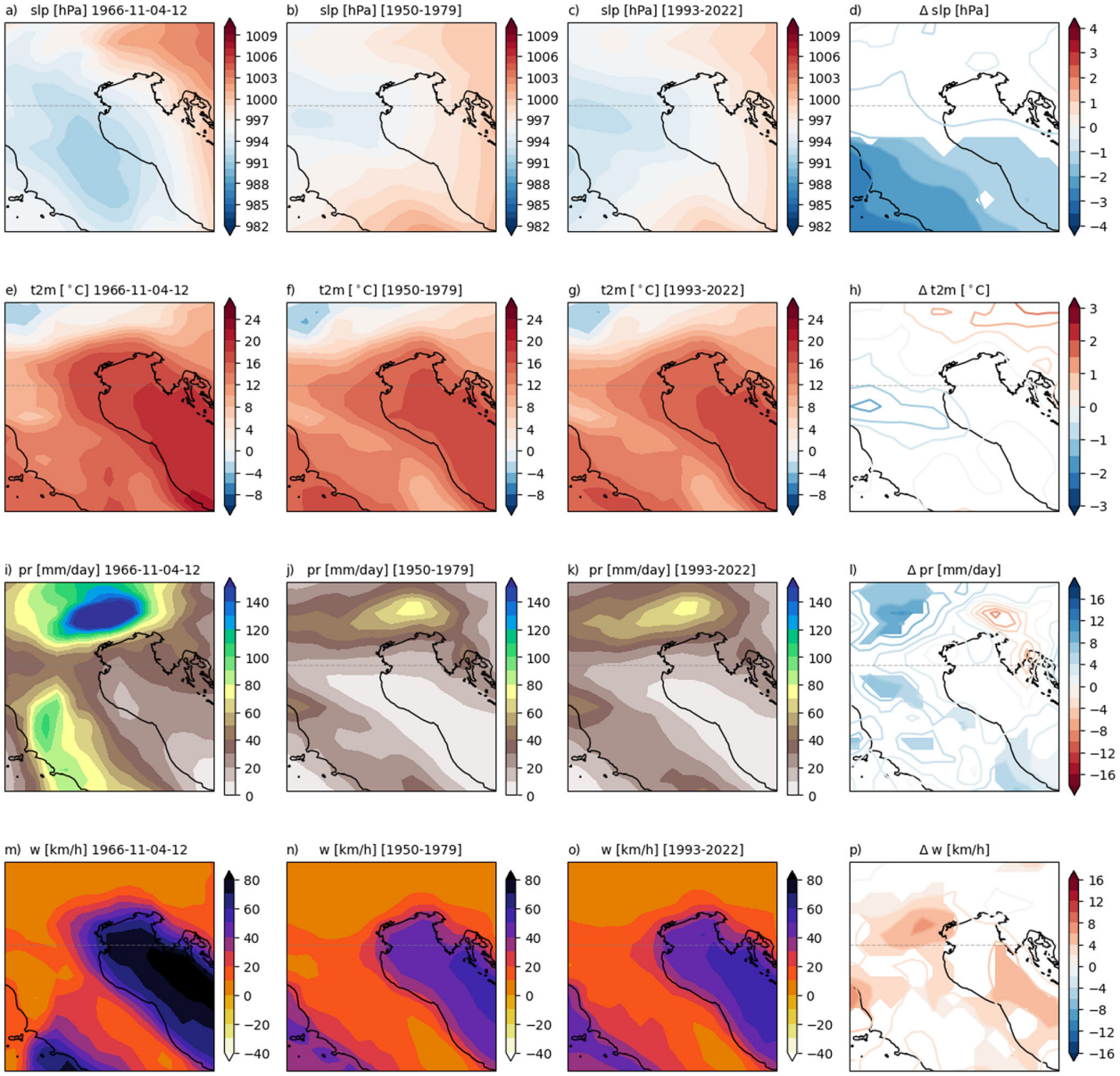

Fig. 2 Analogues Analysis for the 1966 Acqua Alta event in Venice. 6-hourly mean sea-level pressure, slp (**a**), 2-meter temperatures, t2m (**e**), total precipitation accumulated over 24 h, pr (**i**), maximum Scirocco wind component over 24 h, w (**m**), centered at the time of the event. Average of the 17 analogues found for the counterfactual [1950-1979] (**b**) and factual [1993-2022] (**c**) periods and corresponding 2-meter temperatures (**f**, **g**), total precipitation (**j**, **k**) and Scirocco wind speed (**n**, **o**). Δslp (**d**), Δt2m (**h**), Δpr (**l**) and Δw (**p**) between factual and counterfactual periods: coloured-filled areas refer to significant anomalies with respect to the bootstrap procedure (significance is defined as exceeding the 95th percentile in the bootstrap distribution).

Attribution of the 2008, 2018, and 2019 events

The Supplementary Information and Supplementary Fig. 1 describe the diagnostic of the analogues analysis for the 1966 event suggesting that the event is exceptional in both periods analysed. Supplementary Figs. 2–4 show the analogues analyses for the 2008, 2018, and 2019 events, respectively. The 2008 large scale circulation closely resembles that of the 1966 event but with a weaker depression. The 2018 event was associated to Vaia storm and was also characterised by an atmospheric river[31]. Such rivers are not very common in the Mediterranean basin and they could be important contributors to heavy precipitation. In this case, they have presumably influenced the deepening rate of Vaia (see also the huge signal in total precipitation reported in Supplementary Fig. 3). The 2019 event was due to a small-sized, secondary cyclone over the Adriatic sea [32]. Although it is not unusual for local minima to form cyclonic circulations over the Adriatic Sea, often becoming part of a broader low-pressure system that extends east and west of the Italian peninsula, the small-scale cyclone played a significant role in the flooding of Venice. Exploring the potential enhancement of Acqua Alta events through atmospheric and oceanic variability, Supplementary Note 1.4 and Supplementary Fig. 8 shed light on this complex interaction. These materials investigate how four prominent sources of atmospheric and oceanic variability, namely the North Atlantic Oscillation (NAO), the El Nino Southern Oscillation (ENSO), the Pacific Decadal Oscilation (PDO) and the Atlantic Multidecadal Oscillation (AMO)

Table 1. Summary of sea-levels (SL [cm]) and damages [MEUR] during the four considered Acqua Alta events in Venice.

	# MoSE	Variables	Event	[1950–1979] Counterfactual	[1993–2022] Factual (with MoSE)	[1993–2022] Counterfactual (no MoSE)
1966	11 (40%)	SL [cm][b]	194	122 (116,189)	111 (59, 156)	123 (107, 156)
		Damages [MEUR]	4.5	0.13 (0.09,1800)	0.25 (0.07, 28)	0.45 (0.06,28)
2008	09 (33%)	SL [cm][a]	156	119 (114,165)	113(63, 148)	116 (97, 149)
		Damages [MEUR]	28	0.20 (0.10,98)	0.25 (0.06, 11)	0.17 (0.06, 11)
2018	05 (17%)	SL [cm]	156	122 (114,155)	123 (75, 148)	124 (111, 148)
		Damages [MEUR]	28	0.32 (0.10, 27)	0.34 (0.07, 11)	0.38 (0.06, 11)
2019	08 (30%)	SL [cm][b]	187	116 (113,187)	111 (56, 141)	115 (102, 143)
		Damages [MEUR]	1.7	0.13 (0.08, 1800)	0.25 (0.07, 4)	0.12 (0.06, 5)

Mose indicates the number as well as the percentage of MoSE activations during the days anaologues of each event in the present period. Median values and 5-95 percentiles (brackets) of the distributions of analogues are reported for SL and damages during [1950–1979] (counterfactual past), [1993–2022] with MoSE activation (factual present), and [1993–2022] assuming no MoSE activation (counterfactual present).
[a]Indicates significant changes between counterfactual past and factual present (with MoSE activation).
[b]Indicates significant changes between factual present (MoSE activated) and counterfactual present (supposing the MoSE is not activated).
These changes are determined used a Cramer von Mises test at 0.05 significance level [48].

might modify frequency or intensity of Acqua Alta events in Venice. Our analysis suggests that while human-driven climate change remains the dominant driver behind most observed changes, the interplay of atmospheric and oceanic variability could contribute to the intensification of these events. Specifically, these natural factors could potentially exacerbate the conditions leading to 2018 and 2019 Acqua Alta events.

The main question we want to address in the remaining of the section is whether the MoSE is effective in reducing the damages caused by Acqua Alta events in Venice that are similar (analogous) to each of the four observed. To this aim we analyse the relationship between sea level (SL) and damages. In this case we extend the analogues search also one day before and one day after the dates identified as analogues to account for possible time lags. The period [1993–2022] is now partitioned into two different sub-periods: a factual present, corresponding to the actual scenario where the MoSE can be activated, and a counterfactual present, where we assume that the MoSE is not operative. To distinguish these two scenarios in terms of SL we make use of measurements at Punta della Salute (factual present), located within the lagoon (so, its measurements are affected by the MoSE activation), and Piattaforma, located outside the lagoon and being not affected by the MoSE. We retain the previously employed definition of counterfactual past for the period [1950–1979], however to avoid confusion we now rename it as counterfactual past. Potential damages are estimated using an exponential model with considering the daily operational cost of the MoSE, estimated at 0.025 MEUR (https://www.pagellapolitica.it/articoli/costo-mose-venezia), for the factual present. This analysis allows us to evaluate whether the MoSE has already functioned as an effective mitigation strategy. Results of this analysis are reported in Table 1. Figure 3 shows the details of the results for the 1966 event and Supplementary Figs. 9–11 for the other events analysed. First of all, we remark that the SL and the actual damages estimated during all events are larger than both the median values and even of the 95% percentiles of the SL and the damages distribution for all periods. This hints to the exceptionality of the events with respect to their analogues. For the 1966 event, we find 11 analogues where the MoSE has been operated (factual present). Our analysis finds that factual presents show significant reduction of SL with respect to both counteractual past and present periods. Damages for the counterfactual past are on average lower than factual and counterfactual presents with the MoSE system reducing damages from 0.45 MEUR to 0.25 MEUR.

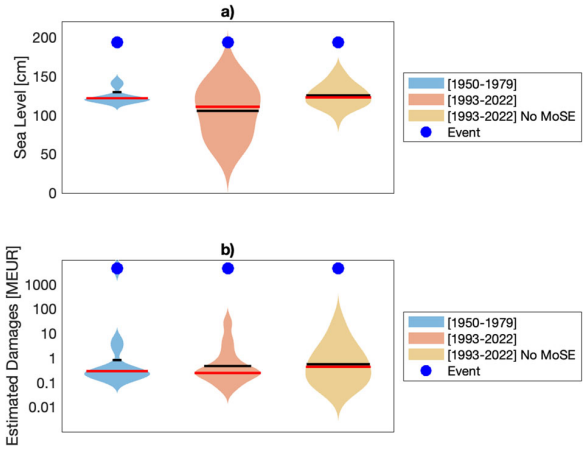

Fig. 3 Sea-levels SL during the analogues of the Acqua Alta 1966 event for past (blue), present (orange) and counterfactual worlds without MoSE (ocre). (**a**), and estimated damages of the flooding events associated (**b**). In the violin plots, red (black) lines represent average (median) values.

For the 2008 event, we find 9 analogues where MoSE has been activated and significantly lower sea-levels for the factual present both when compared to the counterfactual past and counterfactual present. When looking at the damages, the MoSE appears as a non cost-effective measure with a median damage higher than both factual and counterfactual presents. For the 2018 event, there are only 5 analogues situations in the factual present and no significant changes are found. For the 2019 event, we find 8 analogues where the MoSE has been operated (factual present). As for 1966, factual present shows significant reduction of SL with respect to both counteractual past and present periods. When looking at the damages, the MoSE appears as a non cost-effective measure with a median damage higher than both factual and counterfactual presents.

By further inspecting the dates of the analogues (see Table 3 in the counterfactual world none of the 2008, 2018, and 2019 events is analogue to the 1966; conversely, in the factual world both the 2008 and 2018 events are analogues to the 1966 one. This allows us, on one side, to state that, although its uniqueness in terms of impacts, the 1966 is not unique, in a statistical sense; on the other

side, we confirm, instead, that the 2019 is an unprecedented event, also in a statistical view.

DISCUSSION

The analysis presented in this paper aimed at investigating the benefit and effectiveness of the MoSE system in reducing the damages caused by Acqua Alta events in Venice. To achieve this goal, the study used an empirical approach to estimate the relationship between sea level and economic damages, and evaluated the effectiveness of the MoSE system in mitigating the damages caused by events similar to four events in the past.

The results of the analysis show that, for events similar to the 1966, 2008 and 2019 events, the MoSE system has already produced significant protection in terms of number of times of activation of the system, compared to the counterfactual scenario where the MoSE system was not in place. However, our results also highlights the limitations of the MoSE system is used to mitigate damages caused by some specific events, such as the 2018 event.

While our study provides important insights into the relationship between sea level and damages caused by Acqua Alta events in Venice, there are several limitations that should be considered when interpreting our results. First, our analysis relies on identifying analogues based on the sea level pressure, winds and precipitation charts of the event, which may not fully capture all the relevant atmospheric and sea-related conditions that contribute to Acqua Alta. For example, our analysis does not explicitly include the contribution of the atmospheric river associated with the 2018 event [31] and the ERA5 reanalyses are not always adequate to represent mesoscale cyclones as those associated to the 2019 event [32]. Indeed a slight displacement or underestimation of the cyclone can cause errors of several centimeters in the prediction of sea level height in a small basin such as the Venice lagoon. Moreover, our database spans a limited time, and future studies may benefit from incorporating additional data sources and using more advanced machine learning techniques to improve the accuracy of the analogues identification process. Our analysis is based on empirical estimates of the relationship between sea level and damages, which may be subject to errors and biases. In particular, our model assumes an exponential relationship between sea level and damages, which may not hold under changing climatic conditions. Furthermore, our data on damages is limited to reported losses, which may not capture the full extent of the economic and social impacts of Acqua Alta events. Finally, our analysis does not incorporate information from climate models or other types of climate projections, which could help to assess the potential impacts of future climate change on Acqua Alta events in Venice. Incorporating such information would require additional data sources and modeling techniques, and may be subject to uncertainties and biases associated with the models themselves. The use of large ensemble simulations will also help in discriminating the role of anthropogenically driven changes of these patterns from the long term variability of the climate system.

In conclusion, the results of this study have important implications for the management of Acqua Alta events in Venice. While we cannot attribute the observed changes exclusively to one factor, the modifications of atmospheric circulation patterns due to both natural and anthropogenic forced variability leading to Acqua Alta events already greatly affect the city of Venice. Our findings suggest that the MoSE system can be an effective mitigation strategy for events with historical analogues, but additional measures may be needed to address the potential damages caused by unprecedented events[24]. Future research in this area should focus on improving the accuracy of analogues identification, incorporating more sophisticated modeling techniques, and expanding the range of data sources and variables used to assess the impacts of Acqua Alta events. From the point of view of impacts, future research should focus to better understand the effectiveness of the MoSE system in mitigating damages caused by Acqua Alta events and to identify additional measures that can be implemented to reduce the impacts of these events on the city of Venice.

Our study represents one of the first examples that goes beyond identifying the circulation drivers of extreme events to quantifying the changes and their impacts. The framework we presented is general and can be applied to other case studies. However, our study also has limitations, like for example the limited database of sea-level for the past, the limited analogues used, and the fact that we did not use climate models. Despite these limitations, our study provides important insights into the attribution and impacts of extreme events, which are crucial for developing effective mitigation and adaptation strategies. We hope that our work will inspire future research and inform policymakers in their efforts to reduce the risks associated with extreme events.

METHODS

Data

We utilised the latest climate reanalysis data produced by the European Centre for Medium-Range Weather Forecasts (ECMWF) as part of the implementation of the EU-funded Copernicus Climate Change Service (C3S). Specifically, we used the ERA5 dataset, which provides hourly data on atmospheric, land surface, and sea state parameters from 1950 to the present at a horizontal resolution of $0.25^{\circ} \times 0.25^{\circ}$[33]. The choice of using ERA5 data for this study was motivated by the dataset's consistency over a long period of time (73 years), which allowed us to detect changes in the large dynamics associated with Acqua Alta events. In addition, the global nature of the ERA5 dataset allowed us to avoid mixing data from different national weather services and ensured uniform spatial and temporal coverage. While other observational or reanalysis datasets were considered, such as E-OBS, MERRA, NCEP, and CFSR, these were discarded due to the lack of sea-point coverage or insufficient temporal and spatial resolutions. The Centro Previsioni e Segnalazioni Maree (Center for Tides Forecasting and Reporting) of the Venice Municipality provides tide gauge data that is essential for understanding the frequency and intensity of Acqua Alta events in Venice. The tide gauge data records the water levels in the Venetian Lagoon at 16 different locations, including the historical station of Punta della Salute. These measurements are taken every 1 h and are reported in centimeters above the mean sea level, referred to the tidal zero of Punta della Salute. The tide level data are freely available at https://www.comune.venezia.it/it/content/dati-dalle-stazioni-rilevamento.

Analogues methods

The attribution protocol described in Faranda et al.[30] has already been applied and validated for pressure maps leading up to series of extreme events in the year 2021, including floods in Westphalia[34], storm Alex[35], and wind-power changes[36].

Here we apply it for Acqua Alta events in Venice, as follows. Considering that most of the Acqua Alta events analysed were due to rapid, small-scale cyclones, we analyse hourly and 6–hourly data. We divide the ERA5 sea-level pressure data set into two periods: 1950–1979 and 1993–2022 each consisting of 30 years data. We consider the first period to represent a past world with a weaker anthropogenic influence on climate than the second period, which represents our factual world affected by anthropogenic climate change. Here, we assume that 30 years is a long enough period to average out high-frequency interannual variability of the atmospheric motions. This time period is also

recommended by the WMO for the computation of climate normals[37].

To account for the possible influence of low-frequency modes of natural variability in explaining the differences between the two periods, we also consider the possible roles of the El Niño-Southern Oscillation (ENSO), the Atlantic Multidecadal Oscillation (AMO), and the Pacific Decadal Oscillation, the main sources of natural variability.

Our methodology for identifying cyclonic event analogues relies on sea level pressure (slp), total precipitation (pr), and Scirocco wind speed (w) patterns. Scirocco wind represents the south-easterly wind component (135°), calculated using the 10m zonal (u) and meridional (v) wind components (see Eq. (1))

$$w = u_{10m} sin(135^\circ) + v_{10m} cos(135^\circ). \quad (1)$$

To find the analogues we use 6–hourly data. Initially, we select the time step with the minimum sea level pressure from the event data and define the spatial domain covering the cyclonic low that caused the event (Table 2). To ensure comparability and equal weighting, we normalise each field $\phi = \{slp, pr, w\}$ using min-max normalisation, based on the minimum and maximum values observed throughout the 1950–2022 period (see, Eq. (2))

$$\phi_{scaled,i,j} = \frac{\phi(t)_{i,j} - \phi_{\min,i,j}}{\phi_{\max,i,j} - \phi_{\min,i,j}}. \quad (2)$$

Table 2. Time and spatial domain used to find analogues.

TIME	Spatial Box
1966-11-04-12	[10E–15E, 42N–47N]
2018-10-29-18	[5E–16E, 40N–49N]
2019-11-12-18	[5E–16E, 32N–45N]
2008-12-01-00	[5E–16E, 39N–48N]

Table 3. Analogues listed as extreme water heights by[3] for counterfactual and factual periods.

COUNTERFACTUAL		FACTUAL	
1966		1966	
Date	SL (cm)	Date	SL (cm)
1951-11-12	151	2000-11-06	144
1968-11-03	144	2008-12-01[a]	156[a]
		2018-10-29[a]	156[a]
2008		2008	
Date	SL (cm)	Date	SL (cm)
1951-11-12	151	2009-12-24	145
1979-12-22	166	2019-11-15	154
2018		2018	
Date	SL (cm)	Date	SL (cm)
1951-11-12	151	2000-11-06	144
1968-11-03	144	2002-11-16	147
1979-12-22	166	2009-12-23	143
		2010-12-24	144
2019		2019	
Date	SL (cm)	Date	SL (cm)
		2010-12-24	144

[a]Highlights the correspondence between analogues of the 1966 events and other two events analysed in this study.

We then compute the Euclidean distances of the three scaled fields with respect to the event itself. The combined Euclidean distance is determined by aggregating the Euclidean distances of the dynamic field (slp) with that of the physical fields (pr and w) as

$$d(t) = \sqrt{d_{slp}(t)^2} + \sqrt{d_{pr}(t)^2 + d_w(t)^2}. \quad (3)$$

Based on the combined Euclidean distances, we identify the best 17 analogues, corresponding to the records that minimise the combined distance. For the factual period, as is customary in attribution studies, the event itself is excluded. In addition, we prohibit the search for analogues within a 1-week window centered on the date of the event. Some of the analogues found were listed as extreme water heights by[3] for counterfactual and factual periods (Table 3), also reported as exceptional Acqua Alta events (https://www.comune.venezia.it/it/content/le-acque-alte-eccezionali). Finally, once the dates of the analogues are found, we make use of ERA5 hourly data to compute the accumulated precipitation over 24 h and the maximum Scirocco wind speed in 24 h, centered at the time of the event. This approach provides a more comprehensive assessment of the impacts.

We examine the seasonality of the analogues during the relevant season and their association with NAO ENSO, PDO and AMO. We perform this last analysis using monthly indices from NOAA/ERSSTv5 data and retrieved from the Royal Netherlands Meteorological Institute (KNMI) Climate Explorer. In particular, the ENSO index is version 3.4 as defined by Huang et al.[38], and the AMO, PDO index is calculated as described in Trenberth and Shea[39]. When the ENSO 3.4 index is positive, it corresponds to El Niño, and when it is negative, it corresponds to La Niña.

We define several quantities to support our interpretation of analogue-based assignment, including the analogue quality Q, which is the average Euclidean distance of a given day from its 17 closest analogues. If the value of Q for the extreme event belongs to the same distribution of its analogues, then the event is not unprecedented, and the attribution can be performed. If the value of Q is greater than those of its analogues, the event is unprecedented.

We also use dynamical systems theory to compute the local dimension D of each slp map, which is a proxy for the number of degrees of freedom of the field, and the persistence index Θ, which estimates the number of days we are likely to observe a map that is an analogue of the one under consideration[40]. We compute the values of persistence for the extreme event in the past, factual and counterfactual world and the corresponding distributions of the persistence for the analogues.

We count the number of analogues in each month of the extended Autumn season (September, October, November, December) to detect whether there has been a shift in circulation to months earlier or later in the season. This can have strong thermodynamic implications, for example, if a circulation leading to large positive temperature anomalies in early spring becomes more frequent later in the season when average temperatures are much higher.

Economic damage model vs. sea-level

We use an empirical approach to estimate the relation between sea level reached within the lagoon and economic damages to find an analytical function. We based our estimation on the reported damages associated with the four most devastating events (04/11/1966, 01/12/2008, 29/10/2018, and 12/11/2019) which costed 8000 MEUR, 20 MEUR, 47 MEUR, and 1000 MEUR, respectively (https://www.businessinsider.com/flooding-cost-1-billion-of-damage-to-venice-tourist-attractions-2019-12?r=US&IR=T, https://www.bbc.co.uk/newsround/50902267). Damage estimates are adjusted by the inflation (http://resolver.tudelft.nl/uuid:ea34a719-79c1-4c6e-b886-e0d92407bc9d). According to previous employed models for

estimating hazard functions for floods[41–44] we use an exponential law Damage $[MEUR] = a \exp b\, SL^*$, where $SL^* = SL/110$, to link the economic damage (in millions of euros) and the observed sea level change for extreme sea levels larger than 110 cm. The parameters of the fit are estimated by using the Levenberg-Marquardt algorithm whose robustness is assessed by the Least Absolute Residuals (LAR) method to minimise the absolute difference of the residuals. The best-fit parameters are $a = 5.05(3.06, 7.03) \times 10^{-3}$ MEUR and $b = 0.35(0.25, 0.45)$, where in brackets we report the 95% confidence levels, with an adjusted $R^2 = 0.99$ and a Root Mean Squared Error (RMSE = 27). We also used a power-law fit to model the economic damages as a function of the sea level, Damage$[MEUR] = a\, SL^{*b}$, with best-fit parameters $a = 8.97(4.07, 13.09) \times 10^{-3}$ MEUR and $b = 66.19(47.04, 85.34)$, where in brackets we report the 95% confidence levels, with an adjusted $R^2 = 0.84$ and RMSE = 46. However, the results are not statistically confident due to the under-estimation of damages for sea levels <160 cm. We are aware that only 3 events are not sufficient to provide a robust assessment of fitting procedures, however the use of exponential models to describe cost-benefit assessments and risk-hazard results has been widely documented in literature for different scenarios[41–43]. Furthermore, natural hazards are generally characterised by exponential laws in their occurrence as well as in their effects[45] or modeled as cascade processes (i.e. with a power-law model) where the resulting dynamics is a series of mutually interconnected phenomena (as in turbulence[46,47]).

DATA AVAILABILITY

ERA5 data are publicly available at climate explorer (http://climexp.knmi.nl/). Sea level data are made available at https://www.comune.venezia.it/it/content/centro-previsioni-e-segnalazioni-maree from the Centro Previsione e Segnalazione Maree - Protezione Civile, Venice, Italy, under the License Creative Commons Attribution-NonCommercial-ShareAlike 3.0 Italy (CC BY-NC-SA 3.0 IT).

CODE AVAILABILITY

The code to perform the analogues dynamical analysis is available at https://fr.mathworks.com/matlabcentral/fileexchange/95768-attractor-local-dimension-and-local-persistence-computation.

Received: 4 April 2023; Accepted: 27 October 2023;
Published online: 08 November 2023

REFERENCES

1. Tebaldi, C. et al. Extreme sea levels at different global warming levels. *Nat. Clim. Chang.* **11**, 746–751 (2021).
2. Umgiesser, G. et al. The prediction of floods in Venice: methods, models and uncertainty (review article). *Nat. Haz. Earth Sys. Sci.* **21**, 2679–2704 (2021).
3. Lionello, P. et al. Extreme floods of Venice: characteristics, dynamics, past and future evolution (review article). *Nat. Haz. Earth Sys. Sci.* **21**, 2705–2731 (2021).
4. Zanchettin, D. et al. Sea-level rise in Venice: historic and future trends (review article). *Nat. Haz. Earth Sys. Sci.* **21**, 2643–2678 (2021).
5. Malguzzi, P., Grossi, G., Buzzi, A., Ranzi, R. & Buizza, R. The 1966 "century" flood in Italy: A meteorological and hydrological revisitation. *J. Geophys. Res. Atmos.* **111**, D24106 (2006).
6. Ferrarin, C., Lionello, P., Orlić, M., Raicich, F. & Salvadori, G. Venice as a paradigm of coastal flooding under multiple compound drivers. *Sci. Rep.* **12**, 5754 (2022).
7. Cavaleri, L. et al. The 2019 flooding of venice and its implications for future predictions. *Oceanography* **33**, 42–49 (2020).
8. Ferrarin, C. et al. Local and large-scale controls of the exceptional Venice floods of November 2019. *Progress Oceanogr.* **197**, 102628 (2021).
9. Miglietta, M. M., Carnevale, D., Levizzani, V. & Rotunno, R. Role of moist and dry air advection in the development of Mediterranean tropical-like cyclones (medicanes). *Quart. J. Roy. Met. Soc.* **147**, 876–899 (2021).
10. Luppichini, M., Bini, M., Barsanti, M., Giannecchini, R. & Zanchetta, G. Seasonal rainfall trends of a key Mediterranean area in relation to large-scale atmospheric circulation: How does current global change affect the rainfall regime? *J. Hydr.* **612**, 128233 (2022).
11. Flaounas, E. et al. Mediterranean cyclones: current knowledge and open questions on dynamics, prediction, climatology and impacts. *Weath. Clim. Dyn.* **3**, 173–208 (2022).
12. Davolio, S., Silvestro, F. & Gastaldo, T. Impact of Rainfall Assimilation on High-Resolution Hydrometeorological Forecasts over Liguria, Italy. *J. Hydromet.* **18**, 2659–2680 (2017).
13. Davolio, S., Miglietta, M. M., Diomede, T., Marsigli, C. & Montani, A. A flood episode in northern Italy: multi-model and single-model mesoscale meteorological ensembles for hydrological predictions. *Hydr. Earth Sys. Sci.* **17**, 2107–2120 (2013).
14. Otto, F. E. L. Extreme events: The art of attribution. *Nat. Clim. Chang.* **6**, 342–343 (2016).
15. Otto, F. Attribution of extreme weather events: how does climate change affect weather? *Weather* **74**, 325–326 (2019).
16. IPCC. *Climate Change 2022: Mitigation of Climate Change. Contribution of Working Group III to the Sixth Assessment Report of the Intergovernmental Panel on Climate Change* (Cambridge University Press, Cambridge, UK and New York, NY, USA, 2022).
17. Masson-Delmotte, V. et al. *Climate Change 2021: The Physical Science Basis. Contribution of Working Group I to the Sixth Assessment Report of the Intergovernmental Panel on Climate Change*, vol. 2 (Cambridge University Press, Cambridge, United Kingdom and New York, NY, USA, 2021).
18. Van Oldenborgh, G. J. et al. Attributing and Projecting Heatwaves Is Hard: We Can Do Better. *Earth's Future* **10**, e2021EF002271 (2022).
19. Vautard, R. et al. Evaluation of the Large EURO-CORDEX Regional Climate Model Ensemble. *J. Geophys. Res. Atmos.* **126**, e2019JD032344 (2021).
20. van Oldenborgh, G. J. et al. Pathways and pitfalls in extreme event attribution. *Clim. Change* **166**, 13 (2021).
21. Reed, K. A., Wehner, M. F. & Zarzycki, C. M. Attribution of 2020 hurricane season extreme rainfall to human-induced climate change. *Nat. Comm.* **13**, 1905 (2022).
22. Bellprat, O., Guemas, V., Doblas-Reyes, F. & Donat, M. G. Towards reliable extreme weather and climate event attribution. *Nat. Comm.* **10**, 1732 (2019).
23. Strauss, B. H. et al. Economic damages from Hurricane Sandy attributable to sea level rise caused by anthropogenic climate change. *Nat. Comm.* **12**, 2720 (2021).
24. Alberti, T. et al. Dynamical diagnostic of extreme events in Venice lagoon and their mitigation with the MoSE. *Sci. Rep.* **13**, 10475 (2023).
25. Ranasinghe, R. et al. *Climate Change Information for Regional Impact and for Risk Assessment. In Climate Change 2021: The Physical Science Basis. Contribution of Working Group I to the Sixth Assessment Report of the Intergovernmental Panel on Climate Change* (Cambridge University Press, Cambridge, UK and New York, NY, USA, 2021).
26. Sperotto, A. et al. A multi-disciplinary approach to evaluate pluvial floods risk under changing climate: The case study of the municipality of Venice (Italy). *Sci. Tot. Env.* **562**, 1031–1043 (2016).
27. Leonardi, N. The barriers of Venice. *Nat. Geosci.* **14**, 881–882 (2021).
28. Mel, R., Carniello, L. & D'Alpaos, L. Addressing the effect of the Mo.S.E. barriers closure on wind setup within the Venice lagoon. *Est. Coast. Shelf Sci.* **225**, 106249 (2019).
29. Umgiesser, G. & Matticchio, B. Simulating the mobile barrier (MOSE) operation in the Venice Lagoon, Italy: global sea level rise and its implication for navigation. *Ocean Dyn.* **56**, 320–332 (2006).
30. Faranda, D., Pascale, S. & Bulut, B. Persistent anticyclonic conditions and climate change exacerbated the exceptional 2022 European-Mediterranean drought. *Envir. Res. Lett.* **18**, 034030 (2023).
31. Davolio, S., Della Fera, S., Laviola, S., Miglietta, M. M. & Levizzani, V. Heavy Precipitation over Italy from the Mediterranean Storm "Vaia" in October 2018: Assessing the Role of an Atmospheric River. *Mont. Weat. Rev.* **148**, 3571–3588 (2020).
32. Miglietta, M. M. et al. A high-impact meso-beta vortex in the adriatic sea. *Quat. J. Roy. Met. Soc.* **149**, 637–656 (2023).
33. Hersbach, H. et al. ERA5 hourly data on single levels from 1959 to present. *Copernicus Climate Change Service (C3S) Climate Data Store (CDS)* 10.10.24381 (Accessed on 09-11-2022) (2018).
34. Faranda, D. et al. A climate-change attribution retrospective of some impactful weather extremes of 2021. *Weat. Clim. Dyn.* **3**, 1311–1340 (2022).
35. Ginesta, M., Yiou, P., Messori, G. & Faranda, D. A methodology for attributing severe extratropical cyclones to climate change based on reanalysis data: the case study of storm Alex 2020. *Clim. Dyn.* **61**, 229–253 (2023).
36. Rapella, L., Faranda, D., Gaetani, M., Drobinski, P. & Ginesta, M. Climate change on extreme winds already affects off-shore wind power availability in europe. *Envir. Res. Lett.* **18**, 034040 (2023).
37. Arguez, A. & Vose, R. S. The Definition of the Standard WMO Climate Normal: The Key to Deriving Alternative Climate Normals. *Bull. Amer. Met. Soc.* **92**, 699–704 (2011).
38. Huang, B. et al. Reforecasting the ENSO Events in the Past 57 Years (1958-2014). *J. Clim.* **30**, 7669–7693 (2017).
39. Trenberth, K. E. & Shea, D. J. Atlantic hurricanes and natural variability in 2005. *Geophys. Res. Lett.* **33**, L12704 (2006).

40. Faranda, D., Messori, G., Alvarez-Castro, M. C. & Yiou, P. Dynamical properties and extremes of Northern Hemisphere climate fields over the past 60 years. *Nonl. Proc. Geophy.* **24**, 713–725 (2017).
41. Amadio, M. et al. Testing empirical and synthetic flood damage models: the case of italy. *Nat. Haz. Earth Sys. Sci.* **19**, 661–678 (2019).
42. Gerl, T., Kreibich, H., Franco, G., Marechal, D. & Schröter, K. A review of flood loss models as basis for harmonization and benchmarking. *PLOS ONE* **11**, 1–22 (2016).
43. Read, L. K. & Vogel, R. M. Hazard function analysis for flood planning under nonstationarity. *Water Resourc. Res.* **52**, 4116–4131 (2016).
44. Guan, X. Flood risk analysis integrating of bayesian-based time-varying model and expected annual damage considering non-stationarity and uncertainty in the coastal city. *J. Hydr.* **617**, 129038 (2023).
45. Read, L. K. & Vogel, R. M. Hazard function theory for nonstationary natural hazards. *Nat. Haz. Earth Sys. Sci.* **16**, 915–925 (2016).
46. Frisch, U. & Sornette, D. Extreme Deviations and Applications. *J. de Physique I* **7**, 1155–1171 (1997).
47. Alberti, T. et al. Chameleon attractors in turbulent flows. *Chaos Sol. Fract.* **168**, 113195 (2023).
48. Anderson, T. W. On the distribution of the two-sample cramer-von mises criterion. *Ann. Math. Stat.* **33**, 1148–1159 (1962).

ACKNOWLEDGEMENTS

All the authors acknowledge the Centro Previsione e Segnalazione Maree - Protezione Civile, Venice, Italy, for making available tide gauge data. Data are distributed under the License Creative Commons Attribution-NonCommercial-ShareAlike 3.0 Italy (CC BY-NC-SA 3.0 IT). D.F. and E.C. received support from the European Union's Horizon 2020 research and innovation programme under grant agreement No. 101003469 (XAIDA). D.F. and M.G. received support from the European Union's Horizon 2020 Marie Sklodowska-Curie grant agreement No. 956396 (EDIPI). D.F. received further support from the LEFE-MANU-INSU-CNRS grant "CROIRE". We also acknowledge useful discussions with the MedCyclones COST Action (CA19109) community. This research was supported by the SAVEMEDCOASTS2 Project (number 874398 www.savemedcoasts2.eu) funded by the European Commission through the DG-ECHO.

AUTHOR CONTRIBUTIONS

D.F. and T.A. devised the study, D.F. and M.G. performed the analogues analyses and T.A. devised the model of damage. All authors contributed to discussing and writing the paper.

COMPETING INTERESTS

The authors declare no competing interests. No human or animal data have been used in this study.

ADDITIONAL INFORMATION

Supplementary information The online version contains supplementary material available at https://doi.org/10.1038/s41612-023-00513-0.

Correspondence and requests for materials should be addressed to Davide Faranda.

Reprints and permission information is available at http://www.nature.com/reprints

Publisher's note Springer Nature remains neutral with regard to jurisdictional claims in published maps and institutional affiliations.

IOP Publishing Environ. Res. Lett. 18 (2023) 034040 https://doi.org/10.1088/1748-9326/acbdb2

ENVIRONMENTAL RESEARCH
LETTERS

OPEN ACCESS

RECEIVED
4 November 2022

REVISED
16 February 2023

ACCEPTED FOR PUBLICATION
21 February 2023

PUBLISHED
7 March 2023

LETTER

Climate change on extreme winds already affects off-shore wind power availability in Europe

Lia Rapella[1,2,*], Davide Faranda[1,3,5], Marco Gaetani[6], Philippe Drobinski[4] and Mireia Ginesta[1]

[1] Laboratoire des Sciences du Climat et de l'Environnement, UMR 8212 CEA-CNRS-UVSQ, Université Paris-Saclay & IPSL, CE Saclay l'Orme des Merisiers, 91191 Gif-sur-Yvette, France
[2] LMD-IPSL, École Polytechnique, Institut Polytechnique de Paris, CNRS, Palaiseau, France
[3] London Mathematical Laboratory, 8 Margravine Gardens, London W6 8RH, British Islands
[4] LMD-IPSL, École Polytechnique, Institut Polytechnique de Paris, ENS, PSL Research University, Sorbonne Université, CNRS, Palaiseau, France
[5] Laboratoire de Météorologie Dynamique, École Normale Supériore, PSL research University & IPSL, 75005 Paris, France
[6] Scuola Universitaria Superiore IUSS, Palazzo del Broletto, Piazza della Vittoria 15, 27100 Pavia, Italia
[*] Author to whom any correspondence should be addressed.

E-mail: lia.rapella@lmd.ipsl.fr

Keywords: extreme winds, climate change, off-shore wind power availability

Supplementary material for this article is available online

Abstract

Off-shore wind energy in Europe plays a key role in the transition to renewable energy, and its usage is expected to increase in the next few decades. According to the working regimes of a wind turbine, wind energy production can be disrupted by extreme atmospheric events related to low wind speed below the cut-in wind speed and high wind speed above the cut-out wind speed. The purpose of this work is to estimate the behavior of extreme winds on the European panorama, over the period 1950–2020, in order to investigate the large-scale weather regimes related to them and their impact on off-shore wind energy availability. We detected significant changes in the frequency of high and low extreme wind events, proving that climate change or long-term internal climate variability have already affected the off-shore wind power output. Moreover, the analysis of weather regimes showed that high and low extreme wind events can occur simultaneously over Europe. Our results suggest the necessity to implement efficient European energy management policies, to minimize the deficit in wind power supply.

1. Introduction

Climate change is one of the most urgent challenges that humankind confront nowadays. As reported by the Intergovernmental Panel of Climate Change Synthesis Report [34], adaptation and mitigation are the main guidelines to follow in order to reduce and manage the impacts of climate change. Substantial cuts in greenhouse gas emissions are necessary to reduce climate risks in the future (XXI century and beyond) as they can contribute to climate-resilient pathways for sustainable development [34]. To this purpose, the European Union (EU) has planned ambitious strategies: to cut emissions by at least 55% with respect to the values in 1990 by 2030 (and 80% by 2050) and to become, by 2050, the first 'net-zero' carbon continent, i.e. able to compensate all emissions of CO_2 [18], in the world. In this context, renewable energy (RE) plays a key role: on one hand their development and extensive usage can slow down climate change effects and help to obtain the 'net-zero' carbon goal, on the other hand substantial local changes in atmospheric conditions could modify, for better or worse, their efficiency [10, 35, 39, 40], and their demand [36].

Due to its increasing price competitiveness and the development of high-efficiency technologies, wind energy is playing, and it will play more and more in the future, a significant role in the transition to a RE system [46]. To gain the climate targets, the EU is planning to scale up the off-shore wind industry from the 12 GW capacity currently installed to 60 GW by 2030, and to 300 GW by 2050 [17]. Nevertheless, wind energy is one of the most variable and weather-dependent RE, because of its natural dependence on the wind speed, which can vary at different time

scales, ranging from small-scale turbulence to seasonal oscillations and up to long-term climate variability. Moreover, wind energy can be heavily affected by extreme events, since under these conditions winds can easily reach such speeds to force the turbines to be parked or idled, or, conversely, not be strong enough to move them, thus interrupting the energy production.

Indeed, the potential wind power production[7] (W_{pot}), according to the working regimes of a wind turbine [30], depends on the wind speed V by the following relation:

$$W_{pot} = \begin{cases} 0 & \text{if } V < V_i \\ \frac{V^3 - V_i^3}{V_R^3 - V_i^3} & \text{if } V_i \leqslant V < V_R \\ 1 & \text{if } V_R \leqslant V < V_o \\ 0 & \text{otherwise} \end{cases} \quad (1)$$

where V_R is the rated speed (13 m s^{-1}), V_i (3.5 m s^{-1}) and V_o (25 m s^{-1}) are the cut-in and cut-off speed respectively[8] [29].

When the cut-off threshold is overcome, the turbines are stopped for security reasons (*storm control*), and the loss in the wind power production can be high, ranging from the 50% of the installed capacity in half an hour to 70% in 1 h [11]. Similarly, the turbines do not work when the wind speed is lower than the cut-in threshold, with consequent losses in the W_{pot}.

In Europe, high-speed winds are mainly associated with the passage of the so called *extra-tropical* or *mid-latitude cyclones* [23], especially in autumn and winter (supplementary, *Extra-tropycal cyclones*).

Changes in the intensity or frequency of the cyclones (anticyclones) can cause changes in the occurrence of intense storms or low-speed winds events, with possible impacts on the electric power generation. Therefore, it is of strong interest having information about their features and tracks, as well as knowing which weather regimes generate them (supplementary, *Weather regimes*). While Grams *et al* [26] have already analyzed the importance of weather regimes in the average wind energy production by assuming stationarity in weather regimes over the historical period (1979–2015), here we extend this viewpoint by specifically looking at the relationship between extreme high/low-speed wind conditions and weather regimes and by releasing the assumption of weather regime stationary. Indeed, Brönniman *et al* [4] and Corti *et al* [8] evidenced that significant trends in extreme winds frequency in the historical period exist, as well as that natural atmospheric circulation regimes have already changed due to anthropogenic forcing. This motivates the present study.

Identifying which weather regimes are associated with extreme winds[9] is of prominent importance in order to have a complete view of the distribution of the European wind energy resources. In fact, if the same weather regime affects a large area, we could have simultaneous multiple outages in the turbines operation with consequent shortages in the wind energy supply. In a future scenario with only RE, this might even lead to partial or total blackouts, with heavy impacts especially on cities and urban areas. Contrariwise, if the weather regimes that cause extreme wind events differ from area to area, with the perspective of European energy management policies, which provide investments for the construction of infrastructures aimed to distribution, storage and energy transmission, it would be possible to redirect the energy to the affected zones and thus avoid temporary blackouts [25, 32].

In light of these considerations, the general purpose of this work is to estimate the behavior of extreme winds on the European panorama, over the period 1950–2020, in order to investigate the large-scale weather regimes related to them and their impact on off-shore wind energy availability.

The paper is organized as follows. In section 2, we present the data which we will use in our forthcoming analysis. In section 3, we investigate the presence of significant trends in the occurrence of high/low-speed wind events, over selected periods and regions, by means of a non-parametric trend test. Finally, in section 4, we investigate the weather regimes at which the high/low-speed wind events occur, in order to detect changes in their pattern, before drawing our conclusions in section 5.

2. Data and methods

The more recent climate reanalysis released by the European Centre for Medium-Range Weather Forecasts is ERA5, which provides data, from 1950 to present, over different timescales, describing many atmospheric, land-surface and oceans parameters together with estimates of uncertainty. These datasets are publicly available at the Copernicus Climate Data Centre [7] on regular latitude-longitude grid, at 0.25° × 0.25° resolution[10].

For our analysis we used two subsets of ERA5 [27], *ERA5 hourly data on single levels from 1950 to 1978* [15] and *ERA5 hourly data on single levels from 1979 to present* [16], covering a period from 1950 to 2020 and selecting 6-hourly values, at 00:00, 06:00, 12:00 and 18:00. In particular, we selected three variables:

[7] Dimensionless indicator of the potential power production at each location and time.

[8] We chose these values because they are the most common, but we specify that they are not universal and they correspond to a specific wind turbine technology.

[9] See section 2 for the definition of 'extreme winds'.

[10] This resolution corresponds approximately to 27.75 km^2.

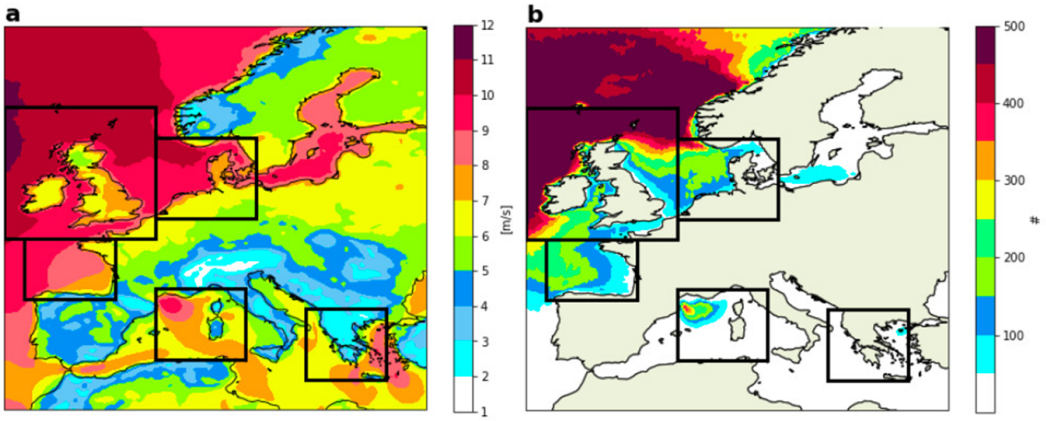

Figure 1. (a) 1950–2020 average 100 m horizontal wind-speed (m s^{-1}). (b) Total number of events # above the 100 m horizontal wind-speed cut-off threshold (25 m s^{-1}) over the period 1950–2020. In order to distinguish more clearly the zones with the highest number of events, we limited the range of values to 500. All the values $\geqslant$500 are mapped with the last color of the colorbar. The black boxes indicate the areas specifically considered in this study: British Islands (12° W−3° E, 49° N−62° N), North Sea (3° E−13° E, 51° N−59° N), Bay of Biscay (10° W−1° W, 43° N−49° N), Central Mediterranean (3° E−12° E, 37° N−44.5° N),Balkan Peninsula (18° E−26° E, 35° N−42° N).

- 100 m u-component of wind, u ([m s^{-1}]): eastward horizontal component of wind speed, measured at 100 m above the Earth surface;
- 100 m v-component of wind, v ([m s^{-1}]): northward horizontal component of wind speed, measured at 100 m above the Earth surface;
- geopotential, z ([m^2 s^{-2}]), at 500 hPa: the gravitational potential energy of a unit mass, at a particular location at the surface of the Earth, relative to mean sea level;

and we extracted a sub-region corresponding to the European area: −12° W−30° E, 32° N−70° N.

To obtain the horizontal wind speed at 100 m[11], V, we combined the u-component of wind with the v-component:

$$V = \sqrt{u^2 + v^2}. \quad (2)$$

To calculate the geopotential height, zh, instead, we simply divided z by the Earth's gravitational acceleration (9.806 65 m s^{-2}).

In figure 1, panel (a), it is represented the mean of the horizontal wind speed at 100 m over the period 1950–2020. As shown by the map, the strongest winds blow off-shore, with a peak of 11 m s^{-1} off the British Islands.

In this paper, we will refer to 'extreme (wind) events' as the wind events with the wind speed in the non-operating regime, according to (1). We will call 'high wind events' the wind events with the wind speed over the cut-off threshold and 'low wind events' those with the wind speed under the cut-in threshold. Moreover, we will consider as event every time-step with the wind speed that satisfies one of these two latter constraints.

To have a clearer view of which zones are affected by high wind events, we first masked the 100 m horizontal wind speed, keeping only the values higher than the cut-off speed. We then counted, grid point by grid point, the number of events during the period 1950–2020 that satisfy this latter constraint (figure 1, panel (b)). As expected, we found that this condition occurs mainly off-shore, and we focused especially on five regions, where high winds are observed more frequently and where most of the farms are installed: British Islands, North Sea, Balkan Peninsula, and the areas off the south of France and north of Spain. These regions are particularly favorable to the installation of offshore wind farms because they experience quasi-constant wind patterns. Specifically, the Bay of Biscay, the British Islands and the North Sea lie on the Atlantic storm track [13]; Central Mediterranean and the Balkan Peninsula are affected by the Mistral and Etesian wind patterns, respectively [43]. During the summer months (June–July–August) no high wind events are detected, while the peak occurs in winter (December–January–February, DJF).

3. Trends in wind events

Focusing on the regions indicated in figure 1, we investigated the existence of significant long-term changes in the occurrence of extreme events during the period 1950–2020. With this aim, we analyzed their trends, separately region by region, by means of the Mann–Kendall test at 95% level of confidence [37]. We computed the test not only considering the

[11] We use the wind speed at 100 m as reference wind speed for the off-shore turbines, which have a typical hub height ranging from 80 m to 120 m.

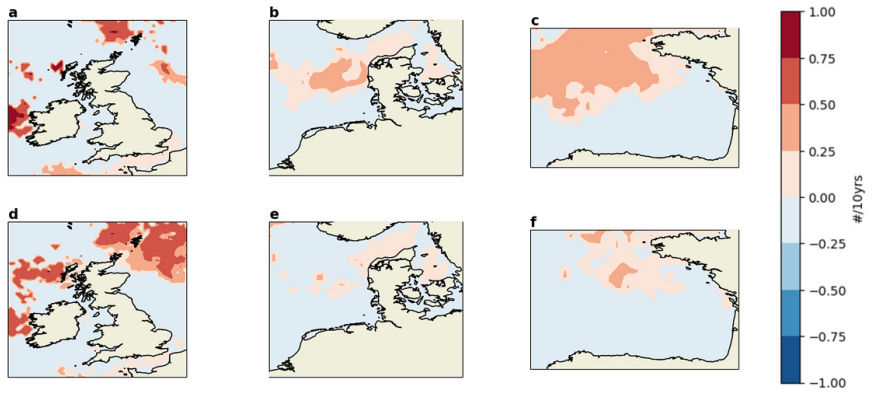

Figure 2. Average change (red: increase, blue: decrease) in the number of high wind events per decade #/ten years over the period 1950–2020, during the whole year (a)–(c) and for the winter months (DJF, (d)–(f)), for British Islands, North Sea and Bay of Biscay. Each map depicts only the grid points that exhibit significant changes.

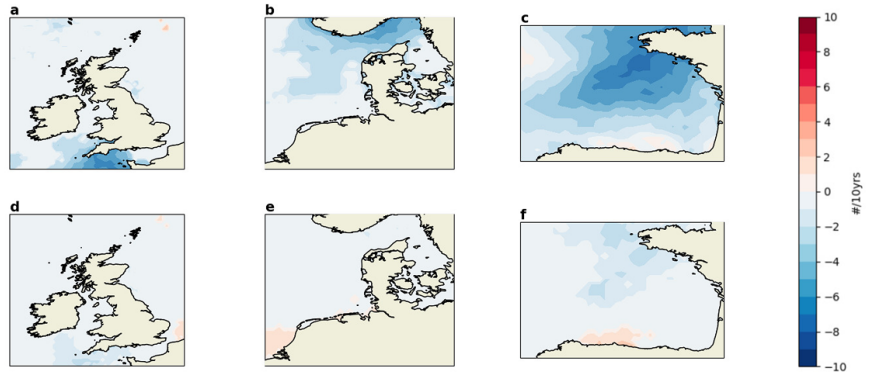

Figure 3. Average change (red: increase, blue: decrease) in the number of low wind events per decade #/ten years over the period 1950–2020, during the whole year (a)–(c) and for the summer months (JJA, (d)–(f)), for British Islands, North Sea and Bay of Biscay. Each map depicts only the grid points that exhibit significant changes.

number of events during the whole year, but also apiece for summer and winter, during which most of the events occur respectively for the low and the high wind events.

Figure 2 shows the average change, per decade, in the number of high wind events, over the period 1950–2020, during the whole year and for the winter months, for British Islands, North Sea, Bay of Biscay. In large part of these regions a significant increasing trend is detected throughout the years and for the DJF period (figure 2), as well as in very small areas of Central Mediterranean. In the Balkan Peninsula (not shown), instead, in both cases, where detected, the trends are significantly decreasing.

Figure 3 shows the average change, per decade, in the number of low wind events, over the period 1950–2020, during the whole year and for the summer months, for British Islands, North Sea, Bay of Biscay. For these latter regions it is observed a general average decrease in the number of these events, with a significant negative trend particularly strong in the number of events during the whole year. Contrariwise, in Central Mediterranean and Balkan Peninsula, the number of low wind events has markedly increased, especially considering its trend during the whole year, as shown in figure 4.

We want to stress that reanalysis is not always the best tool for evaluating wind speed long-term variability, since there are still issues about its ability to reproduce wind-speed trends [19, 42] and different reanalysis can even disagree with each other [2, 47]. In fact, the reanalysis products could be affected by errors in the observations and in the assimilation procedure. Therefore, to have more robust results, it would be recommended to use a multi-reanalysis approach. Nevertheless, Faranda *et al* [21] studied trends in atmospheric circulation using different reanalysis (ERA5, NCEP) and gridded interpolated data (EOBS) finding that the qualitative results of large-scale circulation trends analysis remain largely unaffected. Moreover, three recent works have recently appeared pointing to the possibility of attributing different events to climate change on the basis of reanalysis only: Faranda *et al* [20], Cadiou *et al* [5], Ginesta *et al* [24].

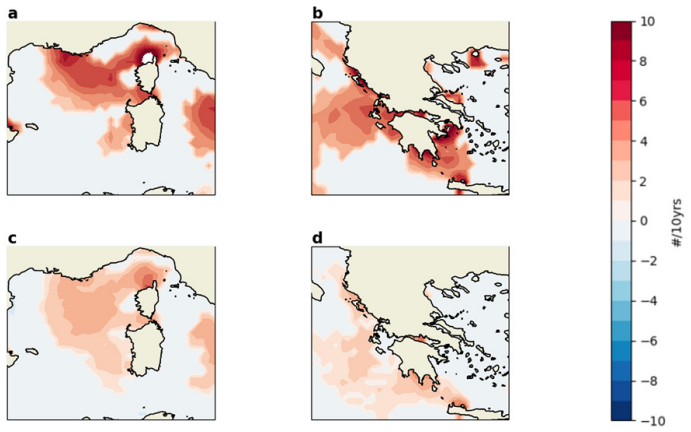

Figure 4. Same as in figure 3, but for Central Mediterranean and Balkan Peninsula. Each map depicts only the grid points that exhibit significant changes.

Table 1. Number of affected grid points with the corresponding spatial area (km^2) above the 95th percentile (high winds) and above the 99th percentile (low winds) for all the areas considered in this study.

Region	High winds		Low winds	
British Islands	419	11627	1104	30636
North Sea	207	5744	668	18537
Bay of Biscay	244	6771	505	14014
Central Mediterranean	85	2359	778	21590
Balkan Peninsula	47	1304	671	18620

4. Weather regimes analysis for high/low wind events

Since we want to investigate the extreme events that may have, in each region, the most widespread impact on the off-shore wind energy production, we restricted the analysis to the events that involve a high number of grid points. To do so, starting from the datasets with only the 6-hourly wind speed values over the cut-off threshold and under the cut-in threshold, we selected, separately for each zone, the time-steps with the number of affected grid points respectively above the 95th percentile and the 99th percentile (table 1).

As expected, the British Islands is the region with the most widespread high winds (457 time-steps identified), followed at a distance by North Sea (97) and Bay of Biscay (85).

In order to identify the different weather regimes associated with the occurrence of extreme wind events and to detect changes in their pattern, we took some preliminary steps.

Firstly, for each region, we computed the anomalies in the geopotential height[12], for the high and low wind events, over the time-steps selected following the procedure mentioned above. To do this, for each time-step we subtracted to ϕ the value of ϕ at the same instant averaged over the month for all the period 1950–2020. For example, to the value of the geopotential height on the 01 February 1953 at 06:00 we subtracted the mean of the geopotential height values on every day of February at 6 a.m. from 1950 to 2020. Then, we grouped the selected time-steps in two sub-periods, past period (1 January 1950–30 June 1985) and present period (1 July 1985–31 December 2020), and we computed the anomalies in the geopotential height averaged over these two time-windows, together with the difference between present and past average anomalies. To test the significance of the differences we applied the bootstrap method, at the 95th level of confidence. Moreover, to better understand the nature of these differences, we analyzed the North Atlantic Oscillation (NAO) index distributions for both periods, by means of a two-sided Cramér–von Mises test at the 95% level of confidence [9] (supplementary, *Weather regimes*).

As shown in figure 5, high winds in British Islands, North Sea and Bay of Biscay occur during the NAO+ phases. In the second period, the positive ϕ anomalies become more intense and widespread over Central-Southern Europe, and the gradient between positive and negative anomalies is accentuated, leading to a higher frequency of these extreme events (table 2) over the zones considered and to stronger winds over the British Islands and North Sea (supplementary, figure 1). For these two regions, a significant change in the NAO distribution between present and past period has been found, with a weak shift

[12] Going forward, the geopotential height will be referred to as ϕ.

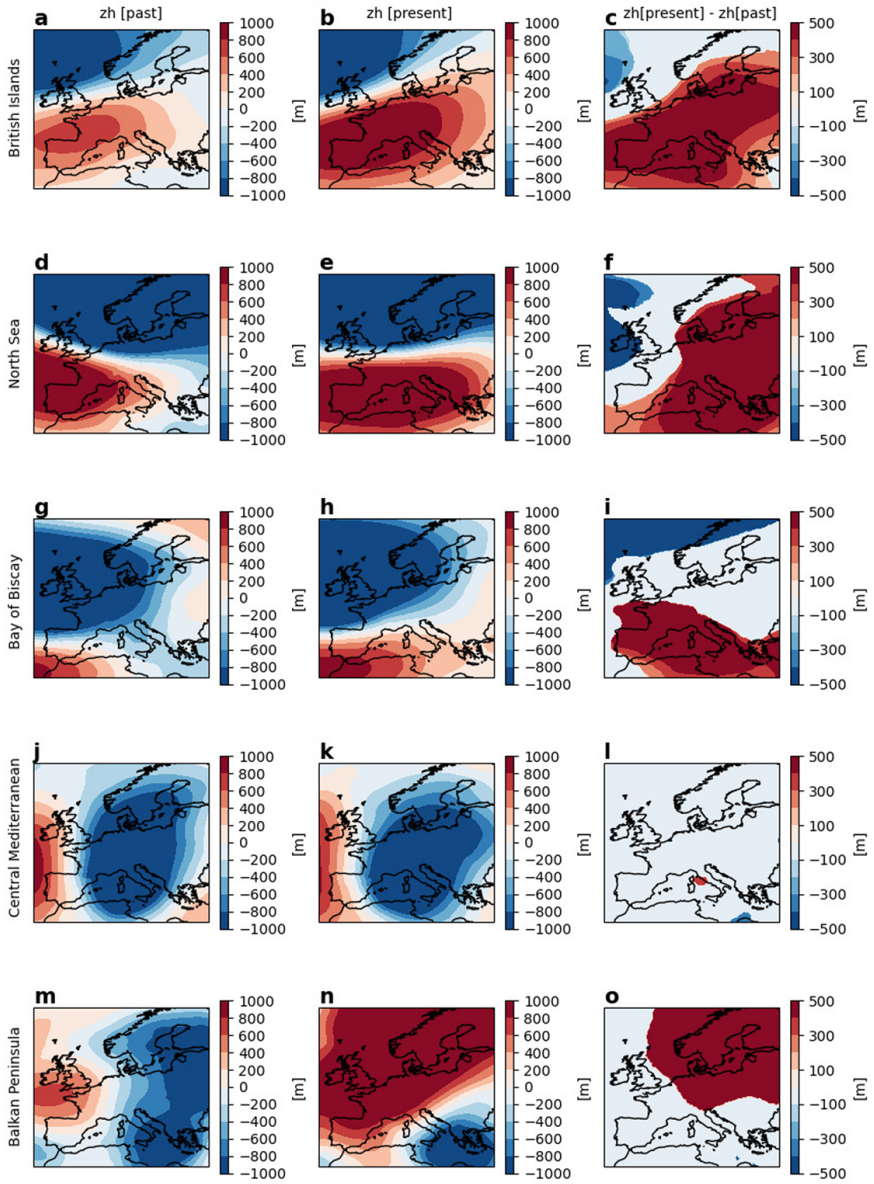

Figure 5. High winds. Composites of the geopotential height anomalies over the time-steps with the number of affected grid points above the 95th percentile for the period 1 January 1950–30 June 1985 (a), (d), (g), (j), (m) and for the period 1 July 1985–31 December 2020 (b), (e), (h), (k), (n); difference between the climatology of present and past anomalies (c), (f), (i), (l), (o). British Islands (a)–(c), North Sea (d)–(f), Bay of Biscay (g)–(i), Central Mediterranean (j)–(l), Balkan Peninsula (m)–(o). In the third column, shadings indicate significant changes.

Table 2. Number of events with the number of affected grid points above the 95th percentile (high winds, left column of each side) and above the 99th percentile (low winds, right column of each side) for the past period (1 January 1950–30 June 1985) and for the present (1 July 1985–31 December 2020) for all the areas considered in this study.

Region	Past period		Present period	
British Islands	176	552	281	382
North Sea	38	493	59	369
Bay of Biscay	29	585	56	389
Central Mediterranean	32	531	31	513
Balkan Peninsula	9	477	10	561

towards more positive (neutral) NAO phases in the present period for the British Islands (North Sea) (supplementary, figures 3 and 4). Instead, an Atlantic ridge pattern is found for the Central Mediterranean (figure 5) and, in the first period, for Balkan Peninsula (figure 5), for which then it shifts to a Scandinavian

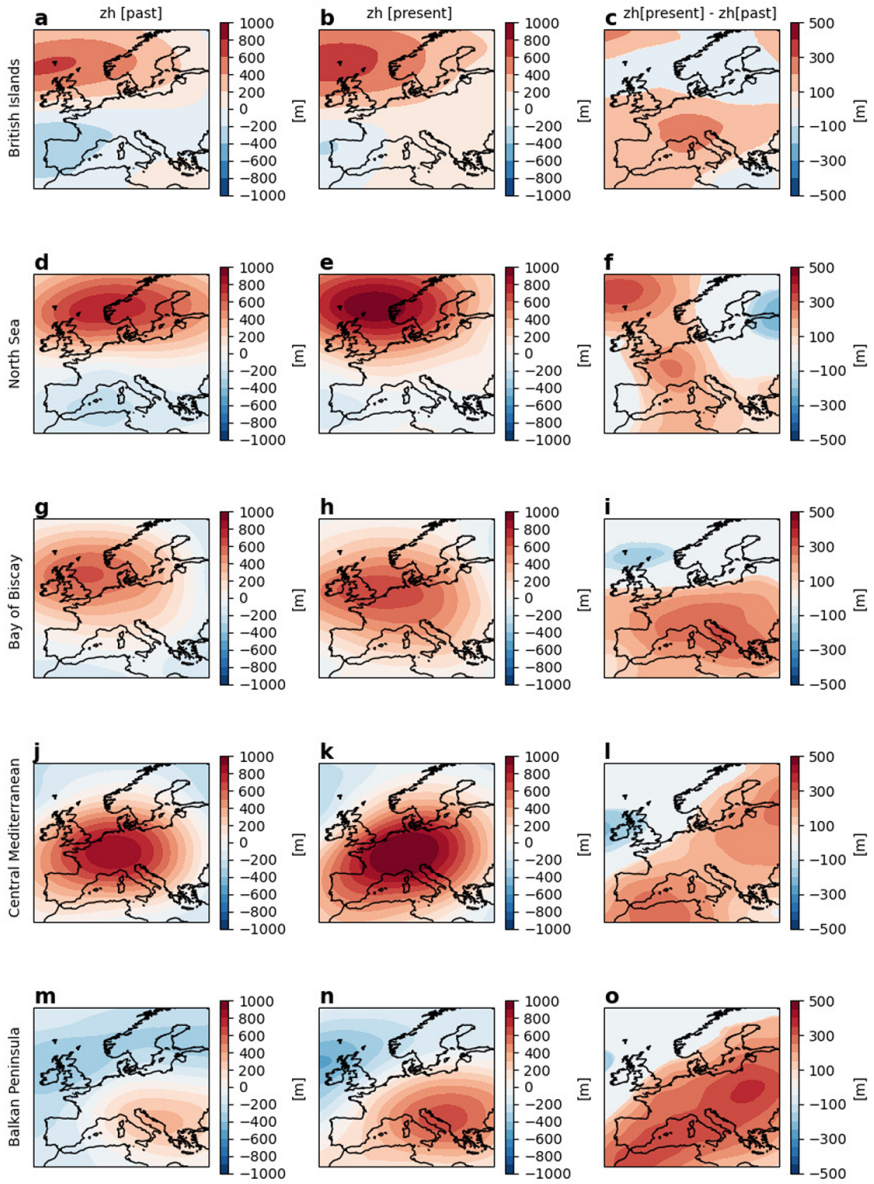

Figure 6. Low winds. Composites of the geopotential height anomalies over the time-steps with the number of affected grid points above the 99th percentile for the period 1 January 1950–30 June 1985 (a), (d), (g), (j), (m) and for the period 1 July 1985–31 December 2020 (b), (e), (h), (k), (n); difference between the climatology of present and past anomalies (c), (f), (i), (l), (o). British Islands (a)–(c), North Sea (d)–(f), Bay of Biscay (g)–(i), Central Mediterranean (j)–(l), Balkan Peninsula (m)–(o). In the third column, shadings indicate significant changes.

blocking, with the center of the low pressure system remaining located over the Balkan Peninsula. According to this behavior, figure 7 (supplementary) displays a significant shift from positive to neutral NAO values in the present period. In both cases, contrary to what happened for the areas in North Europe (British Islands, North Sea and Bay of Biscay), there are substantially no changes in the occurrence of high winds. However, there is a slight decrease in their intensity in Central Mediterranean (supplementary, figure 1) and changes, both positive and negative, in Balkan Peninsula (supplementary, figure 1).

Regarding the low winds, in each period and for each region, their occurrence is related to a blocking pattern with the high pressure zone over the affected area (figure 6), and no significant changes in the NAO distribution between present and past period have been found (figures 8–12, supplementary). In all cases, in the second period the intensity of the positive anomalies increases, leading to stronger pressure gradients and to higher anticyclonic (clockwise) winds, causing a significant reduction in the number of low wind events (table 2). In Balkan Peninsula, on the contrary, we detected a slight increase in the average number of days with low winds: indeed, by looking at the associated ϕ patterns (figure 6), rather than changes in the pressure gradients we observe an extension of the high pressure area over

the Mediterranean. This is consistent with the results presented in [22], where a strengthening in the anticyclones intensity is found over this region.

To account the possible influence of the low-frequency natural variability, the El Niño-Southern Oscillation (ENSO) and the Atlantic Multi-decadal Oscillation (AMO) (supplementary, *ENSO and AMO*) distributions have been studied [20], as done for the NAO index. Regarding the high winds, we detected significant changes between past and present period in the ENSO distribution for British Islands (shift to neutral values), Bay of Biscay and Central Mediterranean (negative shift), and in the AMO distribution for Bay of Biscay, Central Mediterranean (shift to lower values) and Balkan Peninsula (higher values). Therefore, for these mentioned regions, we cannot reject the hypothesis that ENSO and AMO variability have influenced the behavior of the high winds.

For the low winds, we found significant changes in the ENSO and AMO distribution for all the regions, with weak positive shift in the mean values in the present period and/or marked changes in the shape of the distributions between the two periods. This implies that changes in the low wind speed behavior can not be linked only to climate change but they are also related to the internal climate variability, which plays a relevant role.

5. Concluding remarks

In this work, we have estimated the behavior of extreme winds on the European panorama, over the period 1950–2020, and related them to the large-scale weather regimes, drawing conclusions on their potential impacts on off-shore wind energy availability. In particular, we focused on five regions: British Islands, North Sea, Bay of Biscay, Central Mediterranean and Balkan Peninsula. By means of the Mann–Kendall test, we have detected the presence of significant trends in the occurrence of wind events with the wind speed above the cut-out threshold and below the cut-in threshold, during the period 1950–2020. In British Islands, North Sea and Bay of Biscay a significant increasing trend has been observed for high winds, and a decreasing trend for low winds. Contrariwise, in Central Mediterranean and Balkan Peninsula, the number of low wind events has increased. Finally, we have identified the weather regimes at which the extreme wind events occur, analyzing the changes in the average geopotential height anomalies and in the average 100 m horizontal wind speed between the past period (1 January 1950–30 June 1985) and the present period (1 July 1985–31 December 2020). The low winds events are related to blocking patterns with the high pressure zone centered over the affected area. This implies that extreme events with the wind speed under the cut-in threshold can not occur, on average, at the same time at other locations. Conversely, we have found that high winds for British Islands, North Sea and Bay of Biscay were related to the same weather regime, namely the NAO+ phase. This fact could lead, in the future, to widespread shortages in the wind energy supply, possibly leading to partial or total blackouts, with heavy impacts especially on cities and urban areas, in a scenario where energy is produced mostly by renewable sources. We remark that, although the frequency of extreme events related to high winds is relatively modest compared to the low wind ones, they could lead to heavier impacts. In fact, high winds not only prevent the RE infrastructures from operating, because of the storm control, but they may damage and sometimes even destroy the wind turbines, making maintenance interventions necessary and so extending the downtime.

In determining the behavior of low-winds events, only ENSO and AMO played a significant role, while for high winds in British Islands, North Sea and Balkan Peninsula we found a significant link also to NAO phases.

Our analyses, focused on historical climate data for the period 1950–2020, have shown that climate change and internal climate variability intervene together in affecting wind power availability over Europe during extreme weather events. To perform the analyses, as underlined at the end of section 3, we chose to only use ERA5 reanalysis data-sets, and not a multi-reanalysis approach. Furthermore, we did not make use of models due to their limitations in providing a coherent picture of low-frequency modes of variability and their interactions [6], as well as inconsistencies between numerical models and reanalysis when it comes to temporal variations in the atmospheric states—which is at the basis of our analysis [38].

In addition, we point out that in this study we have considered every grid point as a potential location for the installation of wind turbines. However, this is only possible in areas where the sea depth is less than 1 km. Therefore, to increase the relevance of our results, it would be beneficial to only consider the grid points with an average sea depth of less than 1000 m.

A natural continuation of this study will be to look at future climate scenarios. Various studies suggest that climate change will not considerably affect the average near-surface wind speed [28, 41] and therefore the average energy production. However, our analysis could motivate further research by specifically looking at extreme low/high winds that could not necessarily follow the behavior of average wind speed. In this context, it will be appropriate to use the new convection permitting simulations available at high resolutions [1]. A natural strategy to ensure robustness of the results would be the use of *ensembles* climate simulations corresponding to different shared socio-economic pathways.

The results of our work are consistent with the previous literature that analyzed the influence of the

weather patterns, and consequently of the wind conditions, on the wind power generation [3, 14, 45, 48]. In particular, our paper has taken a clue from the work of Grams *et al* [26]. In their paper, Grams *et al* underline the lack of well-deployed installations and of an efficient electric European net that could handle electricity deficit periods. In addition, they stress the necessity to plan the installation of new capacity basing on the meteorological understanding. Combining these considerations with the results of our study, we can state that the planning of new wind farms should take into account also the behavior of the extreme wind events, which can represent a threat to an efficient operation of the installations. We finally remind that, to ensure that meaningful results are obtained, it is fundamental the use of suitable data-sets and an adequate time period to capture detectable trends.

Data availability statement

The data that support the findings of this study are openly available at the following URL/DOI: https://cds.climate.copernicus.eu/#!/home.

Acknowledgments

This work has received support from the European Union's Horizon 2020 research and innovation programme (Grant Agreement No. 101003469, XAIDA) and funding by the Erasmus+ Programme in collaboration with the University of Pavia and by the Commissariat a l'Energie Atomique et aux Energies Alternatives (CEA). This work is a contribution of the Energy4Climate Interdisciplinary Center (E4C) of IP Paris and Ecole des Ponts, supported by 3rd Programme d'Investissements d'Avenir [ANR-18-EUR-0006-02]. This project has received funding from the European Union's Horizon 2020 research and innovation programme under the Marie Sklodowska-Curie grant agreement No. 956396 (EDIPI project).

Author contributions

L R performed the analyses. L R and D F conceived the study and wrote the paper. The authors declare that they have NO affiliations with or involvement in any organization or entity with any financial interest in the subject matter or materials discussed in this manuscript.

References

[1] Ban N *et al* 2021 The first multi-model ensemble of regional climate simulations at kilometer-scale resolution, part I: evaluation of precipitation *Clim. Dyn.* **57** 275–302
[2] Befort D J, Wild S, Kruschke T, Ulbrich U and Leckebusch G C 2016 Different long-term trends of extra-tropical cyclones and windstorms in ERA-20C and NOAA-20CR reanalyses *Atmos. Sci. Lett.* **17** 586–95
[3] Brayshaw D J, Troccoli A, Fordham R and Methven J 2011 The impact of large scale atmospheric circulation patterns on wind power generation and its potential predictability: a case study over the UK *Renew. Energy* **36** 2087–96
[4] Brönnimann S, Martius O, von Waldow H, Welker C, Luterbacher J, Compo G P, Sardeshmukh P D and Usbeck T 2012 Extreme winds at northern mid-latitudes since 1871 *Meteorol. Z.* **21** 13–27
[5] Cadiou C, Noyelle R, Malhomme N and Faranda D 2022 Challenges in attributing the 2022 Australian rain bombs to climate change *Asia-Pac. J. Atmos. Sci.* (https://doi.org/10.1007/s13143-022-00305-1)
[6] Coburn J and Pryor S C 2021 Differential Credibility of Climate Modes in CMIP6 *J. Clim.* **34** 8145–64
[7] Copernicus 2022 (available at: https://cds.climate.copernicus.eu/#!/home)
[8] Corti S, Molteni F and Palmer T N 1999 Signature of recent climate change in frequencies of natural atmospheric circulation regimes *Nature* **398** 799–802
[9] Cramér-von Mises test 2020 (available at: https://encyclopediaofmath.org/wiki/Cramer-von_Mises_test)
[10] Crook J A, Jones L A, Forster P M and Crook R 2011 Climate change impacts on future photovoltaic and concentrated solar power energy output *Energy Environ. Sci.* **4** 3101–9
[11] Cutululis N A, Litong-Palima M and Sørensen P E 2012 *Offshore Wind Power Production in Critical Weather Conditions* (Copenhagen: European Wind Energy Association (EWEA))
[12] Díaz H and Guedes Soares C 2020 Review of the current status, technology and future trends of offshore wind farms *Ocean Eng.* **209** 107381
[13] Dong B, Sutton R T, Woollings T and Hodges K 2013 Variability of the North Atlantic summer storm track: mechanisms and impacts on European climate *Environ. Res. Lett.* **8** 034037
[14] Ely C, Brayshaw D, Methven J, Cox J and Pearce O 2013 Implications of the North Atlantic Oscillation for a UK–Norway Renewable power system *Energy Policy* **62** 1420–7
[15] ERA5 hourly data on single levels from 1950 to 1978 2021 (available at: https://cds.climate.copernicus.eu/cdsapp#!/dataset/reanalysis-era5-single-levels-preliminary-back-extension?tab=overview)
[16] ERA5 hourly data on single levels from 1979 to present 2021 (available at: https://cds.climate.copernicus.eu/cdsapp#!/dataset/reanalysis-era5-single-levels?tab=overview)
[17] European Commission 2022 An EU Strategy to harness the potential of offshore renewable energy for a climate neutral future European Commission 2022 (available at: https://energy.ec.europa.eu/topics/renewable-energy/offshore-renewable-energy_en)
[18] European Commission 2022 2022 (available at: https://climate.ec.europa.eu/eu-action/european-green-deal/delivering-european-green-deal_en)
[19] Fan W, Liu Y, Chappell A, Dong L, Xu R, Ekström M, Fu T and Zeng Z 2021 Evaluation of global reanalysis land surface wind speed trends to support wind energy development using in situ observations *J. Appl. Meteorol. Climatol.* **60** 33–50
[20] Faranda D, Bourdin S, Ginesta M, Krouma M, Noyelle R, Pons F, Yiou P and Messori G 2022 A climate-change attribution retrospective of some impactful weather extremes of 2021 *Weather Clim. Dyn.* **3** 1311–40
[21] Faranda D, Messori G, Jézéquel A, Vrac M and Yiou P 2022 Atmospheric circulation compounds anthropogenic warming and extreme climate impacts in Europe accepted (https://doi.org/10.1073/pnas.2214525120)
[22] Fery L, Dubrulle B, Podvin B, Pons F and Faranda D 2022 Learning a weather dictionary of atmospheric patterns using latent Dirichlet allocation *Geophys. Res. Lett.* **49** e2021GL096184
[23] Froude L S R, Bengtsson L and Hodges K I 2007 The prediction of extratropical storm tracks by the ECMWF and

NCEP Ensemble Prediction Systems *Mon. Weather Rev.* **135** 2545–67
[24] Ginesta M, Yiou P, Messori G and Faranda D 2022 A methodology for attributing extratropical cyclones to climate change: the case study of storm Alex 2020 *Clim. Dyn.* (https://doi.org/10.1007/s00382-022-06565-x)
[25] Gonçalves A, Liberato M L R and Nieto R 2021 Wind energy assessment during high-impact winter storms in southwestern Europe *Atmosphere* **12** 509
[26] Grams C M, Beerli R, Pfenninger S, Staffell I and Wernli H 2017 Balancing Europe's wind-power output through spatial deployment informed by weather regimes *Nat. Clim. Change* **7** 557–62
[27] Gualtieri G 2021 Reliability of ERA5 reanalysis data for wind resource assessment: a comparison against tall towers *Energies* **14** 4169
[28] Hdidouan D and Staffell I 2016 The impact of climate change on the levelised cost of wind energy *Renew. Energy* **101** 575–92
[29] Jerez S, Thais F, Tobin I, Wild M, Colette A, Yiou P and Vautard R 2015 The CLIMIX model: a tool to create and evaluate spatially-resolved scenarios of photovoltaic and wind power development *Renew. Sustain. Energy Rev.* **42** 1–15
[30] Mathew S 2006 *Wind Energy: Fundamentals, Resource Analysis and Economics* (Berlin: Springer)
[31] Moloney N R, Faranda D and Sato Y 2019 An overview of the extremal index *Chaos* **29** 022101
[32] Monforti F, Gaetani M and Vignati E 2016 How synchronous is wind energy production among European countries? *Renew. Sustain. Energy Rev.* **59** 1622–38
[33] Neu U *et al* 2013 IMILAST: a community effort to intercompare extratropical cyclone detection and tracking algorithms *Bull. Am. Meteorol. Soc.* **94** 529–47
[34] Pachauri R K *et al* 2014 Climate change 2014: synthesis report *Contribution of Working Groups I, II and III to the Fifth Assessment Report of the Intergovernmental Panel on Climate Change* (Geneva: IPCC) p 151
[35] Patt A, Pfenninger S and Lilliestam J 2013 Vulnerability of solar energy infrastructure and output to climate change year *Clim. Change* **121** 93–102
[36] Perera A T D, Nik V M, Chen D, Scartezzini J and Hong T 2020 Quantifying the impacts of climate change and extreme climate events on energy systems *Nat. Energy* **5** 150–9
[37] Pymannkendall 1.4.2 2022 (available at: https://pypi.org/project/pymannkendall/)
[38] Rodrigues D, Alvarez-Castro M C, Messori G, Yiou P, Robin Y and Faranda D 2018 Dynamical properties of the North Atlantic atmospheric circulation in the past 150 years in CMIP5 models and the 20CRv2c reanalysis *J. Clim.* **31** 6097–111
[39] Rose S, Jaramillo P, Small M J, Grossmann I and Apt J 2012 Quantifying the hurricane risk to offshore wind turbines *Proc. Natl Acad. Sci.* **109** 3247–52
[40] Steiner A, Köhler C, Metzinger I, Braun A, Zirkelbach M, Ernst D, Tran P and Ritter B 2017 Critical weather situations for renewable energies – Part A: cyclone detection for wind power *Renew. Energy* **101** 41–50
[41] Tobin I, Vautard R, Balog I, Bréon F, Jerez S, Ruti P, Thais F, Vrac M and Yiou P 2015 Assessing climate change impacts on European wind energy from ENSEMBLES high-resolution climate projections *Clim. Change* **128** 99–112
[42] Torralba V, Doblas-Reyes F and Gonzalez-Reviriego N 2017 Uncertainty in recent near-surface wind speed trends: a global reanalysis intercomparison *Environ. Res. Lett.* **12** 114019
[43] Ulbrich U *et al* 2012 Climate of the Mediterranean: synoptic patterns, temperature, precipitation, winds, and their extremes *The Climate of the Mediterranean Region* (Elsevier) pp 301–46
[44] Ulbrich U, Leckebusch G C and Pinto J G 2009 Extra-tropical cyclones in the present and future climate: a review *Theor. Appl. Climatol.* **96** 117–31
[45] Van der Wiel K, Bloomfield H, Lee R, Stoop L, Blackport R, Screen J and Selten F 2019 The influence of weather regimes on European renewable energy production and demand *Environ. Res. Lett.* **14** 094010
[46] Velenturf A P M, Emery A R, Hodgson D M, Barlow N L M, Mohtaj Khorasani A M, Van Alstine J, Peterson E L, Piazolo S and Thorp M 2021 Geoscience solutions for sustainable offshore wind development *Earth Sci. Syst. Soc.* 4
[47] Wohland J, Omrani N, Witthaut D and Keenlyside N S 2019 Inconsistent wind speed trends in current twentieth century reanalyses *J.Geophys. Res.* **124** 1931–40
[48] Zubiate L, McDermott F, Sweeney C and O'Malley M 2016 Spatial variability in winter NAO-wind speed relationships in western Europe linked to concomitant states of the East Atlantic and Scandinavian patterns: variability of winter wind speeds in response to NAO, EA and SCA *Q. J. R. Meteorol. Soc.* **143** 1032–46